General Disclaimer

One or more of the Following Statements may affect this Document

- This document has been reproduced from the best copy furnished by the organizational source. It is being released in the interest of making available as much information as possible.

- This document may contain data, which exceeds the sheet parameters. It was furnished in this condition by the organizational source and is the best copy available.

- This document may contain tone-on-tone or color graphs, charts and/or pictures, which have been reproduced in black and white.

- This document is paginated as submitted by the original source.

- Portions of this document are not fully legible due to the historical nature of some of the material. However, it is the best reproduction available from the original submission.
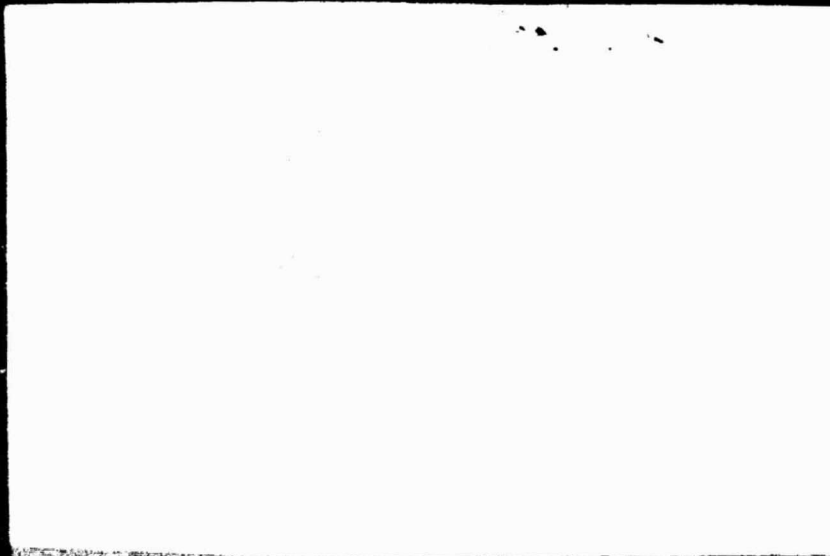
Produced by the NASA Center for Aerospace Information (CASI)

AN IMPROVED SWITCHING CONVERTER

POWER STAGE MODEL USING

DISCRETE-AVERAGE TECHNIQUES

FINAL REPORT

BY

DRS. F. C. LEE and D. J. SHORTT

ELECTRICAL ENGINEERING DEPARTMENT
VIRGINIA POLYTECHNIC INSTITUTE AND STATE UNIVERSITY
BLACKSBURG, VA 24061

Prepared for:

NATIONAL AERONAUTICS AND SPACE ADMINISTRATION

LEWIS RESEARCH CENTER
21000 Brookpark Road
Cleveland, Ohio 44135

AN IMPROVED SWITCHING CONVERTER MODEL

by

Daniel Jeffrey Shortt

Dissertation submitted to the Faculty of the Virginia
Polytechnic Institute and State University in partial
fulfillment of the requirements for the degree of

DOCTOR OF PHILOSOPHY

in

Electrical Engineering

APPROVED:

F.C. Lee, Chairman

D.D. Chen

S.L. Hendricks

L.L. Grigsby

S. Rahman

November, 1982

Blacksburg, Virginia

AN IMPROVED SWITCHING CONVERTER MODEL

ABSTRACT

The nonlinear modeling and analysis of dc-dc converters
in the continuous mode and discontinuous mode has been done by
averaging and discrete-sampling techniques. The averaging
technique is simple to use and averages the output voltage.
The discrete technique is very complex and cumbersome, but
accurately predicts the envelope of the output voltage. A new
model is developed by combining the aforementioned techniques.
This new model, the discrete-average model, accurately predicts
the envelope of the output voltage and is easy to implement in
circuit and state variable forms.

The major points of this dissertation are as follows:

1. The proposed model is shown to be dependent on the
   type of duty cycle control.

2. The proper selection of the power stage model, between
   average and discrete-average, is largely a function
   of the error processor in the feedback loop.

3. The accuracy of the measurement data taken by a con-
   ventional technique is affected by the conditions at
   which the data is collected.

ACKNOWLEDGEMENTS

The author wishes to express his sincere thanks to Drs. D. Y. Chen, L.L. Grigsby, S.L. Hendricks and S. Rahman for serving as members of his committee. Special thanks and sincere appreciation are extended to Dr. F.C. Lee for his guidance and service as the major advisor.

The author is deeply indebted to the Nasa Lewis Research Center for providing the financial support for this research.

The author also wishes to thank Judi Hoover for doing such an excellent job in typing his dissertation. Special thanks are extended to his brother, Joe, who did an excellent job drawing many of the figures.

The author wishes to thank his parents, Glen and Inez Shortt, for their support in his venture to continue his education. And finally, to his wife and daughter, Sandy and Celia, his utmost and sincere thanks are given. Their constant support and love was an inspiration for which the author is truly grateful.

TABLE OF CONTENTS

LIST OF FIGURES

vii

LIST OF TABLES

Chapter I

MODELING TECHNIQUES FOR DC-DC SWITCHING
CONVERTERS

1.1 INTRODUCTION

A switching regulator consists of an input filter, power
switches and an output filter.   The power switch and the
output filter can be assembled to form a large number of
configurations, with the input filter being common to all.
Three basic configurations are illustrated in Fig. 1.1.1; Buck,
Boost and Buck/Boost.   The operation of these switching re-
gulators is nonlinear and discrete; however,   it can be
represented by a cyclic change of power stage topologies.
For the continuous current mode,   there are two topologies;
one for the transistor (switch)   on-time interval, and one
for the off-time interval. Each interval can be represented
by state equations as shown below, during the on-time inter-
val

$$\underline{x} = A_1\underline{x} + B_1\underline{u}$$

$$(1.1.1)$$

$$y = C_1\underline{x}$$

and during the off-time interval

$$\underline{x} = A_2\underline{x} + B_2\underline{u}$$

$$(1.1.2)$$

$$y = C_2\underline{x} \ .$$

1
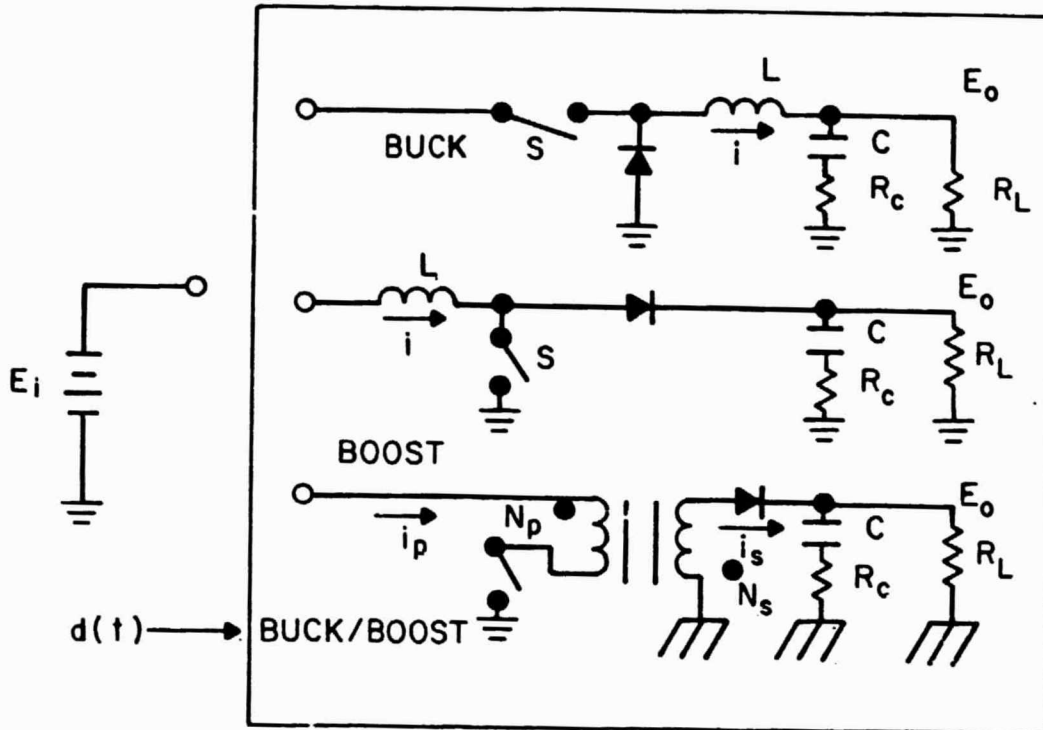
Figure 1.1.1. DC-DC converter with 3 basic power stage
configurations.

For the buck and boost converters, the state variables are

$$\underline{x} = \begin{bmatrix} i_L \\ v_C \end{bmatrix}. \qquad (1.1.3)$$

where i_L is the energy-storage inductor current and v_C is the output filter capacitor voltage. For the buck/boost converter,

$$\underline{x} = \begin{bmatrix} \emptyset \\ v_C \end{bmatrix}. \qquad (1.1.4)$$

where $\emptyset$ is the flux in the two-winding energy storage inductor and v_C is the same as previously stated.

The power stage analysis is linear for each interval; however, for the complete operational cycle, it becomes a piecewise linear problem. The on-time or off-time of one interval will vary from cycle to cycle, further complicating the analysis. Modeling and analysis of the nonlinear, time-varying dc-dc power converter has been achieved through various approaches.

Modeling techniques for dc-dc switching converters can be divided into 2 general categories, numerical (universal) and analytic (mathematical) techniques [1,2]. In analytic techniques, a closed form expression representing the operation of a dc-dc converter is

obtained, enabling a qualitative analysis to be performed [1]. The numerical techniques use various algorithms to produce an accurate quantitative result. However, simple relations among the system parameters are not easily obtainable.

1.2 NUMERICAL MODELING TECHNIQUES

Numerical modeling techniques can be divided into 3 groups. The analog computer has been used to analyze the system using the circuit equations and the classical tools of control theory [1,2]. CSMP (Continuous System Modeling Program) simulates the functions of an analog computer and versions of it exist on IBM computer 1130 and 360/370 [3]. These two methods provide a useful verification of a system design and analysis.

Other programs use topogically based routines which are highly flexible with respect to circuit modifications. IMAG III is a program that uses French or English input data for initial conditions and can perform transient, ac and sensitivity analyses on a nonlinear analog circuit [4]. ECAP (Electronic Circuit Analysis Program) is used as an aid to electric circuit designers in solving some of their problems [5]. It performs dc, ac or transient analyses of electric networks. These techniques allow a simulation of a circuit

using a digital computer rather than laboratory experimentation.

Lee and Yu [6] developed a computer based analysis that employs a discrete time domain technique to derive a recurrent time domain equation that characterizes the converter behavior exactly. This model can be used to study large signal behavior and small signal performance.

In the method of Iwens, Yu and Triner [7], state variable representation is used to derive an accurate, discrete converter model. This is numerically solved and linearized using various numerical techniques and derivative approximations. The method was applied to analyze a Buck converter in the continuous current mode. This approach was generalized to include all types of power stages, duty cycle controllers operating in continuous or discontinuous inductor current mode by Lee, Iwens, Yu and Triner [7,8,9].

All of these methods possess one or more of the following advantages:

1. Accuracy
2. Universality
3. Applicable when no equivalent model exists
4. Ease of use

However, due to the nonlinear, time varying nature of the system, existing circuit analysis programs are time consum-

ing and therefore expensive. Even though, the above methods do provide a good design check, physical relationships in the system are not perceivable due to the numerical nature of the methods, consequently little design insight can be gained.

1.3 ANALYTIC MODELING TECHNIQUES

Analytic techniques can be divided into 2 different system descriptions, discrete and continuous. The discrete system description makes no simplifying assumption or the basis of converter application. This description could be used in any application where the linearization of a periodically changing structure is sought. Prajoux et. al. [10] presented an approach capable of accurately describing any multistructural nonlinear system by a linearized discrete time domain model. It was applied to modeling a boost converter operating in the continuous current mode. Capel et. al. applied this to multiloop buck and boost regulators in both types of conduction in computer aided analysis [11]. Lee, Yu and Triner [12] extended this analysis to the three types of converters: buck, boost and buck/boost operating in continuous and discontinuous current modes. This method is accurate, but very complicated. The analysis is limited to the duty cycle to output voltage transfer function, con-

taining only one parasitic loss--the output filter capacitor ESR. A complete system description cannot be determined without the other input to output transfer functions. The derived expressions are complex and cumbersome, which impedes its practical usefulness and the physical insight into the system operation is not easily obtainable.

Continuous descriptions make simplifying assumptions inherent to switching converters. Thus, the modeling procedure and mathematical results are greatly simplified, but are not as accurate as the discrete descriptions. A converter design requirement is that the output voltage ripple is small. The output filter mentioned previously in section 1.1 is a low-pass filter. Its corner frequency is very much lower than the switching frequency. Using this, 1st and 2nd order approximations for the state transition matrices determined from equations (1.1.1) and (1.1.2) and linear current waveforms are justified. Robin-Jouan [1,2] uses the 1st order approximation for the state transition matrix and Owen et al. [1,2,13] use the 2nd order approximation. In the latter method more complicated expressions are derived, from which little physical insight can be obtained. These methods are accurate but they are complex in nature.

Other continuous techniques use a state space averaging approach. Prajoux et al. [1,2] developed a continuous meth-

od that expressed the output in terms of the input and the average inductor current injected into the output. The DERA method [2] is also based upon the perturbed average current injected into the output, but permits a direct establishment of the small signal model. These two methods are limited to a block diagram, transfer function analysis which gives little physical insight.

An important continuous analytic technique is the averaging technique by Wester and Middlebrook [14]. It is easy to implement and gives physical insight into the operation of a switching converter. Through circuit manipulation, analytical expressions were derived to determine the frequency response to duty cycle modulation. Middlebrook and Cúk in [15,16] modified the technique to average the state space descriptions over a complete cycle. A canonical circuit model with a fixed topology was proposed, that preserved the input-output characteristics of the dc-dc converters. Wong et al. [17] used the technique to analyze a complete functional electrical power system. The model included transistor switching and saturation losses, diode switching and forward drop losses, winding losses and capacitor ESR losses. Polivka et al. [18] examined the effect of saturation, forward drop, winding and ESR losses, including the storage time modulation effect. Recently, Brown and Middlebrook

[19] have developed a new modeling approach combining the average and discrete-sampling techniques. This model did not treat the duty cycle ratio as a smooth, slowly time-varying wave, but as a waveform of discrete pulses. The PWM modeling is capable of predicting high frequency instability and oscillation at the subharmonics of the switching frequency. The power stage model, however, was still based on the average model.

Even though state space averaging possesses a very convenient, continuous time-invariant form and has been applied successfully in many applications, the model accuracy degenerates rapidly as the frequencies of interest approach one half the fundamental frequency of the converters.

1.4 THE NEED FOR AN IMPROVED POWER STAGE MODEL

With the introduction of high gain-bandwidth, high performance dc-dc converters, employing multi-loop control schemes comes the need for an improved model that accurately describes the modulation frequency response up to one half of the switching frequency. Numerical techniques are accurate but give little physical insight into system operation. Continuous analytic techniques are generally easy to implement, but are inaccurate as the frequencies of interest approach one half the fundamental switching frequency. On the

other hand, discrete analytic techniques are accurate, but are very complex and the expressions are cumbersome.

The objective of this paper is to derive a power stage model, that is easy to implement, gives physical insight into system operation, preserves input-output and state variable relationships and is accurate as the modulation frequency approaches one-half of the switching frequency. In order to do this, a continuous and discrete technique are combined. From the modeling techniques that have been discussed, two viable techniques are chosen.

These are the (Prajoux) discrete impulse response method as developed by Lee, Yu and Triner [12] and state space averaging by Wester and Middlebrook [14] and Middlebrook and Cúk [15]. These two techniques model the system using a closed form expression. Modeling and analysis of the three basic dc-dc converter power stages have been achieved through these methods.

A comparison is made between the average model and the discrete impulse response model, particularly in the high modulation frequency (up to one half the switching frequency). Pinpointing the differences and accounting for them leads to the development of a new and improved model - the discrete-average model. This model possesses the advantages of each of the two techniques - easy to use, accurate to one

half of the switching frequency.   Basically, this new model
uses the averaged state space from the averaging technique
and determines the output by a discrete sample.

Chapter II

DISCUSSION OF THE AVERAGE AND DISCRETE TECHNIQUES

In order to make an evaluation and comparison, a review of each technique will be done. The discrete impulse response technique and the averaging technique are described in detail in references [12] and [15], respectively. The purpose of this chapter is to review each technique, presenting the assumptions for each method as they are applied.

2.1 AVERAGE MODEL

For the averaging technique each interval in the cycle is described by its state space representation. In general, the on-time interval is represented by

$$\dot{\underline{x}} = A_1\underline{x} + b_1v_I$$

$$(2.1.1)$$

$$v_O = c_1\underline{x}.$$

and the off-time interval by

$$\dot{\underline{x}} = A_2\underline{x} + b_2v_I$$

$$(2.1.2)$$

$$v_O = c_2\underline{x}.$$

12

The representations are averaged to give a single period re-
presentation, as shown below

$$\dot{\underline{x}} = [dA_1 + d'A_2]\underline{x} + [db_1 + d'b_2]v_I$$

$$(2.1.3)$$

$$v_O = [dc_1 + d'c_2]\underline{x}$$

To study the small-signal behavior, the time varying sys-
tem described in (2.1.3) can be linearized using perturba-
tion techniques. Introducing variations in the line voltage
and duty cycle ratio by the following substitutions:

$$v_I = V_I + \hat{v}_I,$$
$$d = D + \hat{d},$$
$$d' = D' - \hat{d}$$

will cause perturbations in the state and output, as shown
below.

$$\underline{x} = \underline{X} + \hat{\underline{x}}$$
$$v_O = V_O + \hat{v}_O.$$

This results in the following average model:

$$\dot{\underline{x}} = A\underline{X} + bV_I + A\hat{\underline{x}} + b\hat{v}_I$$
$$+ \{[A_1-A_2]\underline{X}+[b_1-b_2]V_I\}\hat{d} + \text{2nd order terms} \quad (2.1.4)$$
$$V_O+\hat{v}_O = c\underline{X}+c\hat{\underline{x}}+(c_1-c_2)\underline{X}\hat{d} + \text{2nd order terms}$$

where
$$A = DA_1 + D^1A_2$$
$$b = Db_1 + D^1b_2$$
$$c = Dc_1 + D^1c_2$$

Assuming that departures of the states from their corresponding steady state values are small compared to the steady state values themselves allows the 2nd order terms in (2.1.4) to be neglected. The average model in its final form is shown below. The dc model is:

$$\underline{0} = A\underline{X} + b\,V_I$$

$$(2.1.5)$$

$$V_0 = c\underline{X}$$

The dc operating point can be determined by solving for $\underline{X}$ in 2.1.5a and substituting into 2.1.5b; the following results are obtained.

$$\underline{X} = -A^{-1}bV_I$$

$$(2.1.6)$$

$$V_0 = -cA^{-1}bV_I$$

The ac model is:

$$\dot{\hat{\underline{x}}} = A\hat{\underline{x}} + b\hat{v}_I + \{(A_1 - A_2)\underline{X} + (b_1 - b_2)V_I\}\hat{d}$$

$$(2.1.7)$$

$$\hat{v}_0 = c\hat{\underline{x}} + (c_1 - c_2)\underline{X}\hat{d}.$$

The transfer functions can be found by taking the Laplace transformation of (2.1.7a) and (2.1.7b) as shown below:

$$s\hat{\underline{x}}(s) = A\hat{\underline{x}}(s) + b\hat{v}_I(s) + \{(A_1 - A_2)\underline{X} + (b_1 - b_2)V_I\}\hat{d}(s) \qquad (2.1.8a)$$

$$\hat{v}_0(s) = c\underline{x}(s) + (c_1 - c_2)\underline{X}\hat{d}(s) \qquad (2.1.8b)$$

solving 2.1.8a for $\hat{x}(s)$

$$\hat{x}(s) = [sI-A]^{-1}[b\hat{v}_I(s) + [(A_1-A_2)\underline{X} + (b_1-$$

$$b_2)V_I]\hat{d}(s) \qquad (2.1.9)$$

and substituting into (2.1.8b) and adding like coefficients

$$\hat{v}_0(s) = c[sI-A]^{-1}b\hat{v}_I(s) \qquad (2.1.10)$$

$$+\{c(sI-A)|^{-1}[(A_1-A_2)\underline{X} + (b_1-b_2) V_I]$$

$$+(c_1-c_2)\underline{X}\}\hat{d}(s),$$

from which the following transfer functions can be obtained.

$$\frac{\hat{v}_0(s)}{\hat{v}_I(s)} = c[sI-A]^{-1}b \qquad (2.1.11)$$

$$\frac{\hat{v}_0(s)}{\hat{d}(s)} = c[sI-A]^{-1}[(A_1-A_2\underline{X} + (b_1-b_2V_I] \qquad (2.1.12)$$

$$+(c_1-c_2)\underline{X}$$

A block diagram of the averaging technique for a dc-dc con-
verter is shown in Fig. 2.1.1.

A canonical equivalent circuit model was determined [15]
for power converters, by putting the above state equations
(2.1.7) into a circuit realizable form. This canonical cir-
cuit model preserves the input/output properties of the ori-
ginal circuit in the small signal sense. However, the ori-
ginal properties of state variable-induction current was
lost in the canonical equivalent circuit representation.

16
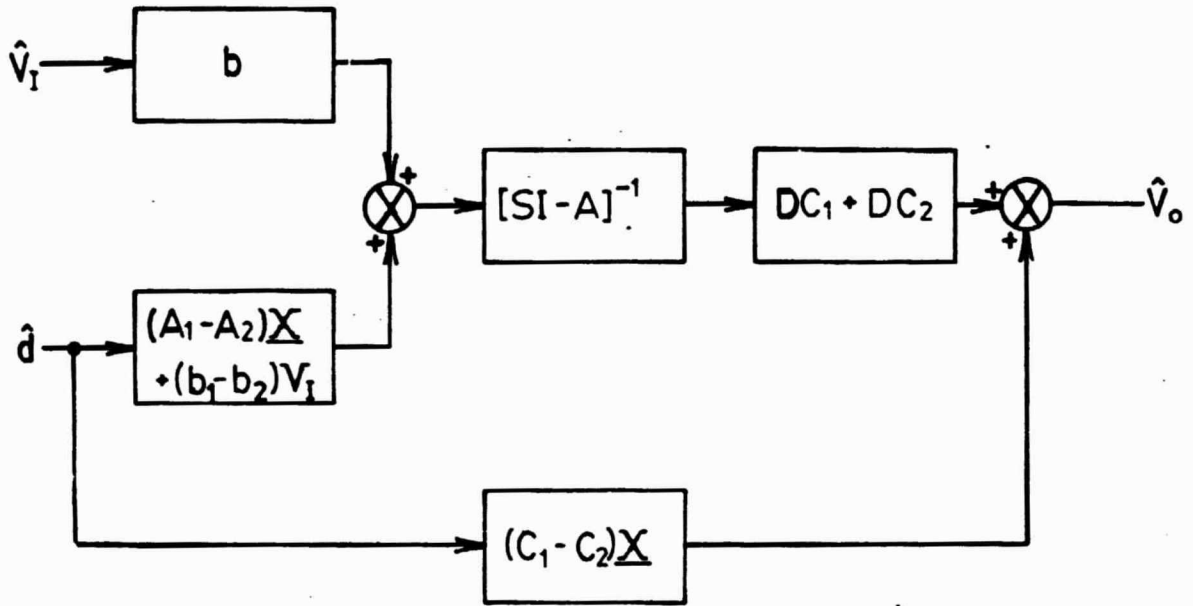
Figure 2.1.1: Block Diagram of the Average Model

Note that this is the average model for a dc-dc converter operating in the continuous current mode (mode 1). A discussion of the average model for a converter in the discontinuous current mode (mode 2) will follow in chapter VII.

2.2 EXTENDED AVERAGE MODEL

The power stage model presented in the previous section has two inputs (input votige and duty cycle ratio) and one output (output voltage). The purpose of this section is to extend the average model to include the load disturbance as another input and the inductor current (mmf) and capacitor voltage as additional outputs.

During T_{ON}, the state equations for each of the converters are expressed by:

$$\underline{\dot{x}} = A_1\underline{x} + b_{v1}v_I \; d \; + b_{i1}i_o \tag{2.2.1}$$

where i_o is the load disturbance, represented by a current injected into the output node.

The output expression is given by:

$$\underline{Y} = c_1\underline{x} + g_1i_o = \begin{bmatrix} v_o \\ i_L \\ v_c \end{bmatrix} \tag{2.2.2}$$

During T_{OFF}, the state equations are expressed by:

$$\underline{\dot{x}} = A_2\underline{x} + b_{v2}v_I + b_{i2}i_o \tag{2.2.3}$$

The output expression is given by:

$$y = c_2 x + g_2 i_o \qquad (2.2.4)$$

The state variable representations are averaged to give a single period representation as shown below:

$$\underline{x} = (dA_1 + d'A_2)\underline{x} + (db_{v1} + d'b_{v2}) v_I$$
$$(db_{i1} + d' b_{i2}) i_o \qquad (2.2.5)$$

$$y = (dc_1 + d'c_2) x + (dg_1 + d'g_2) i_o$$

Introducing variations in the line voltage, duty cycle ratio and load disturbance by the following substitutions

$$v_I = V_I + \hat{v}_I,$$
$$d = D + \hat{d},$$
$$d' = D' - \hat{d},$$
$$i_o = I_o + \hat{i}_o, \quad I_o = 0$$

will cause perturbations in the state and output, as shown below.

$$\underline{x} = \underline{X} + \hat{\underline{x}}$$
$$\underline{y} = \underline{Y} + \hat{\underline{y}}$$

This results in the following model:

$$\dot{\underline{x}} = A \underline{X} + b_v V_I + A \hat{\underline{x}} + b_v \hat{v}_I$$
$$+ [(A_1 - A_2) \underline{X} + (b_{v1} - b_{v2}) V_I] \hat{d} + b_1 \hat{i}_o$$
$$+ \text{2nd order terms} \qquad (2.2.6)$$
$$\underline{Y} + \hat{y} = c \underline{X} + c \hat{\underline{x}} + g \hat{i}_o + (c_1 - c_2) \underline{X} \hat{d} + \text{2nd order terms}$$

where

$$A = D A_1 + D'A_2$$

$$b_v = D b_{v1} + D'b_{v2}$$

$$b_i = D b_{i1} + D'b_{i2}$$

$$g = D g_1 + D'g_2.$$

Asuming that departures of the states from their corresponding steady state vaues are small compared to the steady state values themselves allows the 2nd order terms in (2.2.6) to be neglected. The discrete- average model in its 3 input-3 output form is shown below. The dc model is:

$$\underline{0} = A \underline{X} + b_v V_I$$

$$\underline{Y} = c \underline{X}$$

(2.2.7)

The dc operating point can be determined by solving for X in (2.2.7a.) and substituting into (2.2.7b.), the following results are obtained:

$$\underline{Y} = \begin{bmatrix} V_o \\ I_L \ (or\phi) \\ V_C \end{bmatrix} = -c A^{-1} b_v V_I.$$

(2.2.8)

The ac model is:

$$\dot{\underline{x}} = A\hat{\underline{x}} + b_v\hat{v}_I + \lfloor (A_1-A_2)\underline{X} + (b_{v1}- b_{v2})V_I\rfloor\hat{d}$$

(2.2.9)

$$+b_i\hat{i}_o$$

$$\hat{\underline{y}} = c\hat{\underline{x}} + (c_1-c_2)\underline{X}\hat{d} + g\hat{i}_o$$

The transfer functions can be found by taking the Laplace transformation of (2.2.9b.), solving for x(s) and substituting into (2.2.9a.). This results in:

$$\hat{\underline{y}}(s) = c[sI - A]^{-1} \{b_v \hat{v}_I(s) + [(A_1 - A_2) \underline{X} + (b_{v1} - b_{v2}) V_I] \hat{d}(s)$$
$$+ b_i \hat{i}_o(s)\} + (c_1 - c_2) \underline{X} \hat{d}(s) + g \hat{i}_o(s).$$

(2.2.10)

The duty cycle to output transfer function is:

$$\frac{\hat{\underline{y}}(s)}{\hat{d}(s)} = c[sI - A]^{-1} [(A_1 - A_2)\underline{X} + (b_{v1} - b_{v2}) V_I]$$
$$+ (c_1 - c_2) \underline{X}.$$

(2.2.11)

The load disturbance to output transfer function is:

$$\frac{\hat{\underline{y}}(s)}{\hat{i}_o(s)} = c [sI - A]^{-1} b_i + g.$$

(2.2.12)

The input voltage disturbance to output transfer function is:

$$\frac{\hat{\underline{y}}(s)}{\hat{v}_I(s)} = c [sI - A]^{-1} b_v.$$

(2.2.13)

These transfer functions have been determined for the buck, boost and buck/boost converters are shown in tables 2.2.1, 2.2.2 and 2.2.3, respectively. A block diagram of the averaging technique for a dc-dc converter with 3 inputs and 3 outputs is shown in Fig. 2.2.1.

To illustrate the simplicity and versatility of this model, a circuit model is realized. The average model for the boost converter is:

$$\underline{\dot{x}} = \begin{bmatrix} -\dfrac{R_\ell + d'R_c//R_L}{L} & -\dfrac{d'}{L}\dfrac{R_L}{R_L + R_c} \\[2ex] \dfrac{d'}{C}\dfrac{R_L}{R_L + R_c} & -\dfrac{1}{(R_L + R_c)C} \end{bmatrix} \underline{x} \qquad (2.2.14)$$

$$+ \begin{bmatrix} \dfrac{1}{L} \\[2ex] 0 \end{bmatrix} v_I + \begin{bmatrix} -\dfrac{d'}{L}R_c//R_L \\[2ex] \dfrac{R_L}{C(R_L + R_c)} \end{bmatrix} i_o \quad , \text{ where } \underline{x} = \begin{bmatrix} i_L \\[1ex] v_c \end{bmatrix}$$

$$v_o = [d'R_c//R_L \quad \frac{R_L}{R_L + R_c}] \underline{x} + (R_c//R_L)i_o \qquad (2.2.15)$$

solving for v_c in (2.2.15) and substituting into (2.2.14) results in a circuit realizable set of equations, shown below.

$$\begin{bmatrix} \dot{i}_L \\[2ex] \dot{v}_c \end{bmatrix} = \begin{bmatrix} -\dfrac{R_\ell + dd'R_c//R_L}{L} & -\dfrac{d'}{L} \\[2ex] \dfrac{d'}{C} & -\dfrac{1}{R_L C} \end{bmatrix} \begin{bmatrix} i_L \\[2ex] v_o \end{bmatrix} + \begin{bmatrix} \dfrac{1}{L} \\[2ex] 0 \end{bmatrix} v_I + \begin{bmatrix} 0 \\[2ex] \dfrac{1}{C} \end{bmatrix} i_o$$

$$(2.2.16)$$

Table 2.2.1   Buck Converter

Transfer Function	Transfer Function
$\dfrac{\hat{v}_o(s)}{\hat{d}(s)} = V_I \dfrac{1 + R_c Cs}{G(s)}$	$\dfrac{\hat{i}_L(s)}{\hat{d}(s)} = \dfrac{V_I}{R_L} \dfrac{1 + R_L Cs}{G(s)}$
$\dfrac{\hat{v}_o(s)}{v_I(s)} = D \dfrac{1 + R_c Cs}{G(s)}$	$\dfrac{\hat{i}_L(s)}{\hat{v}_I(s)} = \dfrac{D}{R_L} \dfrac{1 + R_L Cs}{G(s)}$
$\dfrac{\hat{v}_o(s)}{\hat{i}_o(s)} = R_\ell \dfrac{1 + \frac{s}{\omega_1 Q_1} + (\frac{s}{\omega_1})^2}{G(s)}$	$\dfrac{\hat{i}_L(s)}{\hat{i}_o(s)} = - \dfrac{1 + R_c Cs}{G(s)}$

$$G(s) = 1 + \frac{s}{\omega_o Q} + \left(\frac{s}{\omega_c}\right)^2$$

$$\omega_o = \frac{1}{\sqrt{LC}} \quad ; \quad Q = \frac{1}{\omega_o} \frac{1}{\dfrac{L}{R_L} + (R_\ell + R_c)\, C}$$

$$\omega_1 = \frac{1}{\sqrt{LC}} \quad ; \quad Q_1 = \frac{1}{\omega_1} \frac{1}{\dfrac{L}{R_c} + R_\ell C}$$

Table 2.2.2 Boost Converter

Transfer Function	Transfer Function
$\dfrac{\hat{v}_o(s)}{\hat{d}(s)} = \dfrac{V_I}{(D')^2} \dfrac{(1+\frac{s}{\omega_z})(1-\frac{s}{\omega_a})}{G(s)}$	$\dfrac{\hat{i}_L(s)}{\hat{d}(s)} = \dfrac{2V_I}{(D')^3 R_L} \dfrac{1 + \frac{R_L C}{2}}{G(s)}$
$\dfrac{\hat{v}_o(s)}{\hat{v}_I(s)} = \dfrac{1}{D'} \dfrac{1}{G(s)}$	$\dfrac{\hat{i}_L(s)}{\hat{v}_I(s)} = \dfrac{1}{(D')^2 R_L} \dfrac{1 + R_L C}{G(s)}$
$\dfrac{\hat{v}_o(s)}{\hat{i}_o(s)} = R_c + \dfrac{1}{D'}(R_\ell - R_c) \dfrac{1 + \frac{s}{\omega_1 Q_1} + (\frac{s}{\omega_1})^2}{G(s)}$	$\dfrac{\hat{i}_L(s)}{\hat{i}_o(s)} = -\dfrac{1}{D'} \dfrac{1 + R_c C s}{G(s)}$

$$G(s) = 1 + \frac{s}{\omega_0 Q} + \left(\frac{s}{\omega_0}\right)^2 \; ; \quad Q = \frac{D'}{\omega_0} \frac{1}{\frac{L}{D'R_L} + \frac{R_\ell C}{D'} + R_c C}$$

$$\omega_0 = \frac{D'}{\sqrt{LC}}$$

$$\omega_1 = \frac{D'}{\sqrt{LC}} \sqrt{1 + \frac{R_\ell}{D'R_c}} \; ; \quad Q_1 = \frac{1}{\omega_1} \frac{1}{\frac{L}{(D')^2 R_c} + R_\ell C}$$

$$\omega_z = \frac{1}{R_c C} \; ; \quad \omega_a = \frac{(D')^2 R_L}{L}$$

Table 2.2.3 Buck/Boost Converter

Transfer Function	Transfer Function
$\dfrac{\hat{v}_o(s)}{\hat{d}(s)} = -\dfrac{V_I}{(D')^2}\dfrac{N_s}{N_P}\dfrac{(1+\frac{s}{\omega_z})(1-\frac{s}{\omega_a})}{G(s)}$	$\dfrac{\hat{\phi}(s)}{\hat{d}(s)} = \dfrac{V_I}{(D')^3 R_L}\dfrac{L_s}{N_s}\dfrac{1+R_L Cs}{G(s)}$
$\dfrac{\hat{v}_o(s)}{\hat{v}_I(s)} = \dfrac{D}{D'}\dfrac{N_s}{N_P}\dfrac{(1+R_c Cs)}{G(s)}$	$\dfrac{\hat{\phi}(s)}{\hat{v}_I(s)} = \dfrac{D}{(D')^2}\dfrac{L_s}{N_P R_L}\dfrac{1+R_L Cs}{G(s)}$
$\dfrac{\hat{v}_o(s)}{\hat{\imath}_o(s)} = \dfrac{R_s}{(D')^2}\dfrac{1+\frac{s}{Q_1\omega_1}+(\frac{s}{\omega_1})^2}{G(s)}$	$\dfrac{\hat{\phi}(s)}{\hat{\imath}_o(s)} = -\dfrac{1}{D'}\dfrac{L_s}{N_s}\dfrac{1+R_c Cs}{G(s)}$

$$G(s) = 1 + \frac{s}{\omega_c Q} + \left(\frac{s}{\omega_o}\right)^2$$

$$\omega_c = \frac{D'}{\sqrt{L_s C}} \quad ; \quad Q = \frac{D'}{\omega_o}\frac{1}{\frac{L_s}{(D')^2 R_L} + (\frac{R_c}{D'} + \frac{R_s}{(D')^2})C}$$

$$\omega_z = \frac{1}{R_c C} \quad ; \quad \omega_a = \frac{(D')^2 R_L}{D L_s}$$

$$\omega_1 = \frac{1}{\sqrt{L_s C}}\sqrt{\frac{R_s}{R_c}} \quad ; \quad Q_1 = \frac{1}{\omega_1}\frac{1}{\frac{L_s}{R_s} + R_c C}$$
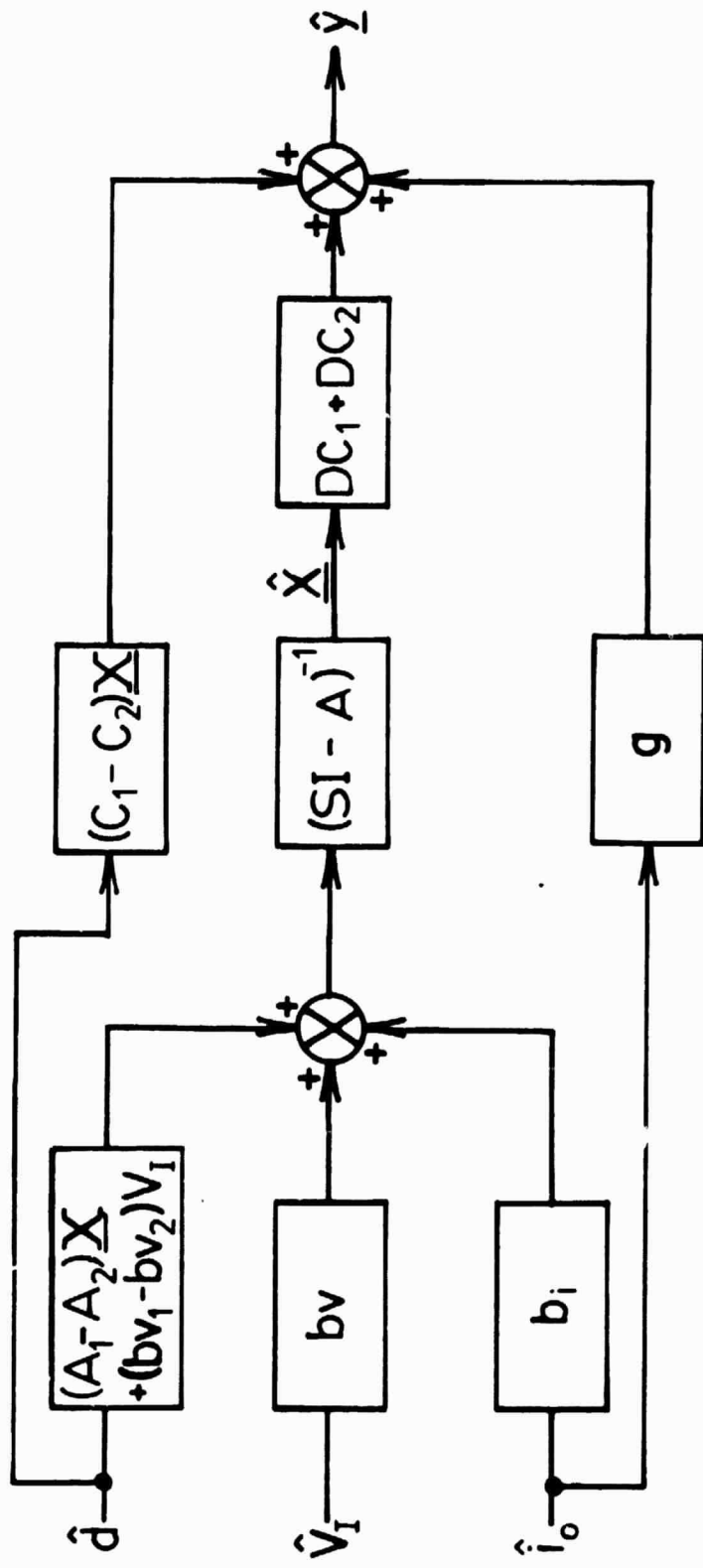
Figure 2.2.1: Block Diagram of the Average Model (3 input-3 output)

This set of equations can be realized into a single circuit with an ideal transformer as shown in Fig. 2.2.2 The average circuit model can be realized for the buck and buck/boost converters, as shown in Fig. 2.2.3 and Fig. 2. 2.4 .

Introducing the perturbations into the state and output, neglecting the small nonlinear terms and simplifying the structure, one obtains the circuits in Figures 2.2.2b.), 2.2.3b.) and 2.2.4b.). At this point the dc operating conditions are determined from equation (2.1.6). They are listed in table 2.2.1 for each type of converter. The small signal circuit model can be found by removing the dc conditions, which give the circuits in Figures 2.2.2c.), 2.2.3c.) and 2.2.4c.).
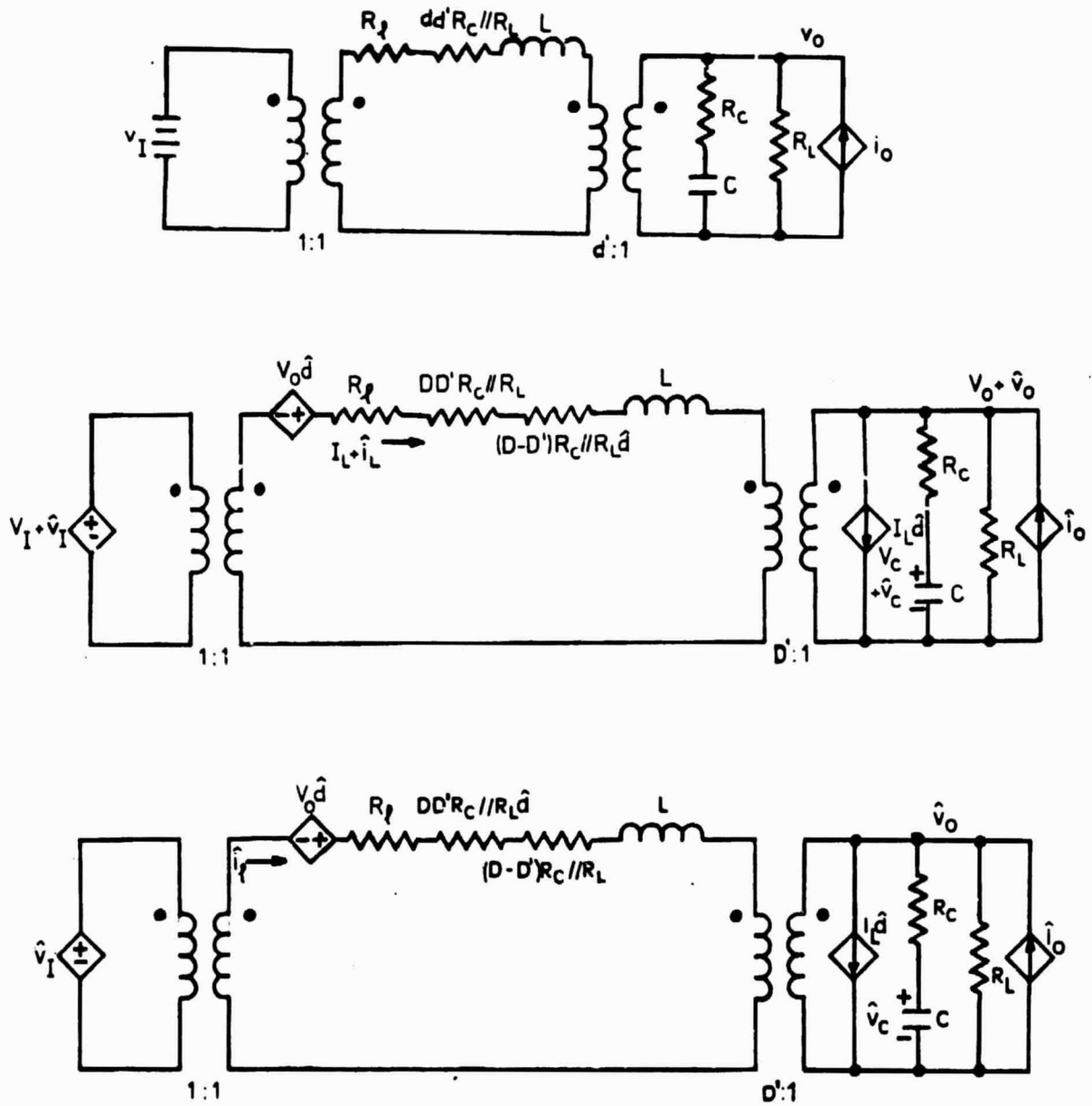
Figure 2.2.2 a.) Unperturbed average circuit model of the boost
converter
b.) Perturbed and linearized circuit model
c.) Small signal model
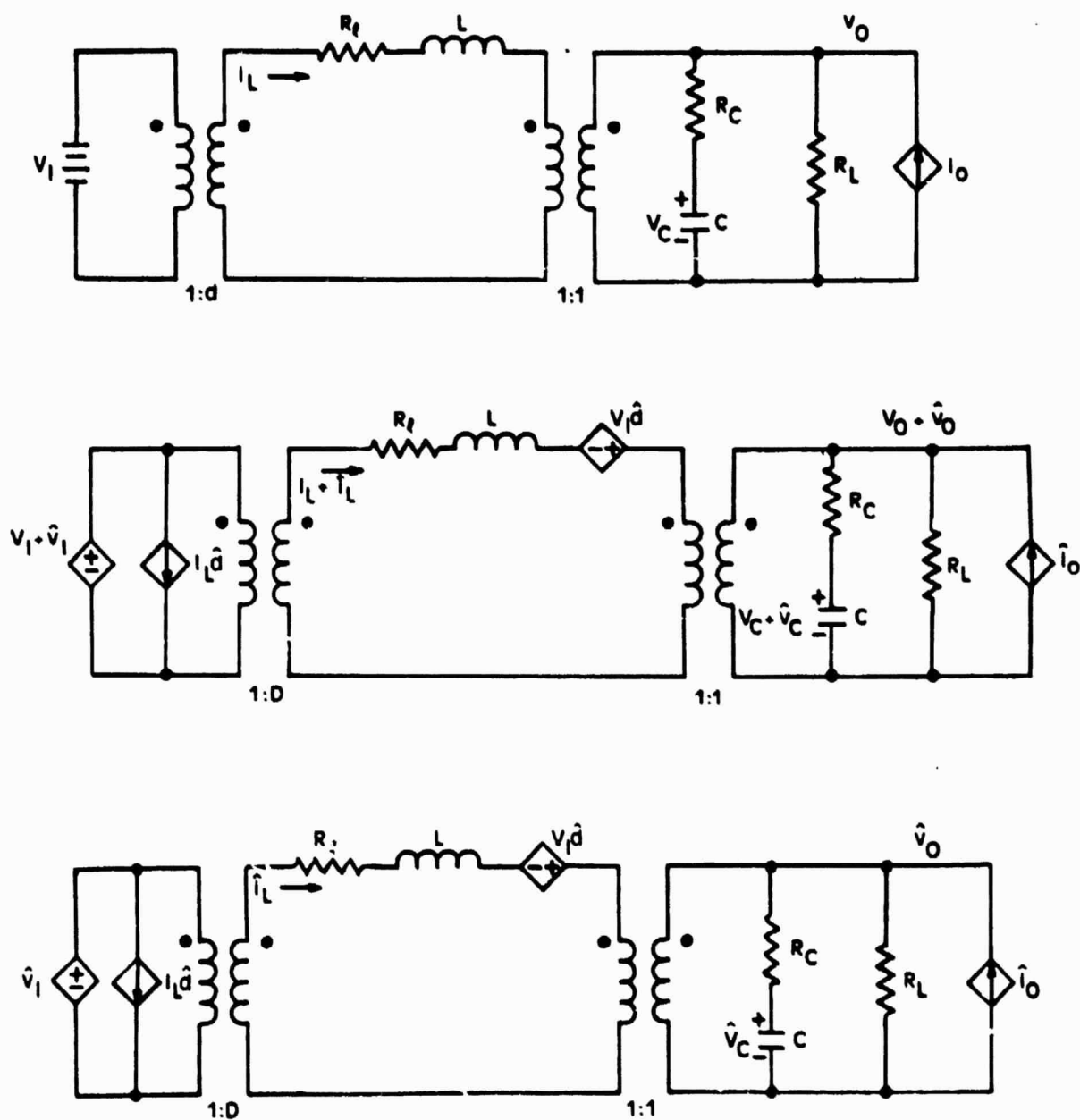
Figure 2.2.3. a.) Unperturbed average circuit model of the buck
               converter
            b.) Perturbed and linearized circuit model
            c.)) Small signal model
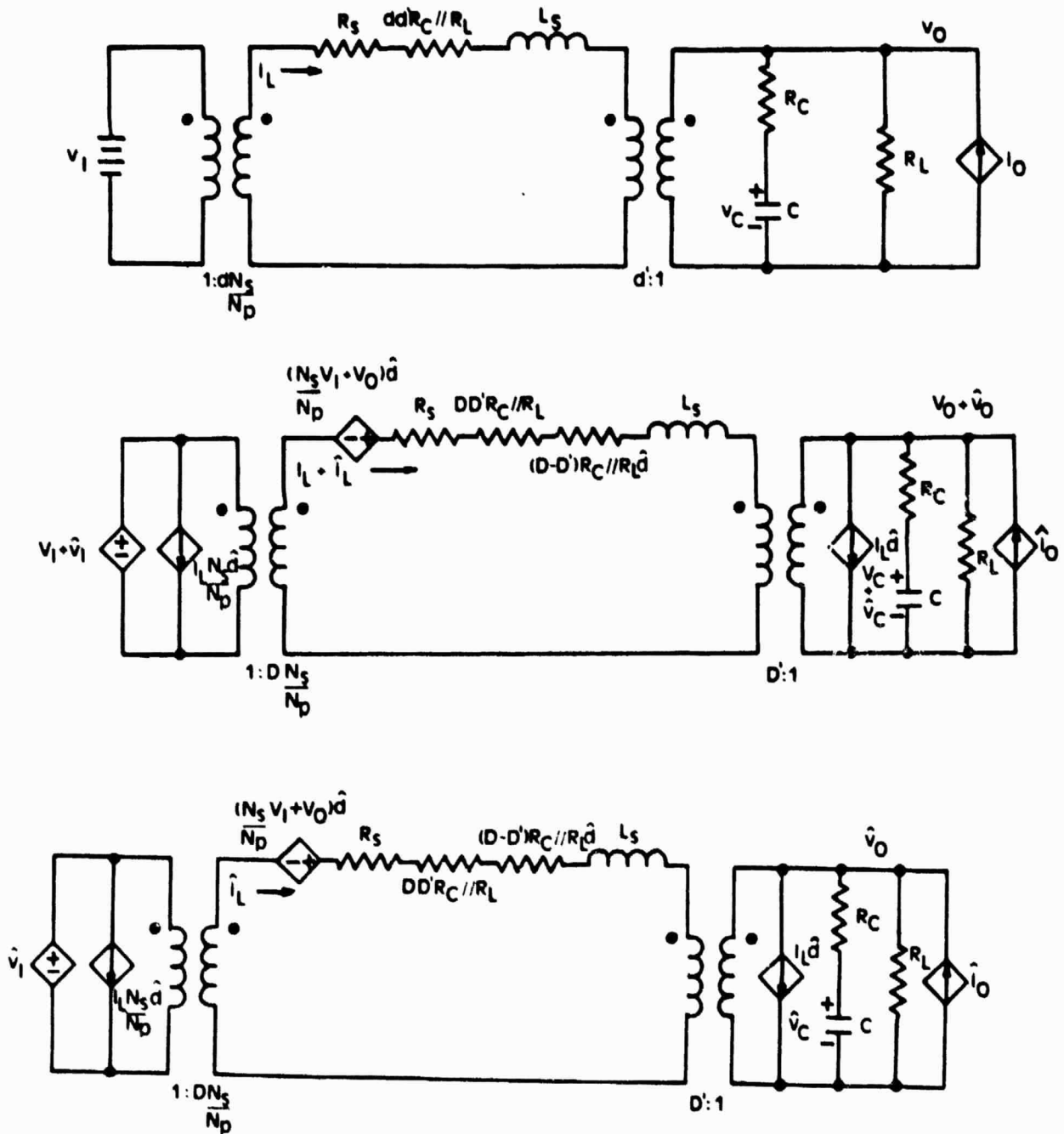
Figure 2.2.4.   a.)   Unperturbed average circuit model of the buck/boost
                      converter
                b.)   Perturbed and linearized circuit model
                c.)   Small signal model

TABLE 2.2.

The Average Approximate dc Model Operating Conditions.

For detailed expressions see Appendix A.

	Buck	Boost	Buck/Boost
I_L	$\dfrac{DV_I}{R_L}$	$\dfrac{V_I}{(D')^2 R_L}$	$\dfrac{D}{(D')^2} \dfrac{N_s}{N_p} \dfrac{V_I}{R_L}$
V_c	DV_I	$\dfrac{V_I}{D'}$	$\dfrac{D}{D'} \dfrac{N_s}{N_p} V_I$
$\dfrac{V_o}{V_I}$	D	$\dfrac{1}{D'}$	$\dfrac{D}{D'} \dfrac{N_s}{N_p}$

2.3 CANONICAL CIRCUIT MODEL

The objective of this section is to present a canonical circuit model that describes the system's small signal operation. This model preserves the input, output and state variable operation of dc-dc converters. Middlebrook and Cuk developed a canonical circuit model in [15] that preserves the input and output properties. However, the state variable information is lost. This model cannot be used in the analysis of multiloop systems, where the state variable information is needed for the feedback network.

Figure 2.3.1 is the canonical circuit model of the buck, boost, and buck/boost converters. Table 2.3.1 lists the necessary parameters. This canonical circuit model can be used in the small signal analysis of dc-dc converters with multiloop feedback. This circuit model preserves the input, output and state variable operation of the system.

2.4 DISCRETE MODEL

The switching regulator power stage, during one cycle of operation, can be represented by three piecewise linear vector differential equations as shown by (2.4.1), (2.4.2) and (2.4.3). For the boost converter these equations represent a specific circuit topology as shown in Fig. 2.4.1.

$$\underline{x} = F1\underline{x} + G1\underline{u} \quad \text{during } T_{F1} \tag{2.4 1}$$

$$\underline{x} = F2\underline{x} + G2\underline{u} \quad \text{during } T_{F2} \tag{2.4.2}$$

Figure 2.3.1. Canonical Circuit Model

33
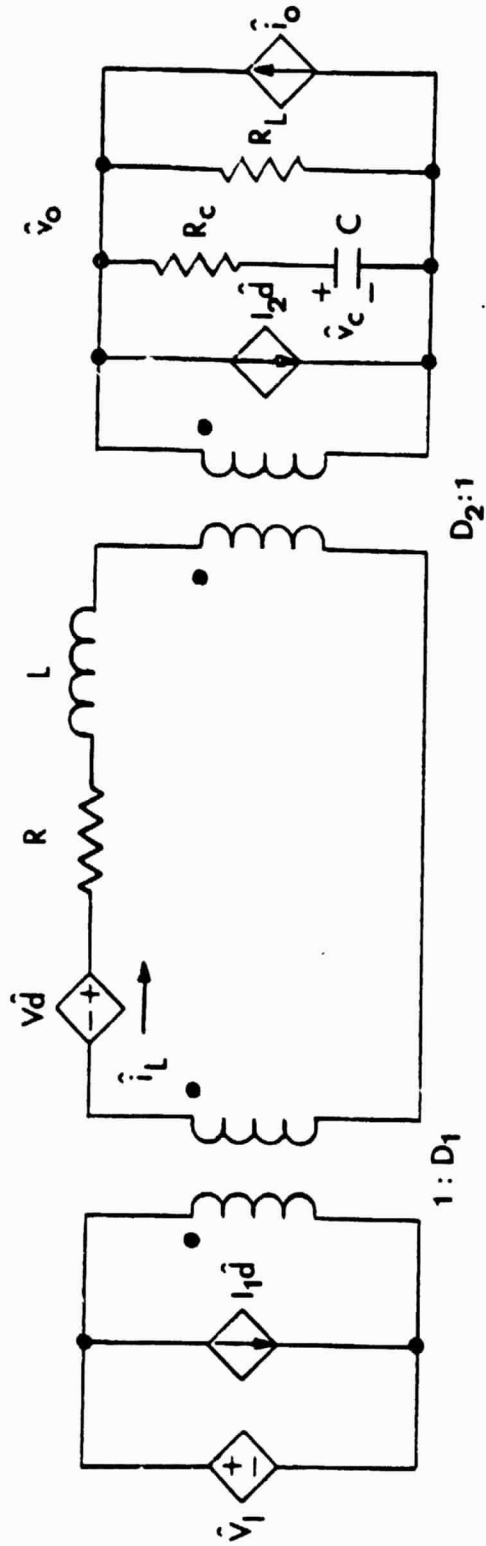
Table 2.3.1 Canonical Circuit Model

	Buck	Boost	Buck/Boost
I_1	I_L	0	$\dfrac{N_s}{N_p} I_L$
I_2	0	I_L	I_L
D_1	D	1	$\dfrac{N_s}{N_p} D$
D_2	1	D'	D'
R	R	$R + DD'R_c//R_L + (D-D')R_c//R_L\,d$	$R_s + DD'R_c//R_L + (D-D')R_c//R_L\,d$
L	L	L	L_s
V	V_I	V_o	$\dfrac{N_s}{N_p} V_I + V_o$

ORIGINAL PAGE IS
OF POOR QUALITY
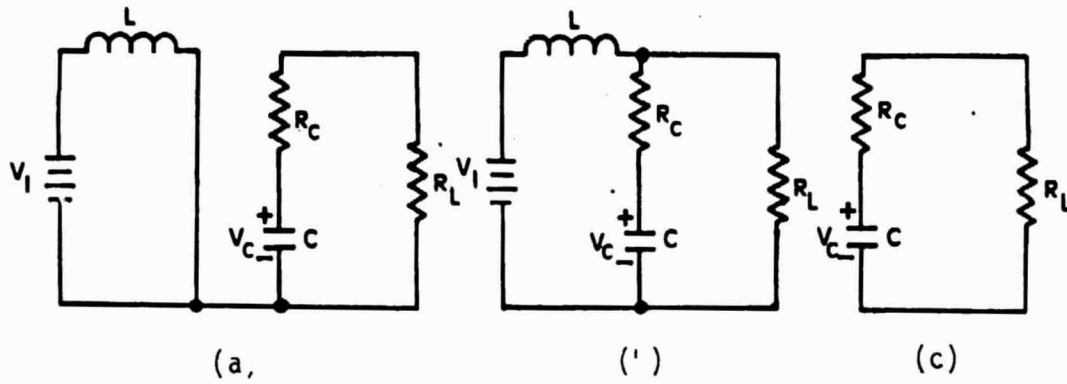
Figure 2.4.1.   Topologies for the Boost Converter
        a.) T_{on} Topology
        b.) T_{F1} Topology
        c.) T_{F2} Topology

$$\underline{x} = F3\underline{x} + G3\underline{u} \quad \text{during } T_{ON} \tag{2.4.3}$$

The time intervals T_{F1}, T_{F2} and T_{ON} are defined in Fig. 2.4.2. It should be noted that for mode 1 operation, the time interval T_{F2} does not exist. Therefore, the vector differential equation (2.4.2) can be neglected.

Consider a duty cycle signal

$$d(t) = \begin{cases} 1, \text{during the on-time } (T_{ON}) \\ \\ 0, \text{during the off-time } (T_{OFF}) \end{cases}$$

whose leading edge of T_{ON} is always initiated by a clock signal. When the converter is subjected to a small disturbance, the duty-cycle signal is modified as shown in Fig. 2.4.3. This perturbed duty-cycle signal can be idealized as an impulse train when the perturbation is vanishingly small. If the perturbed output voltage resulting from a small duty cycle disturbance at the kth switching cycle can be computed after n cycles of propagation, a linearized discrete impulse response which describes the small signal behavior of the power stage about its equilibrium state can be obtained. This concept is elaborated by the following equation.
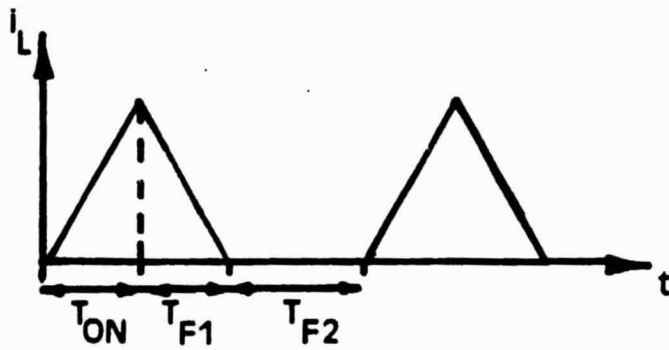
Figure 2.4.2. Inductor current plotted versus time
illustrating the discontinuous mode
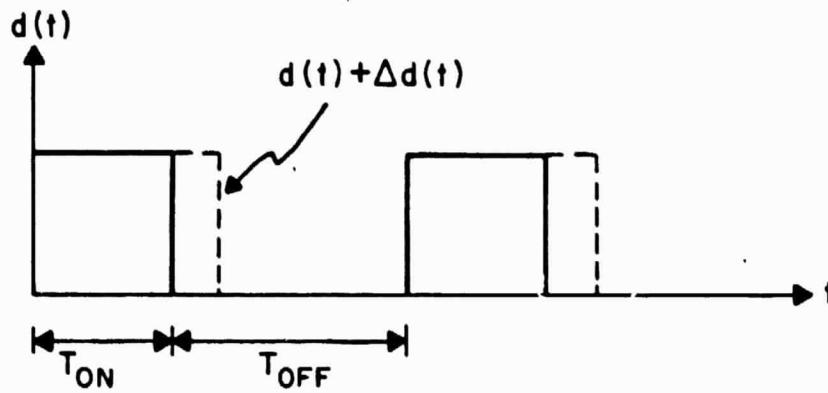
Figure 2.4.3: The duty-cycle signal at steady state d(t) and after small perturbation d(t) + Δd(t)

$$\frac{v_0(t_{k+n})}{\Delta t_k} = g(nT_p) \tag{2.4.4}$$

where Δt_k is a small duty cycle disturbance at the kth switching cycle and $v_0(t_{k+n})$ is the resulting output voltage variation at the (k+n)th cycle. The sampling rate is equal to the switching frequency $1/T_p$.

The propagation of the perturbed state can be illustrated in Fig. 2.4 4. The steady state with a superscript "0" is shown as the solid curve, while the perturbed state with a superscript "*" is represented by the dotted curve. The perturbed state after one cycle of propagation is expressed as

$$\underline{x}^*(t_{k1}^o) = \emptyset_1(t_{k1}^o - t_k^*)\underline{x}^*(t_k^*) + \emptyset_1(t_{k1}^o) \int_{t_k^*}^{t_{k1}^o} \emptyset(-s)ds G1\underline{u} \tag{2.4.5}$$

$$\underline{x}^*(t_{k2}^o) = \emptyset_2(t_{k2}^o - t_{k1}^*)\underline{x}^*(t_{k1}^*)$$

$$+ \emptyset_2(t_{k2}^o) \int_{t_{k1}^*}^{t_{kz}^o} \emptyset(-s)ds G2\underline{u} \tag{2.4.6}$$

$$\underline{x}(t_{k+1}^o) = \emptyset_3(t_{k+1}^o - t_{k2}^*)\underline{x}^*(t_{k2}^*)$$
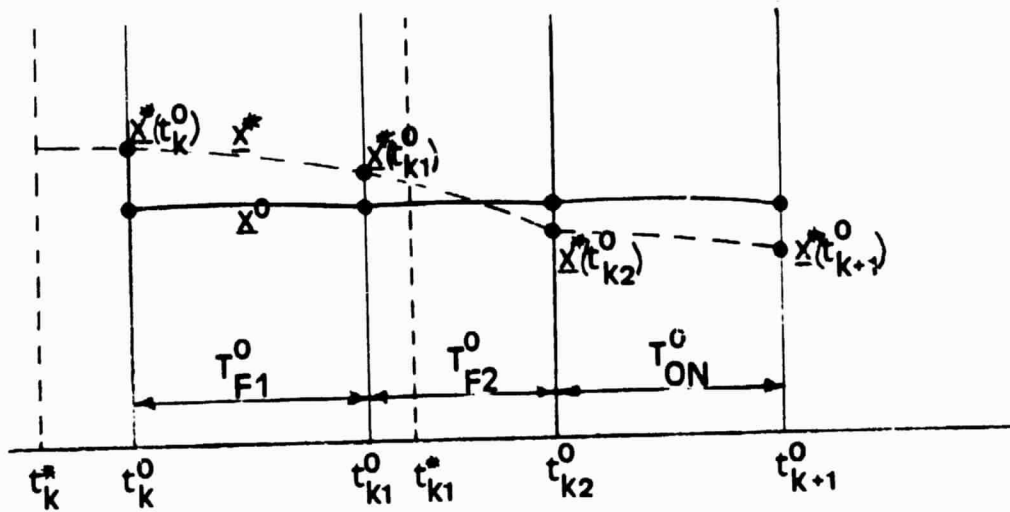
Figure 2.4.4 : State trajectories for the steady state (solid curve) and perturbed state (dotted curve).

$$+ \phi_3(t^o_{k+1}) \int_{t^*_{k2}}^{t^o_{k+1}} \phi_3(-s) ds G3 \underline{u} \qquad (2.4.7)$$

where the ϕ_i's are the state transition matrices defined as

$$\phi_i(t) = \underline{e}^{F_i t} \qquad i = 1, 2, 3.$$

Since the clock signal initiates the turn-on time, the time instant t^*_{k2} is equal to t^0_{k2} in equation (2.4.7).

The corresponding discrete impulse response for each switching power stage, represented by (2.4.4) can be obtained by performing the following vector differentiation.

$$g(nT_p) = \frac{dv_0}{dt^*_k} = c \frac{d\underline{x}^*(t^0_{k+n})}{dt^*_k} \qquad (2.4.8)$$

where $v_0 = c\underline{x}$ and c is a constant row matrix. Applying the chain rule to (2.2.8) and simplifying

$$\frac{d\underline{x}^*(t^o_{k+n})}{dt^*_k} = \left[\frac{d\underline{x}^*(t^o_{k+1})}{d\underline{x}^*(t^o_k)} \right]^n \frac{d\underline{x}^*(t^o_k)}{dt^*_k}, \qquad (2.4.9)$$

where

$$\frac{d\underline{x}^*(t^o_{k+1})}{d\underline{x}(t^o_k)} = \frac{d\underline{x}^*(t^o_{k+1})}{d\underline{x}^*(t^o_{k2})} \frac{d\underline{x}^*(t^o_{k2})}{d\underline{x}^*(t^o_{k1})} \frac{d\underline{x}^*(t^o_{k1})}{d\underline{x}^*(t^o_k)}, \qquad (2.4.10)$$

for mode 2 operation.

$$\frac{d\underline{x}^*(t_{k+1}^o)}{d\underline{x}^*(t_k^{o*})} = \frac{d\underline{x}^*(t_{k+1}^o)}{d\underline{x}^*(t_{k1}^o)} \frac{d\underline{x}^*(t_{k1}^o)}{d\underline{x}(t_k^o)}, \tag{2.4.11}$$

for mode 1 operation.

It is proved in   for all 3 converters

$$\frac{d\underline{x}^*(t_{k+1}^o)}{d\underline{x}^*(t_k^o)} = \emptyset(T_p) = \emptyset_3(T_{ON}^o)\emptyset_2 \begin{vmatrix} 0 & 0 \\ 0 & 1 \end{vmatrix} \emptyset(T_{F1}^o) \tag{2.4.12}$$

for mode 2

$$= \emptyset_1(T_{ON}^o)\emptyset_2(T_{F1}^o) \tag{2.4.13}$$

for mode 1

and

$$\frac{d\underline{x}^*(t_k^o)}{dt_k^*} = B = (A_1 - A_2)\underline{x}^o(t_k^o) + (b_1 - b_2)V_I \tag{2.4.14}$$

where $\underline{x}^0(t_k^)$ is the state at the instant of sampling.

Substituting (2.4.12), (2.4.14) into (2.4.9)

$$\frac{d\underline{x}^*(t_{k+n}^0)}{dt_k^*} = \emptyset^n(T_p)B \text{ and} \tag{2.4.15}$$

the linearized discrete impulse response is obtained by sub-stituting (2.4.15) into (2.4.8)

$$g(nT_p) = c\emptyset^n(T_p)B. \tag{2.4.16}$$

The derivation for $\emptyset^n(T_p)$ is presented in [12]. If one is willing to neglect the detail of the waveforms between sam-

ples and study the long range trend of the converter, an equivalent continuous linear impulse response $g(t)$ can be obtained simply by substituting $t = nt_p$ into the expression for $g(nT_p)$. This is possible due to the systems response being much slower than the sampling rate. Every converter power stage inherently has a low-pass LC filter that attenuates the high frequency switching ripple. The natural resonant frequency of the output filters is designed on the order of a decade lower than the switching frequency to obtain good output voltage regulation.

2.5 DISCUSSION OF THE AVERAGE AND DISCRETE MODELING CONCEPT

Fig 2.5.1. illustrates the averaging and discrete concept in modeling. The example that is used, is the inductor current of a boost converter. The average technique models the duty cycle control ratio as a continuous function rather than a series of discrete pulses, as shown in Figure 2.5.1a.) and the jagged inductor current waveform is effectively smoothed out.

The discrete technique samples the waveform at the points indicated in Figure 2.5.1b.). The continuous linear impulse response is shown by a dashed curve.

The two modeling techniques look similar in the low modulation frequency range, but the difference is notable when the modulation frequency is high.

The average model is relatively easy to obtain. Since the model can be expressed in state equation, circuit and transfer function; physical insight into the system operation can be perceived. However, as the modulation frequency gets higher the model's accuracy decreases.

The discrete model's accuracy doesn't decrease as the frequency gets higher; but the obtainment of the model is very complex and the expressions are cumbersome. Since the model is expressed in just the transfer function form little physical insight into the system operation can be perceived.
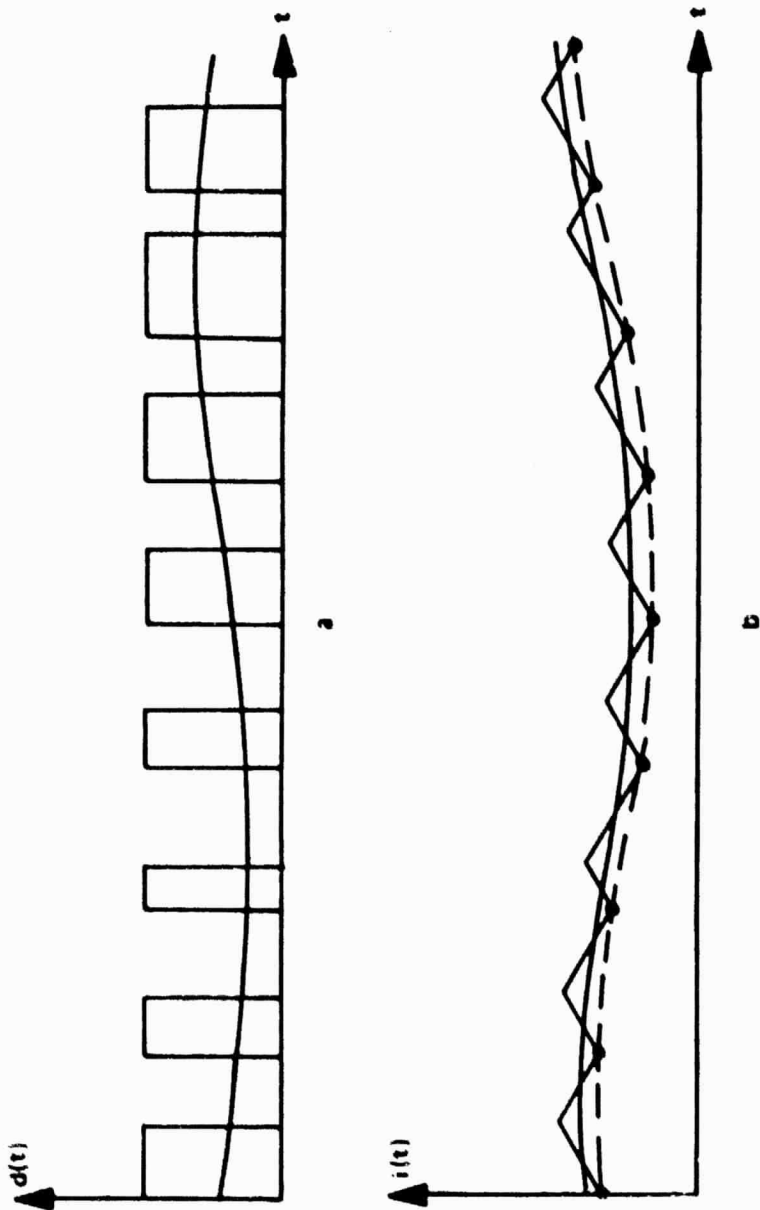
Figure 2.5.1. a.) Duty Cycle Control Ratio

b.) Boost Converter Inductor Current.

Chapter III

COMPARISON OF THE AVERAGE AND DISCRETE MODEL

A comparison of the average and discrete model is made on the basis of transfer functions, an equivalent state space representation and a numerical camparison, using a computer simulation. The boost converter will be used as the example throughout this chapter.

3.1   TRANSFER FUNCTION COMPARISON

In order to determine the transfer function for the boost converter, the state equations for the switch on-time and switch off-time must be determined.

Figure 3.1.1 shows the power stage topologies from which the state equations for each interval will be written.

For the on-time interval

$$\dot{\underline{x}} = \begin{bmatrix} 0 & 0 \\ 0 & -\dfrac{1}{R_L + R_c} \end{bmatrix} \begin{bmatrix} i_L \\ v_c \end{bmatrix} + \begin{bmatrix} \dfrac{1}{L} \\ 0 \end{bmatrix} v_I \qquad (3.1.1)$$

$$v_o = \begin{bmatrix} 0 & \dfrac{R_L}{R_L + R_c} \end{bmatrix} \begin{bmatrix} i_L \\ v_c \end{bmatrix}$$

45
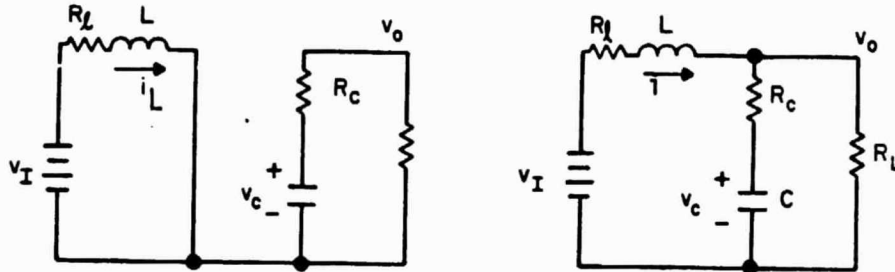
Figure 3.1.1 . Topologies for the boost converter during a
complete cycle of operation

and for the off-time interval

$$\underline{\dot{x}} = \begin{bmatrix} \dfrac{-R_c//R_L}{L} & \dfrac{-R_L}{R_L + R_c} \cdot \dfrac{1}{L} \\ \dfrac{R_L}{R_L + R_c} \cdot \dfrac{1}{C} & -\dfrac{1}{C(R_L + R_c)} \end{bmatrix} \begin{bmatrix} i_L \\ v_c \end{bmatrix} + \begin{bmatrix} \dfrac{1}{L} \\ 0 \end{bmatrix} v_I \quad (3.1.2)$$

$$v_0 = \begin{bmatrix} R_c//R_L & \dfrac{R_L}{R_L + R_c} \end{bmatrix} \begin{bmatrix} i_L \\ v_c \end{bmatrix} .$$

Using the averaging technique these two sets of state equations can be combined into a single period representation, shown below.

$$\underline{\dot{x}} = \begin{bmatrix} \dfrac{-D'R_c//R_L}{L} & -\dfrac{D}{L} \cdot \dfrac{R_L}{R_L + R_c} \\ \dfrac{D'}{C} \cdot \dfrac{R_L}{R_L + R_c} & -\dfrac{1}{C(R_L + R_c)} \end{bmatrix} \begin{bmatrix} i_L \\ v_c \end{bmatrix} + \begin{bmatrix} \dfrac{1}{L} \\ 0 \end{bmatrix} v_I \quad (3.1.3)$$

$$v_0 = \begin{bmatrix} D'R_c//R_L & \dfrac{R_L}{R_L + R_c} \end{bmatrix} \begin{bmatrix} i_L \\ v_c \end{bmatrix}$$

Using equation 2.1.11 the duty cycle to output voltage transfer function can be determined. The $\dfrac{\hat{v}_0(s)}{\hat{d}(s)}$ transfer function is shown below.

$$\frac{\hat{v}_0(s)}{\hat{d}(s)} = \frac{V_I}{(D')^2} \cdot \frac{1 + \frac{R_C}{R_L}}{1 + \left(\frac{R_C}{D'R_L}\right)^2} \cdot \frac{1 + s\left(\frac{1}{\omega_z} - \frac{1}{\omega_a}\right) - \frac{s^2}{\omega_a \omega_z}}{1 + \frac{s}{\omega_0 Q} + \left(\frac{s}{\omega_0}\right)^2} \qquad (3.1.4)$$

where $\omega_z = \dfrac{1}{R_C C}$; $\omega_a = \dfrac{(D')^2 R_L \dfrac{R_L}{R_L + R_C}}{L}$

$$\omega_0 = \frac{D'}{\sqrt{LC}} \quad \frac{R_L}{R_L + R_C} \quad \sqrt{1 + \frac{R_C}{D'R_L}}$$

$$Q = \frac{D'}{\omega_0} \quad \frac{R_L}{R_L + R_C} \quad \frac{1 + \frac{R_C}{D'R_L}}{\frac{L}{D'R_L} + R_C C}$$

The transfer function as determined by the discrete technique is [12]:

$$\frac{\hat{v}_0(s)}{\hat{d}(s)} = \frac{V_I}{(D')^2} \frac{1 + \dfrac{s}{\omega_a}}{1 + \dfrac{s}{\omega_0 Q} + \left(\dfrac{s}{\omega_0}\right)^2} \qquad (3.1.5)$$

where

$$\omega_a = \frac{\dfrac{R_L}{R_L + R_c}\left(1 + \dfrac{R_c}{D'R_L}\right)}{-\dfrac{R_L}{R_L + R_c}\dfrac{L}{(D')^2 R_L} - \dfrac{D}{2}\dfrac{R_L}{R_L + R_c} T_p + \dfrac{R_c C}{D'}}$$

$$\approx \frac{1}{-\dfrac{L}{(D')^2 R_L} + \dfrac{R_c C}{D'}}$$

assuming $\left[\dfrac{-L}{(D')^2 R_L} + \dfrac{R_c C}{D'}\right] >> \left[\dfrac{D}{2} T_p\right]$

and $R_c << R_L$.

$$\omega_0 = \frac{D'}{\sqrt{LC}} \frac{R_L}{R_L + R_c} \sqrt{1 + \frac{R_c}{D'R_L}}$$

$$Q = \frac{D'}{C} \frac{R_L}{R_L + R_c} \frac{1 + \dfrac{R_c}{D'R_L}}{\dfrac{L}{D'R_L} + R_c C}$$

The average and discrete transfer functions are shown to have the same natural resonant frequency ω_0 and the same Q-factor.

Under the assumption $R_L \gg R_C$, the dc gain and the second order poles are essentially the same, comparing (3.1.1) with (3.1.2); however, the zeroes of the two expressions exhibit some discernible differences.

$$\text{Zeroes of the Average Model} = 1 + \left(s\, R_c C - \frac{L}{(D')^2 R_L} \right) - \frac{s^2}{\dfrac{(D')^2 R_L}{R_c LC}} \quad (3.1.6)$$

and

$$\text{zeroes of the Discrete Model} = 1 + s\left(\frac{R_c C}{D'} - \frac{L}{(D')^2 R_L} \right) , \quad (3.1.7)$$

where $\dfrac{L}{(D')^2 R_L} > \dfrac{R_c C}{D'}$ under most design conditions. Comparing the above two equations, the zero-order and first-order terms are almost the same, except the effect due to the output filter capacitor ESR is exhibited in a somewhat different form. In the case of low modulation frequency,

$$\frac{s^2 \omega_0^2}{(D')^2 R_L/R_C} \ll 1,$$

the above two expressions are almost identical. The zeroes of the average model start to depart from that of the discrete model when the modulation frequency is considerably higher than the filter resonant frequency ω_0.

To elaborate the subtle yet important discrepancies between the two models, the following comparisons are made. The gain and phase plots computed from both techniques are illustrated in Figures 3.1.2-3.1.4 with the following numerical values:

$$T_p = 100 \, \mu \, sec, \; L = 6 \; mh, \; C = 41.7 \, \mu f,$$
$$R_L = 60 \, \Omega \, , \; R_C = 1 \, \Omega \, , \; R_1 = 0 \, , \; v_I = 60v.$$

The value for D is .25 for Fig. 3.1.2; .5 for fig. 3.1.3; .75 for Fig. 3.1.4.

There is a difference in the dc gain that increases as D increases. This is due to the difference in the power stage gain derived from the two techniques. The frequency response difference between the two becomes significant when the frequency is greater than 1 kHz. The average model has larger gain and phase angle. This is primarily due to the different effects of the capacitor ESR as described by the two different modeling techniques. A stronger contribution of ESR to the phase lead is shown in the average model, due

Figure 3.1.2   Frequency response for the boost converter
power stage from the discrete analysis and the
average model.   D=.25

Figure 3.1.3 : Frequency response for the boost converter power stage from the discrete analysis and the average model. D=.50

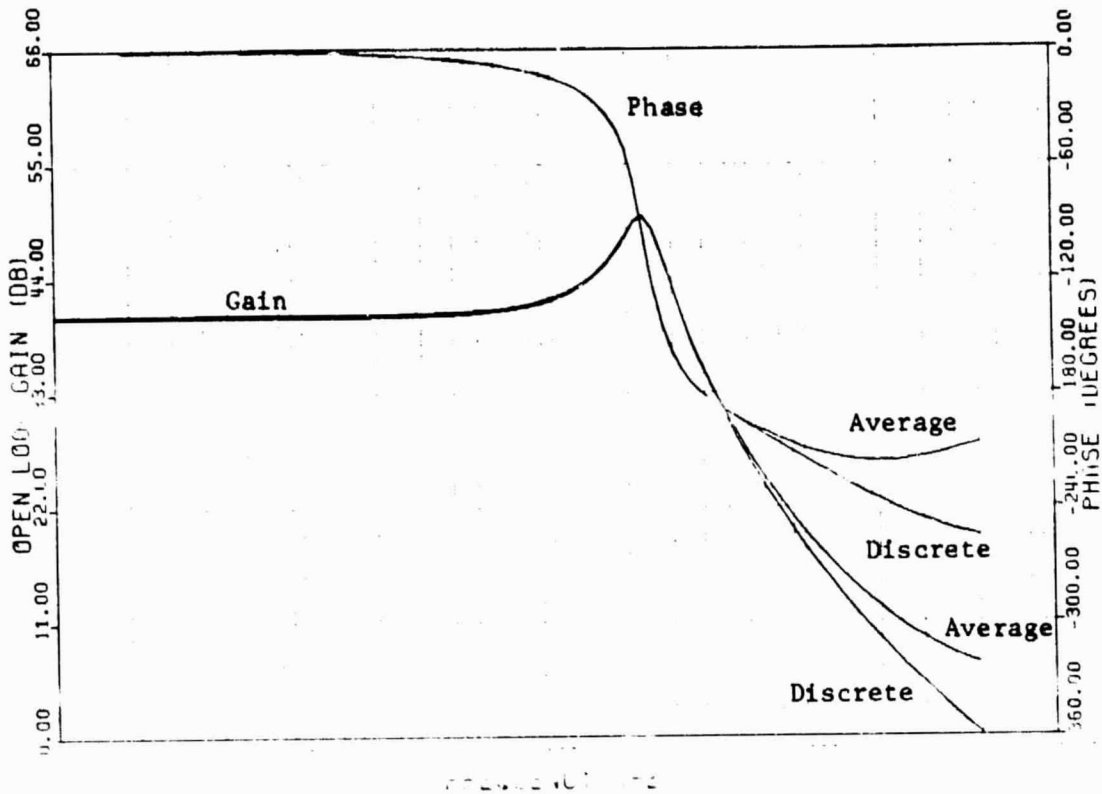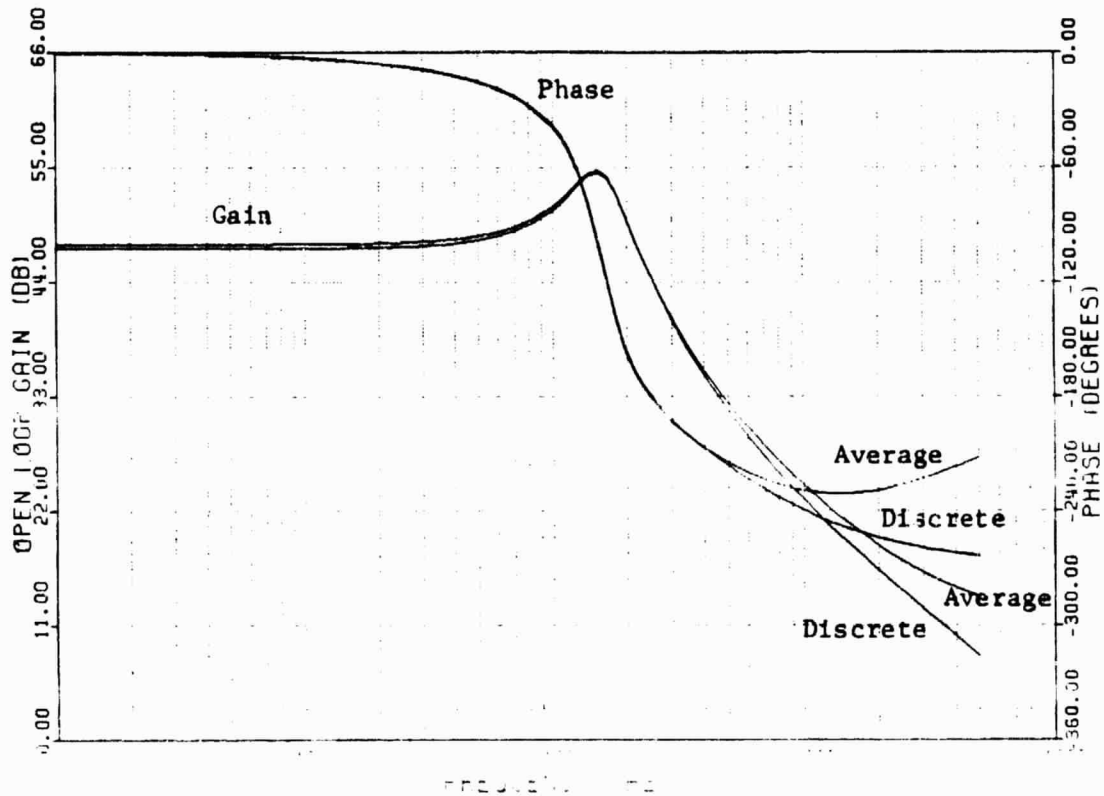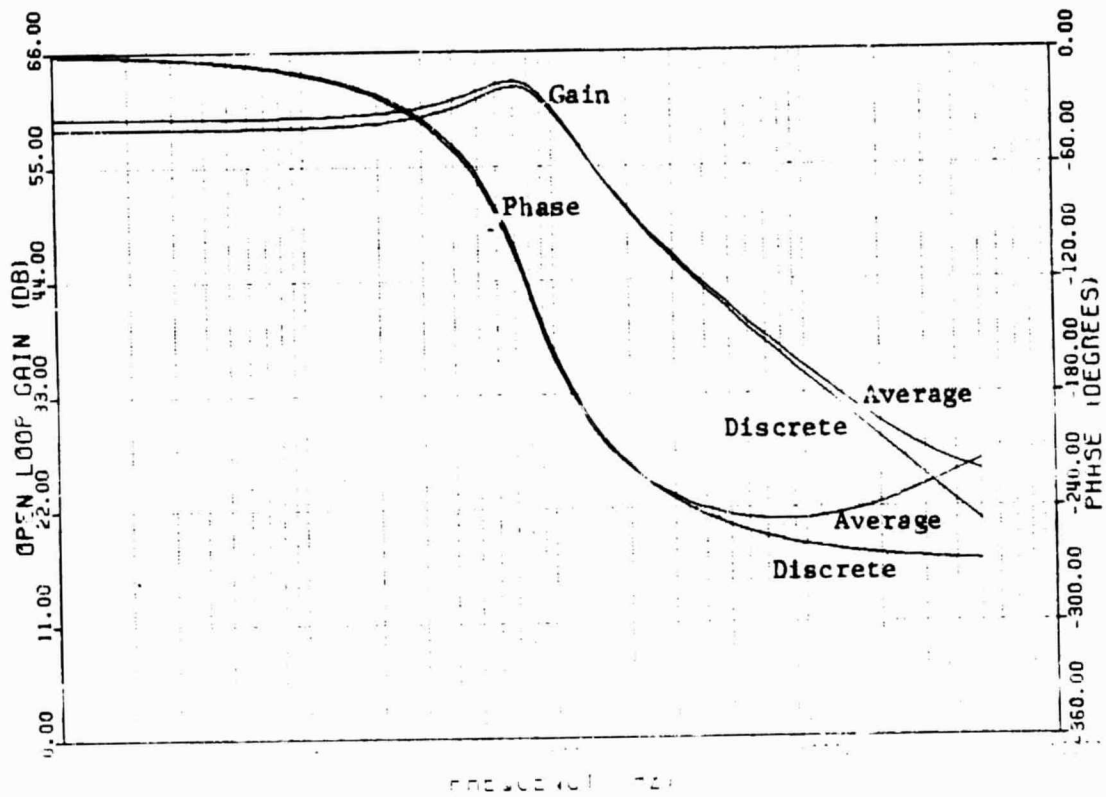Figure 3.1.4 : Frequency response for the boost converter
power stage from the discrete analysis and the
average model.   D=.75

to the second-order term, $- \frac{s^2}{\omega_z \omega_a}$. This term adds additional phase lag to the system, in the high modulation frequency range. For a high performance converter, employing multi-loop feedback schemes and providing high gain wide bandwidths, the amount of differences can be sufficiently large to mislead the stability prediction.

3.2 EQUIVALENT CIRCUIT REPRESENTATION

The significant difference in the two techniques has been identified to be in the $- \frac{s^2}{\omega_z \omega_a}$ term of the average model. The origin of this term must be found so that the differences can be identified and used to develop a new model which more accurately describes the system performance.

At this point, in trying to identify the differences, it would be helpful to express both transfer functions in the same form, a state variable representation. As shown in Figure 3.2.1 the averaging technique's transfer function can be expressed in the state variable form. From the state variable diagram, a linear set of equations can be obtained. This set of equations is not necessarily defined by the state variables of the system, but this system can be obtained by a linear transformation on the previous set of equations. The same operation could be applied to the discrete technique transfer function and result in a "similar" state variable model.
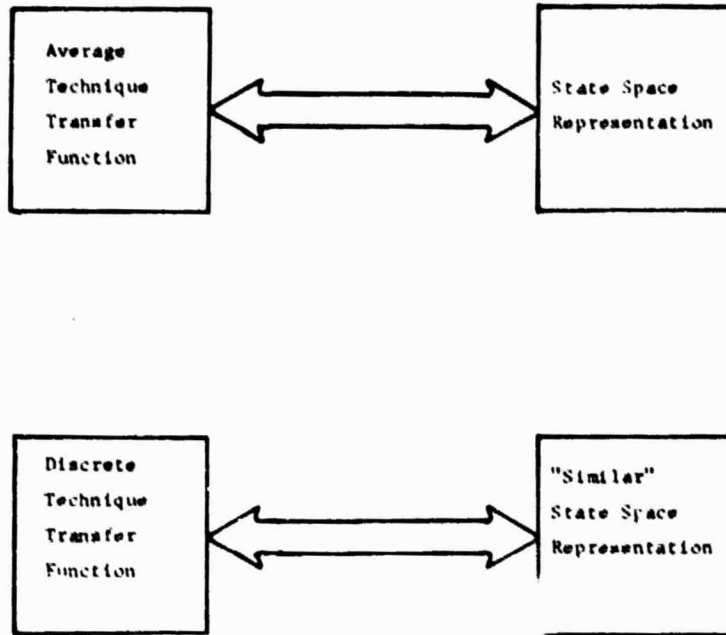
Figure 3.2.1 . Block Diagram representation of the
transformation from transfer function to state
space for each technique

The transformation from the transfer function form to a state variable form is not unique. Among the infinite possible transformations, there exists one that could lead to a state variable representation representing the state variable properties of the original system.

First, an algorithm is needed that will transform a system description from a transfer function to one of state variables. Gilbert [20] describes just such an algorithm.

If the transfer function of a physical system is given it is generally impossible to derive the corresponding differential equation representation. It is possible to find a set of differential equations which yields the same transfer function and does not necessarily describe the original system. This set of equations is in the normal form as shown below:

$$\dot{\underline{z}} = \Lambda\underline{z} + Bd \tag{3.2.2}$$
$$\dot{v}_0 = \gamma\underline{z} + Fd \ .$$

where $\Lambda = \begin{bmatrix} \lambda_1 & 0 \\ 0 & \lambda_2 \end{bmatrix}$

λ_1, λ_2 are the distinct eigenvalues of the system. To determine β, the transfer function is put into the form:

$$H(s) = \frac{\hat{v}_0(s)}{\hat{d}(s)} = \frac{k_1}{s - \lambda_1} + \frac{k_2}{s - \lambda_2} + E \qquad (3.2.3)$$

where $k_i = \lim_{s \to \lambda_i} (s - \lambda_i) H(s)$,

$$E = \lim_{s \to 0} H(s)$$

can then be calculated in terms of γ.

Let $\gamma = [\gamma_1 \gamma_2]$, $\quad \beta = \begin{bmatrix} \dfrac{k_1}{\gamma_1} \\ \dfrac{k_2}{\gamma_2} \end{bmatrix}$ $\qquad (3.2.4)$

The transformation matrix $\underline{R}$ is not unique, there are infinite transformations from a normal model to a state space model. A unique $\underline{R}$ can be determined in this case, however. This is because the normal model and state space model are both known for the average technique. Applying this transformation to the discrete normal model, an equivalent state space model is obtained.

To determine the unique transformation matrix $\underline{R}$ in Fig. 3.2.2, the relationship of the normal form and state space form is discussed. The normal form is related to the state space form by the following:
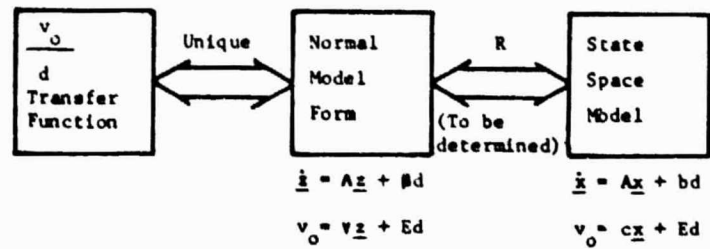
Figure 3.2.2 : Block diagram representation of the two step transformation

$$\underline{R}^{-1} \Lambda \underline{R} = A \tag{3.2.5}$$

$$\underline{R}^{-1} \beta = b \tag{3.2.6}$$

$$\gamma \underline{R} = c. \tag{3.2.7}$$

To determine R, equation (3.2.5) is used to obtain:

$$\Lambda \underline{R} = \underline{R}A \tag{3.2.8}$$

Let $R = \begin{bmatrix} r_{11} & r_{12} \\ \\ r_{21} & r_{22} \end{bmatrix}$ $\tag{3.2.9}$

The coefficient matrix A as determined by the average model can be represented in general as:

$$A = \begin{bmatrix} a_{11} & a_{12} \\ \\ a_{21} & a_{22} \end{bmatrix} . \tag{3.2.10}$$

$$\Lambda = \begin{bmatrix} \lambda_1 & 0 \\ \\ 0 & \lambda_2 \end{bmatrix} \tag{3.2.11}$$

where λ_1, λ_2 are the eigenvalues of the coefficient matrix A. Substituting (3.2.9), (3.2.10), and (3.2.11) into (3.2.8) and multiplying, results in:

$$\begin{bmatrix} \lambda_1 r_{11} \lambda_1 r_{12} \\ \\ \lambda_2 r_{21} \lambda_2 r_{22} \end{bmatrix} = \begin{bmatrix} r_{11} a_{11} + r_{12} a_{21} & r_{11} a_{12} + r_{12} a_{22} \\ \\ r_{21} a_{11} + r_{22} a_{21} & r_{21} a_{12} + r_{22} a_{22} \end{bmatrix} \tag{3.2.12}$$

The components of each of the above matrices are equal, so that the components of the $\underline{R}$ matrix can now be determined. Thus the transformation from transfer function form to state variable form is now complete.

For the boost converter, the equivalent state space model from the discrete transfer function is:

$$
\underline{\dot{\hat{x}}} = \begin{bmatrix} \dfrac{-D'R_c//R_L}{L} & -\dfrac{D'}{C}\dfrac{R_L}{R_L + R_c} \\[3mm] \dfrac{D'}{C}\dfrac{R_L}{R_L + R_c} & -\dfrac{1}{c(R_L + R_c)} \end{bmatrix} \underline{\hat{x}} + \begin{bmatrix} \dfrac{1 + \dfrac{R_c}{R_L} - \dfrac{1}{\omega_a}\dfrac{DD'R_c}{L}}{\dfrac{D'}{C}(1+\dfrac{R_c}{R_L}) - \dfrac{(D')^2 R_c^2}{L}D} G\hat{d} \\[6mm] \dfrac{1+\dfrac{R_c}{R_L}(-D'R_c)+\dfrac{1}{\omega_a}\dfrac{D'}{C}(1+\dfrac{R_c}{R_L}}{\dfrac{D'}{C}(1+\dfrac{R_c}{R_L} - \dfrac{D(D')^2 R_c}{L}} \end{bmatrix}
$$

$$\tag{3.2.13}$$

$$
\hat{v}_0 = \begin{bmatrix} D'R_c//R_L & \dfrac{R_L}{R_L + R_c} \end{bmatrix} \underline{\hat{x}}
$$

$$
\text{where } G = \frac{V_I}{LC}\,\frac{R_L}{R_L + R_c}\,(1 + \frac{R_c}{D'R_L}) \ .
$$

The state space representation that results from this transformation cannot be guaranteed to be the same state space as in the average model. However, this transformation does give a result which illustrates the discrete model with

a circuit. Using this circuit, physical insight into the modeling by the discrete technique can be obtained. This insight can be used to determine the basic differences between the modeling techniques.

An equivalent circuit can be realized from the above by solving for v_0 in equation (3.2.13b) and substituting into equation (3.2.13a). Using this equation to realize the circuit results in the one shown in figure 3.2.3.

The average model for the boost converter can be put into an equivalent circuit form by solving for v_c in equation (2.1.7b) and substituting (2.1.7a). Simplifying the expression results in:

$$
\begin{bmatrix} \dfrac{d\hat{i}_L}{dt} \\[2mm] \dfrac{d\hat{v}_c}{dt} \end{bmatrix} = \begin{bmatrix} \dfrac{-DD'R_c//R_L}{L} & \dfrac{-D'}{L} \\[2mm] \dfrac{D'}{C} & -\dfrac{1}{R_L C} \end{bmatrix} \begin{bmatrix} \hat{i}_L \\[2mm] \hat{v}_0 \end{bmatrix} + \begin{bmatrix} \dfrac{1}{L} \\[2mm] 0 \end{bmatrix} \hat{v}_I
$$

$$
+ \begin{bmatrix} 1 + \dfrac{D}{D'}\dfrac{R_c}{R_L} \\[3mm] -\dfrac{1}{D'R_L C}(1+\dfrac{R_c}{R_L}) \end{bmatrix} \dfrac{V_I/D'}{1 + \dfrac{R_c}{D'R_L}} \hat{d}
$$

$$(3.2.14)$$

Note that the 1st equation of 3.2.14 is Kirchoff's voltage law applied to a loop and the 2nd equation is Kirchoff's current law applied to a node. These two equations can be
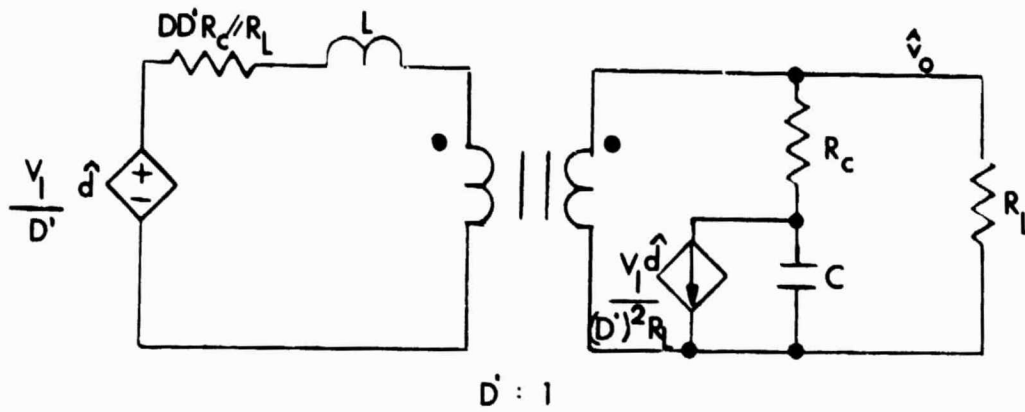
Figure 3.2.3: Equivalent circuit model obtained from the discrete technique.

represented by one circuit if an ideal transformer is used. The equivalent average model circuit for the boost converter is shown in figure 3.2.4. When the output filter capacitor ESR is equal to zero, the models are the same. Therefore, the two techniques model the effect of the ESR differently.

3.3 NUMERICAL COMPARISON

In order to determine the effect of modeling the output filter capacitor ESR for the two techniques, an example has been programmed, where a duty cycle perturbation is injected into the boost converter example of 3.1. The PWM is modeled by a naturally sampled circuit, as discussed in [21] and shown in Fig. 3.3.1 . This circuit was programmed for a dc value of the duty cycle to be .5 and as illustrated by the waveforms, in Fig. 3.3.1 introduces no phase lag. The inductor current, capacitor voltage and output voltage waveforms were plotted for 4 different modulation frequencies, as shown in Figures 3.3.2-3.3.5. The jagged curve in all figures was determined by the actual circuit equations (3.1.1) and (3.1.2); the smoother continuous curve by the averaged equation (3.1.3). As shown in Figures 3.3.2-3.3.5, the state variable waveforms determined by the average model effectively smooths out the switching ripple with no discernible phase shift, giving a smooth waveform that portrays
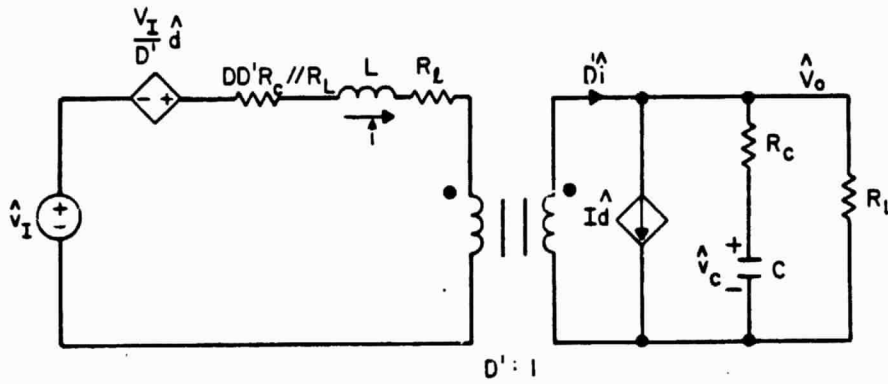
Figure 3.2.4 . Average small-signal circuit model for the
boost converter.
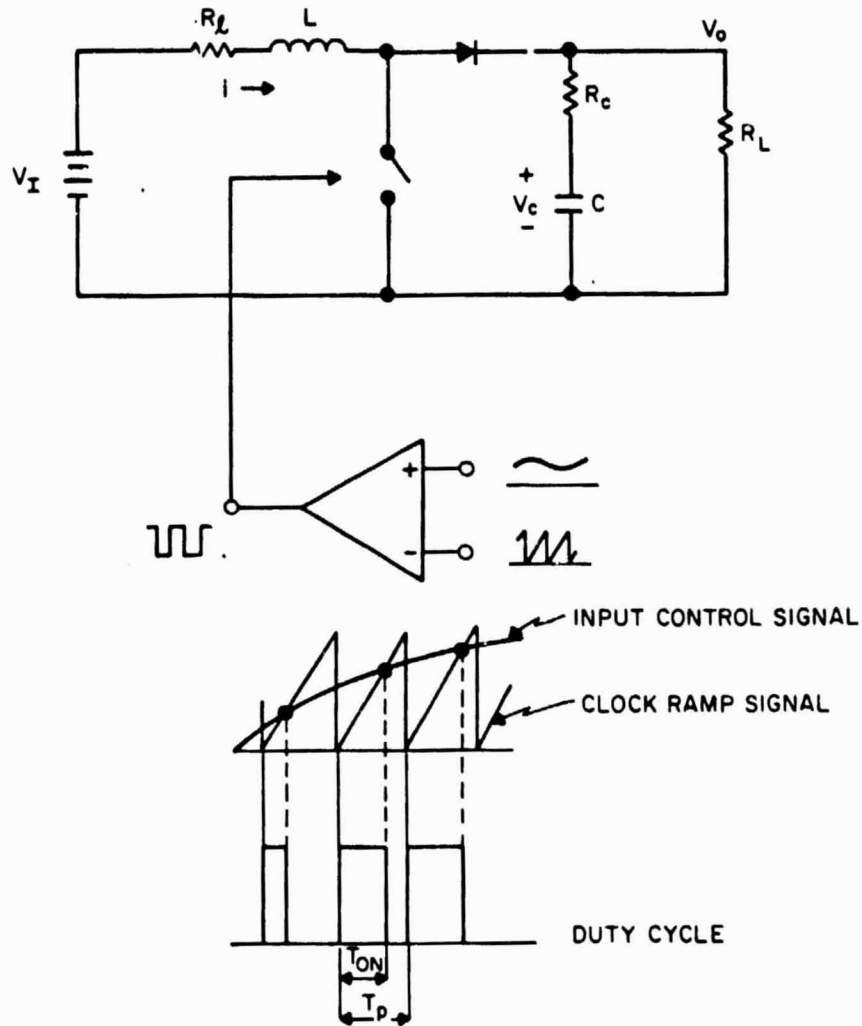
Figure 3.3.1 : Duty cycle determination by the naturally
sampled modulator.

ORIGINAL PAGE IS
OF POOR QUALITY
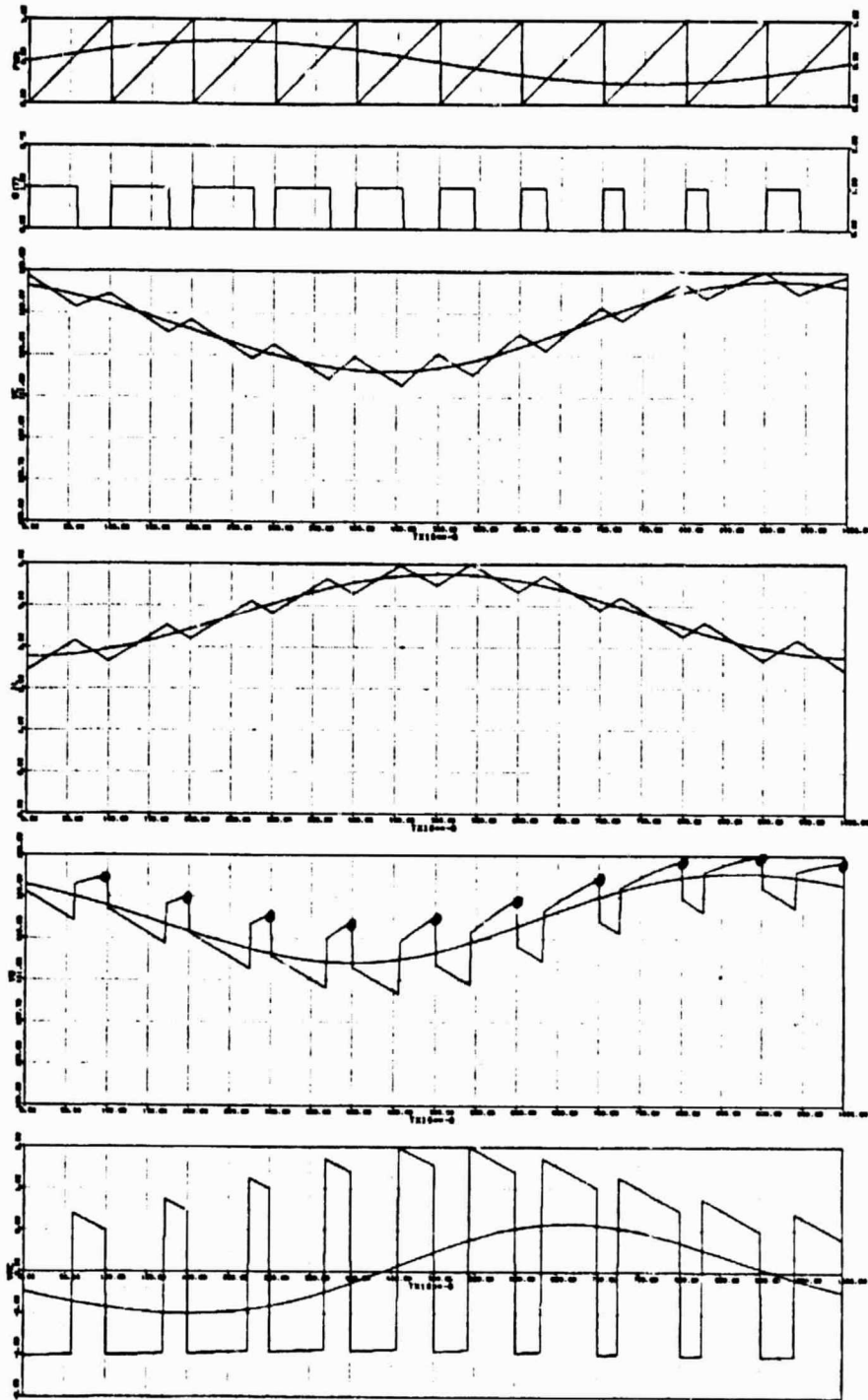
Figure 3.3.2 Computer simulated waveforms for boost converter for
one-tenth switching frequency modulation.
Continuous waveform --- Average Model
Dots --- Discrete Model
Switching Waveform --- Actual circuit behavior

**ORIGINAL PAGE IS
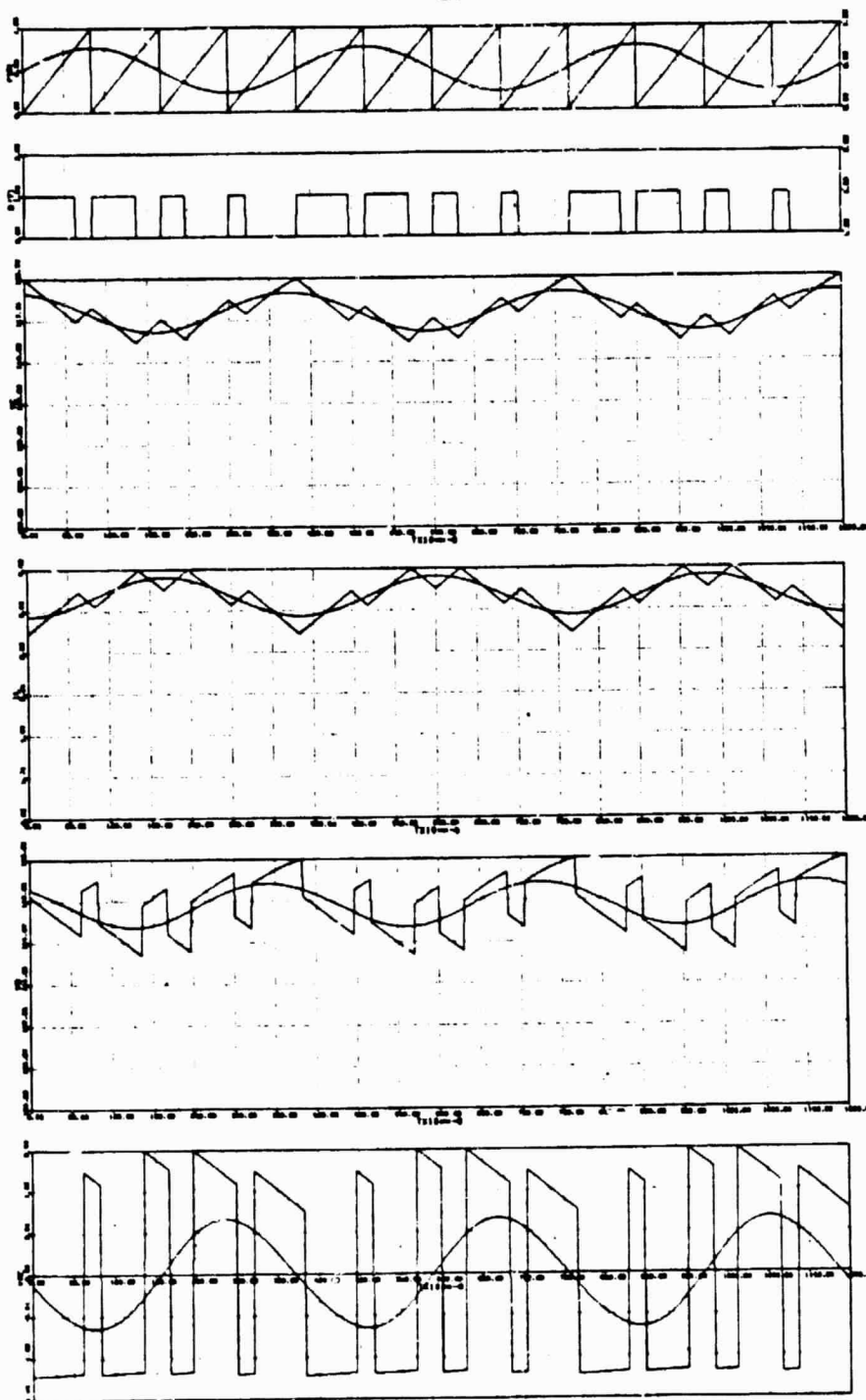OF POOR QUALITY**

Figure 3.3.3.   Computer simulated waveforms for boost
converter for one-fourth switching frequency
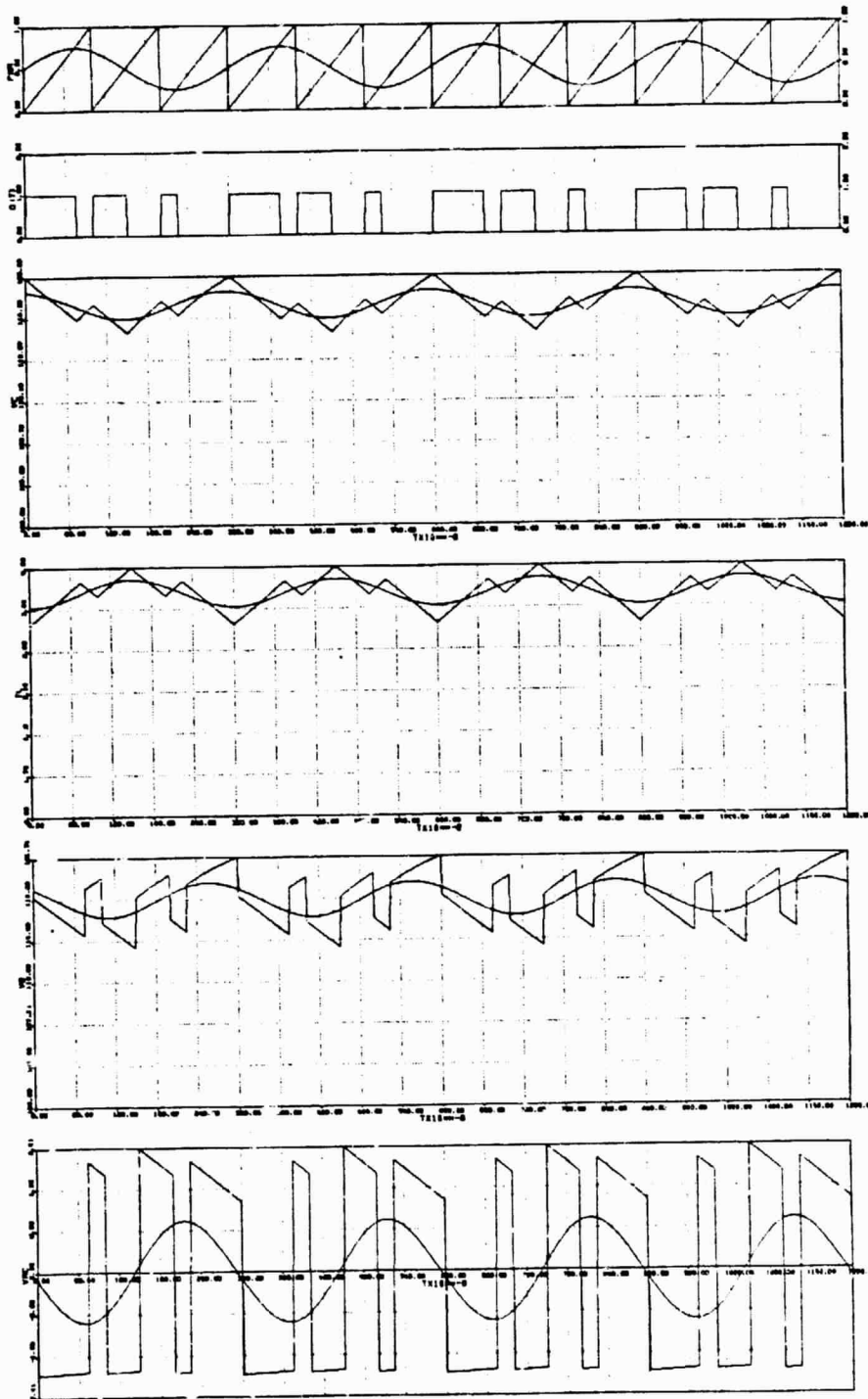modulation.

Figure 3.3.4   Computer simulation for boost converter for
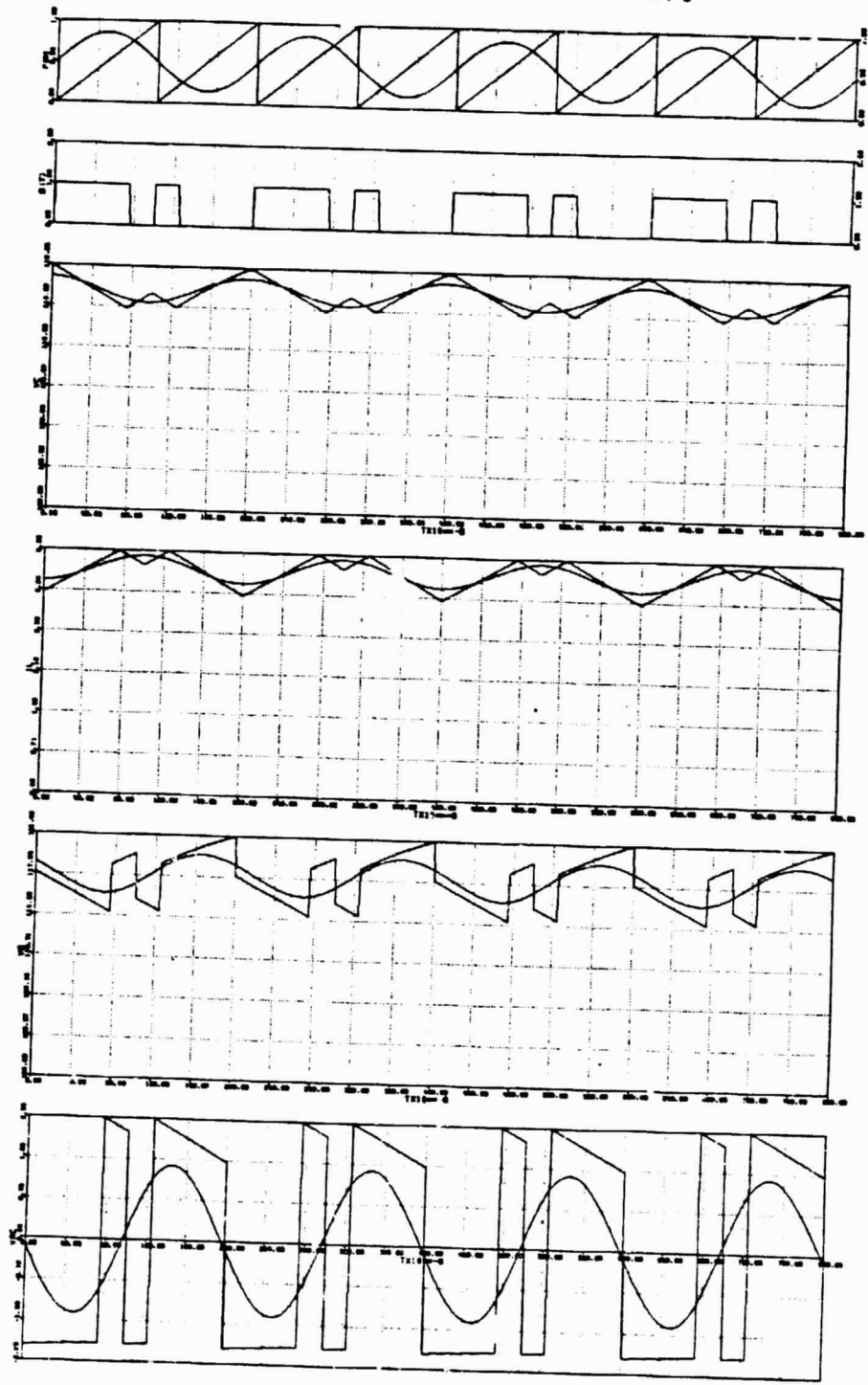one-third switching modulation.

Figure 3.3.5   Computer simulation for boost converter for
one-half switching frequency modulation.

the long range trend. The output voltage waveform, deter-
mined by the average model, leads the actual waveform by
approximately 8° in Fig. 3.3.2, and 31° in Fig. 3.3.3, 38°
in Fig. 3.3.4 and 51° in Fig. 3.3.5. This agrees with the
difference in phase shown in Fig. 3.1.2, for the frequencies
of 1000 Hz (1/10 of the switching frequency), 2500 Hz (1/4
of the switching frequency), 3,333Hz (1/3 of the switching
frequency) and 5000Hz (1/2 of the switching frequency).
Therefore as shown by this discussion and example, the out-
put voltage, as determined by the average model, does not
agree with the actual case and this is the origin of the
difference between the average and discrete techniques.

The output voltage is equal to the sum of the capacitor
voltage and the capacitor ESR voltage. Careful examination
of Figures 3.3.2-3.3.7, illustrate that the ESR waveform
consists of two modulation components: amplitude modulation
and pulse-width modulation; the former is due to the induc-
tor-current-modulation effect and the latter is due to the
duty-cycle-modulation effect. There is an obvious phase
difference between these two modulation components, as shown
in parts (a) and (b) of figures 3.3.2-3.3.5. A modulation
voltage of this type carries a phase lead with respect to
the capacitor voltage.

At one-tenth switching frequency the amplitude of the capacitor modulation voltage is larger compared to the ESR modulation voltage, but as the frequency increases to one-fourth, one-third and one-half of the switching frequency, the amplitude of the capacitor modulation voltage remains almost constant. This is shown by Figures 3.3.2-3.3.5. The effect is to cause the averaged output voltage waveform to lead in phase with respect to the envelope of the actual output voltage waveform.

As mentioned previously, the average model and the discrete model are the same when the ESR is equal to zero. To illustrate this, examine figures 3.3.3, 3.3.6 and 3.3.7. These are the simulated waveforms with the ESR equal to 1Ω, $.1\Omega$ and $.01\Omega$, respectively. The figures show that the average output voltage waveform approaches the discrete output voltage as R_c approaches zero. The effect of the ESR waveform is reduced as the ESR goes to zero, because the maximum modulation value of the ESR voltage is reduced. Therefore, since the source of the difference between the averaged and discrete waveforms is reduced to an insignificant amount the averaged output voltage tends to approach the discrete output voltage.

From the control point of view, the error processor does not observe the average output voltage and the duty cycle is
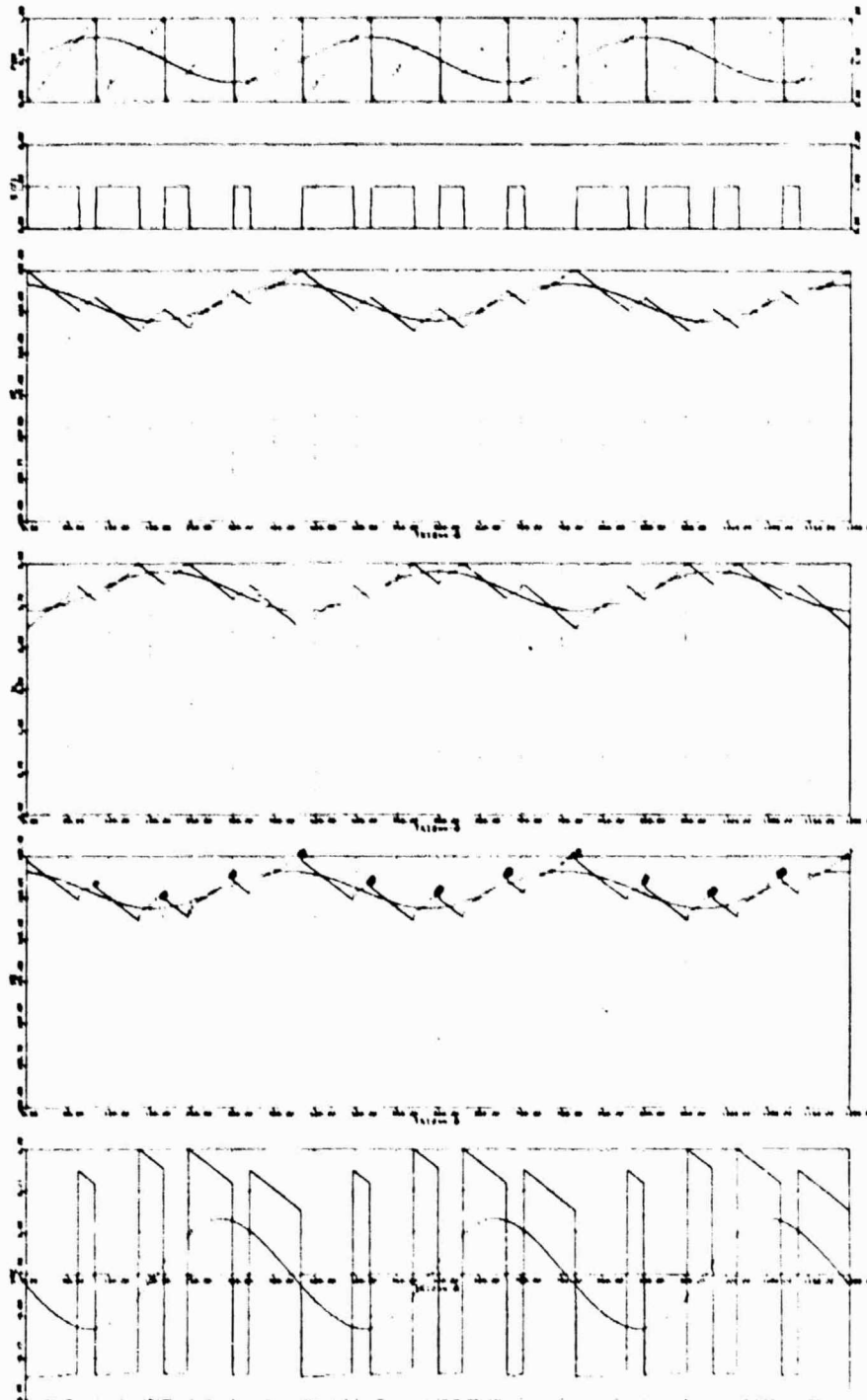
Figure 3.3.6. Computer simulated waveforms for boost converter for
one-fourth switching frequency. ESR = .1Ω
Continuous Waveform -- 'verage Model
Dots --- Discrete Model
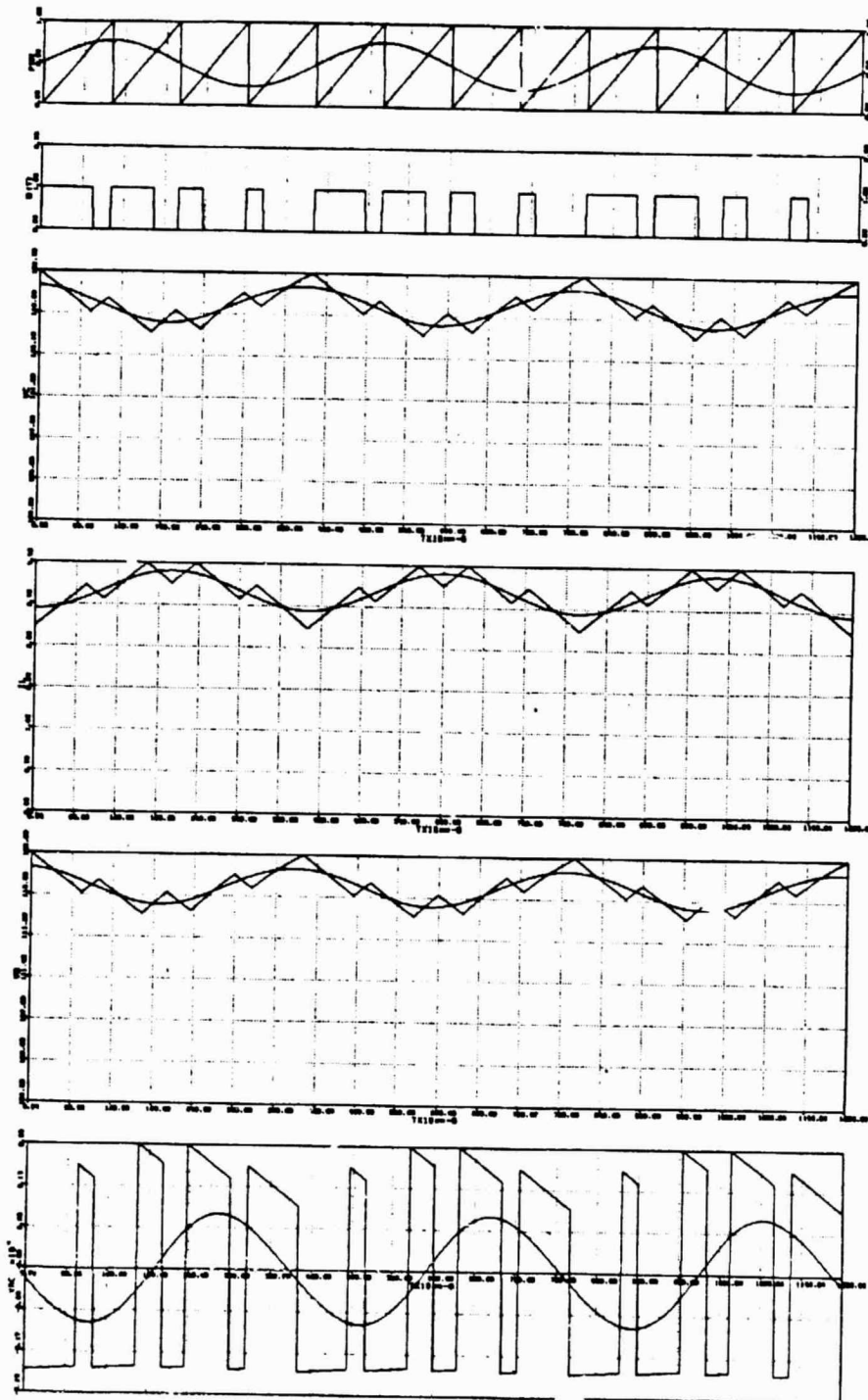Switching Waveform --- Actual circuit behavior

ORIGINAL PAGE IS
OF POOR QUALITY

Figure 3.3.7. Computer simulated waveforms for boost converter
for one-fourth switching frequency.   ESR-.01Ω

implemented based on the actual output voltage waveform (on an instantaneous basis). Therefore, the discrete modeling technique provides a more accurate power stage model than that derived from the average technique.

Chapter IV

PRESENTATION OF THE NEW POWER STAGE MODEL

As shown in the previous chapter the average model does not accurately simulate the power stage output voltage operation as the modulation frequency gets higher. With the advent of high gain bandwidth power converters, the model must accurately describe converter operation so that stability requirements can be determined accurately. Otherwise, a system could become unstable when the model has forecasted it to be stable.

This chapter addresses itself to the presentation of a new power stage model. The new model combines the discrete sampling technique with the averaging technique, determining a model that is accurate at high modulation frequencies.

4.1 THEORETICAL DEVELOPMENT

The average model has been shown by example to model the state variables very well; but the output voltage is not modeled accurately, because of the effect of the output filter capacitor ESR. Where does the difference in modeling originate? Could it be from an assumption that was made?

The average model as shown in Appendix C of [15] assumes that

$$\underline{e} \quad d'A_2T_p \underline{\underline{e}} \; dA_1T_p \underline{\underline{=}} \underline{e} \; (dA_1 + d'A_2)T_p$$

This equation is satisfied exactly when $A_1A_2 = A_2A_1$. This approximation is shown in [15] to introduce insignificant error (approximately 2%) because the switching frequency is sufficiently greater than the natural frequencies of the output filter. The conclusion is that even for the natural frequencies slightly more than a decade apart from the switching frequency, satisfactory results are obtained using a linear approximation for the exponential matrices. Therefore, one can reasonably assume that insignificant error is introduced in the modeling of the state variables.

The difference must be introduced when the output voltage expression is averaged. The averaged output voltage has already been shown to lead the envelope established by the discrete output voltage. Thus, the difference occurs at the point in the averaging technique when the discountinuous output voltage waveform is averaged. An expression is needed that will allow the envelope of the discrete output voltage to be determined. The way to determine this expression is to sample the actual output voltage at a constant frequency. The controller is operating at a constant frequency, with the period equal to T_p.

As shown in Fig. 3.3.1 the input control signal intersects the clocked ramp signal, causing the duty cycle to go

low, which causes the switch in the power stage to turn off. As shown in Fig. 4.1.1., the input control signal is the compensated error feedback signal for the regulated output voltage of the converter. Essentially, this signal is the compensated and inverted output ripple voltage. Consider that the error signal is discontinuous, Fig. 4.1.2 illustrates the action of constant frequency controller in steady state. At the beginning of the cycle, the duty cycle goes high signalling the power stage switch to turn on, when the error signal intersects the clocked ramp the duty cycle goes low. Fig. 4.1.3 illustrates the constant frequency controller when the error signal is perturbed. The duty cycle goes high every T_p sec, but the T_{ON} and T_{OFF} are modulated according to the modulation frequency of the error signal. The intersection occurs at the top part of the error signal. This corresponds to the bottom part of the compensated output voltage ripple.

The bottom part of the output voltage ripple corresponds to the time that the switch is on. Therefore, a modulation in the duty cycle would correspond to a modulation in the T_{ON} part of the output voltage ripple. Thus, for a constant frequency controller, the sampling point should be chosen at the beginning of the cycle.

The output is determined at $t=T_p$ (the beginning of the cycle). From equation (1.1.2) it is found to be:

$$Y_2(T_p) = c_1 \underline{x}_2(T_p).$$

(4.1.1)
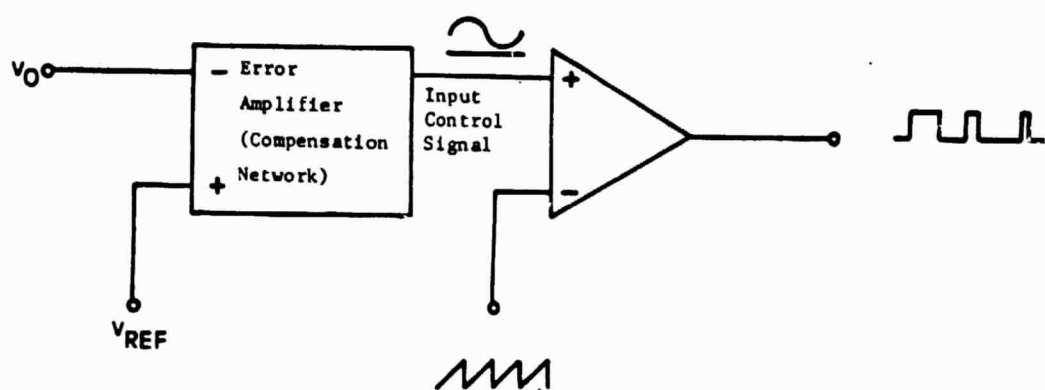
Figure 4.1.1.   Determination of Input Control Signal

error signal (a.) constant ramp

T_{ON} T_{OFF} T_{ON} T_{OFF}

T 2T 3T . . . (b.)
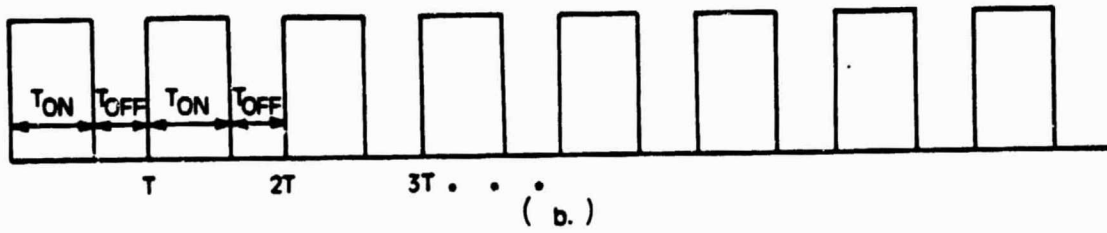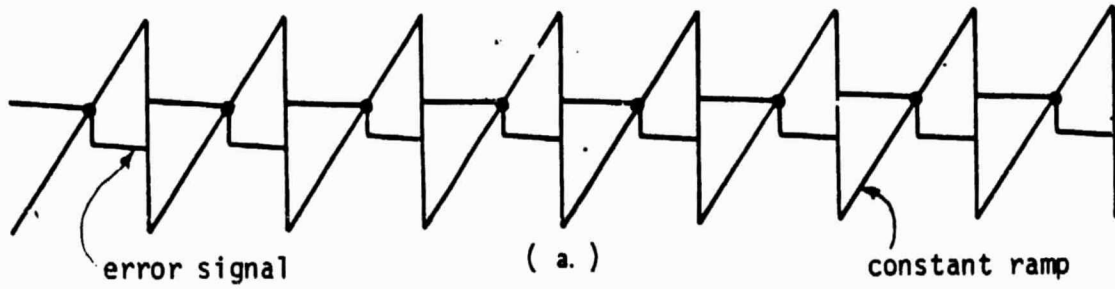
Figure 4.1.2. Constant frequency controller in steady state
      a.) Input control signal and clocked ramp signal
      b.) Duty cycle

81

error signal (a.) constant ramp

T_{ON}^1 T_{OFF}^1 T_{ON}^2 T_{OFF}^2
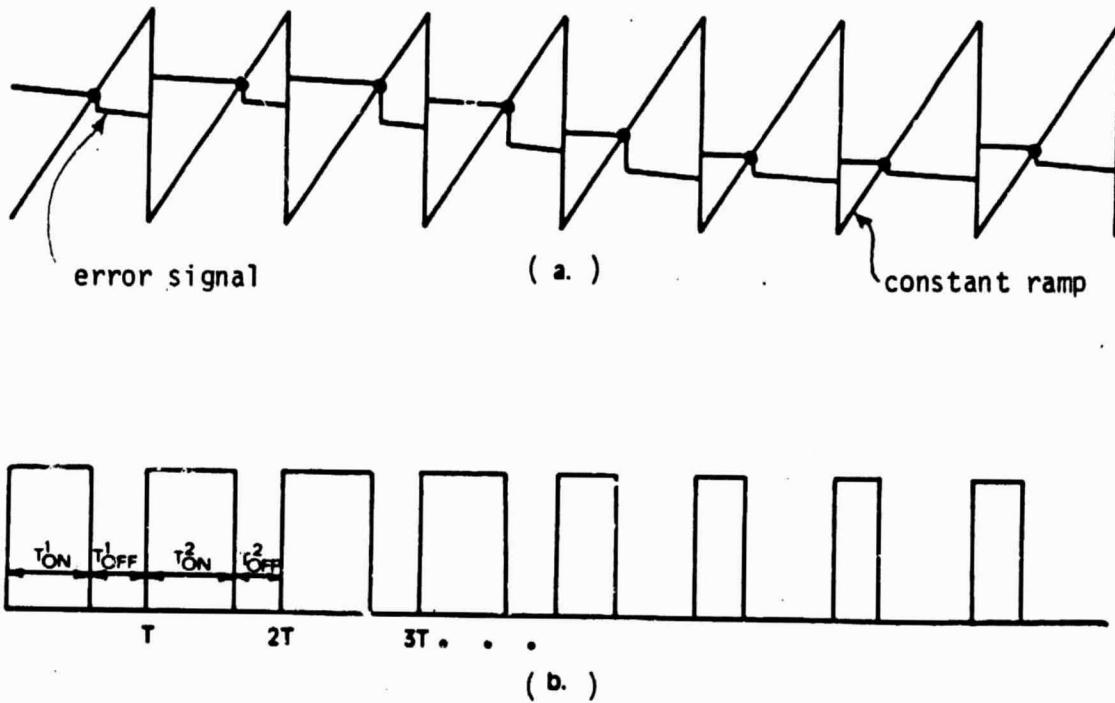
T 2T 3T • • •

(b.)

Figure 4.1.3. Constant frequency controller with perturbed input
control signal
a.) Input control signal and clocked ramp signal
b.) Duty cycle

The above equation can be generalized to obtain the nth point resulting in:

$$\underline{Y}_2(nT_p) = c_1\underline{x}_2(nT_p) \tag{4.1.2}$$

Since the purpose of this model will be to study the long range trend of the converter, an equivalent continuous linear output expression can be obtained by substituting $t = nT_p$. The average state variable, $\underline{x}$ has been determined to model $\underline{x}_2$ accurately, therefore, one can substitute $\underline{x} = \underline{x}_2$ and $\underline{y} = \underline{y}_2$. This results in the following output expression.

$$\underline{y}(t) = c_1\underline{x}(t). \tag{4.1.3}$$

The averaged output expression is:

$$\underline{y} = (dc_1 + d'c_2)\underline{x}(t) \tag{4.1.4}$$

For the output (4.1.3) to be equal to the averaged output (4.1.4), the sum $dc_1 + d'c_2$ must be equal to c_1 which is true for the buck converter and boost converter when the output filter capacitor ESR is zero. It should be noted that the expression of (4.1.3) is limited to a power converter employing constant frequency control. It can't be used for other duty cycle control models indiscriminately. The sam-

pling point selected during the cycle, before or after the jump of the output voltage waveform plays a significant role in the accuracy of the power stage model.

Applying the discrete sampled output expression of equation (4.1.3) to the average state variable model a single period representation can be obtained. The perturbation analysis described in Chapter II can be applied on this model to the analyze the converter.

The unperturbed discrete-average model is

$$\underline{x} = A\underline{x} + b\ v_I \qquad\qquad (4.1.5)$$

$$\underline{y} = v_0 = c_1\underline{x},$$

where $\quad A = dA_1 + d'A_2 \qquad b = db_1 + d'b_2$

The line voltage and duty cycle variations, introduced as they were previously in chapter II, produce a perturbation in the state and output variables. Substituting those variables into the above equation and assuming negligibly small departures from the steady state values, results in:

$$\dot{\hat{\underline{x}}} = A\underline{x} + b\ V_I + A\ \hat{\underline{x}} + b\ \hat{v}_I +$$

$$[(A_1 - A_2)\underline{x} + (b_1 - b_2)V_I]\hat{d} \qquad (4.1.6)$$

$$\underline{y} + \hat{\underline{y}} = V_0 + \hat{v}_0 = c_t\underline{x} + c_1\hat{\underline{x}},$$

The discrete-average in its final form is shown below. The dc model is:

$$0 = A\underline{x} + b\ V_I \qquad\qquad (4.1.7a)$$

$$V_o = c_1 \underline{X}, \tag{4.1.7b}$$

From which the dc operating point can be determined by solving for $\underline{X}$ in (4.1.7a) and substituting into (4.1.7b), the following results are obtained.

$$\underline{X} = -A^{-1}b \ V_I \tag{4.1.8a}$$

$$V_o = -c_1 A^{-1}b \ V_I. \tag{4.1.8b}$$

The ac model is

$$\hat{\underline{x}} = A\hat{\underline{x}} + b\hat{v}_I + [(A_1 - A_2)\underline{X} + (b_1 - b_2)V_I]\hat{d} \tag{4.1.9a}$$

$$\hat{v}_o = c_1 \hat{\underline{x}} \tag{4.1.9b}$$

The transfer functions can be found by taking the Laplace transformation of (4.1.9a) and (4.1.9b) as shown below.

$$s\hat{\underline{x}}(s) = A\hat{\underline{x}}(s) + b\hat{v}_I(s) + \{ (A_1 - A_2)\underline{X} + (b_1 - b_2)V_I] \}\hat{d}(s) \tag{4.1.10a}$$

$$\hat{v}_o(s) = c_1 \hat{\underline{x}}(s) \tag{4.1.10b}$$

Solve 4.1.10a for $\underline{x}$ (s)

$$\hat{\underline{x}}(s) = [sI-A]^{-1}\{ b\hat{v}_I(s) + [(A_1 - A_2)\underline{X} + (b_1 - b_2 V_I]\hat{d}(s) \} \tag{4.1.11}$$

and substitute for x(s) into (4.1.10b), adding like coefficients.

$$\hat{v}_o(s) = c_1 [sI-A]^{-1}[b\hat{v}_I(s)]$$
$$\quad + c_1 [sI-A]^{-1}[(A_1 - A_2)\underline{X} + (b_1 - b_2)V_I]\hat{d}(s) \tag{4.1.12}$$

from which the following transfer functions can be obtained:

$$\frac{\hat{v}_0(s)}{\hat{v}_I(s)} = c_1[sI-A]^{-1}b \tag{4.1.13}$$

$$\frac{\hat{v}_0(s)}{\hat{d}(s)} = c_1[sI-A]^{-1}[(A_1-A_2)\underline{X}+(b_1-b_2)V_I] \tag{4.1.14}$$

An equivalent circuit can also be determined for a specific type of converter, by putting the above state equations (4.1.10) into a realizable form. This will be illustrated in the next section.

4.2   ILLUSTRATION WITH AN EXAMPLE CONVERTER

The $\dfrac{\hat{v}_0(s)}{\hat{d}(s)}$ transfer function determined by the discrete-

average model for the boost converter is:

$$\frac{\hat{v}_o}{\hat{d}(s)} = \frac{V_I}{(D')^2}\left(1 - \frac{R_\ell}{D'R_L}\left(1 + \frac{R_c}{R_L}\right)\right)\frac{1 + \frac{s}{\omega_a}}{1 + \frac{s}{\omega_0 Q} + \left(\frac{s}{\omega_0}\right)^2} \tag{4.2.1}$$

$$\text{where } \omega_a = -\frac{(D')^2 R_L}{L}\frac{R_L}{R_L + R_c}\left(1 - \frac{R_\ell}{D'R_L}\left(1 + \frac{R_c}{R_L}\right)\right)$$

$$\simeq -\frac{(D')R_L}{L} \quad , \quad R_c \quad R_L$$

$$\omega_0 = \frac{D'}{\sqrt{LC}} \; \frac{R_L}{R_L + R_c} \; \sqrt{1 + \frac{R_c}{D'R_L} + \frac{R_\ell}{(D')^2 R_L}\left(1 + \frac{R_c}{R_L}\right)}$$

$$Q = \frac{D'}{\omega_0} \; \frac{R_L}{R_L + R_c} \; \frac{1 + \dfrac{R_c}{D'R_L} + \dfrac{R_\ell}{(D')^2 R_L}\left(1 + \dfrac{R_c}{R_L}\right)}{\dfrac{L}{D'R_L} + \dfrac{R_\ell C}{D'} + R_c C + \left(1 + \dfrac{R_\ell}{D'R_L}\right)}$$

Compare the discrete-average transfer function with the previously developed ones.

1. The transfer function has one zero that is positive.

2. There is no 2nd order term in the numerator of the discrete-average model. The average model transfer function has the 2nd order term $\dfrac{s^2}{\omega_z \omega_a}$, which has been determined to cause the differences, noted previously in chapter III.

3. The natural resonant frequency and Q factor are the same for all three models. The power stage gain with $R_c = 0$ is the same as with the discrete model.

To illustrate the simplicity of this model, a circuit model will be realized. The discrete-average model for the boost converter is:

$$\underline{\dot{x}} = \begin{bmatrix} \dfrac{-d'R_c//R_L}{L} & \dfrac{-d'}{L}\dfrac{R_L}{R_L + R_c} \\[2ex] \dfrac{d'}{C}\dfrac{R_L}{R_L + R_c} & -\dfrac{1}{(R_L + R_c)C} \end{bmatrix} \underline{x} + \begin{bmatrix} \dfrac{1}{L} \\[1ex] 0 \end{bmatrix} v_I \qquad (4.2.2)$$

$$v_0 = \begin{bmatrix} 0 & \dfrac{R_L}{R_L + R_c} \end{bmatrix} \underline{x}, \text{ where } \underline{x} = \begin{bmatrix} i_L \\ v_c \end{bmatrix} \qquad (4.2.3)$$

Solving for v_c in (4.2.3) and substituting into (4.2.2) results in a circuit realizable set of equations, shown below.

$$\begin{bmatrix} i_L \\[1ex] \dot{v}_c \end{bmatrix} = \begin{bmatrix} -\dfrac{d'R_c//R_L}{L} & \dfrac{-d'}{L} \\[2ex] \dfrac{d'}{C}\dfrac{R_L}{R_L + R_c} & \dfrac{-1}{R_L C} \end{bmatrix} \begin{bmatrix} i_L \\[1ex] v_0 \end{bmatrix} + \begin{bmatrix} \dfrac{1}{L} \\[1ex] 0 \end{bmatrix} v_I \qquad (4.2.4)$$

This set of equations can be realized into a single circuit with an ideal transformer as shown in Figure 4.2.1.
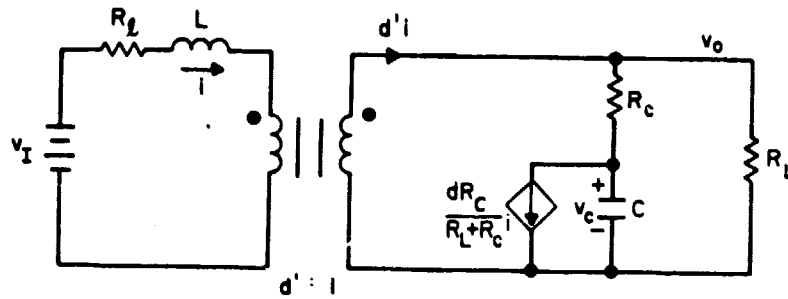
Figure 4.2.1. : Unperturbed discrete-average circuit model
of the boost converter.

Introducing the perturbations noted previously into the
state and output into the circuit of fig. 4.2.1, neglecting
negligibly small departures, simplifying the structure and
assuming $R_c \ll R_L$ one obtains the circuit of Fig. 4.2.2. This
circuit model preserves the input-output properties of the
boost converter and also preserves the properties of the
state variables, inductor current and capacitor voltage, in
the averaged range. The source of the difference discussed
in chapter III can be seen by making a comparison with Fig-
ure 3.2.4. There is no $DD'R_c//R_L$ resistance in Figure 4.2.2
and the average model doesn't contain the two current cont-
rolled sources across R_c. These differences would account
for the variation in modeling the output voltage between the
average and discrete models.

4.3 NUMERICAL EXAMPLE

Using the example that is in Chapter III, a comparison
betwee the Bode plot of the discret-average model and the
discrete models can be made. Figures 4.3.1-4.3.3 show
the Bode plot of the discrete- average model with the dis-
crete model. There is excellent agreeement over all the mo-
dulation frequency range and duty cycle range. There is a
small difference in gain between the two at the higher fre-
quency range above the resonant frequency that is more pro-
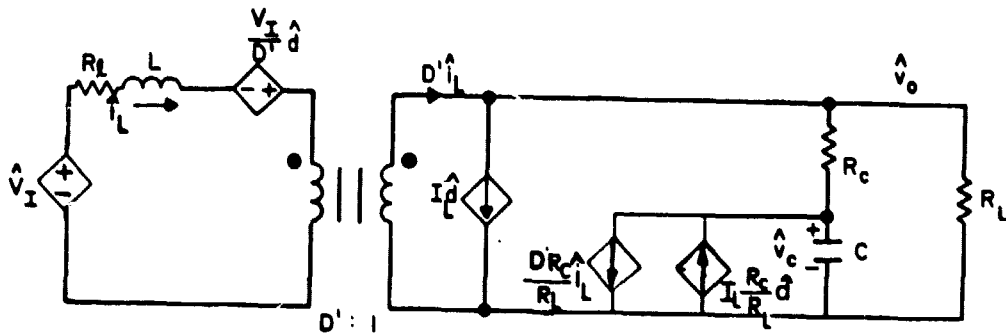
Figure 4.2.2   Perturbed and linearized discrete-average
        circuit model of the boost converter, assuming
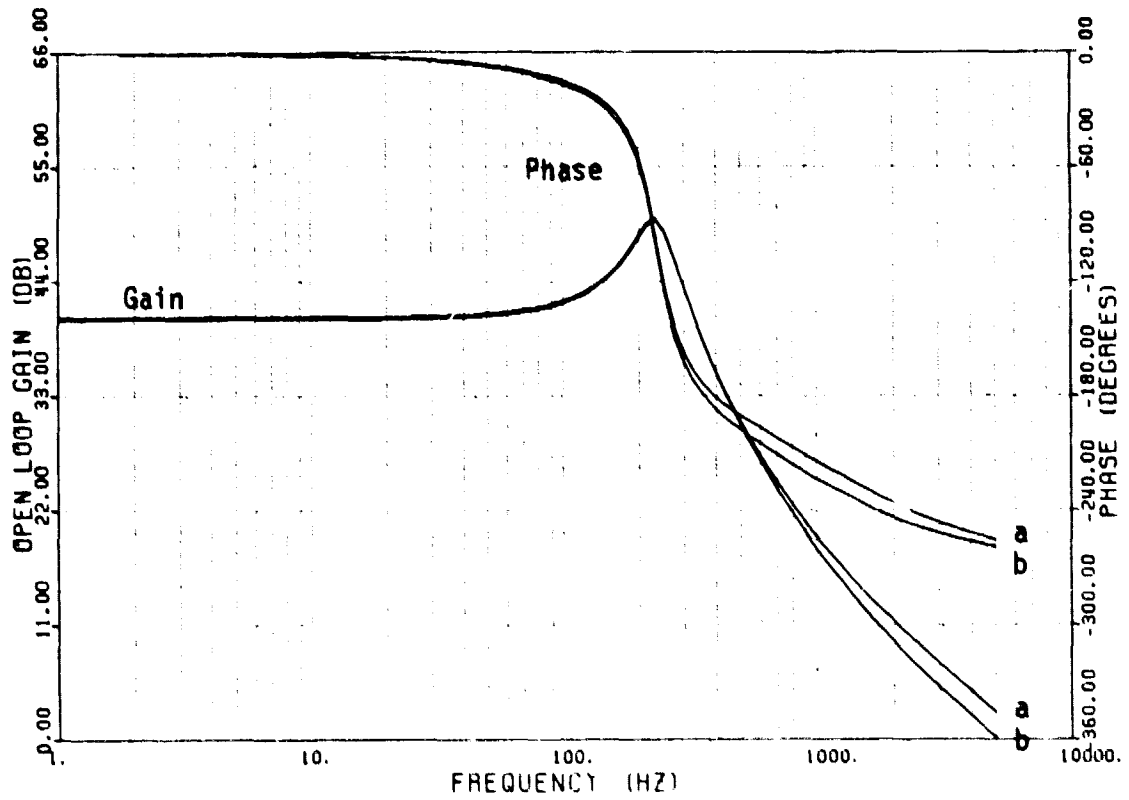 $R_c \ll R_L$

ORIGINAL PAGE IS
OF POOR QUALITY

Figure 4.3.1. Frequency response for the boost converter power stage
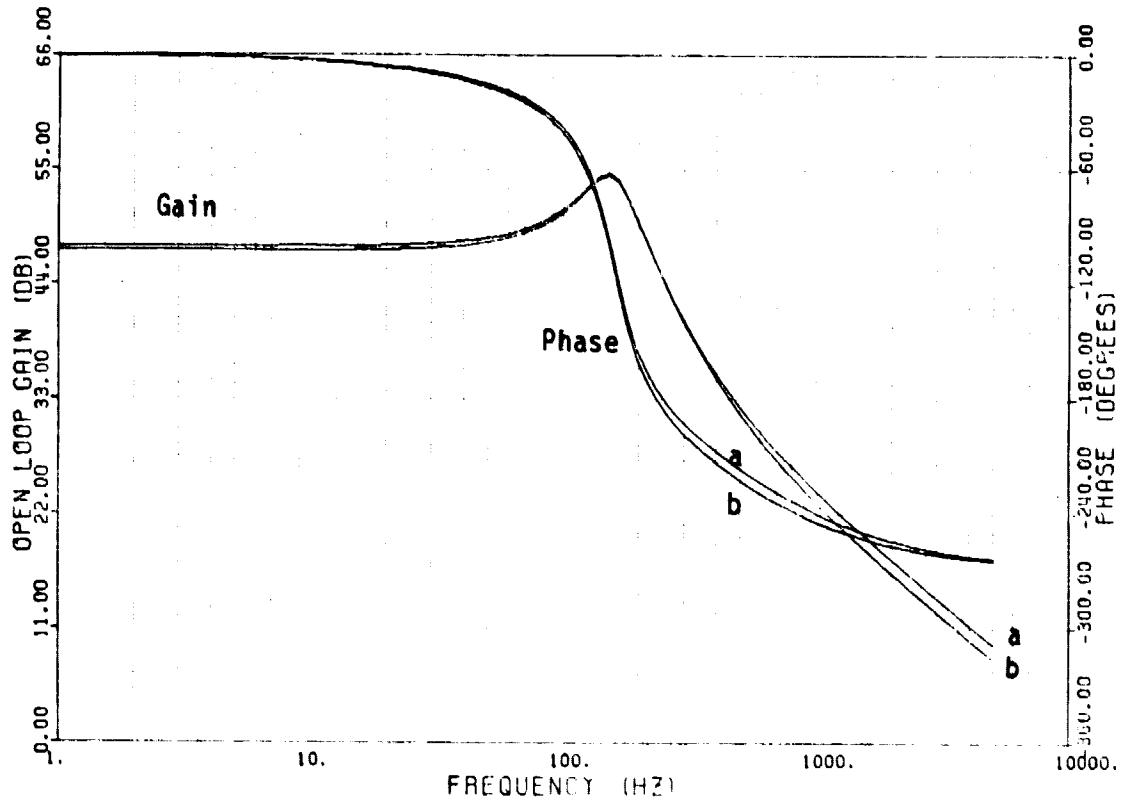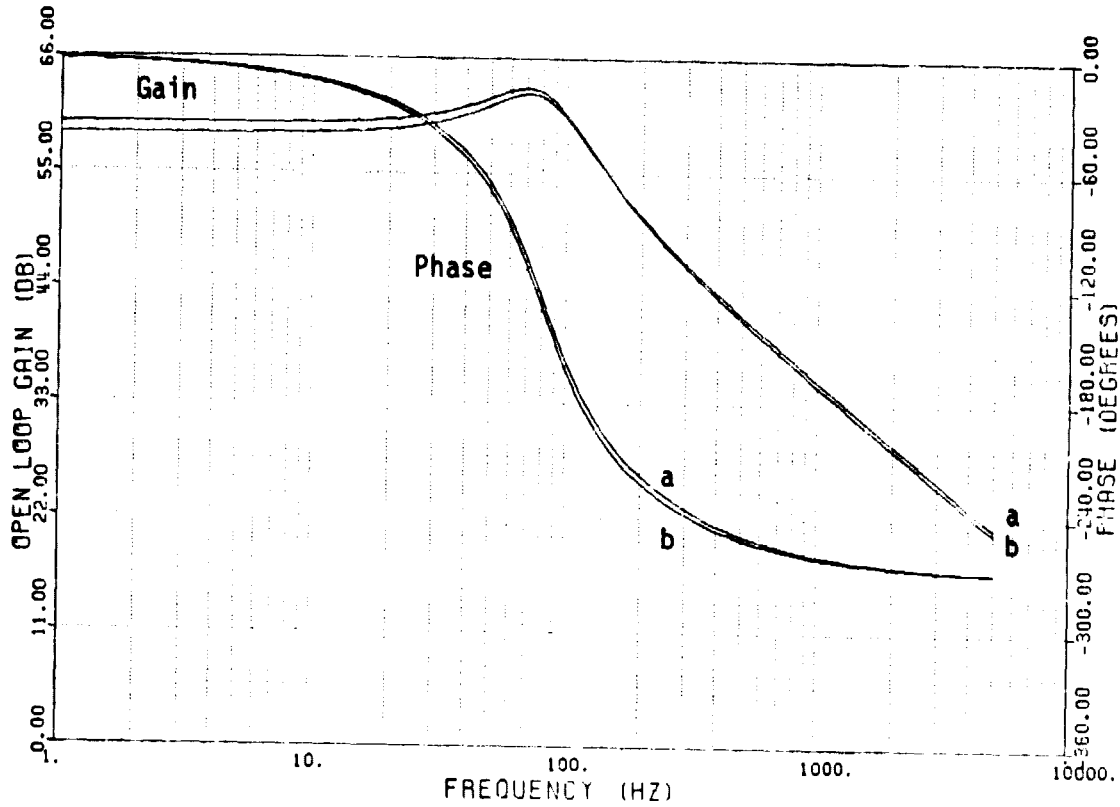with D = .25.
a --- Discrete/Average Model
b --- Discrete Model

Figure 4.3.2. Frequency response for the boost converter power stage
with D = .50.
a ---- Discrete/Average Model
b ---- Discrete Model

Figure 4.3.3. Frequency response for the boost converter power stage
with D = .75.
a --- Discrete/Average Model
b --- Discrete Model

nounced as the duty cycle ratio is increased. This is due
to the small difference in the expressions for the zero giv-
en by each technique. There is no easily discernible bet-
ween the phases.

Figs. 4.3.4-4.3.6 show the Bode plot of the discrete-
average model with the average model. The frequency response
difference between the two becomes significant when the fre-
quency is greater than 1 kHz. The average model has larger
gain and phase angle.

The accuracy of the discrete-average model can be further
demonstrated in the following. Figs. 4.3.7-4.3.10 show the
results obtained from the discrete-average model simulation.
The output voltage waveform is simulated very well in all
the cases. Figures 4.3.8a.), b.), c.), are the simulated
waveforms with the modulation frequency equal to one-fourth
of the switching frequency and the ESR equal to 1., .1 and
.01 ohm, respectively. They show that the discrete-average
output voltage model follows the envelope of the output vol-
tage. Therefore, the model is shown to accurately simulate
the waveform as the ESR of the output filter changes.
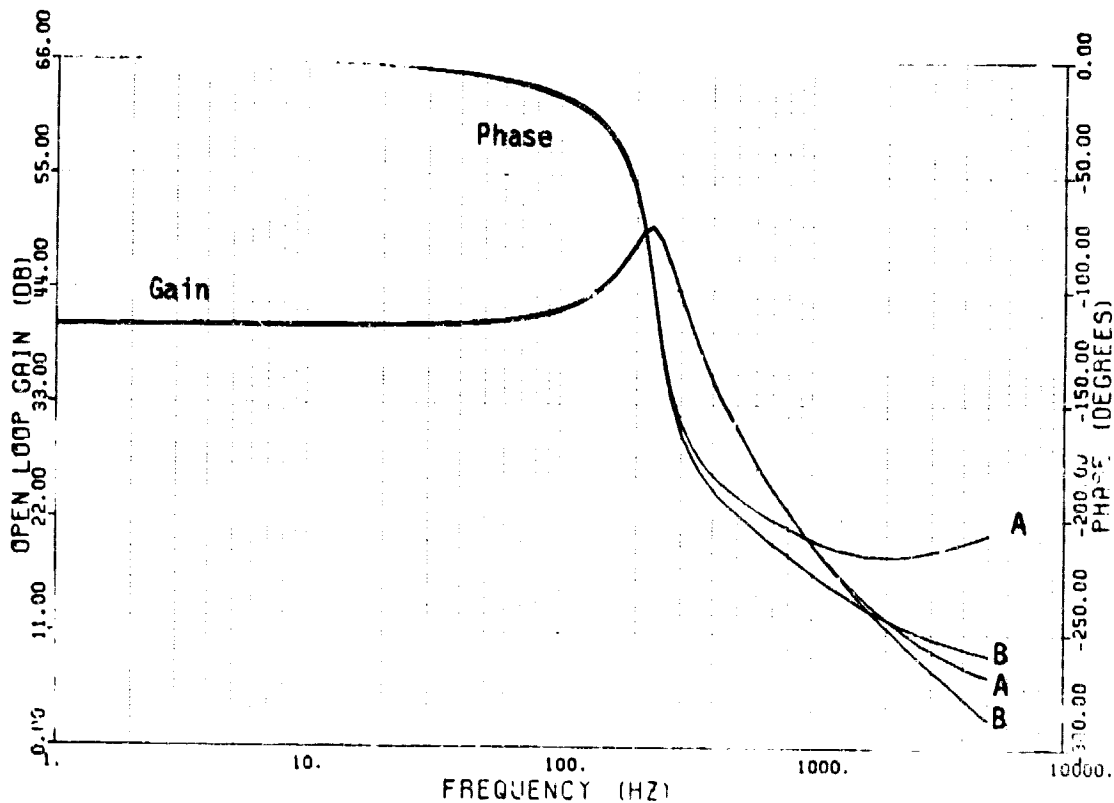
Figure 4.3.4.   Frequency response of the boost converter
        power stage with D=.25.

        A --- Average Model
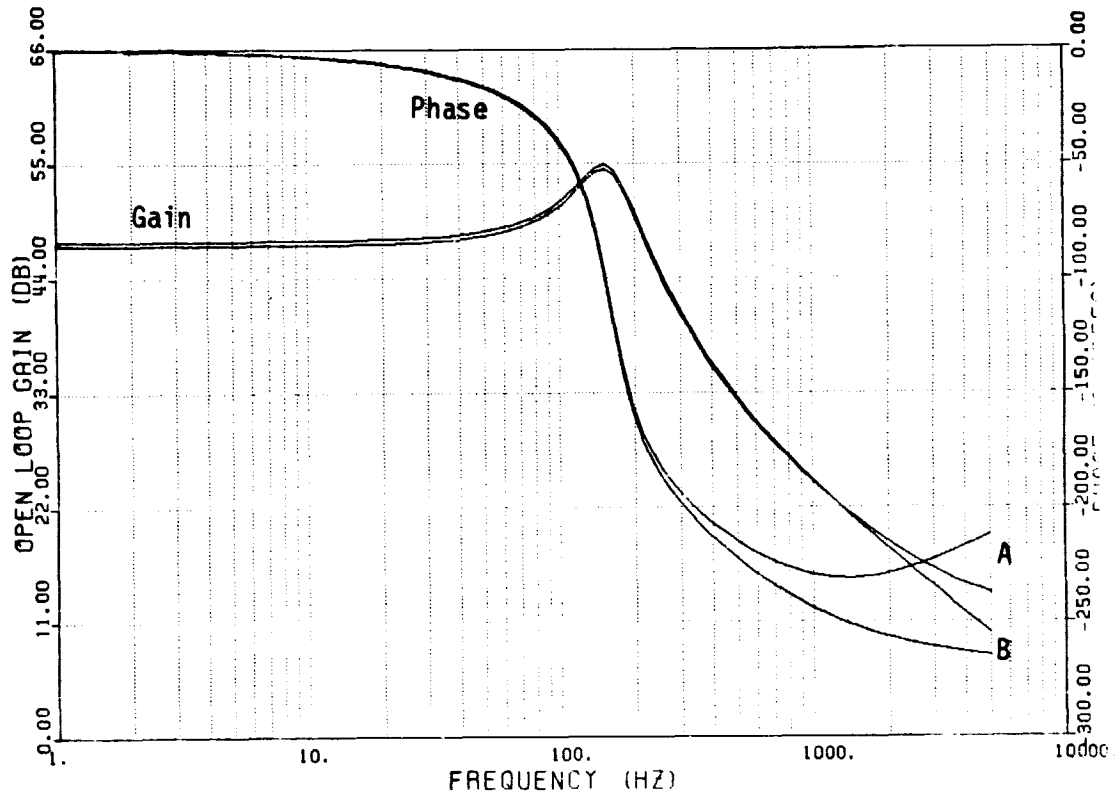   B --- Discrete/Average Model

ORIGINAL PAGE IS
OF POOR QUALITY

Figure 4.3.5.   Frequency response of the boost converter
power stage with D=.5.
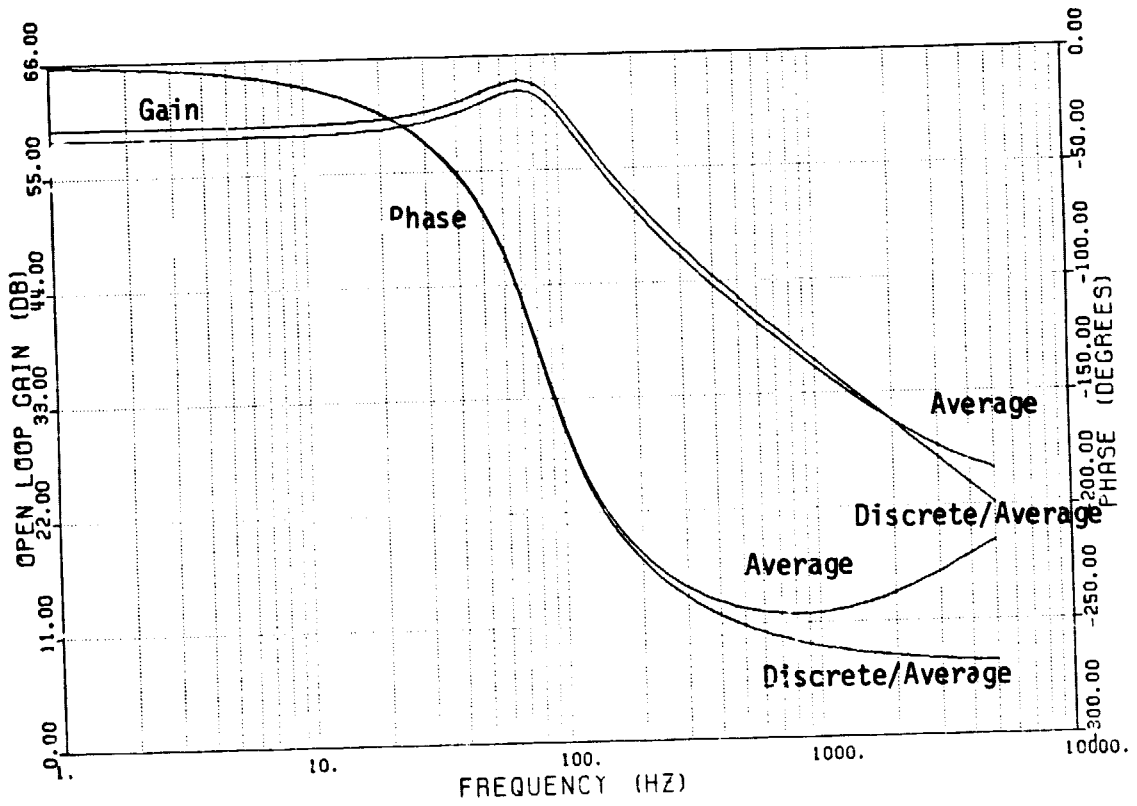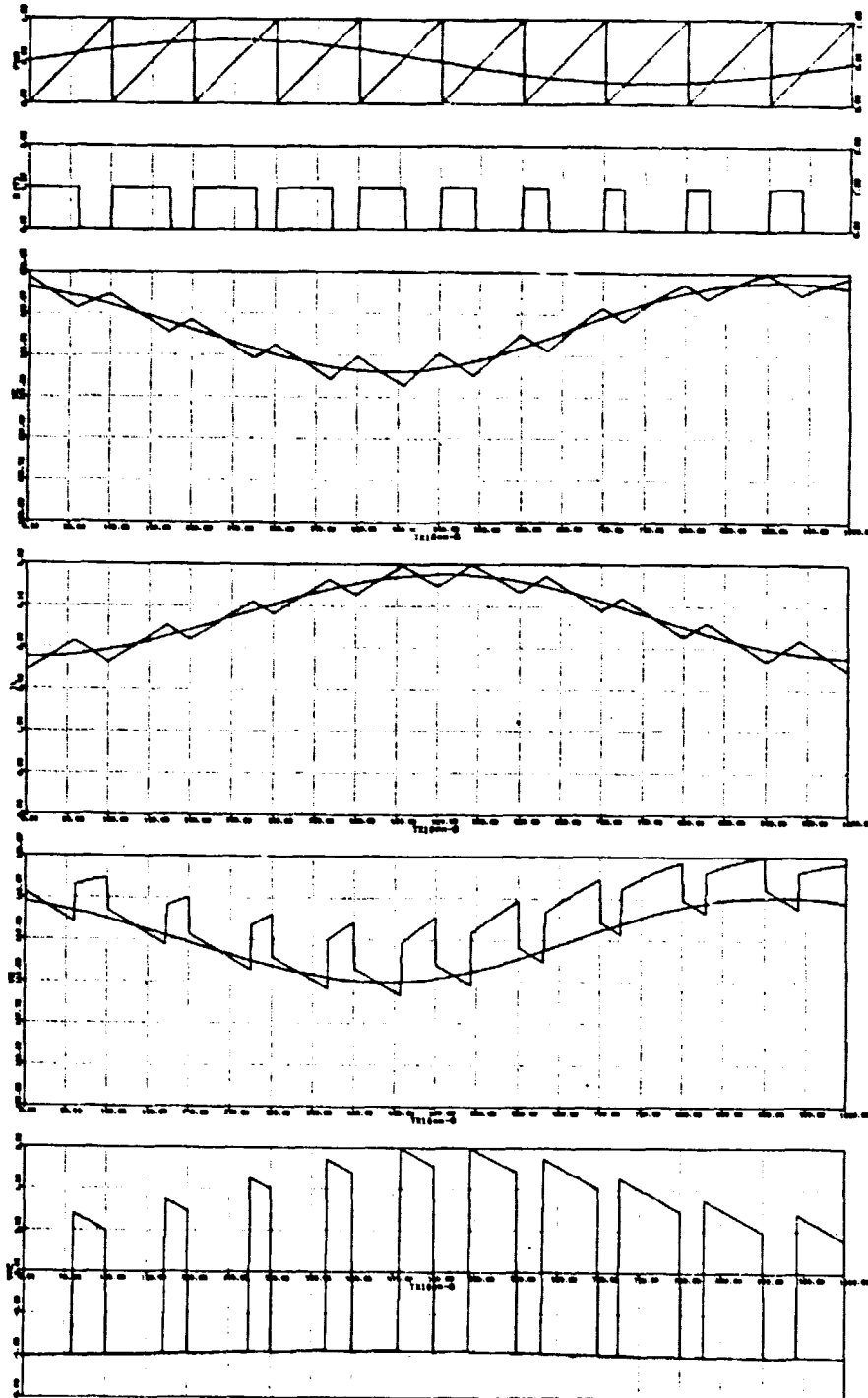A --- Average Model
B --- Discrete/Average Model

Figure 4.3.6.   Frequency response of the boost converter
power stage with D= .75.

Figure 4.3.7. Computer simulated waveforms for boost converter for
one-tenth switching frequency modulation.
Continuous waveforms --- Discrete/Average Model
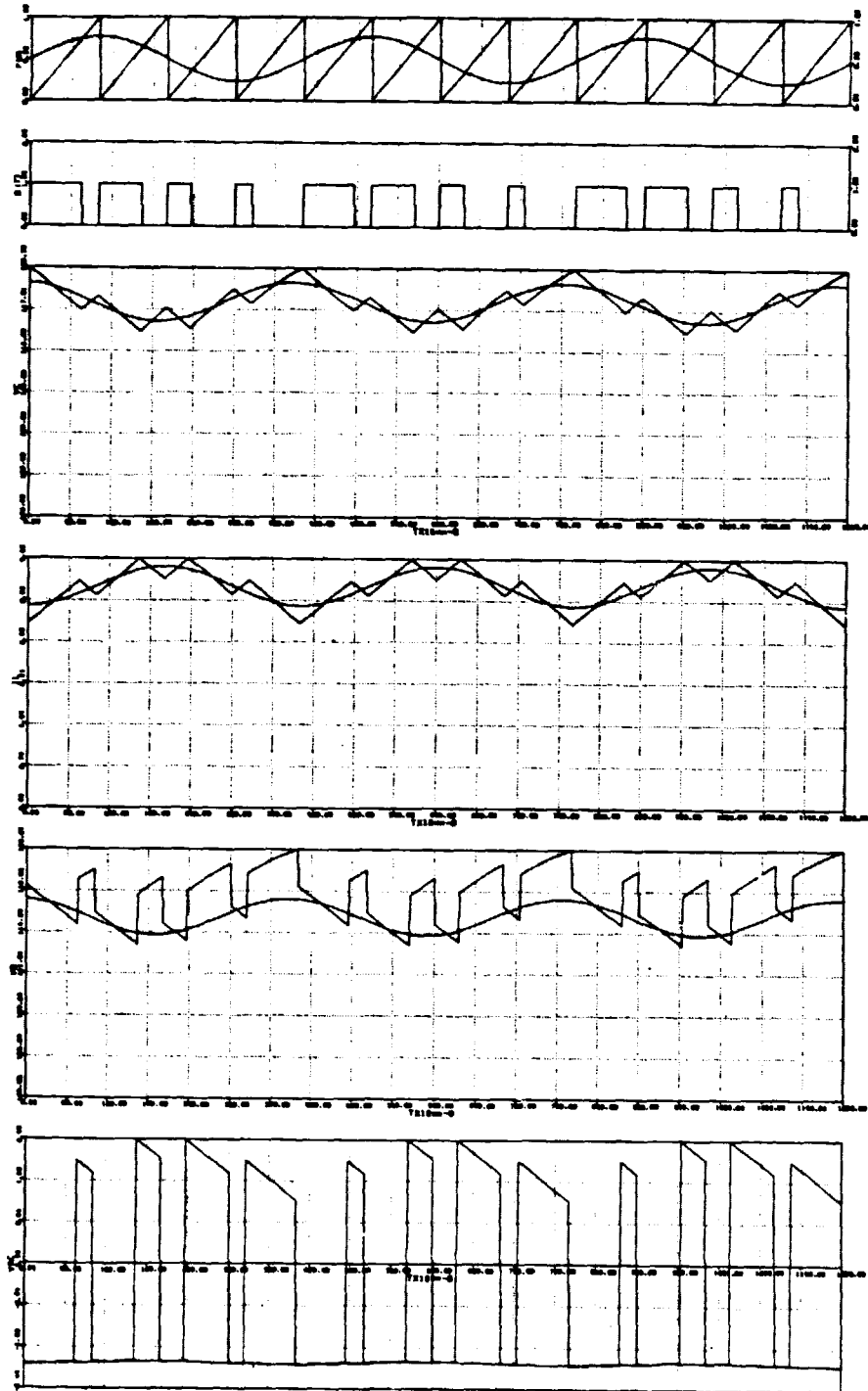Switching waveforms --- Actual circuit behavior

Figure 4.3.8a.   Computer simulation for Boost Converter for
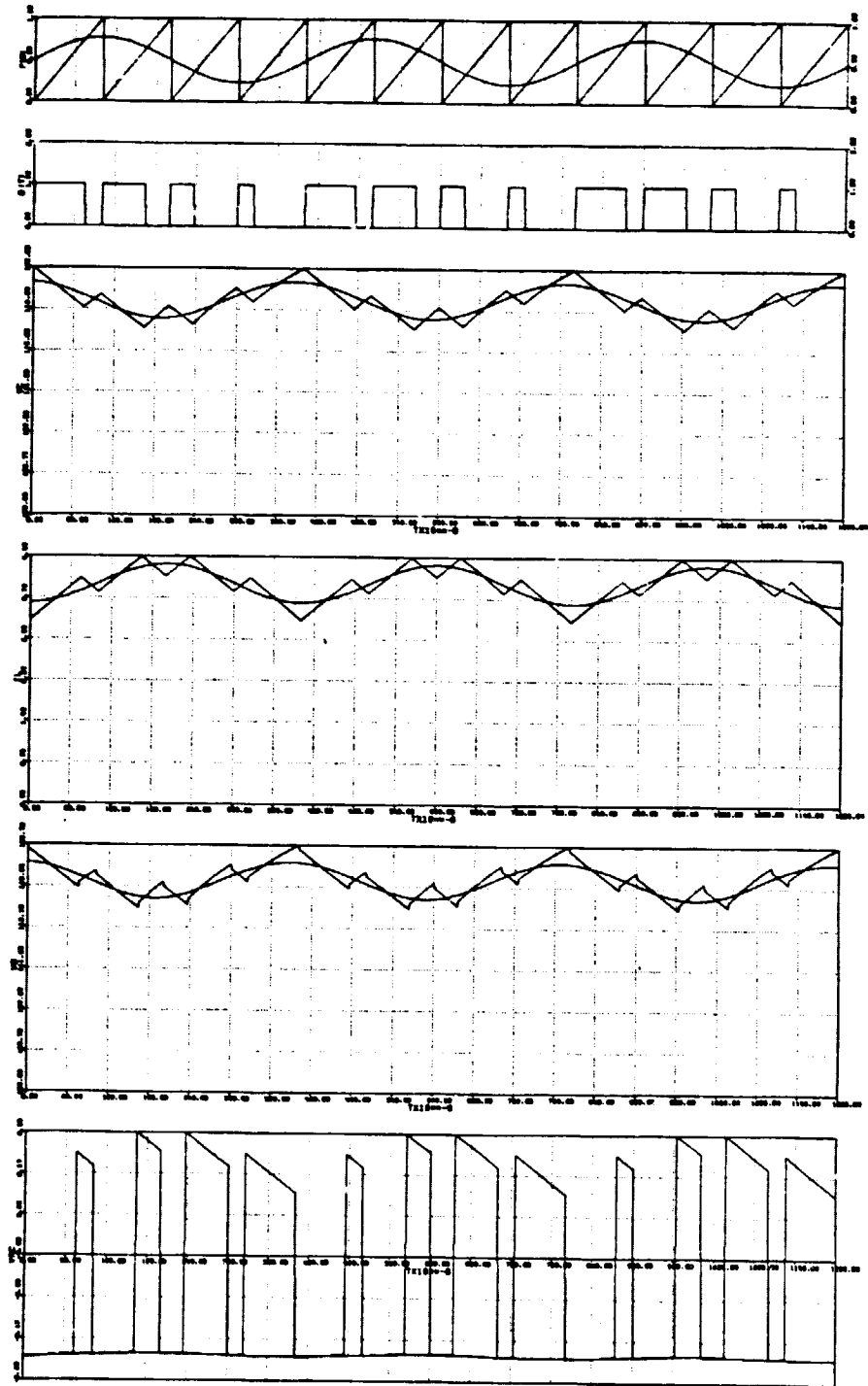one-fourth switching frequency modulation. Rc=
1Ω .

Figure 4.3.8b.   Computer simulation for boost converter for
one-fourth switching frequency.   ESR = .1Ω

101

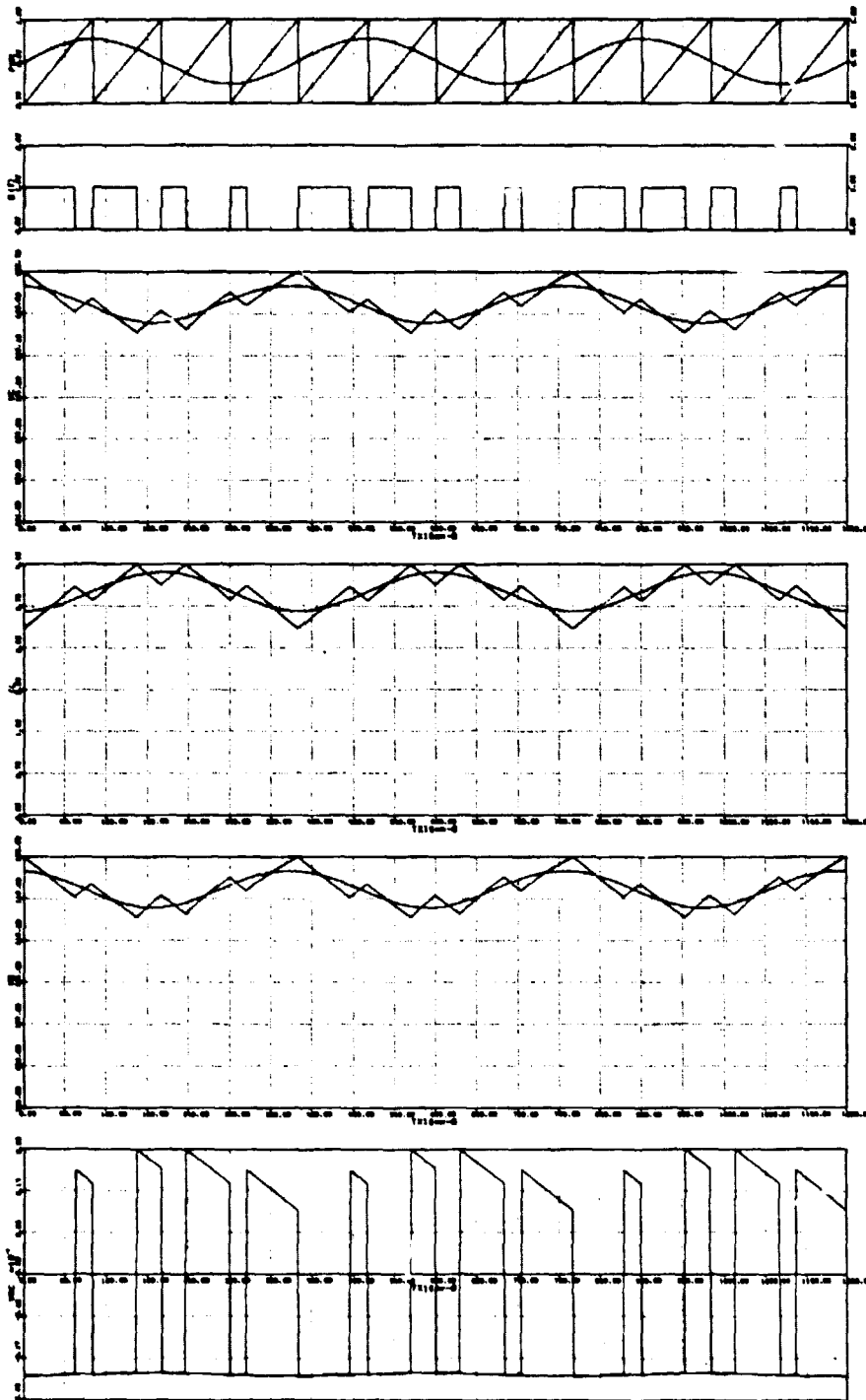Figure 4.3.8c.   Computer simulation for boost converter for
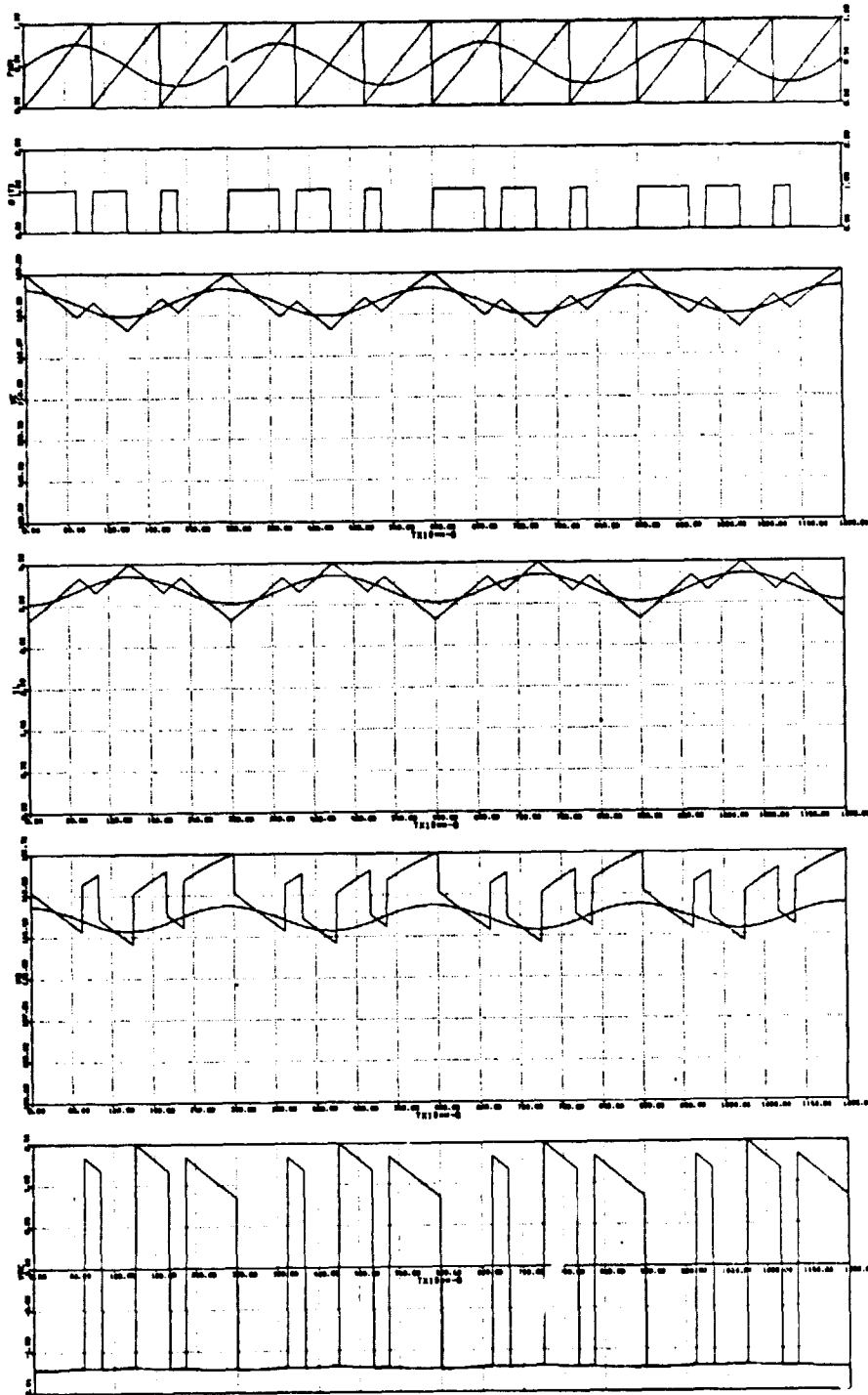one-fourth switching frequency modulation.   ESR
= .01Ω

Figure 4.3.9.   Computer simulation for boost converter for
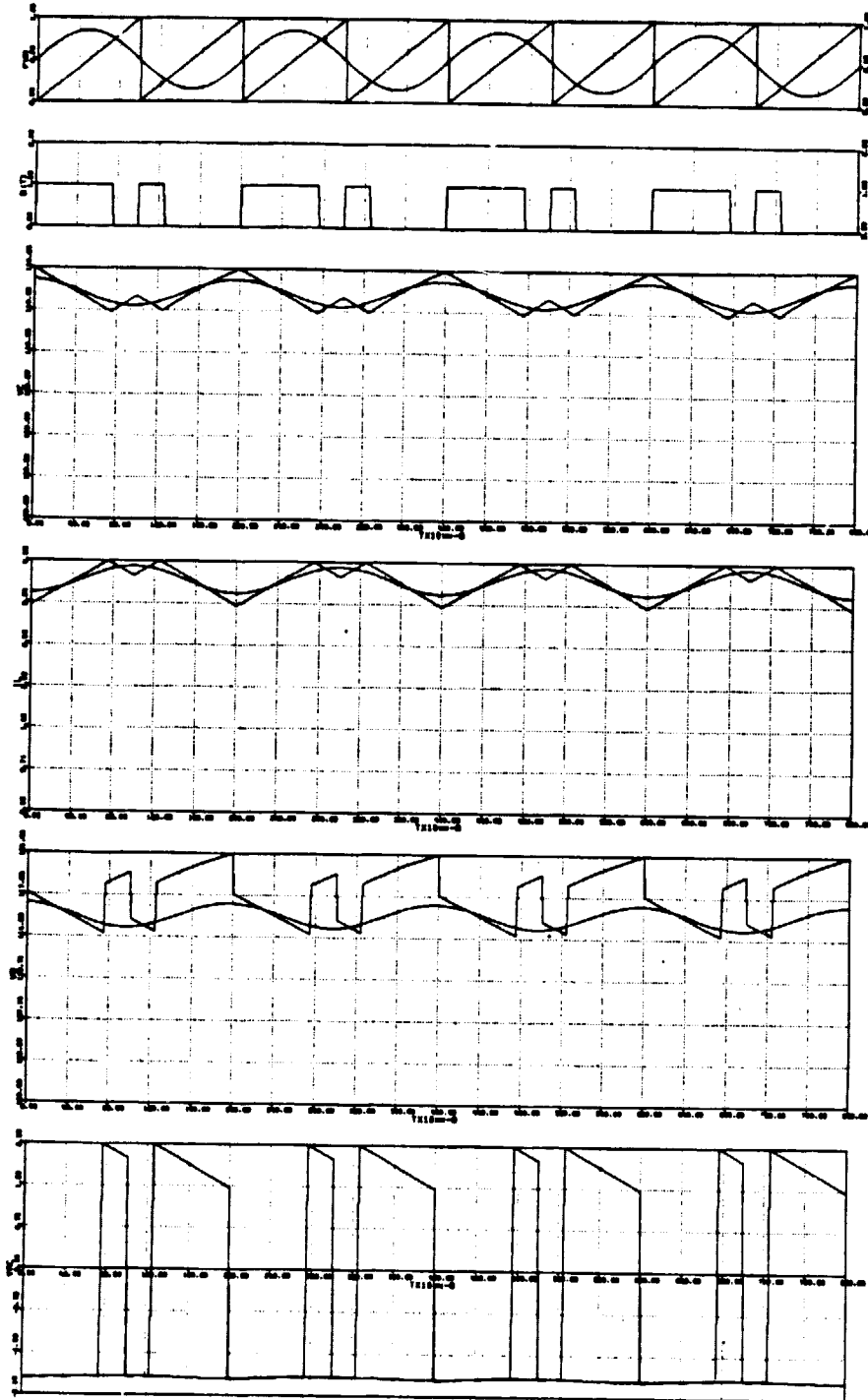one-third switching frequency modulation.

Figure 4.3.10.   Computer simulation for boost converter for
one-half switching frequency modulation.

In verifying the model, attention must be called to the measurement technique. The conventional measurement technique using a network analyzer (gain and phase meter) takes the average of the examined waveforms. This results in an inaccurate prediction for the output voltage waveform as discussed in detail previously and demonstrated in various computer simulation results. Therefore, another verification method is selected, similar to the one reported in [14]. The procedure is as follows:

1. Sample the output voltage.

2. Find the fundamental component of the sampled data of the output voltage waveform.

3. Obtain the gain and phase at each modulatory frequency and plot them along with the analytical results of the discrete-average and average models.

The example that is used for illustration is the same example that has been previously mentioned. Fig. 4.3.11-4.3.13 show the analytical results and experimental data obtained at duty cycle ratios equal to .25, .50 and .75 respectively. For Figures 4.3.11 and 4.3.12, the discrete-average model estimates the data better than the average model.

The following summaries are note worthy:

1. There is good agreement in the low frequency range among the three modeling techniques: discrete, average and discrete-average modeling.
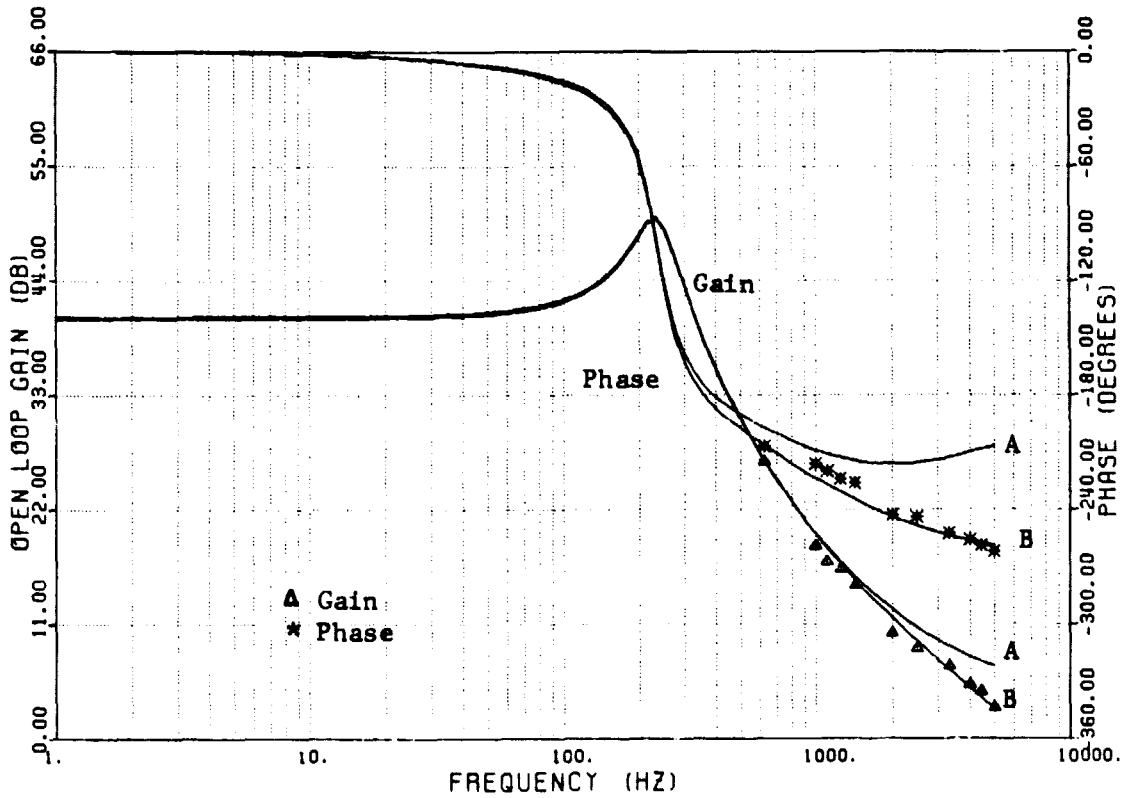
ORIGINAL PAGE IS
OF POOR QUALITY

Figure 4.3.11.   Bode Plots for discrete-average and average transfer
functions.   Constant frequency duty dydle control, D=.25
A -- Average Model
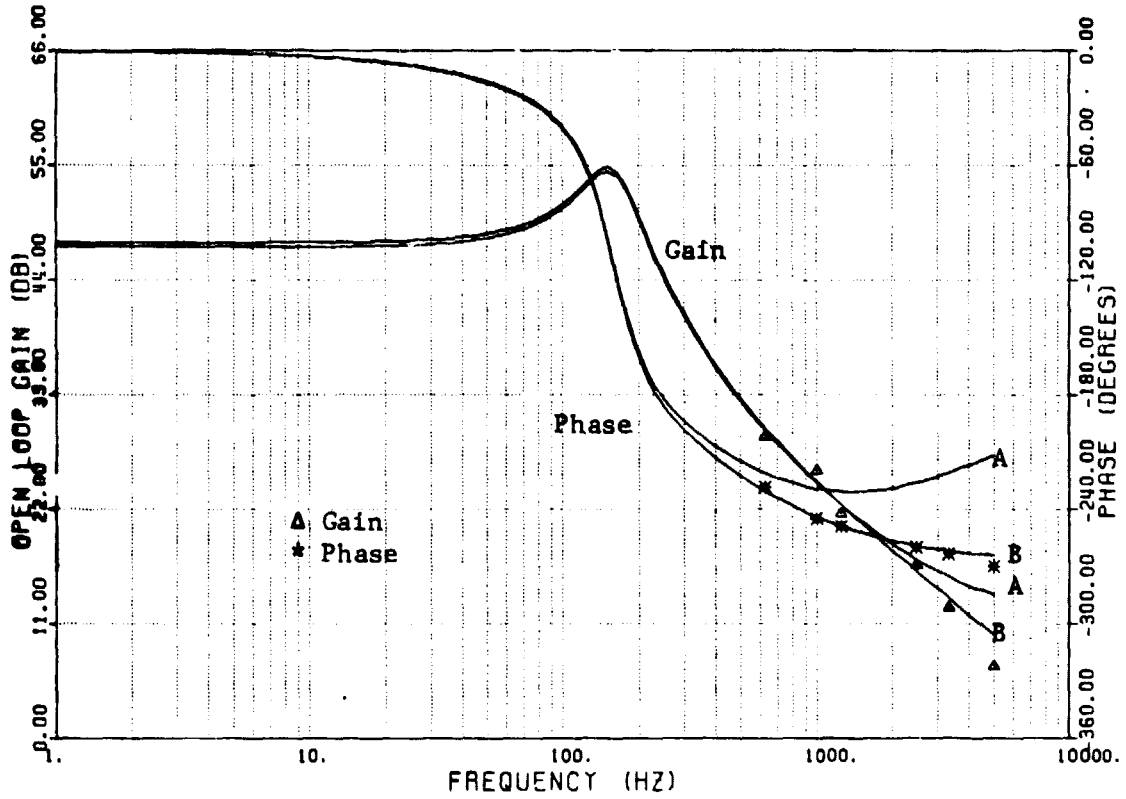B -- Discrete Model

ORIGINAL PAGE IS
OF POOR QUALITY

Figure 4.3.12. Bode Plots for discrete-average and average transfer
functions. Constant frequency duty cycle control, D=.50
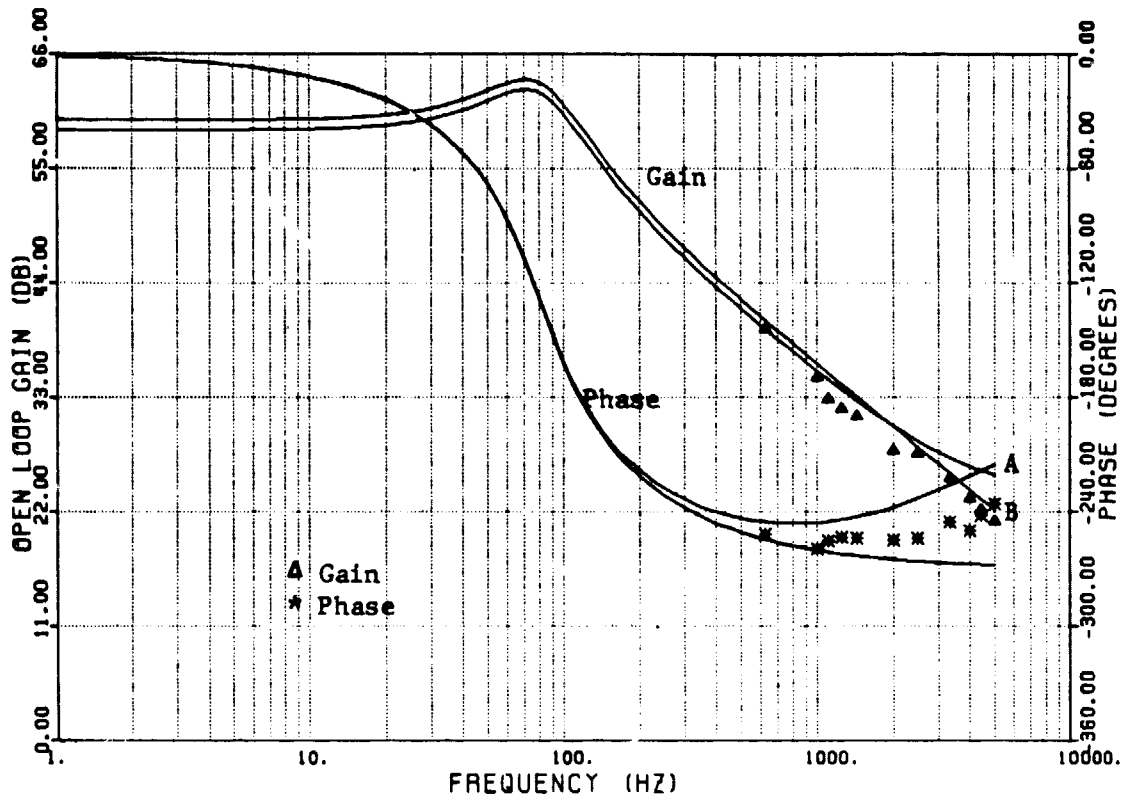A -- Average Model
B -- Discrete-Average Model

Figure 4.3.13. Bode Plots for discrete-average and average transfer
functions with data. Constant frequency duty cycle
control, D=.75
A -- Average Model
B -- Discrete-Average Model

2. The average transfer function tends to diverge from the discrete-average transfer function as the frequency increases above 1 kHz.

3. The discrete-average transfer function remains close to the data as frequency increases.

4. There is good agreement for the phase and gain over the entire frequency range between the data measurement and the discrete-average transfer function.

For Figure 4.3.13, the average state modeling is less accurate than at the lower duty cycles. The discrete-average model estimates the gain better than the average model in the high frequency range and indicates the trend of the phase.

4.4 CONSTANT T_{OFF} & CONSTANT T_{ON} DUTY CYCLE CONTROLLERS

The previous derivation, discussion and example concerned a constant frequency duty cycle controller. This section will discuss the constant T_{OFF} and constant T_{ON} controllers.

4.4.1 Constant T_{OFF} Duty Cycle Controller

Figure 4.4.1. shows the input control signal and ramp with the appropriate duty cycle for a constant T_{OFF} in steady state operation. The duty cycle goes high signalling the power stage
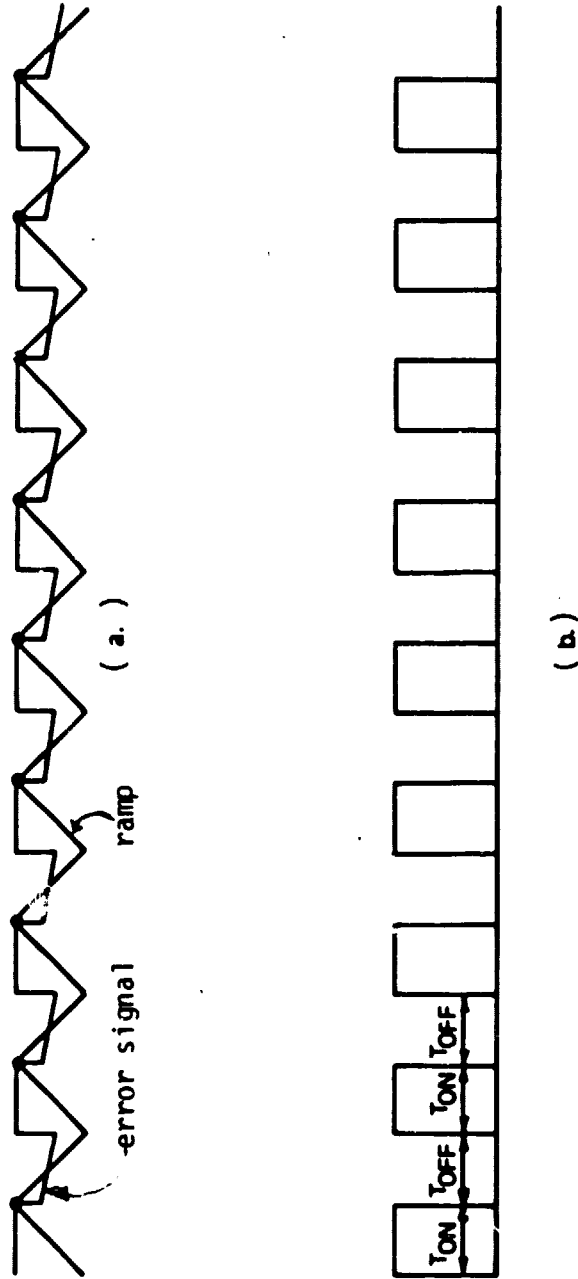
ORIGINAL PAGE IS
OF POOR QUALITY

error signal   ramp

(a.)

T_{ON} T_{OFF} T_{ON} T_{OFF}

(b.)

Figure 4.4.1.   Constant T_{off} controller in steady state

a.)   Input control signal and constant T_{off} ramp signal
b.)   Duty cycle

switch to turn on, when the input control signal intersects the ramp the duty cycle goes low, after a fixed T_{OFF} sec the duty cycle again goes high and the process is repeated. Figure 4.4.2 illustrates the controller when the input control signal is perturbed. After a fixed time T_{OFF} sec the duty cycle signal goes high and when the input control signal intersects the ramp the duty cycle goes low. The T_{ON} time varys from cycle to cycle but T_{OFF} remains constant.

The intersection occurs at the top part of the input control signal, which is the same case as the constant frequency controller. Thus, as with constant frequency controller, for the constant T_{OFF} controller the sampling point for the discrete-average model should be chosen at the beginning of the cycle.
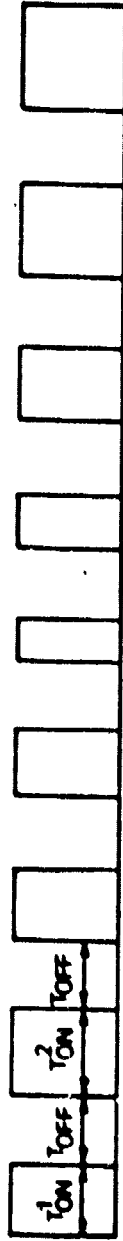
4.4.2   Constant T_{ON} Duty Cycle Controller

Fig. 4.4.3. shows the input control signal and ramp with the appropriate duty cycle for a constant T_{ON} in steady state operation. The duty cycle goes high and remains high for a constant time T_{ON} sec and then goes low. This begins the T_{OFF} interval. The T_{OFF} interval ends when the ramp intersects the input control signal. As discussed previously, the input control signal is essentially the compensated and inverted output voltage ripple. The ramp

Figure 4.4.2. Constant I_{off} with a perturbed input control signal.

a.) Input control signal and constant I_{off} ramp signal
b.) Duty cycle

112

(a.)

error signal

ramp

(b.)

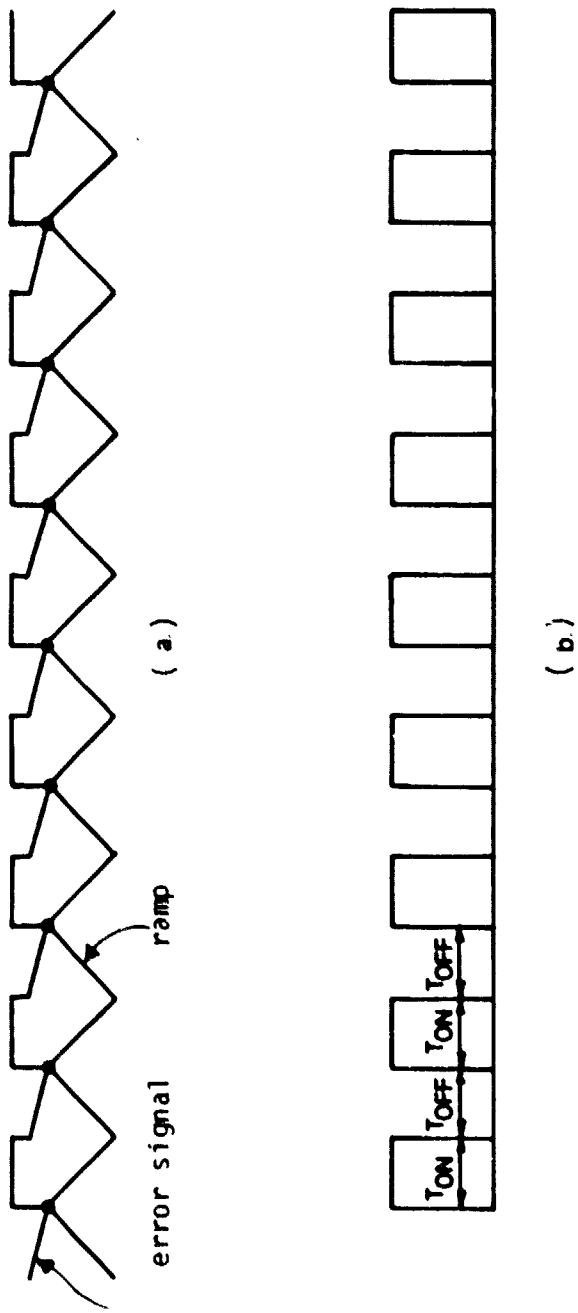T_{ON} T_{OFF} T_{ON} T_{OFF}

Figure 4.4.3. Constant T_{on} controller in steady state.

a.) Input control signal and constant T_{on} ramp signal
b.) Duty cycle
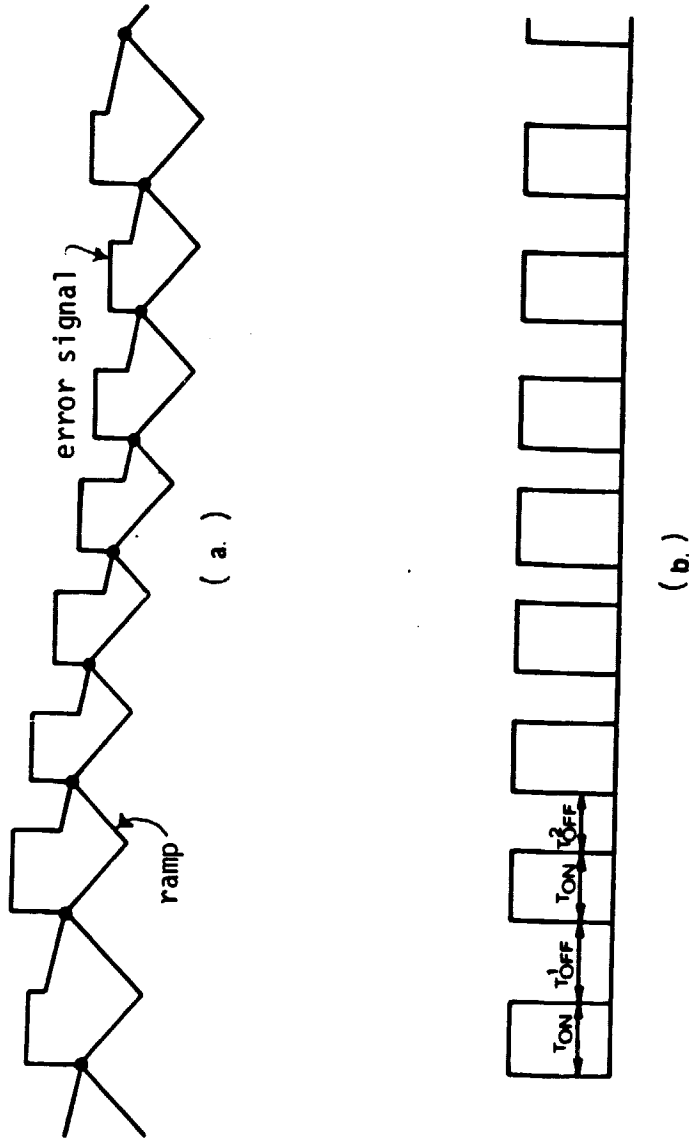
ORIGINAL PAGE IS
OF POOR QUALITY

Figure 4.4.4. Constant T_{on} controller with perturbed input control signal.

a.) Input control signal and constant T_{on} ramp signal
b.) Duty cycle

intersects the bottom part of the error signal. This corresponds to the output voltage ripple during the time that the switch is off. Therefore, a modulation in the duty cycle would correspond to a modulation in the T_{OFF} part of the output voltage ripple. Thus, for a constant T_{ON} controller, the sampling should be chosen at the end of the cycle.

The derivation is the same as shown in section 4.1 except that the output is determined at the end of the cycle so that equation 4.1.3 becomes

$$y(t) = c_2 X(t) \tag{4.4.1}$$

In fact the expressions that are derived are basically the same as those for the constant frequency controller except that the output coefficient vector c_1 is replaced by c_2 The dc model becomes

$$V_o = -c_2 A^{-1} b V_I \tag{4.4.2}$$

The ac model becomes

$$\frac{\hat{v}_o(s)}{\hat{v}_I(s)} = c_2 [sI - A]^{-1} b \tag{4.4.3}$$

$$\frac{\hat{v}_o(s)}{\hat{d}(s)} = c_2 [sI - A]^{-1} [(A_1 - A_2)\underline{X} + (b_1 - b_2)V_I] \tag{4.4.4}$$

Using the boost converter for an example, the $\dfrac{\dot{v}_0(s)}{\hat{d}(s)}$ transfer function determined by the discrete-average model with constant T_{ON} controller for the boost converter is:

$$\frac{\dot{v}_0(s)}{\hat{d}(s)} = \frac{V_I}{(D')^2} \frac{\left(1+\dfrac{R_c}{D'R_L}\right)^2 - \dfrac{R_1}{(D')^2 R}\left(1+\dfrac{R_c}{R_L}\right)}{\left|1+\dfrac{R_c}{D'R_L} + \dfrac{R_L}{(D')^2 R_L}(1+\dfrac{R_c}{R_L})\right|} \cdot \frac{1 + \dfrac{s}{\omega_a}}{1+\dfrac{s}{\omega_0 Q} + \left(\dfrac{s}{\omega_0}\right)^2} \qquad (4.4.5)$$

where $\omega_a = \dfrac{\dfrac{R_L}{R_L + R_c}\left\{\left(1+\dfrac{R_c}{D'R_L}\right)^2 - \dfrac{R_1}{(D')^2 R_L}\left(1+\dfrac{R_c}{R_L}\right)\right\}}{\dfrac{R_c C}{D'}\left\{1+\dfrac{R_c}{D'R_L} + \dfrac{R_1}{D'R_L}\left(1+\dfrac{R_c}{R_L}\right)\right\} - \dfrac{L}{(D')^2 R_L}}$

$\approx \dfrac{1}{\dfrac{R_c C}{D} - \dfrac{L}{(D')^2 R_L}}$, $R_c \ll R_L$

ω_0, Q are the same as in 4.2.1. Comparing this with the previously developed ones.

1. The transfer function has one zero that is positive under most design conditions. ω_a is approximately the same as the one from the discrete transfer function.

2. The 1st order term of the numerator for the discrete, average and constant T_{ON} control discrete-average transfer functions is approximately the same.

3. Zeroes of the transfer function for constant T_{ON} and constant frequency control differ by an amount approximately equal to R_cC.

4. There is no 2nd order term in this the discrete-average transfer function.

5. The natural resonant frequency and Q factor are the same for all models. The power stage gain with $R_\ell = 0$ is the same as with the discrete model.

The difference, as discussed in the above no. 3, between the top envelope (constant T_{ON} duty cycle controller) and the bottom envelope (constant frequency and constant T_{OFF} duty cycle control) is R_cC, approximately. This difference is a small amount, as illustrated in Figure 4.4.5. The figure is a bode plot of the top and bottom envelope of the output voltage ripple. The example is the one that has been used previously, with D = .5. The gain difference is approximately 5db at one-half the switching frequency; the phase difference is a maximum of $10°$ at one-tenth of the switching frequency.

Figure 4.4.6. shows a computer simulated waveform at one-tenth switching frequency. The top and bottom envelope are close in gain and phase.

Figure 4.4.7. shows the bode plot of the top and bottom envelope of the output voltage ripple, when the difference is greater. The example presented here is from chapter VI and
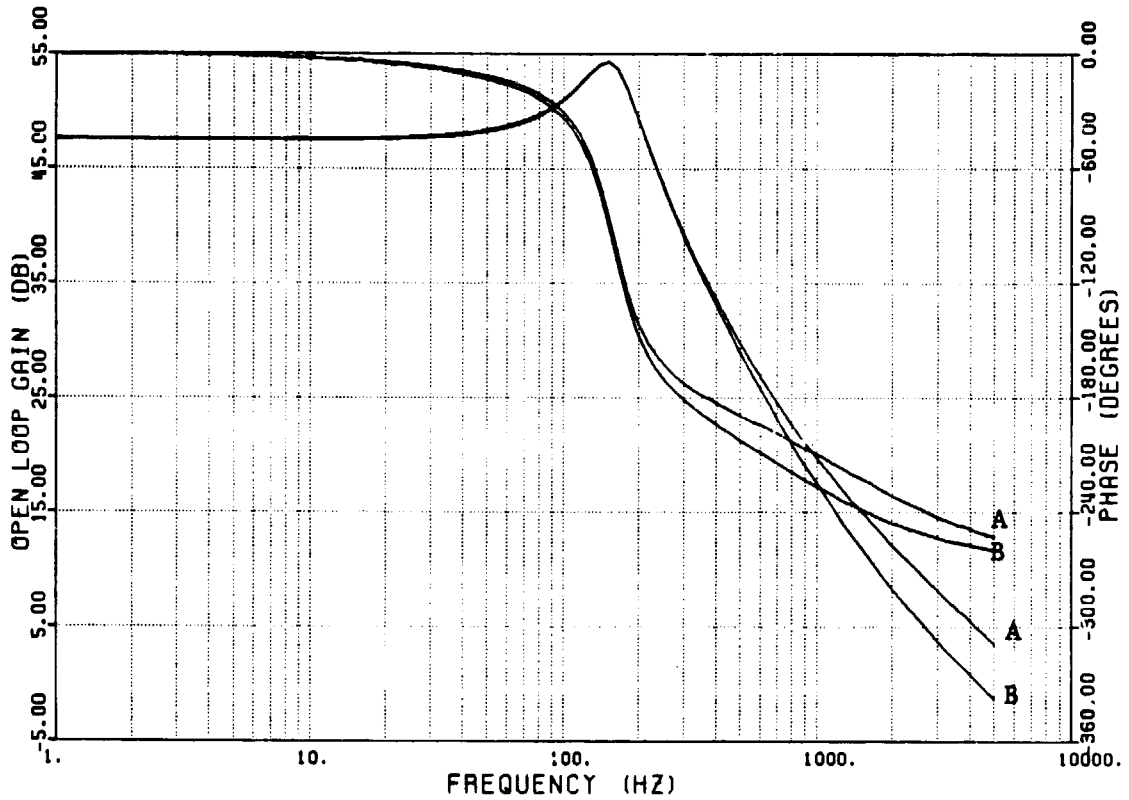
Figure 4.4.5. Bode Plots of the discrete-average transfer function

A -- Constant T_{on} Control

B -- Constant Frequency and Constant T_{off} Controls
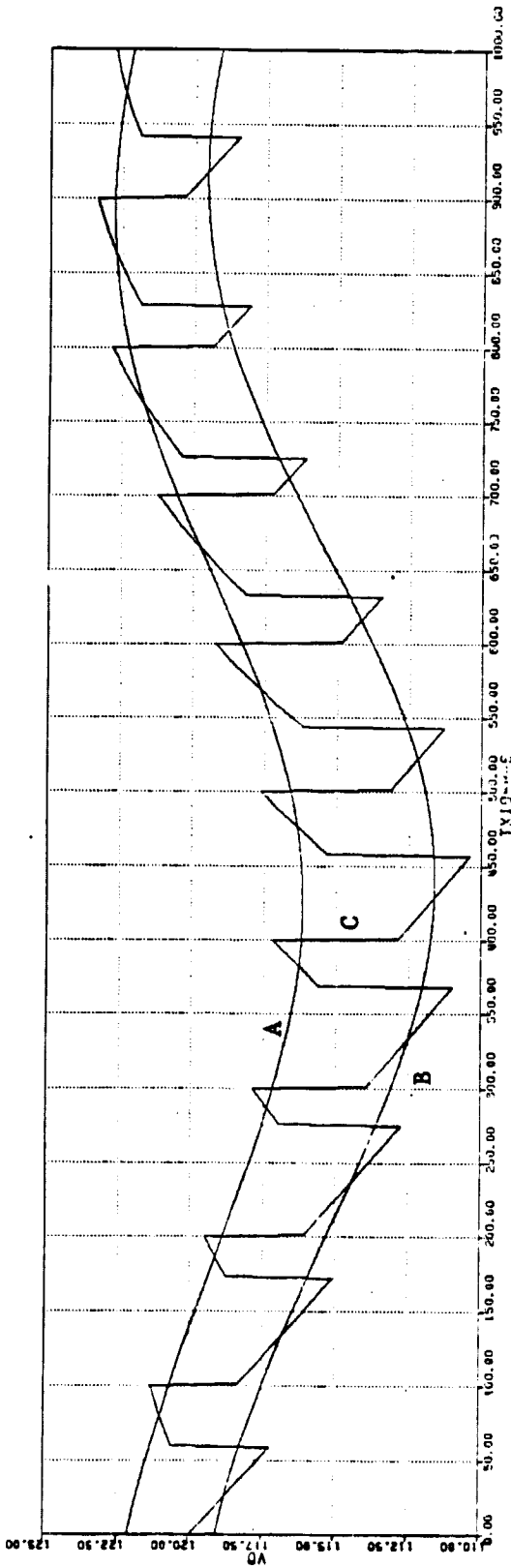
ORIGINAL PAGE IS
OF POOR QUALITY

Figure 4.4.6.   Computer simulation for Boost Converter for one-tenth
switching frequency modulation.

A -- Constant T_{on} Control

B -- Constant Frequency and Constant T_{off} Controls

C -- Discrete waveform

will be discussed later. The zero of equation 4.4.4 is now a negative one, so that the phase delay of the top envelope is much smaller than the bottom envelope. An important observation can be made here that for this system a constant T_{ON} control would be more preferable to use than the others. Since the phase delay is much smaller and the operation of the system would be more stable.

Figure 4.4.8 shows computer simulated waveforms at one-tenth switching frequency. The bottom envelope is more clearly seen in Figure 4.4.8b.) where the discrete waveform has been removed. The difference in gain and phase is obvious. The numerical example that was used in section 4.3 is used to show the accuracy of the constant T_{ON} control discrete-average model. The difference in the example is that a constant T_{ON} duty cycle controller is used to determine the duty cycle. The same method for obtaining data is used.

Figures 4.4.9-4.4.11 show the analytical results and experimental data obtained at duty cycle ratios equal to .25, .50 and .75, respectively. The results are the same shown in the previous section for the discrete-average model. There is excellent agreement for the phase and gain over the entire frequency range between the data measurement and the discrete-average transfer function.
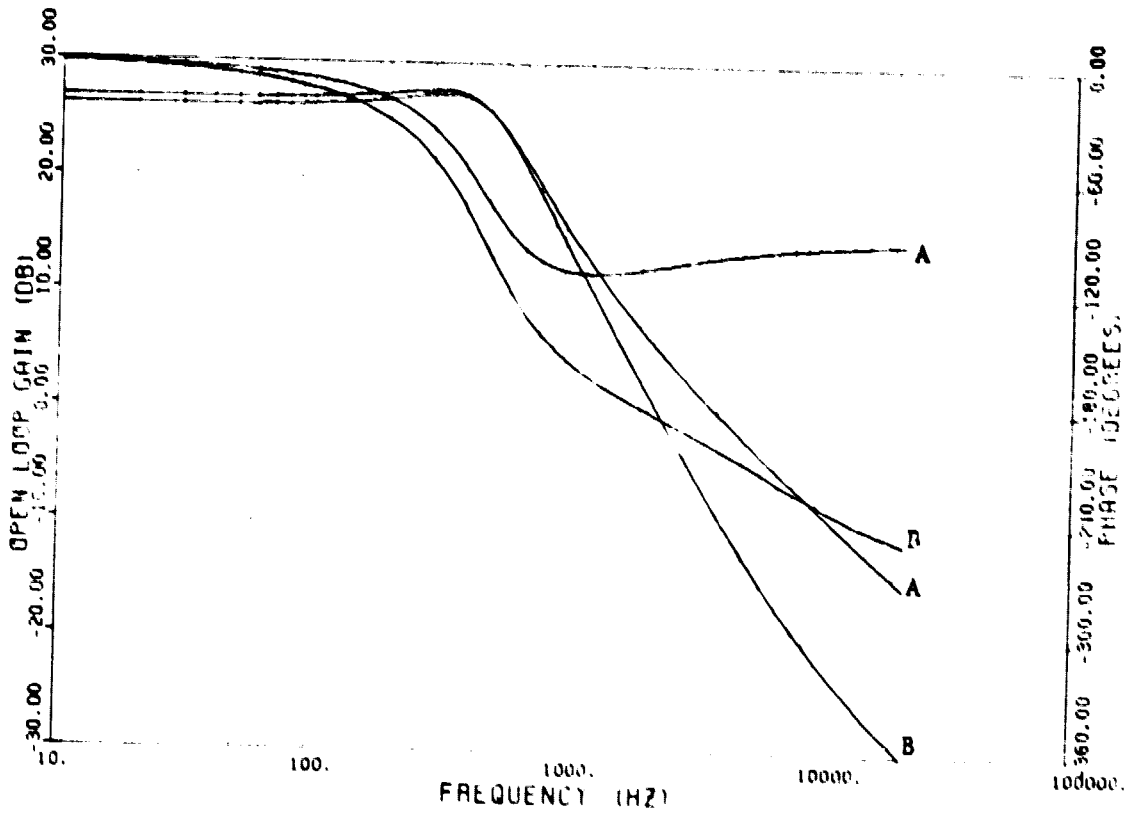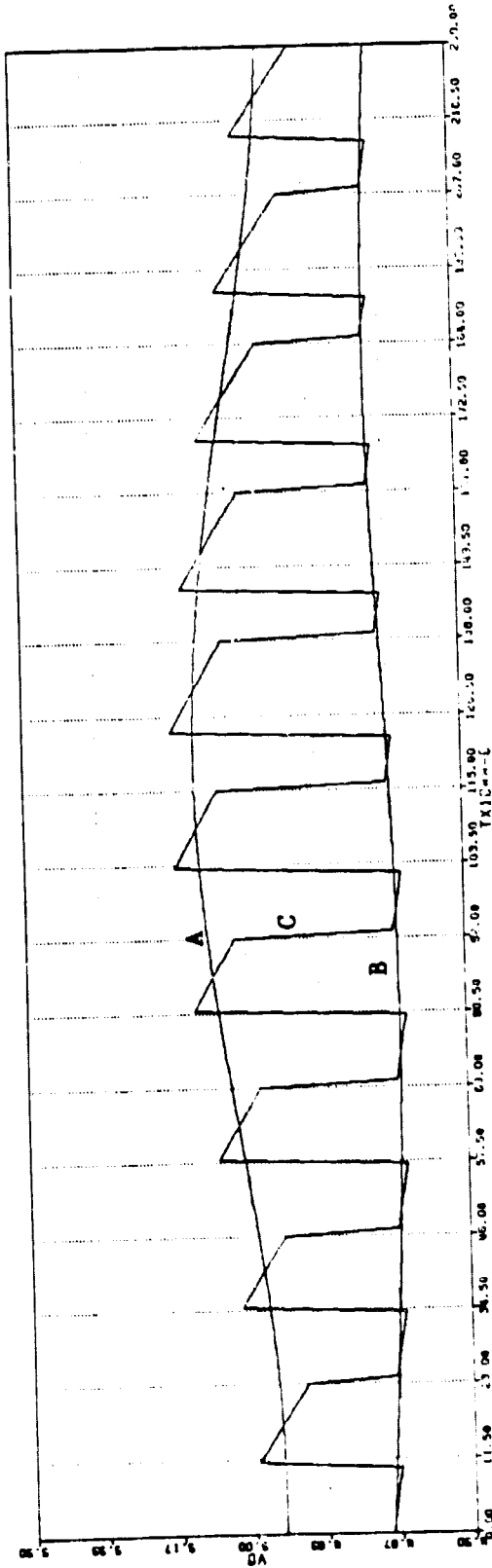
Figure 4.4.7. Bode Plots of discrete-average transfer function.
A -- Constant T_{on} Control
B -- Constant Frequency and Constant T_{off} Controls

Figure 4.4.8 a.) Computer simulation for Boost Converter for one-tenth switching frequency
modulation

A -- Constant T_{on} control

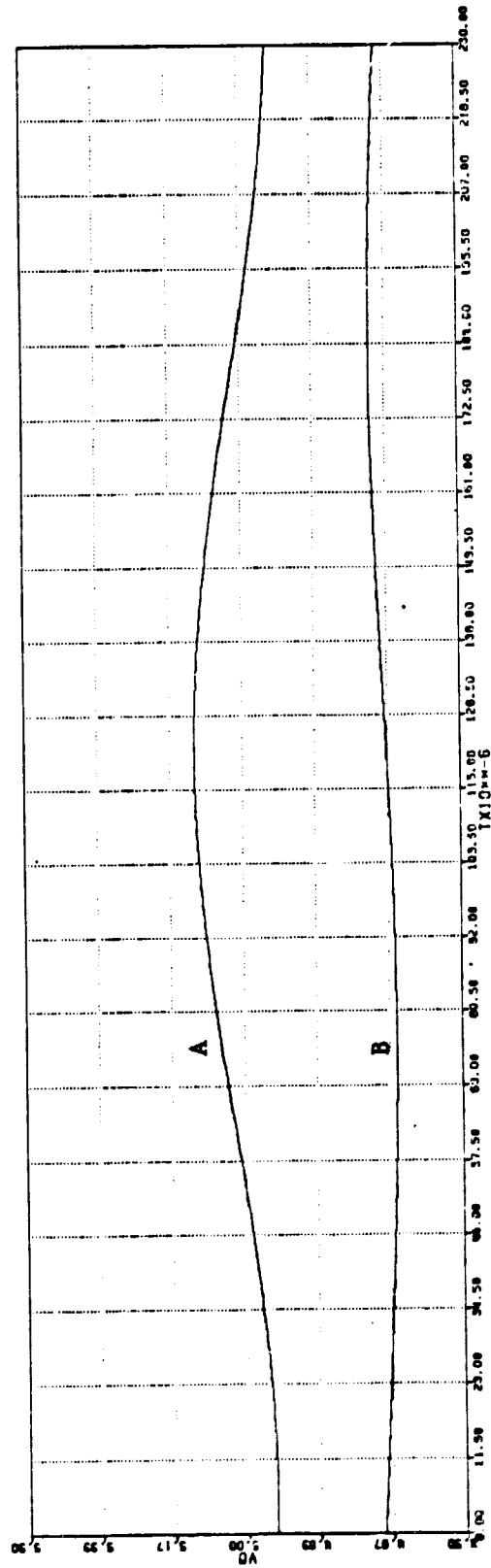B -- Constant frequency and constant T_{off} controls

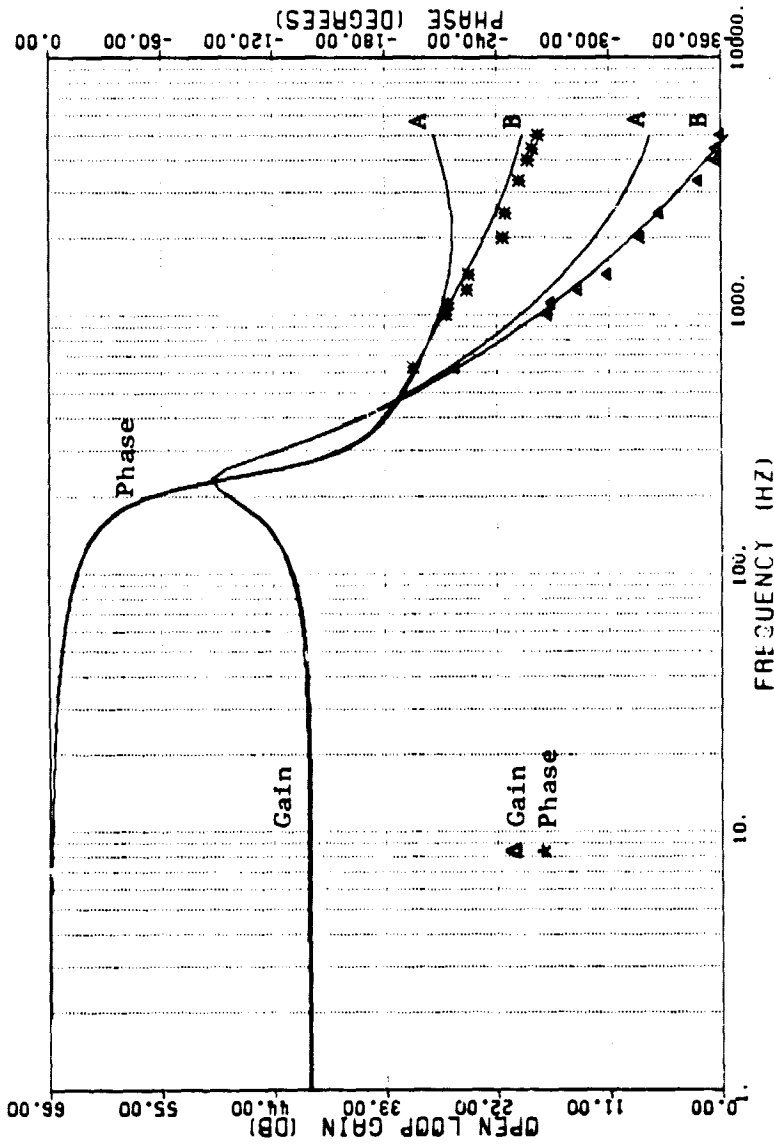C -- Discrete waveform

122

Figure 4.4.8 b.)

Figure 4.4.9. Bode Plots for discrete-average and average transfer functions with data, D=.25. Constant T_{on} duty cycle control.

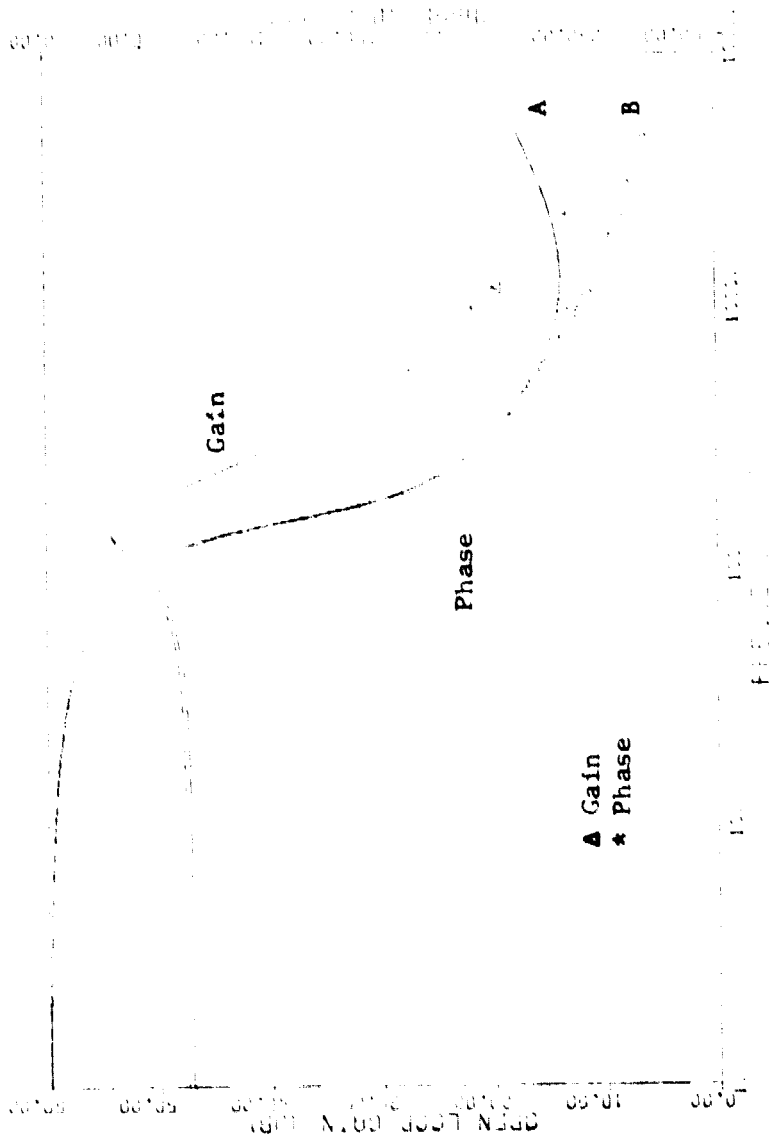A -- Average Model
B -- Discrete-Average Model

Figure 4.4.10. Bode Plots for discrete-average and average transfer functions
with data, D=.50. Constant T_{on} duty cycle control.
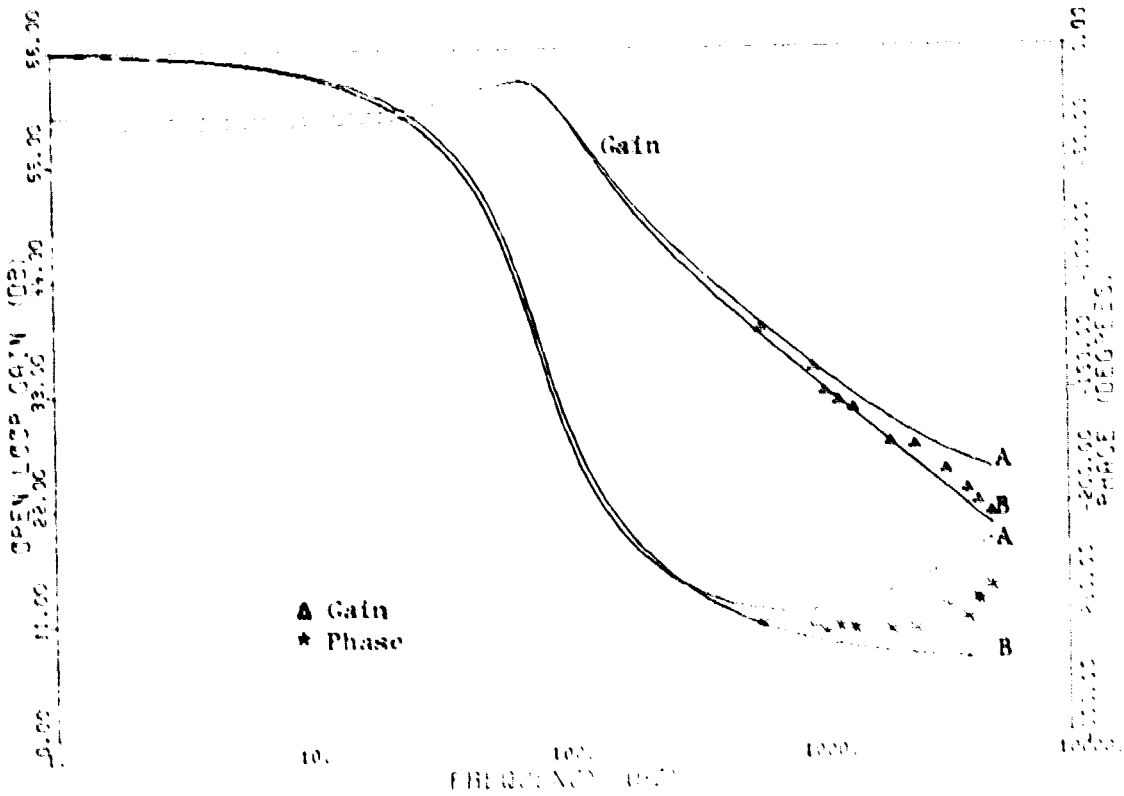A -- Average Model
B -- Discrete-Average Model

Figure 4.4.11. Bode Plots for discrete-average and average transfer
functions with data, D=.75. Constant T_{on} duty cycle
control.
A -- Average Model
B -- Discrete-Average Model

For figure 4.4.7, the average state modeling is less accurate than at the lower duty cycles. The discrete-average model estimates the gain better than the average model in the high frequency range and indicates the trend of the phase.

Chapter V

CONTINUOUS TIME MODELS OF THE BUCK, BOOST AND BUCK/BOOST CONVERTERS

The power stage model presented in the previous chapter has two inputs (input voltage and duty cycle ratio) and one output (output voltage). The purpose of this chapter is to extend the discrete-average model to include the load disturbance as another input and the inductor current (mmf) and capacitor voltage as additional outputs.

5.1 THREE INPUT THREE OUTPUT MODEL DEVELOPMENT

During T_{ON}, the state equations for each of the converters are expressed by:

$$\dot{\underline{x}} = A_1 \underline{x} + b v_1 V_I + b i_1 i_o \tag{5.1.1}$$

where i_o is the load disturbance, represented by a current injected into the output node.

During T_{OFF}, the state equations are expressed by:

$$\dot{\underline{x}} = A_2 x + b v_2 V_I + b i_2 i_o. \tag{5.1.2}$$

The output expression is given by:

$$y = c_2\underline{x} + gi_o = \begin{bmatrix} v_o \\ i_L(\emptyset) \\ v_c \end{bmatrix} \qquad (5.1.3)$$

The state variable representations are averaged to give a single period representation as shown below:

$$\dot{\underline{x}} = (dA_1 + d'A_2)\underline{x} + (db_{v1} + d'b_{v2})v_I$$
$$+ (db_{i1} + d'b_{i2})i_o \qquad (5.1.4)$$

and $\underline{y} = c_2\underline{x} + gi_o$.

Introducing variations in the line voltage, duty cycle ratio and load disturbance by the following substitutions

$$v_I = V_I + \hat{v}_I,$$
$$d = D + \hat{d},$$
$$d' = D' - \hat{d},$$
$$i_o = I_o + \hat{i}_o, \quad (I_o = 0)$$

will cause perturbations in the state and output, as shown below.

$$\underline{x} = \underline{X} + \hat{\underline{x}}$$
$$\underline{y} = \underline{Y} + \hat{\underline{y}}.$$

This results in the following model:

$$\dot{\underline{x}} = A\underline{X} + b_v V_I + b_v \hat{v}_I$$

$$+ (A_1 - A_2 \underline{X} + (b_{v1} - b_{v2})V_I]\hat{d}$$

$$+ b_i \hat{i}_o + \text{2nd order terms}$$

$$\underline{Y} + \hat{\underline{y}} = c_1 \underline{X} + c_1 \hat{\underline{x}} + g\hat{i}_o$$

where $A = DA_1 + D'A_2$

$\quad b_v = Dbv_1 + D'bv_2$

$\quad b_i = Dbi_1 + D'bi_2.$

Assuming that departures of the states from their corresponding steady state values are small compared to the steady state values themselves allows the 2nd order terms in (5.1.5) to be neglected. The discrete-average model in its 3 input-3 output form is shown below. The dc model is:

$$0 = A\underline{X} + b_v V_I$$

$$(5.1.6)$$

$$\underline{Y} = c_1 \underline{X}.$$

The dc operating point can be determined by solving for $\underline{X}$ in (5.1.6a) and substituting into (5.1.6b); the following results are obtained

$$Y = \begin{bmatrix} V_o \\ I_L(\emptyset) \\ V_c \end{bmatrix} = -c_1 A^{-1} b_v V_I. \qquad (5.1.7)$$

The ac model is:

$$\dot{\underline{x}} = A\hat{\underline{x}} + b_v\hat{v}_I + [(A_1 - A_2)\underline{X}$$
$$+ (bv_1 - bv_2)V_I]\hat{d} + b_i\hat{i}_o \qquad (5.1.8)$$
$$\hat{\underline{y}} = c_1\hat{\underline{x}} + g\hat{i}_o$$

The transfer functions can be found by taking the Laplace transformation of (5.1.8), solving for $\underline{x}$ (s) and substituting into (5.1.8b). This results in:

$$\hat{\underline{y}}(s) = c_1[sI-A]^{-1}\{b_v\hat{v}_I(s)$$
$$[(A_1 - A_2)\underline{X} + (bv_1 - bv_2)V_I]\hat{d}(s)$$
$$+bi\hat{i}_o(s)\} + g\hat{i}_o(s) \qquad (5.1.9)$$

The duty cycle to output transfer function is:

$$\frac{\hat{\underline{y}}(s)}{\hat{d}(s)} = \begin{bmatrix} \dfrac{\hat{v}_0(s)}{\hat{d}(s)} \\[2ex] \dfrac{\hat{i}_L(s)(\theta)}{\hat{d}(s)} \\[2ex] \dfrac{\hat{v}_c(s)}{\hat{d}(s)} \end{bmatrix} = c_1[sI - A]^{-1}[A_1-A_2\underline{X} + (bv_1-bv_2)V_I].$$

$$(5.1.10)$$

The load disturbance to output transfer function is:

$$\frac{\hat{y}(s)}{\hat{i}_o(s)} = \begin{bmatrix} \dfrac{\hat{v}_0(s)}{\hat{i}_0(s)} \\[2em] \dfrac{\hat{i}_L(s)(\emptyset)}{\hat{i}_0(s)} \\[2em] \dfrac{\hat{v}_c(s)}{\hat{i}_0(s)} \end{bmatrix} = c_1[sI - A]^{-1}b_i + g \ .$$

(5.1.11)

The input voltage disturbance to output transfer function is:

$$\frac{\hat{y}(s)}{v_I(s)} = \begin{bmatrix} \dfrac{\hat{v}_0(s)}{v_I(s)} \\[2em] \dfrac{\hat{i}_L(s)(or\ \emptyset(s))}{v_I(s)} \\[2em] \dfrac{\hat{v}_c(s)}{v_I(s)} \end{bmatrix} = c_1[sI - A]^{-1}b_v .$$

(5.2.12)

5.2 DISCRETE AVERAGE CIRCUIT REALIZATION

The objective of this section is to realize a circuit model for the buck, boost and buck/boost converters with constant frequency, constant off time or constant on time duty cycle control. To illustrate the process by which a circuit model is obtained, the boost converter with constant frequency duty cycle control will be used as an example.

For the boost converter the discrete-average model is:

$$
\underline{\dot{x}} = \begin{bmatrix} -\dfrac{R_\ell + d'R_c//R_L}{L} & \dfrac{-d'R_L}{L(R_L + R_c)} \\ \dfrac{d'}{C}\dfrac{R_L}{R_L + R_c} & -\dfrac{1}{(R_L + R_c)C} \end{bmatrix} \underline{x} + \begin{bmatrix} \dfrac{1}{L} \\ 0 \end{bmatrix} v_I + \begin{bmatrix} \dfrac{-d'R_c//R_L}{L} \\ \dfrac{1}{C}\dfrac{R_L}{R_L+R_c} \end{bmatrix} i_0
$$

$$(5.2.1)$$

$$
\underline{y} = \begin{bmatrix} v_0 \\ i_L \\ v_c \end{bmatrix} = \begin{bmatrix} 0 & \dfrac{R_L}{R_L + R_c} \\ 1 & 0 \\ 0 & 1 \end{bmatrix} \underline{x} + \begin{bmatrix} R_c//R_L \\ 0 \\ 0 \end{bmatrix} i_0 \quad .
$$

In the first output equation, solve for v_c in terms of v_o and i.

$$v_c = (1 + R_c/R_L) v_o - R_c i_o \tag{5.2.2}$$

or in matrix form:

$$\begin{bmatrix} i_L \\ v_c \end{bmatrix} = \begin{bmatrix} 1 & 0 \\ 0 & 1 + \dfrac{R_c}{R_L} \end{bmatrix} \begin{bmatrix} i_L \\ v_0 \end{bmatrix} + \begin{bmatrix} 0 \\ -R_c \end{bmatrix} i_0 \tag{5.2.3}$$

Substituting equation (5.2.3) into (5.2.1), an equation in terms of i_L and v_o is determined

$$\begin{bmatrix} i_L \\ v_c \end{bmatrix} = \begin{bmatrix} -\dfrac{R_\ell}{L} & -\dfrac{d'}{L} \\ \\ \dfrac{d'}{C} \dfrac{R_L}{R_L + R_c} & -\dfrac{1}{R_L C} \end{bmatrix} \begin{bmatrix} i_L \\ v_0 \end{bmatrix} + \begin{bmatrix} \dfrac{1}{L} \\ 0 \end{bmatrix} v_I + \begin{bmatrix} 0 \\ \dfrac{1}{C} \end{bmatrix} i_0 \tag{5.2.4}$$

By examining the first equation in (5.2.4) it can be noted that it is the application of Kirchoff's voltage law for a loop.

$$(R_1 + d'R_c // R_L) i_L + L \, di_L/dt + d'v_o - v_I = 0 \tag{5.2.5}$$

It is realized as shown in figure 5.2.1a. The second equation is

$$c \frac{dv_c}{dt} - d'i_L \frac{R_L}{R_L + R_C} + \frac{v_o}{R_L} - i_o = 0 \qquad (5.2.6)$$

and can be realized by noting that it is the application of Kirchoff's Current Law at a node. The realization is shown in figure 5.2.1b. The circuit realization as shown in Fig. 5.2.1. also must satisfy the state equations as given in equation (5.2.1). The two circuits in figure 5.2.1 can be connected with an ideal transformer as shown in Fig. 5.2.2a.

Introducing the perturbations $v_I = V_I + \hat{v}_I$, $i_L = I_L + \hat{i}_L$, $d = D + \hat{d}$, $d' = D' - \hat{d}$, $v_c = V_c + \hat{v}_c$ results in a perturbation in the output $v_o = V_o + \hat{v}_o$. Substituting these equations into the above circuit model results in figure 5.2.2b. Removing the $-\hat{d}$ term from the transformer turns ratio results in figure 5.2.2c. Assuming that departures of the states from their corresponding steady state values are small compared to the steady state values themselves allows the second order terms in figure 5.2.2c to be neglected; resulting in figure 5.2.2d. At this point the dc operating condition may be determined. From equation (4.1.8), the dc values for the inductor current, capacitor voltage and output voltage are calculated.
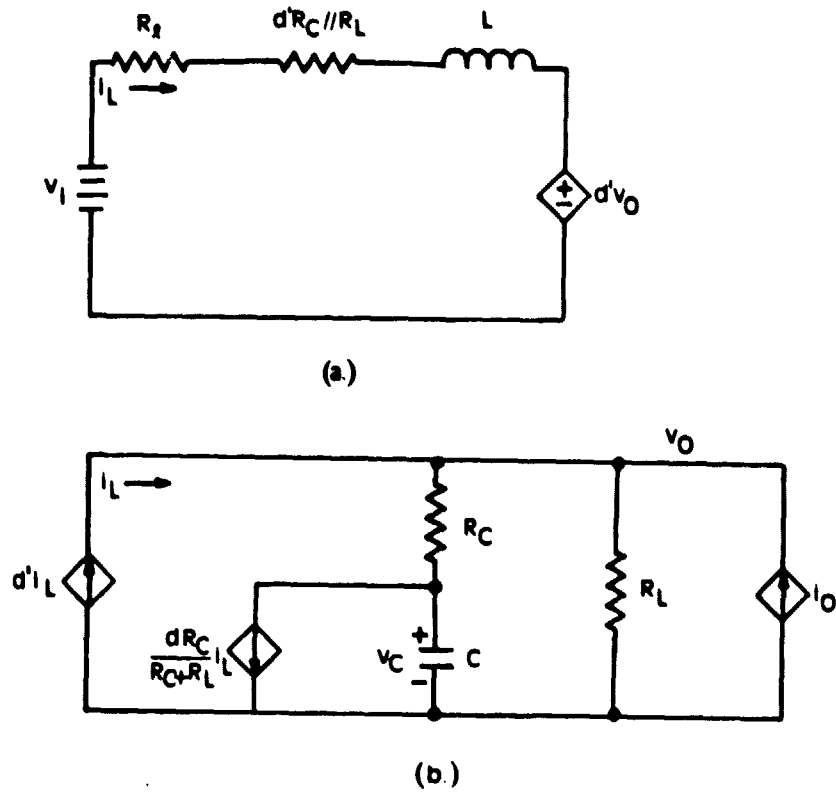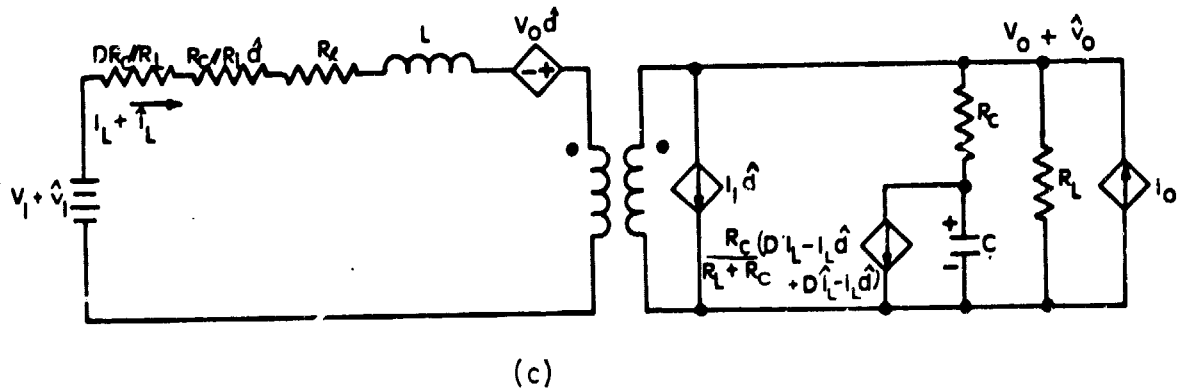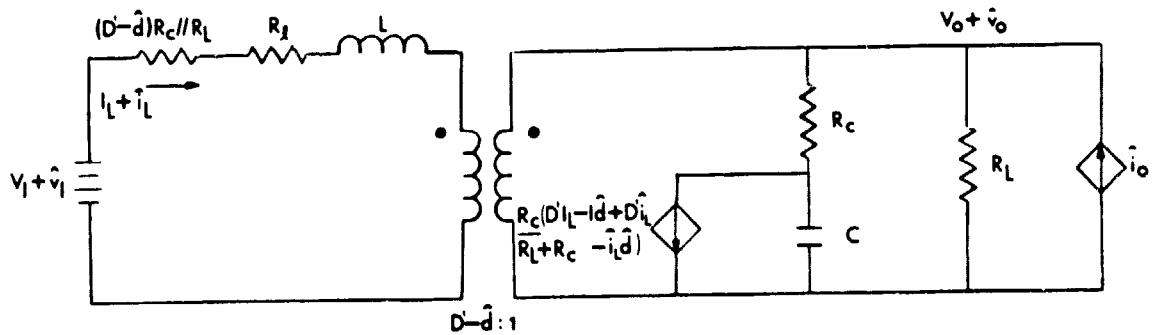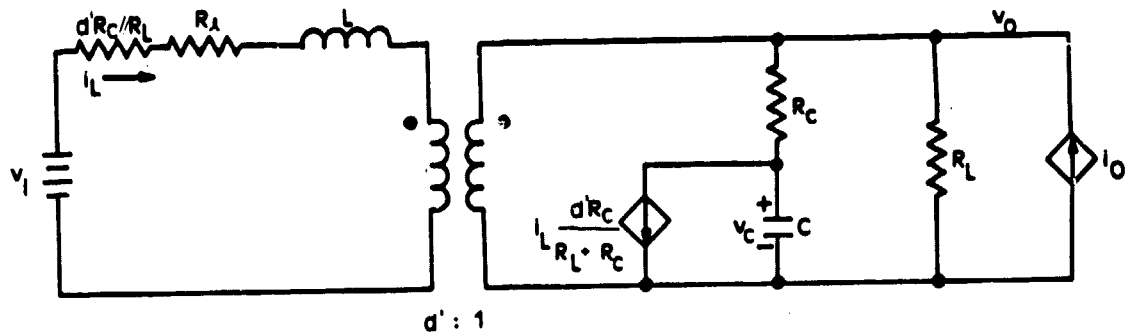
(a.)

(b.)

Figure 5.2.1 : Boost converter circuit model realizations.

136

Figures 5.2.2a-5.2.2e. Boost converter circuit model perturbation
and linearization.

(d)

(e)
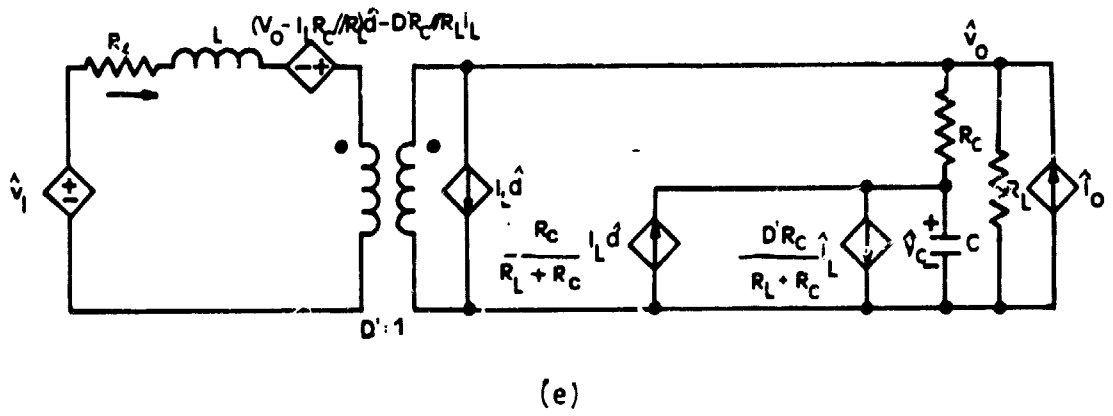
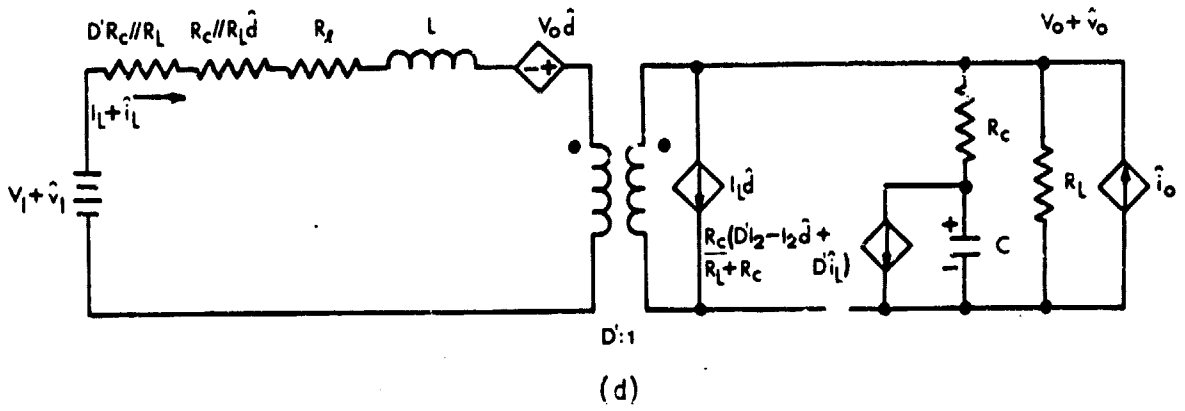Figure 5.2.2a - 5.2.2e   (continued)

138

$$\underline{X} = \begin{bmatrix} I_L \\ V_c \end{bmatrix} = - \begin{bmatrix} \dfrac{-R_\ell + D'R_{\bar{c}}//R_L}{L} & -\dfrac{D'}{L}\dfrac{R_L}{R_L + R_{\bar{c}}} \\ \dfrac{D'}{C}\dfrac{R_L}{R_c + R_L} & -\dfrac{1}{C(R_L + R_c)} \end{bmatrix} \begin{bmatrix} \dfrac{V_I}{L} \\ 0 \end{bmatrix} \qquad (5.2.7)$$

$$V_0 = - \begin{bmatrix} 0 & \dfrac{R_L}{R_c + R_L} \end{bmatrix} \underline{X}$$

I, V_c and V_0 can be found from equation (5.2.7).

$$I_L = \frac{V_I}{(D')^2 R_L} \cdot \frac{1 + \dfrac{R_c}{R_L}}{1 + \dfrac{R_c}{R_L} + \dfrac{R_\ell}{(D')^2 R_L}\left(1 + \dfrac{R_c}{R_L}\right)} \qquad (5.2.8)$$

$$V_c = \frac{V_I}{D'} \cdot \frac{1 + \dfrac{R_c}{R_L}}{1 + \dfrac{R_c}{D'R_L} + \dfrac{R_\ell}{(D')^2 R_L}\left(1 + \dfrac{R_c}{R_L}\right)} \qquad (5.2.9)$$

and

$$V_0 = \frac{V_I}{D'} \cdot \frac{1}{1 + \dfrac{R_L}{D'R_L} + \dfrac{R_\ell}{(D')^2 R_L}\left(1 + \dfrac{R_c}{R_L}\right)} \qquad (5.2.10)$$

The dc input voltage to dc output voltage ratio is found from equation (5.2.10).

$$\frac{V_0}{V_I} = \frac{1}{D'} \cdot \frac{1}{1 + \dfrac{R_c}{D'R_L} + \dfrac{R_\ell}{(D')^2 R_L}\left(1 + \dfrac{R_c}{R_L}\right)} \qquad (5.2.11)$$

The small signal circuit model can now be found by removing the dc operating conditions and rearranging the parameters into the circuit of Figure 5.2.2e. This circuit model preserves the input, output and average state variable properties of the boost converter.

The same process can be applied to the buck converter and the buck/boost converter. The discrete-average state equations can be determined for each of the above converters with constant frequency control. These sets of equations are then realized into a single circuit with an ideal transformer as shown in Figs. 5.2.3. and 5.2.4. Introducing the perturbations into the state and output, neglecting the small nonlinear terms and simplifying the structure, one obtains the circuits in Figures 5.2.3b.) and 5.2.4b). At this point the dc operating conditions are determined from equation (4.1.8). They are listed in Table 5.2.1. for each type of converter. The small signal circuit model can be found by removing the dc operating conditions, which give the circuits in Figures 5.2.3c.) and 5.2.4c.).
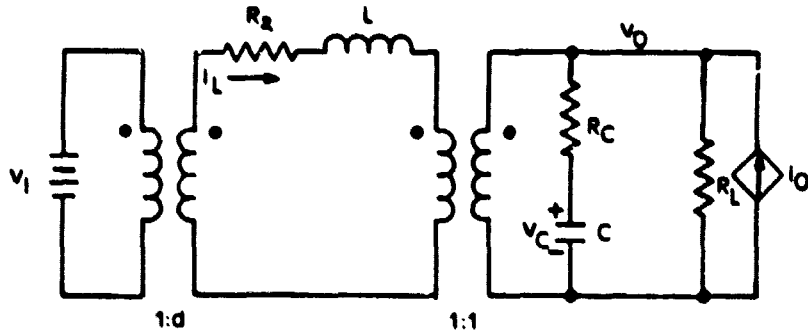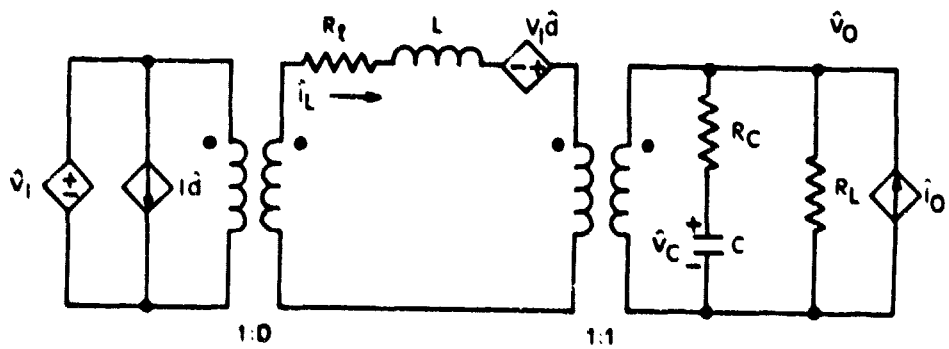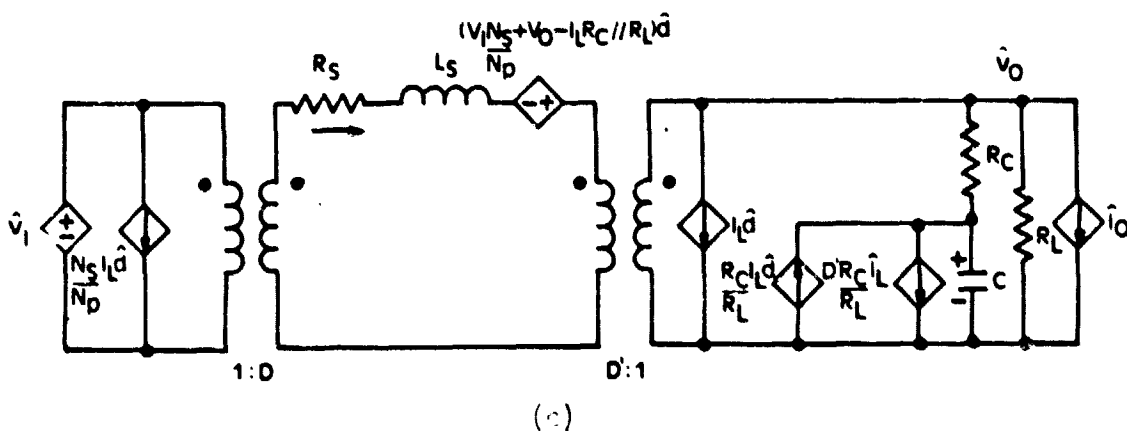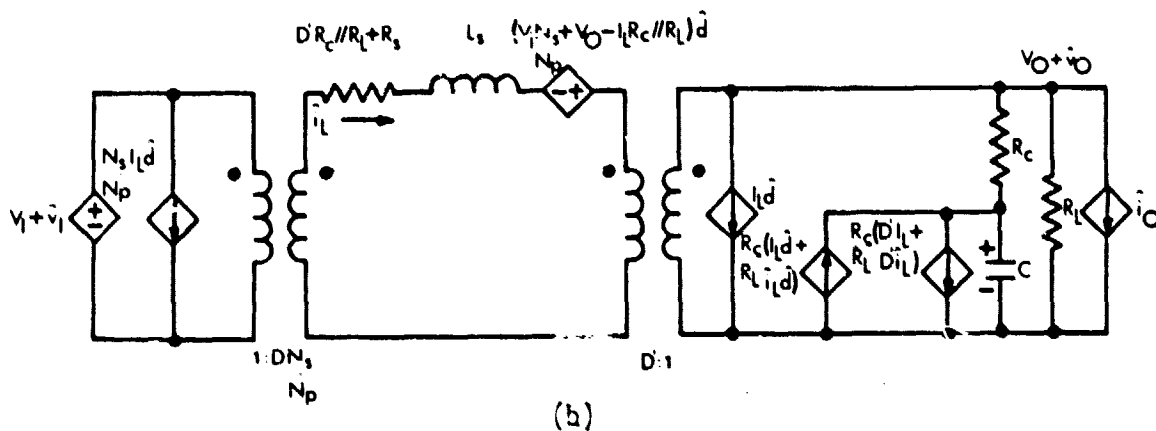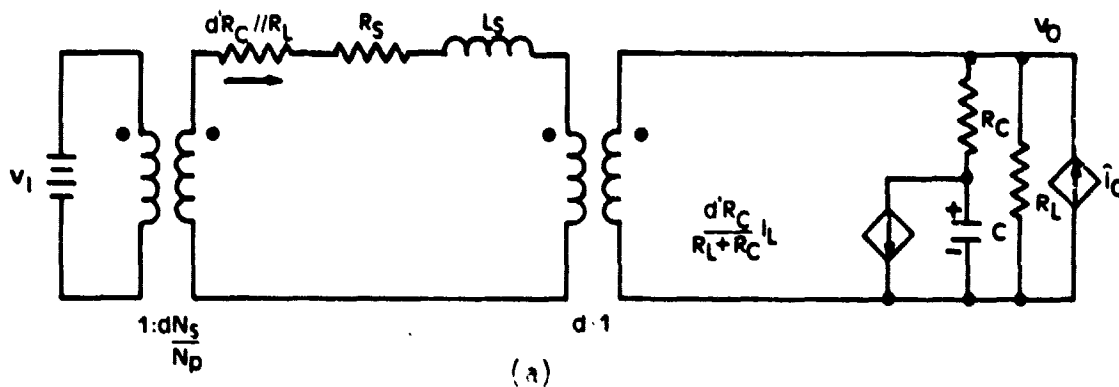
(a)
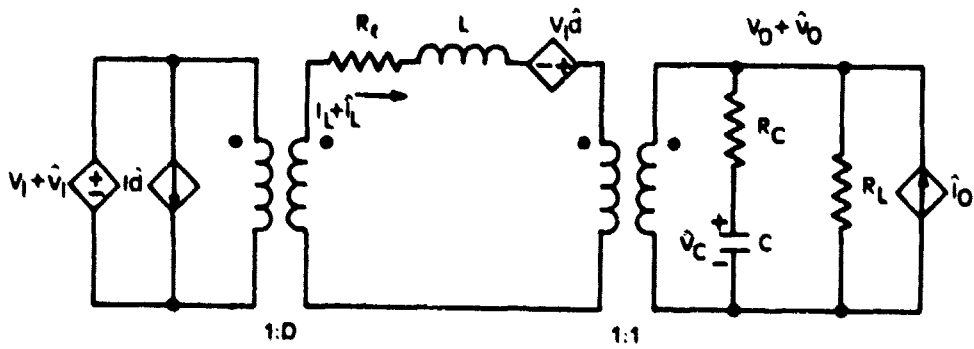
(b)

(c)

Figures 5.2.3a-5.2.3c. Buck Converter Circuit Model

(a)

(b)

(c)

Figures 5.2.4a-5.2.4c. Buck/Boost Converter Circuit Model

TABLE 5.2.1

The discrete-average approximate dc model operating conditions.
The detailed dc operating conditions are listed in Appendix A.

	BUCK	BOOST	BUCK/BOOST
I_L	$D\dfrac{V_I}{R_L}$	$\dfrac{V_I}{(D')^2 R_L}$	$\dfrac{D}{(D')^2}\dfrac{N_s}{N_p}\dfrac{V_I}{R_L}$
V_C	DV_I	$\dfrac{V_I}{D'}$	$\dfrac{D}{D'}\dfrac{N_s}{N_p}V_I$
$\dfrac{V_o}{V_I}$	D	$\dfrac{1}{D'}$	$\dfrac{D}{D'}\dfrac{N_s}{N_p}$

To determine the small signal circuit model with constant on time duty cycle control, the previously mentioned process is repeated.

A small signal canonical circuit model is presented in the next section, that will describe the buck, boost or buck/boost converter with constant frequency, constant off time or constant on time duty cycle control.

5.3 CANONICAL CIRCUIT MODEL

The objective of this section is to present a canonical circuit model that describes the system's small signal operation. This model preserves the input, output and state variable operation of dc-dc converters. Middlebrook and Cúk developed a canonical circuit model in [15] that preserves the input and output properties, however, the state variable information is lost. That model can't be used in the analysis of multiloop systems, where the state variable in formation is needed for the feedback network.

Fig.5.3.1 is the canonical circuit model that can be used for the small signal analysis of the buck, boost and buck/boost converters with constant frequency, constant off time or constant on time control. Table 5.3.1 lists the necessary parameters. This canonical circuit model can be used in the small signal analysis of dc-dc converters with multiloop

Figure 5.3.1. Canonical Circuit Model
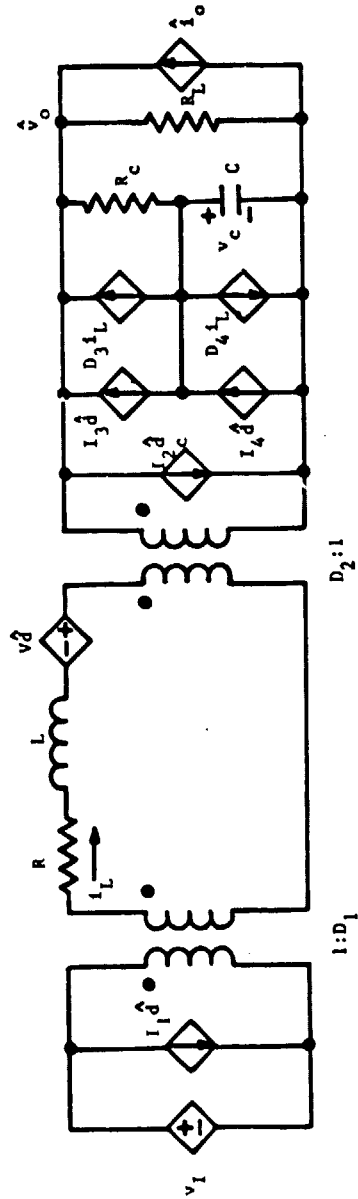
ORIGINAL PAGE IS OF POOR QUALITY

Table 5.3.1   Canonical Circuit Model Parameters

		Buck	Boost	Buck/Boost
Constant Frequency, Constant off time, Constant on time	I_1	I_L	0	$\dfrac{N_S}{N_P} I_L$
	I_2	0	I_L	I_L
	D_1	D	1	$\dfrac{N_S}{N_P} D$
	D_2	1	D'	D'
	R	R	R	R_S
	L	L	L	L_S
Constant Frequency, Constant off time	V	V_I	$V_o - I_L R_c // R_L$	$\dfrac{N_S}{N_P} V_I + V_o - I_L R_c // R_L$
	I_3	0	0	0
	I_4	0	$\dfrac{R_c}{R_L + R_c} I_L$	$\dfrac{R_c}{R_L + R_c} I_L$
	D_3	0	0	0
	D_4	0	$\dfrac{R_c}{R_L + R_c} D'$	$D' \dfrac{R_c}{R_L + R_c}$
Constant on time	V	V_I	V_o	$\dfrac{N_S}{N_P} V_I + V_o$
	I_3	0	$\dfrac{R_L}{R_L + R_c} I_L$	$\dfrac{R_L}{R_L + R_c} I_L$
	I_4	0	0	0
	D_3	0	D	D
	D_4	0	0	0

feedback. This circuit model preserves the input, output and state variable operation of the system.

5.4 TRANSFER FUNCTION REPRESENTATION

The input to output transfer functions are determined from equations (5.1.10), (5.1.11) and (5.1.12). These transfer functions have been determined for the buck, boost and buck/boost converters. Fig. 5.4.1. is the block diagram of the transfer functions for the converters. Tables 5.4.1. and 5.4.2. contain the definitions of the block diagram for each converter. These tables assume that $R_c \ll R_L$, for the detailed expressions see Appendix A.
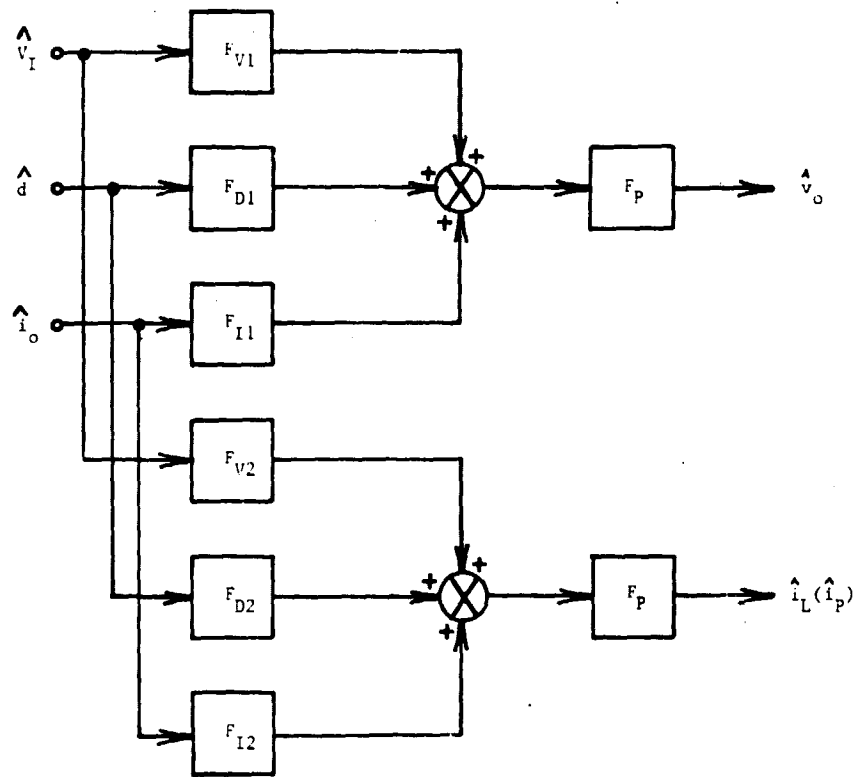
Figure 5.4.1. Block Diagram of Transfer Functions for Buck, Boost, and Buck/Boost Converters

Table 5.4.1a Constant frequency and constant off time duty cycle, control transfer functions.

	Buck	Boost	Buck/Boost
F_{v1}	$D(1 + R_c Cs)$	$\dfrac{1}{D'}$	$\dfrac{D}{D'}$
F_{v2}	$\dfrac{D}{R_L}(1 + (R_L + R_c)Cs)$	$\dfrac{V_I}{(D')^2}(1 + (R_L+R_c)Cs)$	$\dfrac{D}{(D')^2 R_L}\dfrac{L_s}{L_p}(1+(R_L+R_c)Cs)$
F_{D1}	$V_I(1 + R_c Cs)$	$\dfrac{V_I}{(D')^2}\left(1 - \dfrac{L}{(D')^2 R_L}s\right)$	$\dfrac{V_I}{(D')^2}\dfrac{N_s}{N_p}\left(1 - \dfrac{DL_s}{(D')^2 R_L}s\right)$
F_{D2}	$\dfrac{V_I}{R_L}(1 + (R_L+R_c)Cs)$	$\dfrac{V_I}{(D')^3 R_L}(2 + (R_L+R_c)Cs)$	$\dfrac{V_I}{(D')^3 R_L}\dfrac{L_s}{L_p}(1 + D + (R_L+R_c)Cs)$
F_{I1}	$R_\ell\left(1 + (\dfrac{L}{R_c}+R_\ell C)\dfrac{R_L}{R_\ell}s + s^2 LC\dfrac{R_L}{R_\ell}\right)$	$\dfrac{R_\ell}{(D')^2}(1 + \dfrac{L}{R_\ell}s)$	$\dfrac{R_c//R_L}{D'}(1 + \dfrac{L_s}{D'R_c}s)$
F_{I2}	$-(1 + R_c C s)$	$-\dfrac{1}{D'}(1 + R_c Cs)$	$-\dfrac{L_s}{D'L_p}\dfrac{N_p}{N_s}(1 + R_c Cs)$
F_P	$\dfrac{1}{1 + \dfrac{s}{\omega_0 Q} + \left(\dfrac{s}{\omega_0}\right)^2}$		

Table 5.4.1b Constant frequency and constant off time duty cycle, control transfer functions.

	Buck	Boost	Buck/Boost
ω_0	$\dfrac{1}{LC}$	$\dfrac{D'}{LC}$	$\dfrac{D'}{L_sC}$
Q	$\dfrac{1}{\omega_0}(\dfrac{L}{R_L} + (R_c+R)C)^{-1}$	$\dfrac{D'}{\omega_0}(\dfrac{L}{D'R_L} + (R_c +\dfrac{R}{D'})C)^{-1}$	$\dfrac{D'}{\omega_0}(\dfrac{L_s}{(D')^2 R_L} + (\dfrac{R_c}{D'} + \dfrac{R_s}{(D')^2})C)^{-1}$

$\dfrac{s}{}$

Table 5.4.2. Constant on time duty cycle control transfer functions.

	Buck	Boost	Buck/Boost
F_{V1}	$D(1 + R_c Cs)$	$\dfrac{1}{D'}(1 + \dfrac{R_c C}{D'} s)$	$\dfrac{D}{D'}\dfrac{N_s}{N_p}(1 + \dfrac{R_c C}{D} s)$
F_{D1}	$V_I(1 + R_c Cs)$	$\dfrac{V_I}{(D')^2}(1+(\dfrac{R_c C}{D'} - \dfrac{DL_s}{(D')^2 R_L})s)$	$\dfrac{V_I}{(D')^2}\dfrac{N_s}{N_p}(1+(\dfrac{R_c C}{D} - \dfrac{DL_s}{(D')^2 R_L})s)$
F_{I1}	$R(1+(\dfrac{L}{R_c} + R_\ell C)\dfrac{R_L}{R}s + s^2 LC\dfrac{L}{R})$	$R_c(1+\dfrac{1}{D'})\dfrac{\dfrac{L}{R_c} + R_c}{1 + \dfrac{R}{(D')^2 R_c}}s$ $\dfrac{\dfrac{LC}{2}(D')^2 + s^2 \dfrac{R}{1 + \dfrac{R}{(D')^2 R_c}}}{}$	$\dfrac{R_s}{(D')^2}(1+\dfrac{L_s}{R_s} +R_c C)s + s^2 L_s C(\dfrac{R_c}{R_s})$

Chapter VI

PROPER MODEL SELECTIONS BETWEEN THE AVERAGE MODEL AND THE DISCRETE-AVERAGE MODEL AND SOME MEASUREMENT CONCERNS

6.1 INTRODUCTION

The ESR of the output filter capacitor results in the discontinuous waveform of the output voltage for the boost and buck/boost converters. Examining the output voltage, as shown in Figure 6.1.1, one can see a double envelope. The bottom envelope, (Fig. 6.1.1b), tracks closely with the capacitor voltage and the top envelope, (Fig. 6.1.1a), is determined by two components: the capacitor voltage and the voltage drop across the ESR of the output filter capacitor, which is the product of the inductor current and the ESR of the output filter capacitor. These two envelopes with distinct phase shift represent different modulation effects. In addition, there exists a third kind of modulation signal, the duty cycle modulation, that is embedded in the output voltage waveform.

The output voltage waveform is processed by an error amplifier and certain kind of compensation network to form an error signal, that is fed into a Pulse Width Modulator (PWM) to implement the duty cycle control.
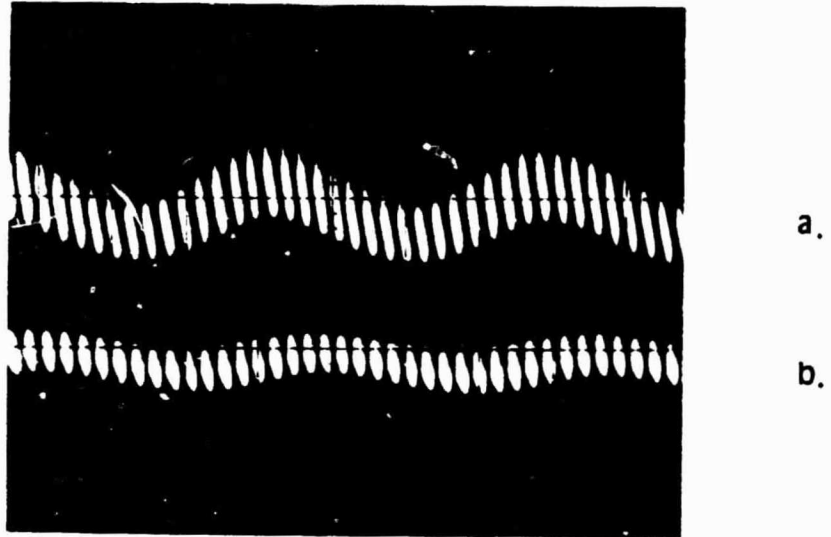
Figure 6.1.1   Output voltage waveform.
              a.)   Top envelope.
              b.)   Bottom envelope.

The average model takes the average of the entire output voltage waveform. It combines all of the three above mentioned effects and assumes the average waveform adequately represents the original properties of the system. The discrete-average model samples the output voltage at an appropriate time, depending on the specific mechanism of ramp and error signal interaction which in turn determines the type of duty cycle controller used.

If the error processor is such that it performs a good integration (averaging) of the output voltage so that all three modulation components at the output voltage are combined and together are formed as an i. egral part of the error signal, then the average model s the more accurate one to use. If the error processor is not a good low pass filter or only performs limited integration, the average model will not be accurate. The discrete-average model is then a better model to use.

In summary, the proper selection of power stage converter model between average model and discrete-average model largely depends on the type of error processor in use. Three examples are presented to illustrate model selection tailored to the compensation network design.

6.2 MEASUREMENT CONCERNS

Measurement of loop gain is often done in closed loop fashion [24] by injecting an ac signal into an appropriate location of the feedback loop. If the waveform at the point where the injected signal is placed is "smooth" and well behaved, then the measurement data is accurate. However, if the waveform at the place where the disturbance is injected is of a discontinuous fashion then the measurement data is not accurate. Since the output voltage of the boost and buck/boost converter is of a discontinuous fashion, the loop gain measurement needs to be performed with great care.

For simplicity, consider the following case: the converter output voltage is approximated by a duty cycle modulated, square wave as shown in Figure 6.2.1a. A sinusoidal waveform is injected in series with it, the composite waveform ($v_o + v_s$), Figure 6.2.1b, is both amplitude and pulse width (duty cycle) modulated. The amplitude modulation component of the waveform is primarily responsible for the desired duty cycle modulation; the pulse width modulated component of the waveform is merely an effect of the duty cycle modulation and is not responsible for the modulation of the duty cycle.

Under this circumstance, the measured data obtained from the gain and phase meter, no longer provide results correlating to the model prediction.
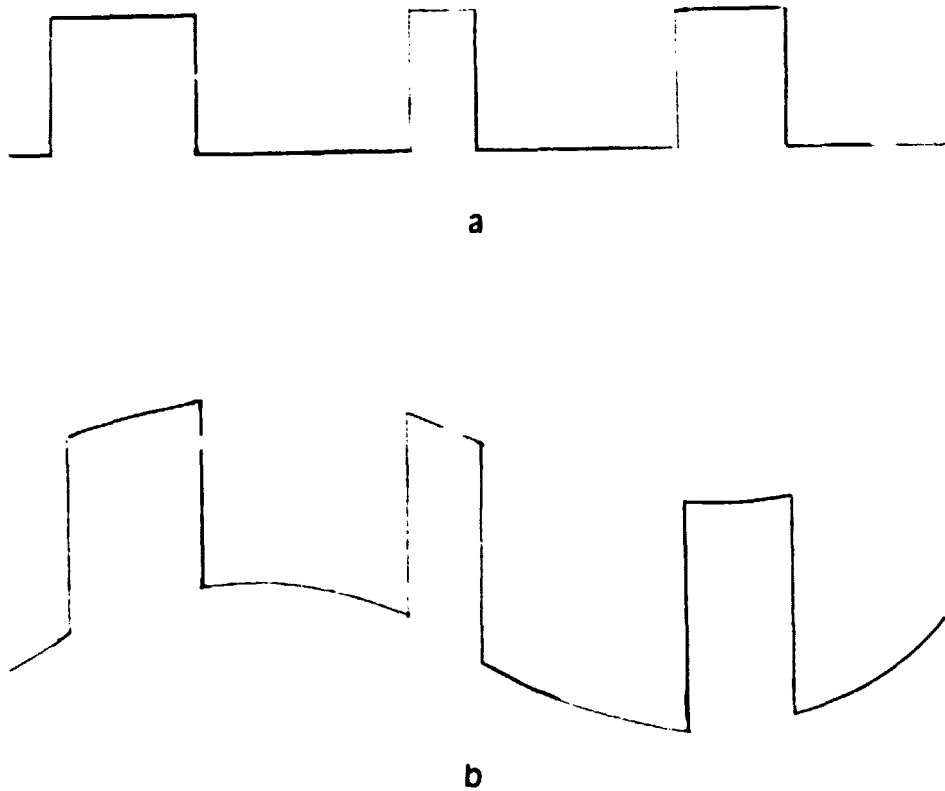
a

b

Figure 6.2.1 a.) Approximate output voltage waveform.
            b.) Output voltage plus injected signal waveform
                 both amplitude and pulse width modulated.

When the circumstances determined that the measurement was proper, the model verification was performed by opening the loop between the compensation network and the PWM and inserting an a‿ signal. The loop-gain measurement was performed with a gain and phase meter and the measurement data then compared with the analytical predictions. If the control loop waveforms are such that it circumvents proper measurement of gain and phase, the model can be verified only at a particular operating point at which system instability occurs. The system instability can be induced by changing the gain of the feedback loop, as will be discussed in the next section.

6.3 THE OPEN LOOP TRANSFER FUNCTION

The buck/boost dc‑dc converters with a single loop feedback and a constant frequency (43.5 KHz) duty cycle controller is used to verify the model. The circuit diagram is shown in Figure 6.3.1, the numerical values are:

R_s = .2Ω, R_c = .27Ω, R_L = 6Ω, C = 330μf,

L = 130μh, V_o = 5$_v$

and .23 < D < .78.

The expression of interest for this verification is the open loop transfer function. This is found by opening the loop at point X, indicated in Figure 6.3.1, and determining the transfer function from A to B. Starting at A and pro-

ORIGINAL PAGE IS
OF POOR QUALITY
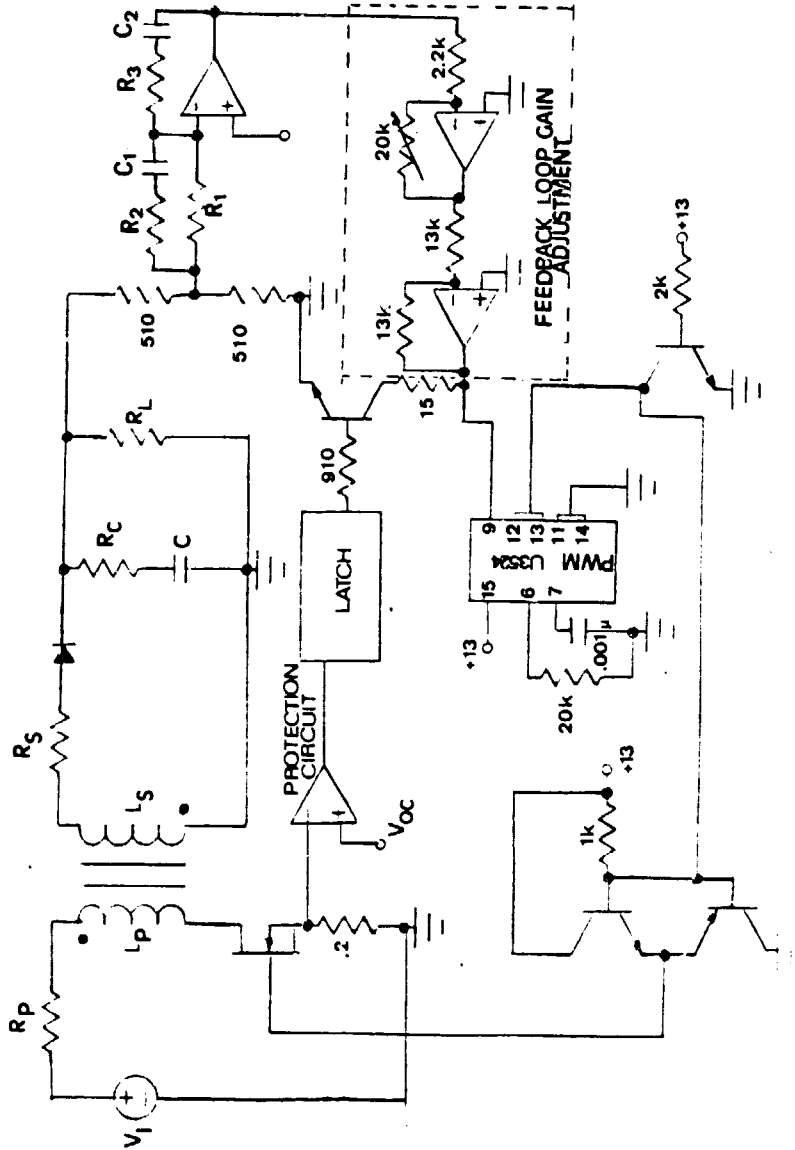
Figure 6.3.1 Buck/Boost dc-dc converter circuit diagram for
model and measurement data collection.

ceeding clockwise, each portion of the loop is examined as
follows.

The PWM is a naturally sampled modulator . The describ-
ing function is a simple dc term, Gm and from [23] is equal
to the inverse of the peak to peak voltage of the clocked
ramp signal. For this system Gm is equal to .36. The duty
cycle to output voltage transfer functions for the average
and discrete-average models are found in chapters III and
IV, respectively. The duty cycle to output voltage transfer
functions are termed $G_A(S)$ for the average model and $G_{DA}(S)$
for the discrete-average model. Finally, the compensation
network transfer function needs to be determined. Note the
two series, inverting op amps with a variable resistor in
the feedback of one op amp and a unity gain configuration
for the second. This network is used to push the system
into instability by increasing the loop gain by a factor, G.
This is for the purpose of verifying the point at which sys-
tem instability occurs, when the gain and phase measurement
are determined to be inaccurate. The transfer function for
the compensation network is:

$$G_c(s) = \frac{1}{2} G \frac{(s(R_1 + R_2) C_1 + 1)(sR_3C_2 + 1)}{sR_1C_2(sR_2C_1 + 1)} \quad (6.3.1)$$

The open loop transfer function is:

$$G_{OL}(s) = G_m G_A(s) G_c(s) \qquad (6.3.2)$$

for the average model and

$$G_{OL}(s) = G_m G_{DA}(s) G_c(s) \qquad (6.3.3)$$

for the discrete-average model.

6.4 TYPE 1 COMPENSATION NETWORK

Figure 6.4.1 is a sketch of the gain asymptotic plot of the 1st compensation. Essentially, it is an integrator with a large amount of attenuation. The numerical values for this type of compensation are:

$R_1 = 750$ KΩ, $R_2 = 9.1$KΩ, $R_3 = 0.$, $C_1 = 3900$pf and $C_2 = 8200$pf.

The compensation network transfer function is:

$$G_c(s) = \frac{1}{2} G \frac{(s(R_1 + R_2) C_1 + 1)}{sR_1 C_2(sR_2 C_1 + 1)} \qquad (6.4.1)$$

Figure 6.4.2a shows the converter output voltage waveform. Figure 6.4.2b and c show the output of the compensation network, the error processor signal, and the clocked ramp signal. This photograph was taken with $V_I = 20$V. The effect of the high attenuation can be clearly seen.
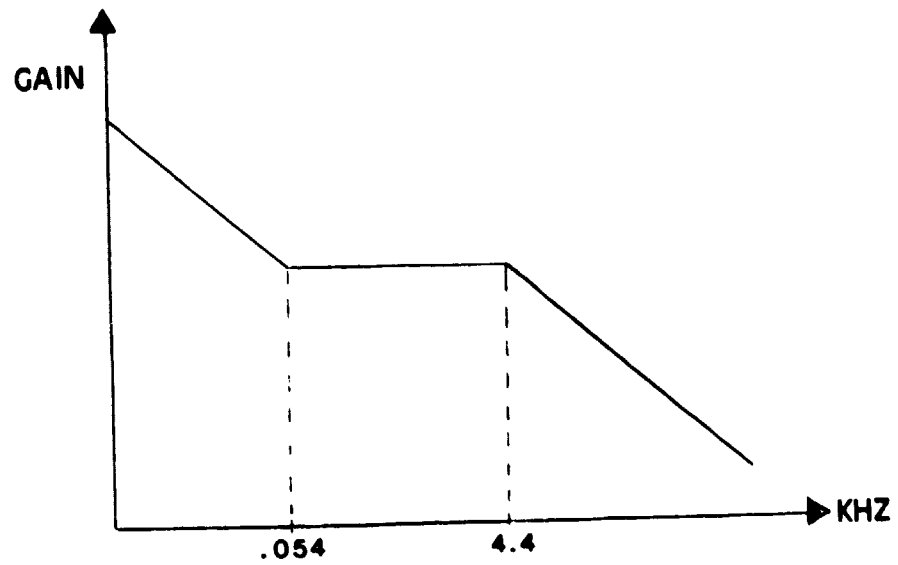
Figure 6.4.1 Asymptotic plot of the 1st compensation transfer function.

a.

b.

c.
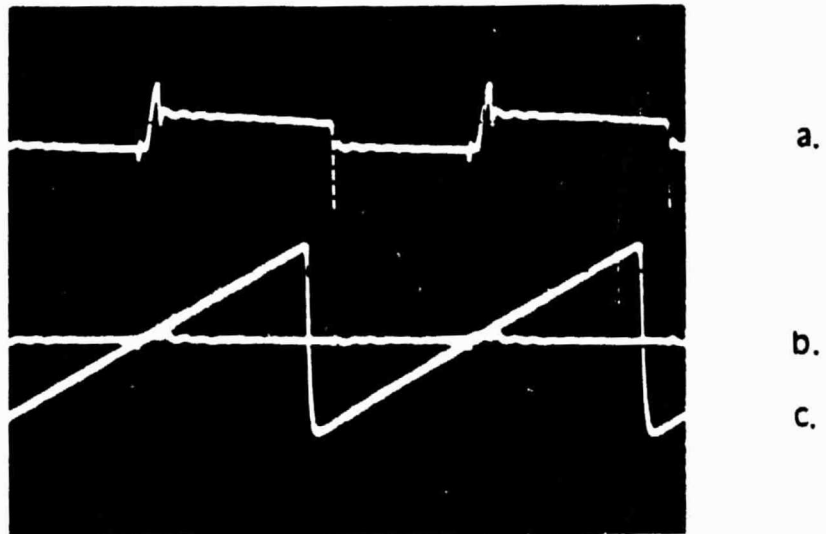
Figure 6.4.2 a.) Output voltage.
b.) Error processor signal.
c.) Clocked ramp signal.

Scale: vertical 1v/div.
horizontal 5 µs/div.

To establish the accuracy of the average model over a range of duty cycle, three different duty cycles were examined with G=1. Figure 6.4.3 is a Bode plot of the open loop transfer function and measurement data with $V_I = 45_v$ and D =.23. The data follows closely with the average model, over the entire frequency range. Increasing the duty cycle to .40 ($V_I = 20^v$) Figure 6.4.4 shows that the data follows the average model Bode plot. For a high duty cycle equal to .78 and $V_I = 6$ V, Figure 6.4.5 shows that the gain measurement data tracks closer to the average model prediction and the phase is not closely followed by either model. From Figures 6.4.3 - 6.4.5, the average model is more accurate at lower duty cycles.

To ascertain that the both model and measurement data describe accurately the physical behavior of the circuit, the following experiment was conducted. The system is pushed into instability by increasing G, keeping the duty cycle constant. The value for D is chosen to be .40. As shown in Figure 6.4.6, the discrete-average model predicts the system to be unstable for G = 3. But in Figure 6.4.7, the average model predicts the system to go unstable for G = 18. Figures 6.4.8 - 6.4.10, show the open loop transfer function bode plot with measurement data at G equal to 3, 5 and 7, respectively. In each case the data follows the average mo-
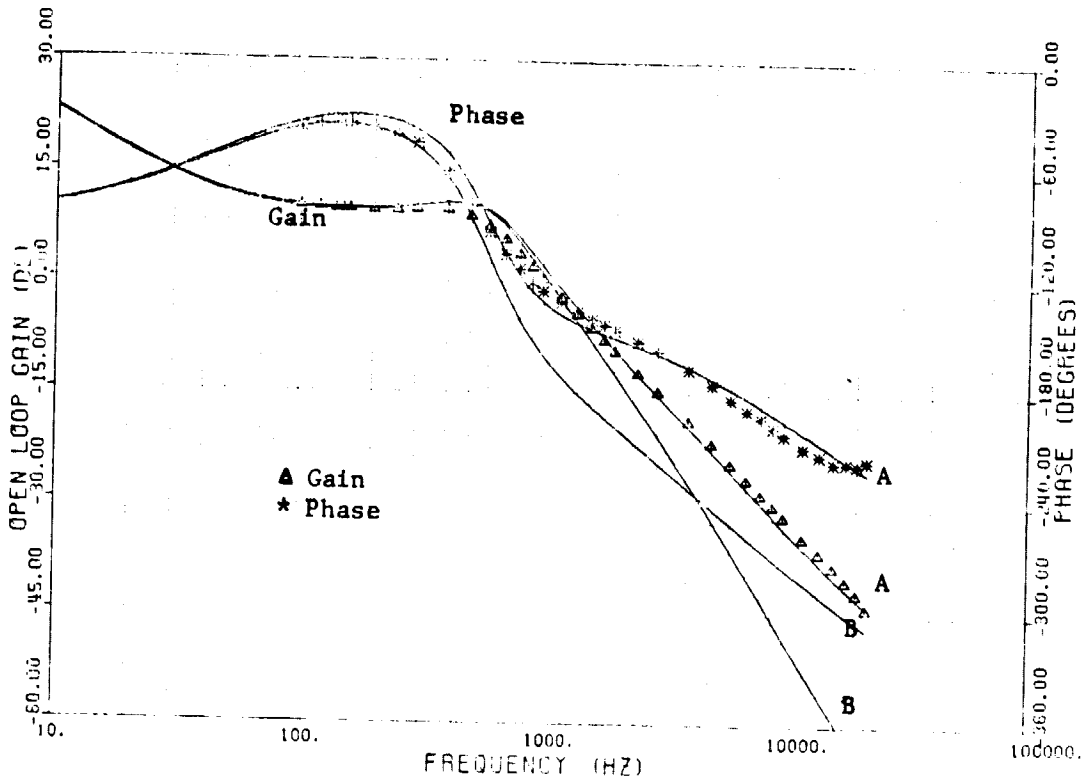
Figure 6.4.3 Open loop transfer function bode plot with the
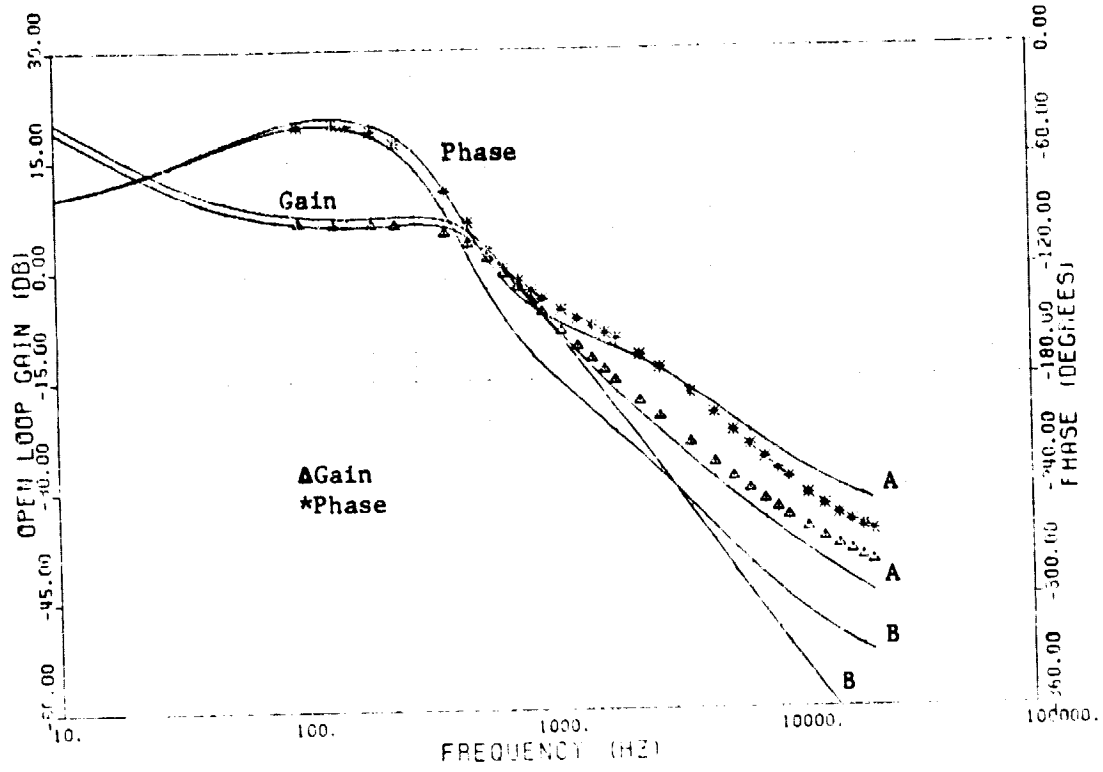1st compensation.
G=1, D=.23
A - Average
B - Discrete/Aver~ge

Figure 6.4.4 Open loop transfer function bode plot with the
1st compensation.
G=1, D=.40
A - Average
B - Discrete/Average

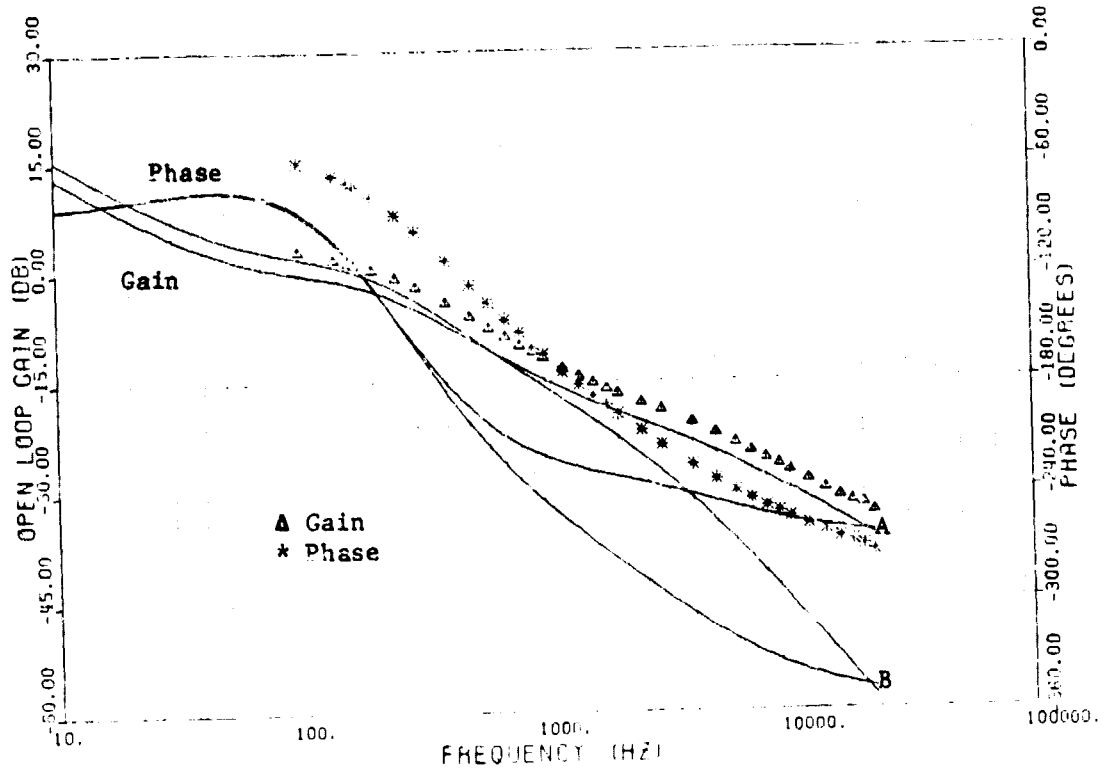Figure 6.4.5   Open loop transfer function bode plot with the
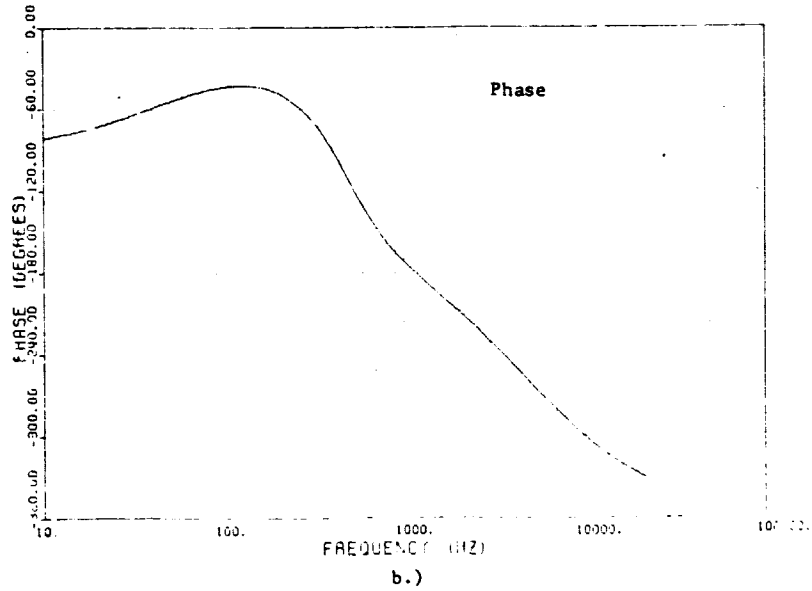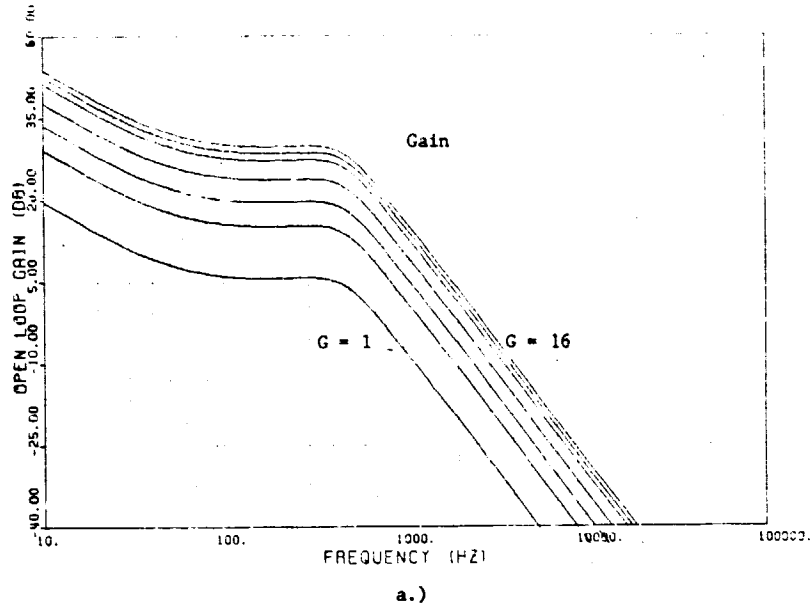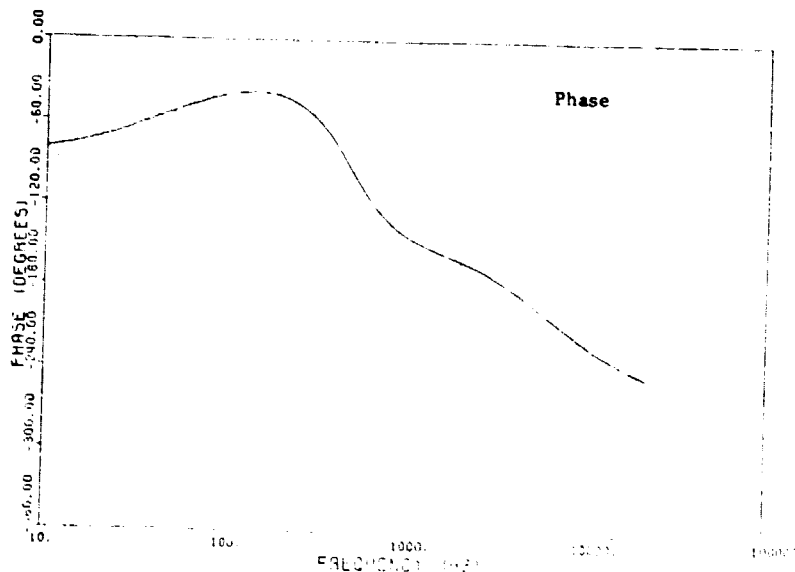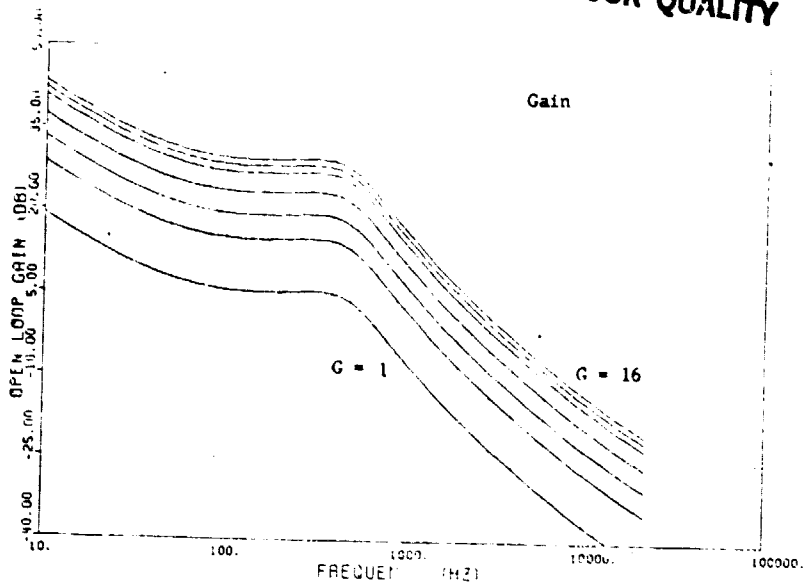1st compensation.
G=1, D= .78
A - Average
B - Discrete/Average

166

Figure 6.4.6 Discrete-Average open loop transfer function bode
plot for G=1, 3, 5, 8, 12, 14, 16 (1st compensation.)

Figure 6.4.7 Average open loop transfer function bode plot
for G=1, 3, 5, 8, 12, 14, 16 (1st compensation.)
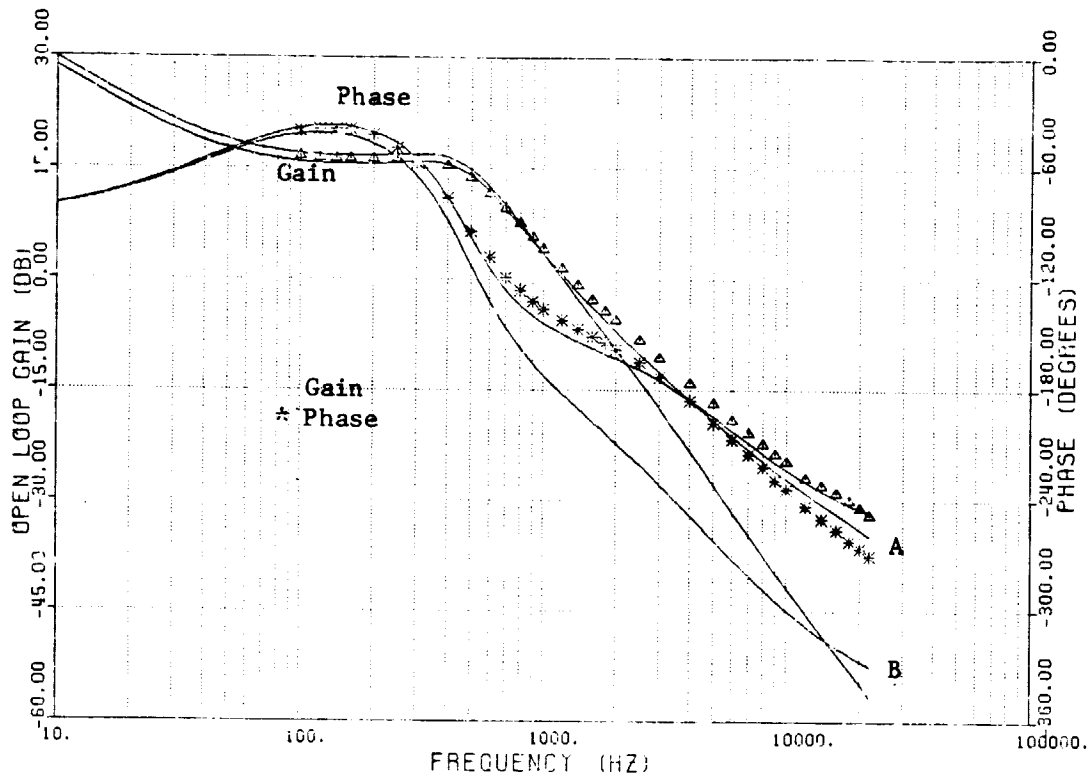
Figure 6.4.8 Open loop transfer function bode plot (1st com-
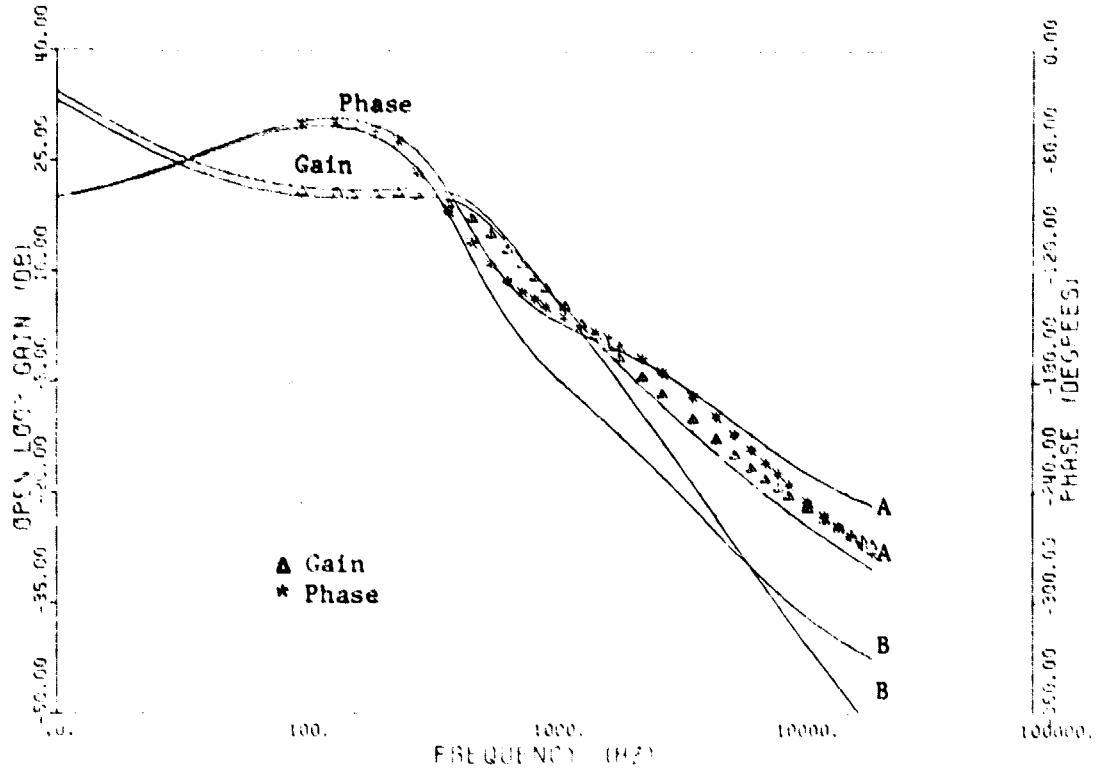pensation.)
G=3, D= .40
A - Average
B - Discrete/Average

Figure 6.4.9   Open loop transfer function bode plot (1st com-
              pensation.)
              G=5, D= .40
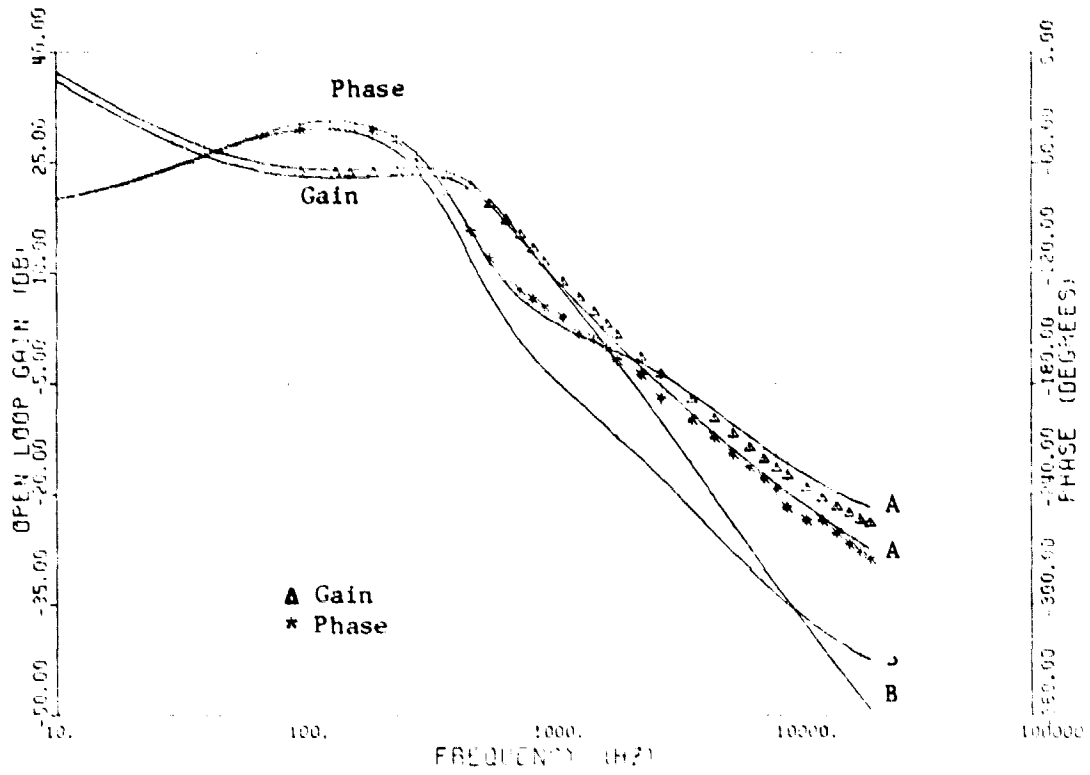   A - Average
              B - Discrete/Average

Figure 6.4.10 Open loop transfer function bode plot (1st compensation.)
G=7, D= .40
A - Average
B - Discrete/Average

del. Figure 6.4.11 shows the output voltage waveform prior to the occurrence of instability. At G = 14.25 the system goes unstable with the resultant output voltage shown in Figure 6.4.12. This is only 2 db lower than the average model prediction. At this value of G the average model indicates a phase margin of approximately $8°$.

Based on the above presented measurement data, it is quite obvious that the average model is more accurate than the discrete-average model. This is due to the fact that the particular chosen compensation network performs a good integration (averaging) of the output voltage so that all modulation components (mentioned in 6.1) of the output voltage are combined and together form an integral part of the error signal.

6.5 TYPE 2 COMPENSATION NETWORK

Figure 6.5.1 is a sketch of the gain asymptotic plot of the 2nd compensation. This type of compensation does not integrate or highly attenuate the error signal at high frequencies. The numerical values for this compensation are:

R_1=750KΩ, R_2=9.1KΩ, R_3=9.1KΩ, C_1=3900pf

and C_2=8200pf.

The compensation network transfer function is:

$$G_c(s) = \frac{1}{2} G \frac{(s(R_1+ R_2) C_1 + 1)(sR_3C_2+ 1)}{sR_1C_2(sR_2C_1 + 1)} \quad (6.5.1)$$
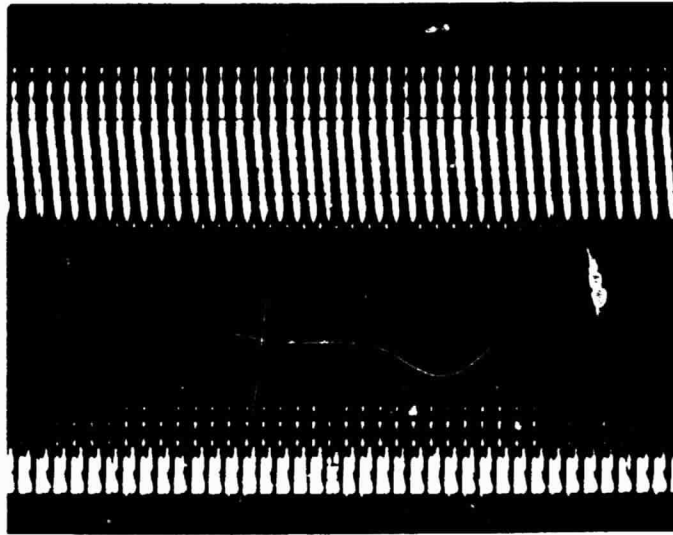
172

Figure 6.4.11 Output voltage.
          Scale: vertical   .1v/div.
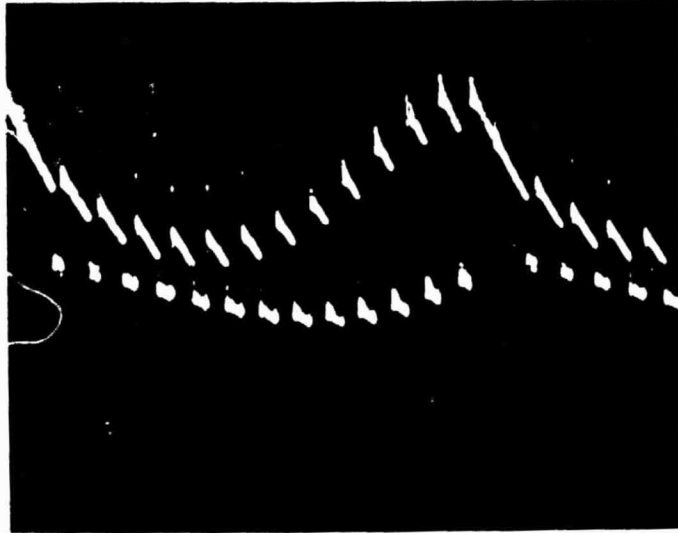   horizontal .1ms/div.

Figure 6.4.12 Output voltage (unstable).
G= 14.25
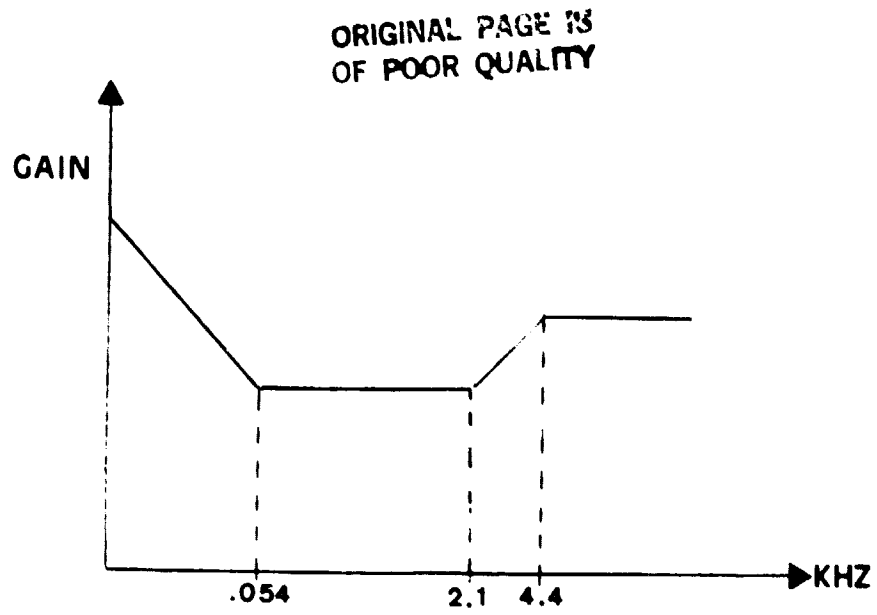Scale: vertical   .2v/div.
   horizontal 50 µs/div.

Figure 6.5.1 Asymptotic plot of the 2nd compensation transfer function.

Figure 6.5.2a shows the converter output voltage wave-
form. Figure 6.5.2b and c show the output of the compensa-
tion network, the error signal and the clocked ramp signal.
Notice the discontinuity of the error voltage waveform.

Figure 6.5.3 is the Bode plot of the discrete-average
open loop transfer function. This plot indicates that the
system will go unstable at a gain equal to 10. Figure 6.5.4
is the average model's Bode plot. This figure indicates
that this system will not go unstable for an arbitrary high
loop gain. The measurement data for G equal to 1, 2 and 3
is plotted with the discrete-average and average model in
Figures 6.5.5-6.5.7. The measurement data is taken from a
wave form that is discontinuous. Under this circumstance the
measurement data obtained from the gain and phase meter no
longer provide results correlating to the model prediction,
for it is quite obvious if one observes the rather erratic
measurement data give in Figures 6.5.5-6.5.7.

Figure 6.5.8 shows the error processor signal just before
instability. The gain is determined by measuring the ripple
of the error processor signal and comparing it with that of
the output voltage. The gain, G, just before instability
was determined to be equal to 4.6. The output voltage is
shown in Figure 6.5.9. For G greater than this gain value,
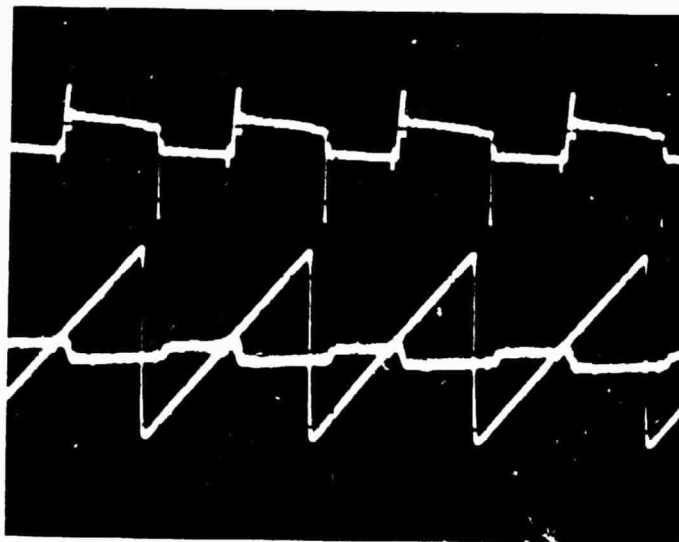
a.

b.

c.

Figure 6.5.2 a.) Output voltage.
              b.) Error processor signal.
              c.) Clocked ramp signal.
              Scale: vertical   1v/div.
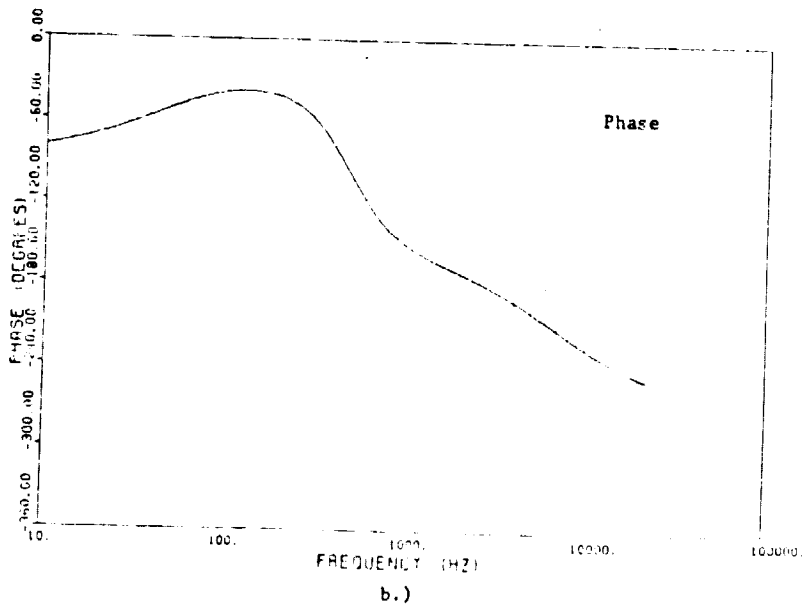   horizontal 10 μs/div.
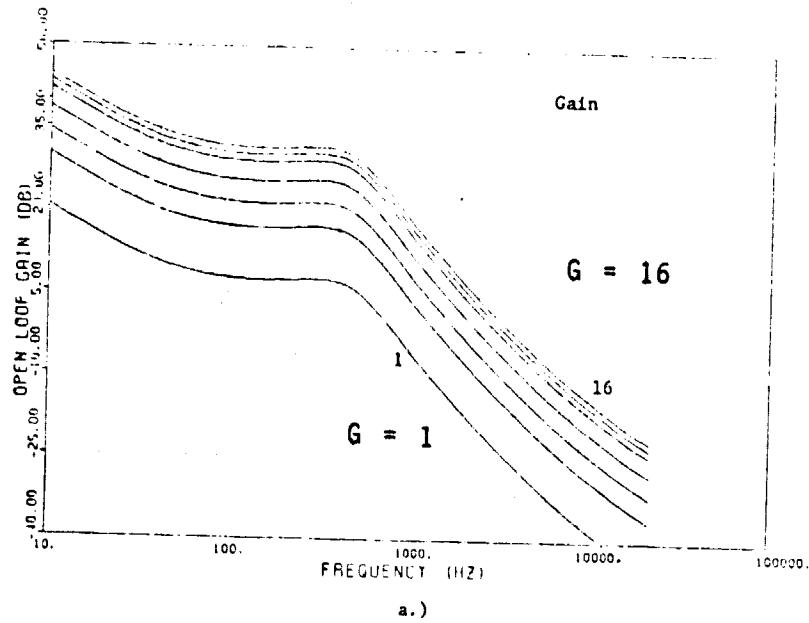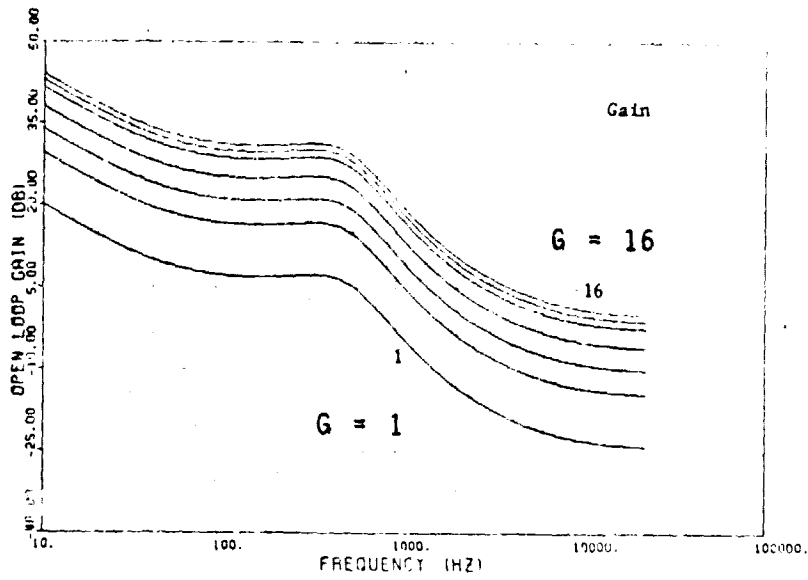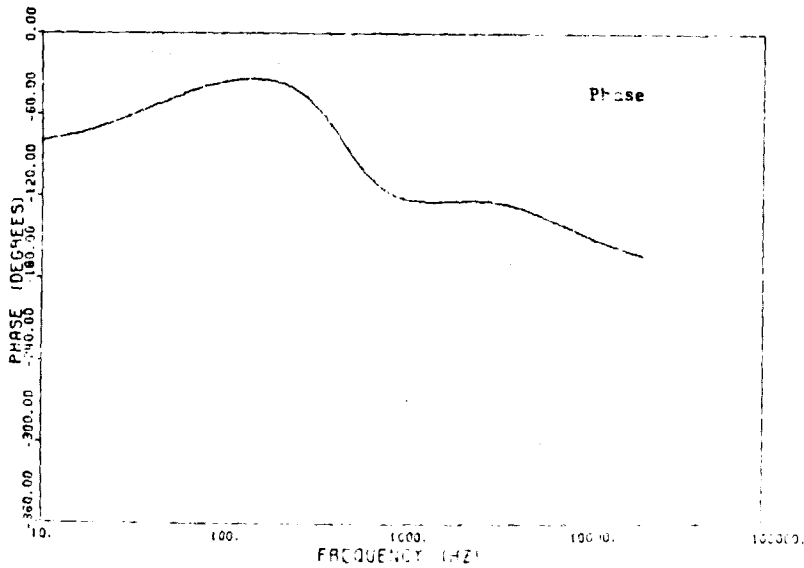
a.)

b.)

Figure 6.5.3   Discrete-Average open loop transfer function bode
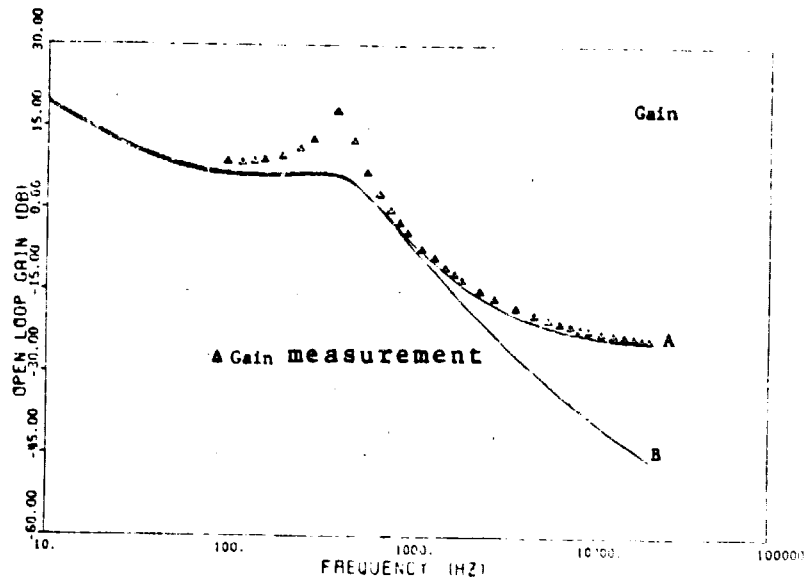plot (2nd compensation.)
G=1, 3, 5, 8, 12, 14, 16.
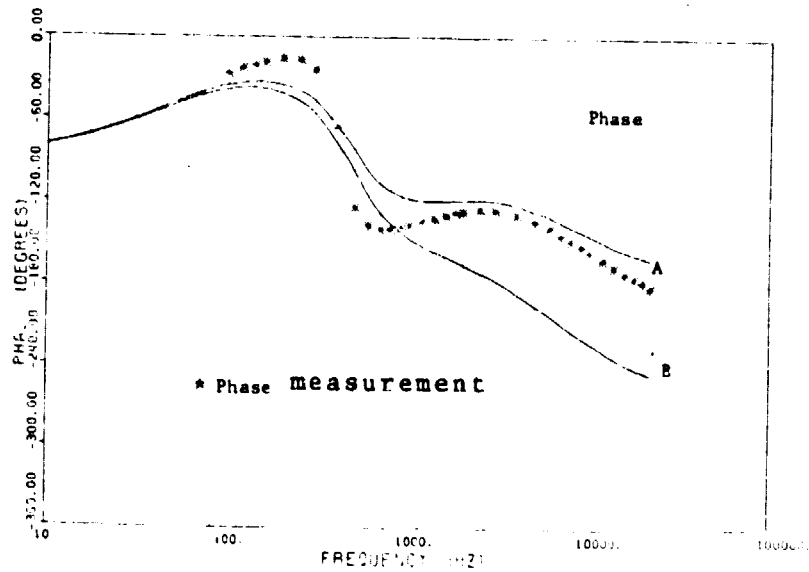
Figure 6.5.4 Average open loop transfer function bode plot
(2nd compensation).
G = 1, 3, 5, 8, 12, 14, 16.

a.)

b.)

Figure 6.5.5   Open loop transfer function Bode plot
(2nd compensation).
G = 1, d = .40
A - Average Model
B - Discrete-Average Model
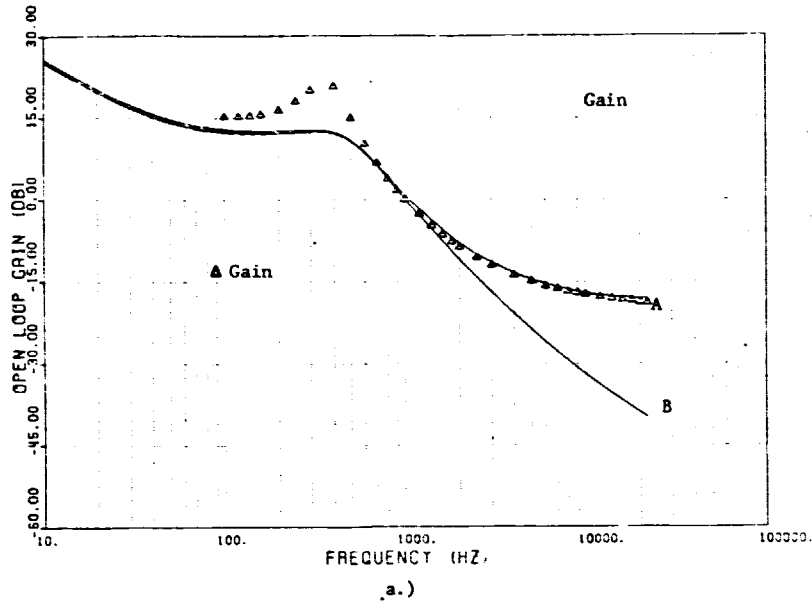
Figure 6.5.6 Open loop transfer function bode plot
(2nd compensation)
G = 2, D = .40
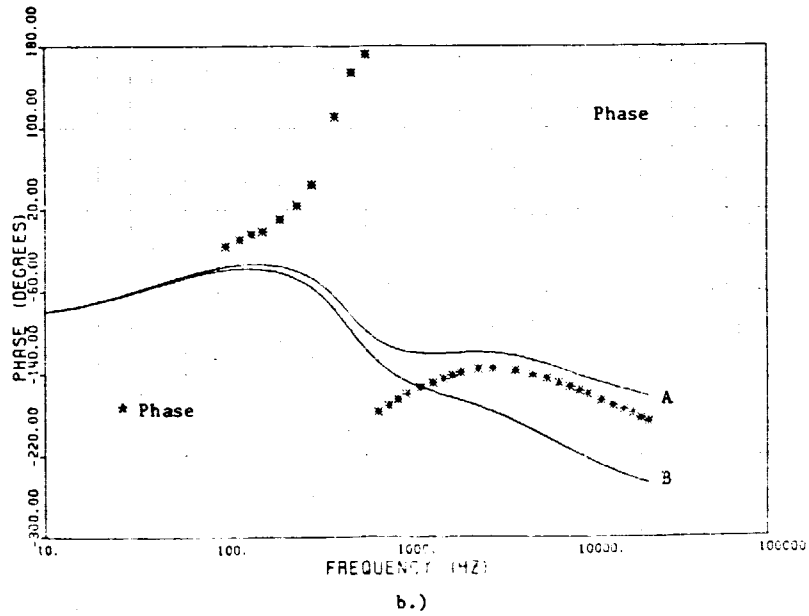A - Average
B - Discrete-Average
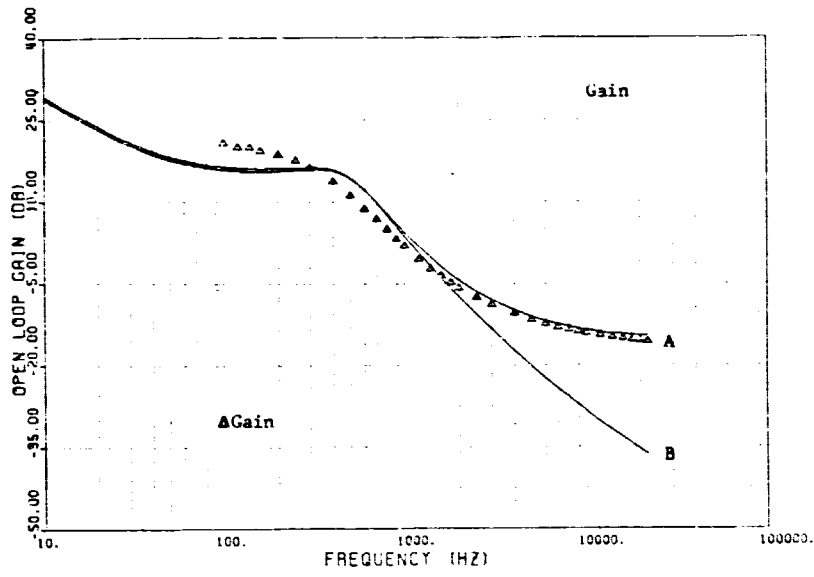
a.)
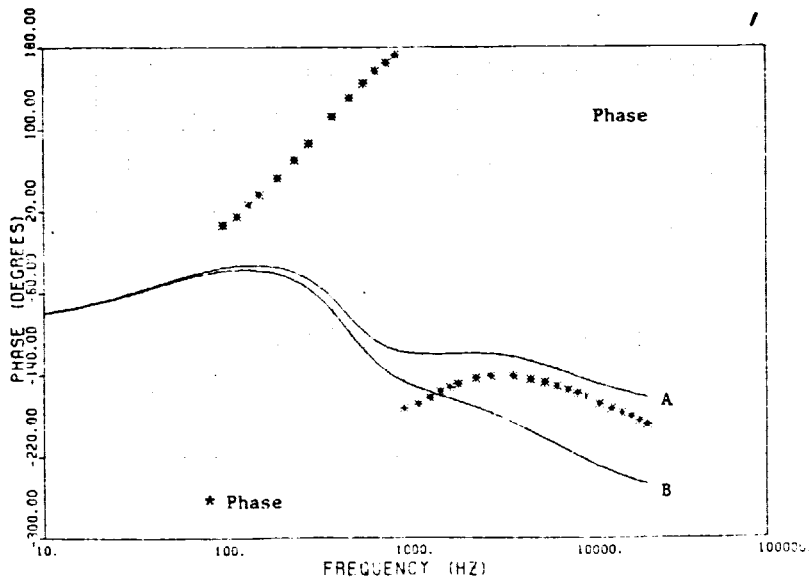
b.)

Figure 6.5.7 Open loop transfer function bode plot
(2nd compensation)
G = 3, D = .40
A - Average
B - Discrete-Average

ORIGINAL PAGE IS
OF POOR QUALITY

Figure 6.5.8   Error processor signal just before system
              instability.
              Scale: vertical   .2v/div.
                       horizontal 5 µs/div.

ORIGINAL PAGE IS
OF POOR QUALITY

Figure 6.5.9 Output voltage.
            Scale: vertical   .2v/div.
                     horizontal 50 μs/div.

the system goes into unstable operation, indicated by the output voltage in Figure 6.5.10. This is lower than the discrete-average prediction. However, the phase margin det-ermined by the discrete-average model at this value of G is approximately 14°. The average model phase margin is approximately 57°.
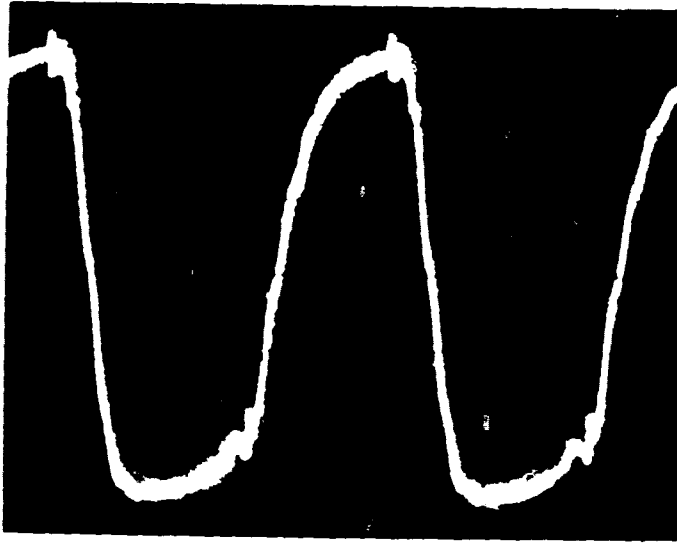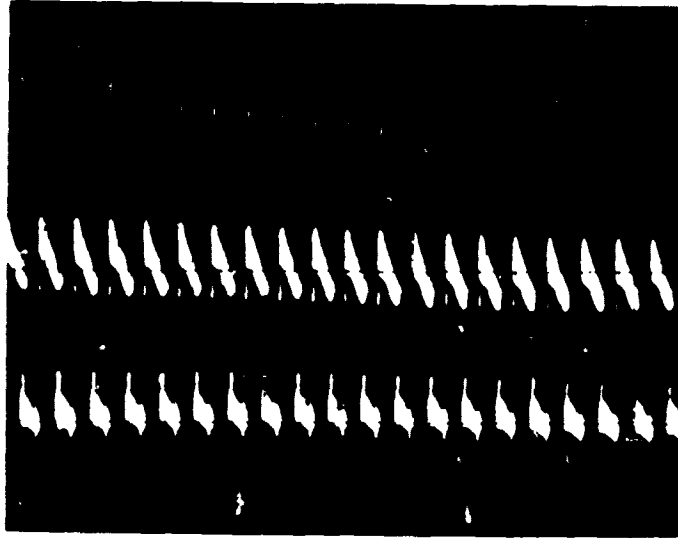
Since this type of compensation is not a good low-pass filter which performs only limited integration, at low frequencies, the discrete-average model is more accurate.

6.6 TYPE 3 COMPENSATION NETWORK

Figure 6.6.1 is a sketch of the gain asymptotic plot of the third compensation. This compensation has the following numerical values:

R_1=750KΩ, R_2=20KΩ, R_3=4.7KΩ, C_1=3900pf
and C_2 = 8200 pf.

The compensation network transfer function is:

$$G_c(s) = \frac{1}{2} G \frac{(s(R_1 + R_2)C_1 + 1)(sR_3C_2 + 1)}{sR_1C_2(sR_2C_1 + 1)} \quad (6.6.1)$$

Figure 6.6.2 shows the output of the compensation, the error processor signal, the output voltage and the voltage drop across the power stage FET, V_{DS} Notice the discontinuity in the output voltage.
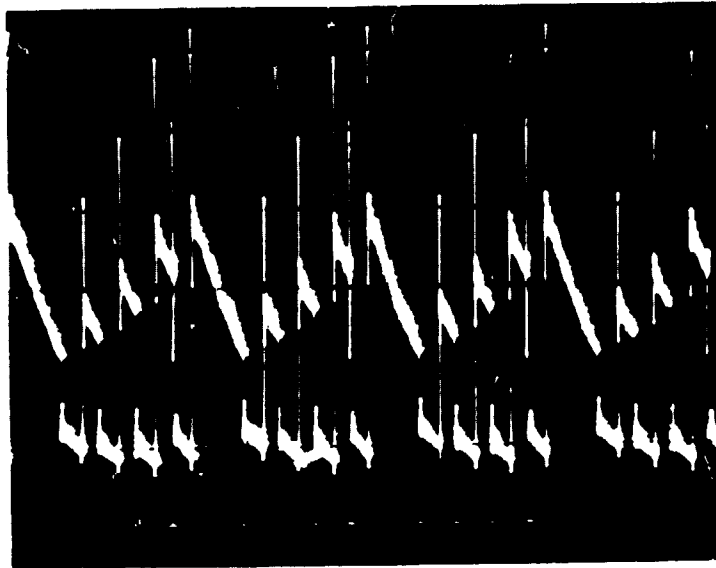
Figure 6.5.10 Output voltage (unstable).
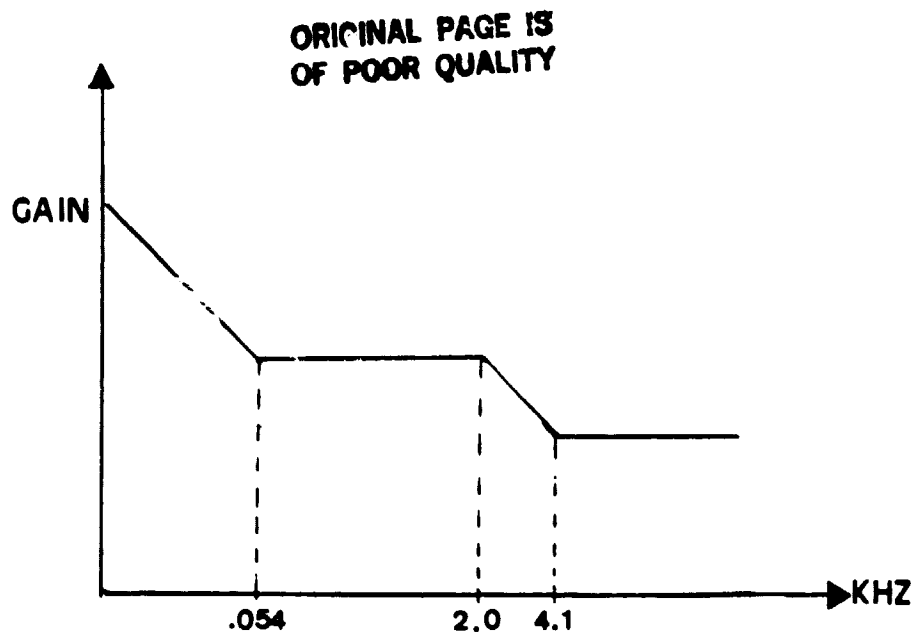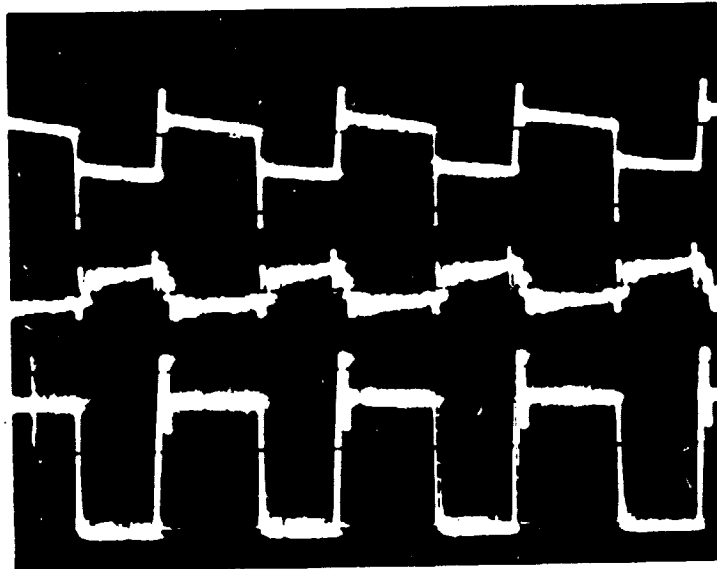   Scale: vertical   .2v/div.
                    horizontal 50 μs/div.

Figure 6.6.1   Asymptotic plot of the 3rd compensation transfer
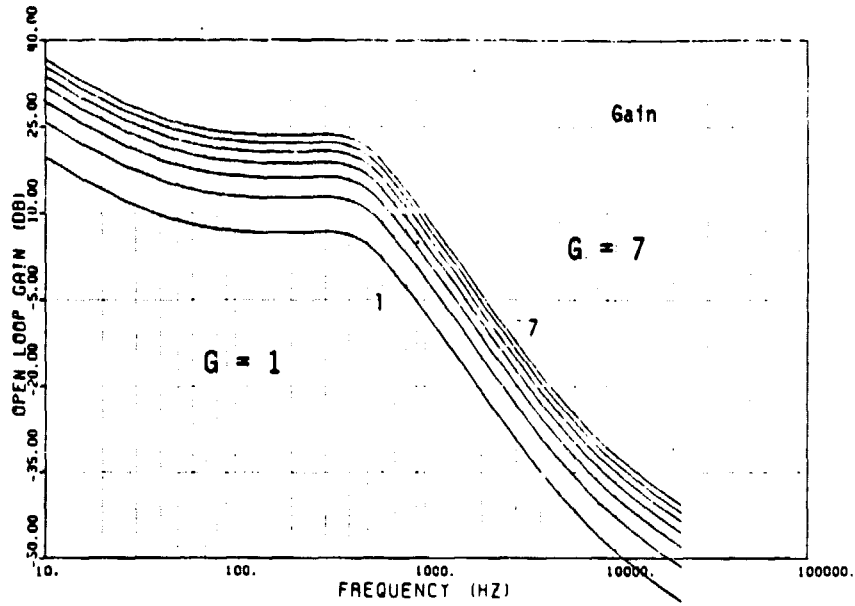function.

a.

b.

c.

Figure 6.6.2   a.) Output voltage.
Scale: vertical 1v/div.
b.) Error processor signal.
Scale: vertical .2v/div.
c.) V_{DS}
Scale: vertical 20v/div.
horizontal 10 µs/div.

Figure 6.6.3 is the Bode plot of the discrete-average open loop transfer function. Figure 6.6.4 is the average model's Bode plot. This figure indicates that this system will never go unstable. Figure 6.6.5 is the measurement data, the discrete-average and average model for G equal to 1. Figure 6.6.6 is the measurement data for G equal to 1.75, 3.17, 3.75 and 4.7. There is a great difference in phase as the gain, G, is increased. There is also a noticeable change in the shape of the gain plot as G is increased. The measurement data is taken from a waveform that is dicontinuous with amplitude and pulse width modulation. Under this circumstance the measurement data obtained from the gain and phase meter no longer provide results correlating to the model prediction .

Figure 6.6.7 shows the error processor signal just before instability occurs. Comparing this with the output voltage, the gain, G, is determined to be 4.7. The output voltage waveform and voltage across the FET is shown in Figure 6.6.8. For G greater than 4.7, the system goes to unstable operation as indicated in Figure 6.6.9. This is very close to the discrete-average model prediction of G=4. The average model at G=4 predicts a 30° phase margin.

This type of compensation network is commonly used. It, however, only provides a certain fixed gain attenuation at

a.)
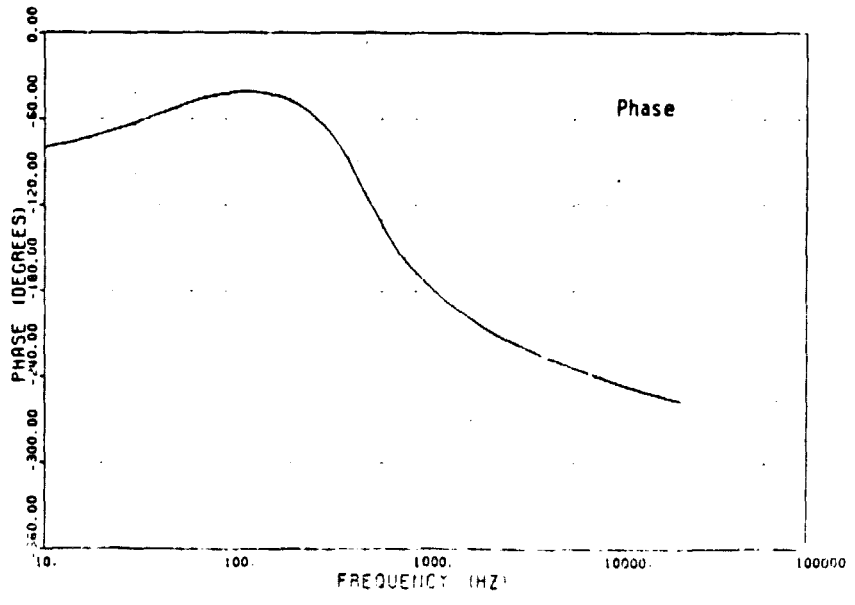
b.)

Figure 6.6.3 Discrete-Average open loop transfer function
bode plot (3rd compensation).
G = 1, 2, 3, 4, 5, 6, 7.
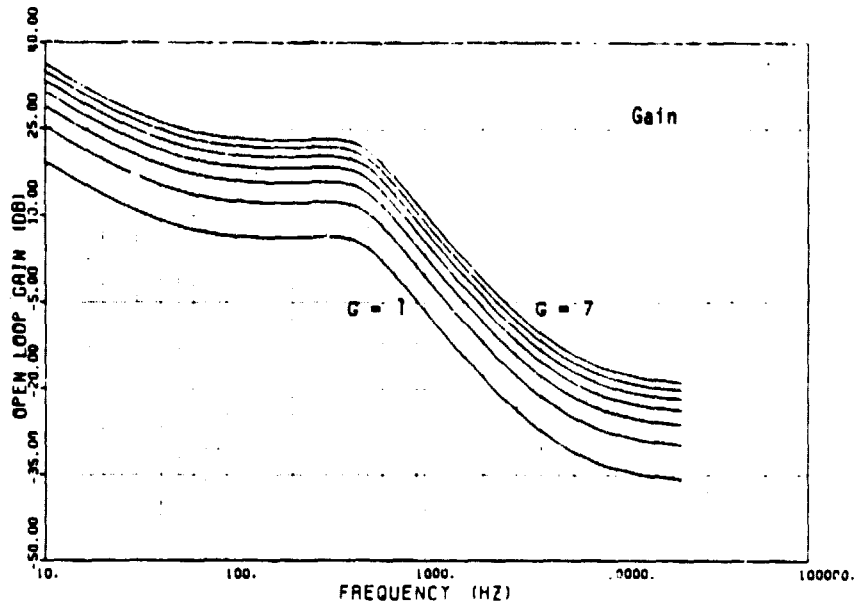
a.)
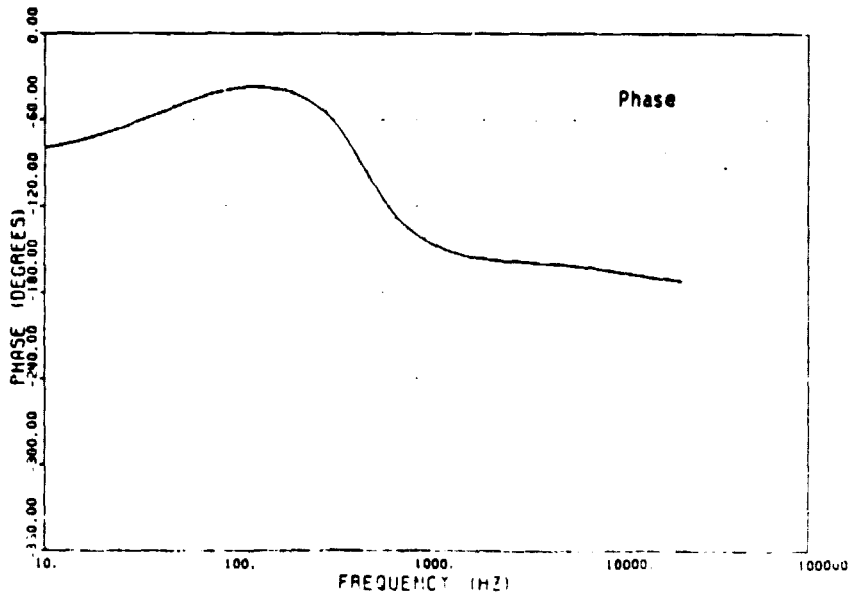
b.)

Figure 6.6.4   Average open loop transfer function bode plot
(3rd compensation).
G = 1, 2, 3, 4, 5, 6, 7.
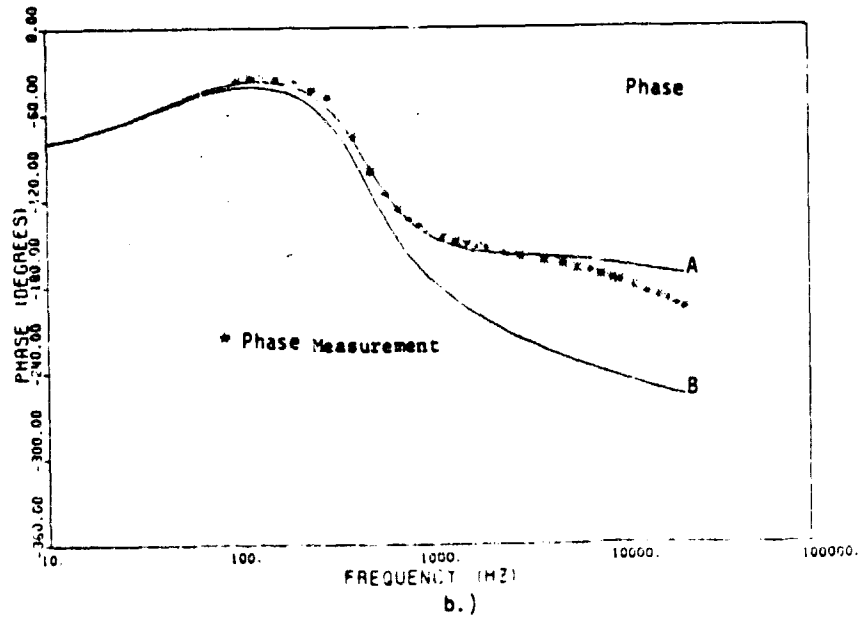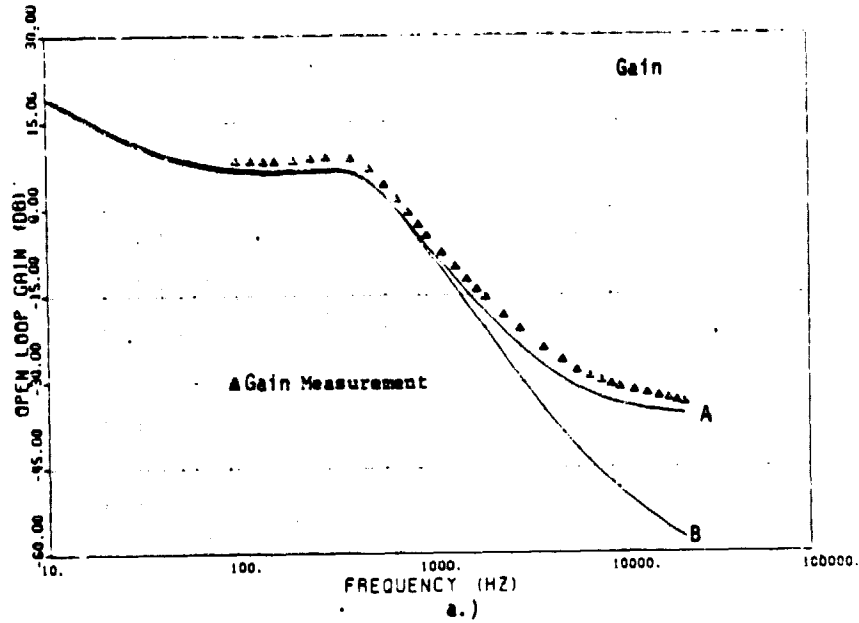
Figure 6.6.5 Open loop transfer function bode plot
(3rd compensation).
G = 1, D = .40
A - Average, B - Discrete-Average
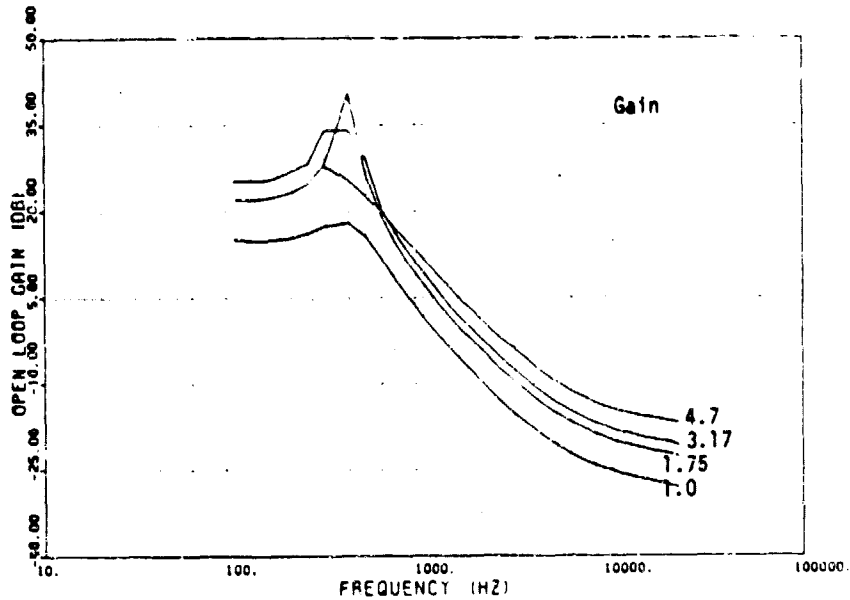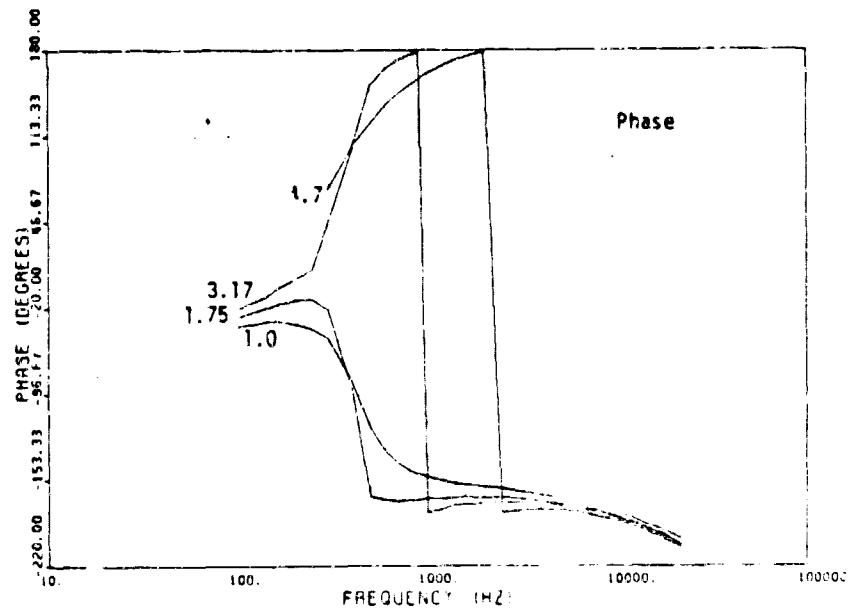
Figure 6.6.6   Open loop measurement data.
(3rd compensation).
G = 1, 1.75, 3.17, 4.7.
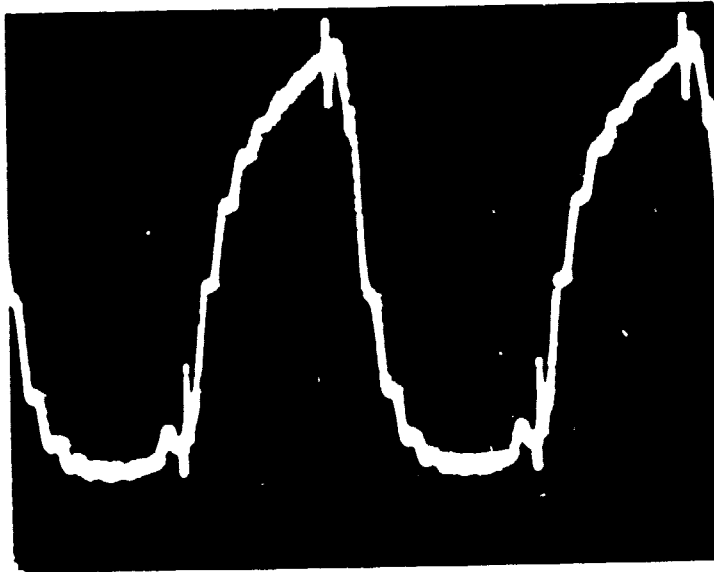
Figure 6.6.7   Error processor signal just before
system instability.
Scale: vertical .2v/div.
horizontal 5 μs/div.
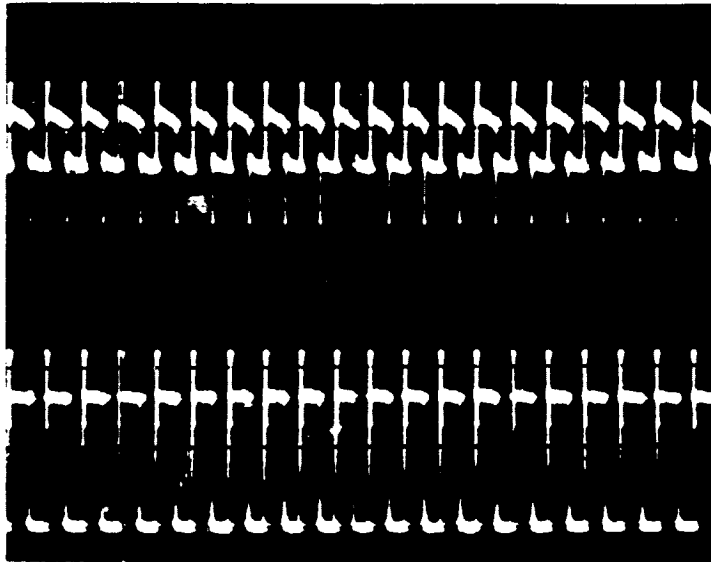
a.

b.

Figure 6.6.8   a.) Output voltage.
             Scale: vertical   1v/div.
             b.) V_{DS}
             Scale: vertical   20v/div.
                     horizontal 50 μs/div.

195

a.

b.
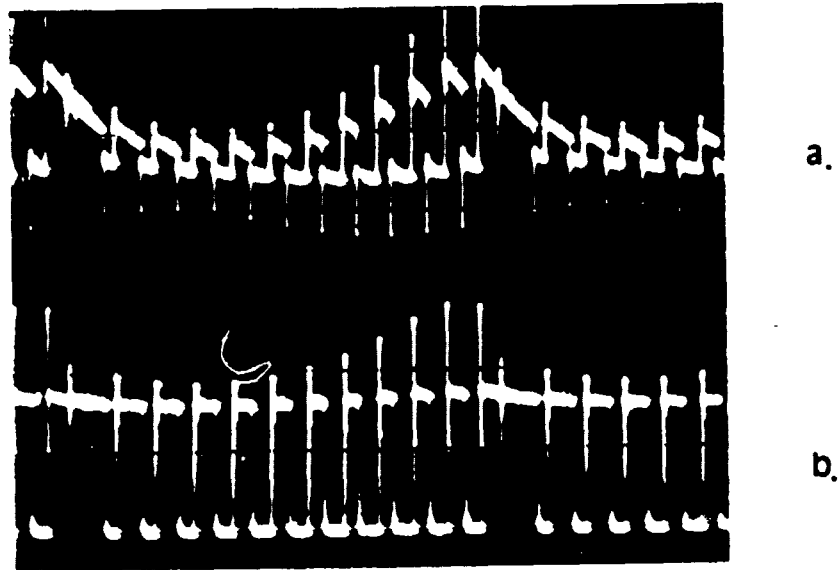
Figure 6.6.9 a.) Output voltage (unstable).
Scale: vertical   1v/div.
b.) V_{DS} (unstable).
Scale: vertical   20v/div.
horizontal 50 µs/div.

high frequencies. Although, measurement data tracks closely
with the average model as illustrated in Figure 6.6.5, both
informations are incorrect. It is quite evident that the
discrete-average model is more accurate.

6.7 SUMMARY

As illustrated in this chapter, the nature of the compen-
sation network determines the appropriate model to use.
When the compensation performs a good integration(an effec-
tive low-pass filter) so that all modulation components at
the output voltage are combined and form an integral part of
the error signal, the average power stage model is the more
accurate one. When the compensation is not an effective
low-pass filter or only performs limited integration, the
discrete-average model is the more accurate one.

In addition, the measurement data is not accurate if the
waveform to be evaluated is of a discontinuous nature.
Since the output voltage of the boost and buck/boost con-
verters are of a discontinuous fashion, the measurement needs
to be performed with great care. When the compensation per-
forms a good integration, the measurement data can accurate-
ly be obtained by opening the loop between the compensation
and the PWM. The loop should not be opened right after the
.converter output, because of the discontinuous nature of the
output voltage. The measurement data is inaccurate when the

compensation is not a good low-pass filter.

Chapter VII

MODELING OF DC-DC CONVERTERS IN THE
DISCONTINUOUS MODE

7.1 INTRODUCTION

A dc-dc converter enters the discontinuous mode when the
energy stored in the inductor during the T_{ON} interval (men-
tioned in Chapter II) is completely released to the load pri-
or to the end of one complete switching cycle. The discon-
tinuous mode of operation can be caused by a reduction of
inductance in the energy storage inductor, a reduction of
the switching frequency or an increase in the load resis-
tance. This results in the switch and diode current becom-
ing a zero value for a portion of the switching period. The
condition that the inductor curent is zero is only true for
the conventional inductive energy storage converters such as
the buck, boost and buck/boost converters. However, for a
capacitive energy storage converter such as the Cuk Convert-
er [22] the inductor current value is nonzero; yet it is
maintained at a constant value during a portion of the T_{OFF}
interval.

Certain abrupt changes often can be observed in the
converter breadboard performance, when the discontinuous
mode is entered. [12] For example, the system order

is reduced by one, the transient response may change from oscillatory to well damped and the audio susceptibility is improved. The stability nature can be changed from an unstable system to a stable one. However, to maintain the same inductor current dc level as in the continuous mode, the switch is subjected to higher stress and switching losses.

Various modeling techniques have been presented, describing the converter in the discontinuous mode. These have been mentioned previously in Chapter I. The purpose of this chapter is to evaluate these modeling techniques and, to determine a power stage model that is easy to implement, gives physical insight into system operation and preserves the input-output and state variable relationships. The model should be general and the process by which it is determined, straight forward , so that it could be applied to any converter. From the modeling techniques that have been mentioned in Chapter I, two viable techniques are discussed. They are the Discrete Impulse Response Technique [12] (already discussed in Chapter II) and the averaging method of Middlebrook and Cúk [16].

A comparison is made between the average model and the discrete model. There is virtually no difference in the results of these two models. However, the average model is not a general and straight forward one and the discrete mo-

del is complex and cumbersome with little physical insight. The discrete-average model for the discontinuous mode is introduced. The model gives the same results as the average model but is general and straight forward.

7.2 AVERAGE MODEL

The switching regulator power stage, during one cycle of operation, can be represented by three piecewise linear vector differential equations as shown by (7.2.1), (7.2.2) and (7.2.3). For the boost converter these equations represent a specific circuit topology as shown in Figure 2.3.1.

$$\dot{x}_1 = A_1 x_1 + b_1 v_I \qquad \text{during } T_{ON} \qquad (7.2.1)$$

$$\dot{x}_2 = A_2 x_2 + b_2 v_I \quad \text{during } T_{F1} \qquad (7.2.2)$$

$$\dot{x}_3 = A_3 x_3 + b_3 v_I \quad \text{during } T_{F2} \quad (7.2.3)$$

The time intervals T_{ON}, T_{F1} and T_{F2} are defined in Figure 7.2.1. The representations are averaged in the same fashion as in the continuous mode to give a single period representation, as shown below

$$\dot{x} = [d_1 A_1 + d_2 A_2 + d_3 A_3] \underline{x} + [d_1 b_1 + d_2 b_2 + d_3 b_3] v_I$$

$$\dot{\underline{x}} = A\underline{x} + bv_I \qquad (7.2.4)$$

$$v_0 = [d_1 c_1 + d_2 c_2 + d_3 c_3] \underline{x}$$

$$v_0 = c\underline{x}$$
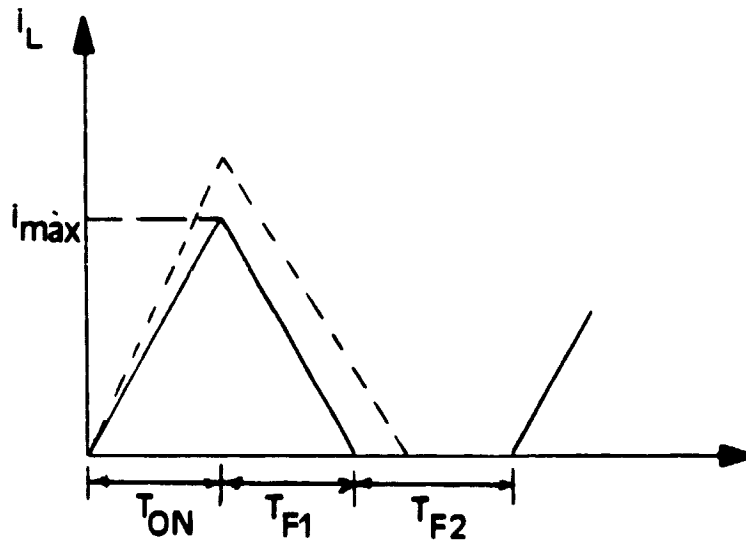
Figure 7.2.1 Instantaneous inductor current.

———steady state

------perturbed state

average state $\underline{x}$ is continuous and is equal to the average inductor current, i_L and average capacitor voltage, V_c In order to explain the observation of the order reduction in the system, the concept of discrete derivation is introduced.

As seen in Figure 7.2.1, the instantaneous current is restricted in its trajectory since

$$i_L(0) = i_L(T_{ON} + T_{F1}) = i_L(T_{ON} \ T_{F1} + T_{F2}) = 0 \qquad (7.2.5)$$

and $i(t) = 0$ for $T_{ON} + T_{F1} < t < T_{ON} + T_{F1} + T_{F2}$

This is an incorrect general assumption on the inductor current since the inductor current in the Cuk converter does not fall to zero.

The discrete derivative for the inductor current is defined as

$$\frac{i_L(T_{ON} + T_{F1} + T_{F2}) - i_L(0)}{T_{ON} + T_{F1} + T_{F2}} \qquad (7.2.6)$$

and under the conditions in (7.2.5) is equal to zero. However, this is a discrete equation used to determine the condition on the inductor current after it has been averaged. This discrete condition is then introduced into the continuous average model in order to justify the reduction of system order. The authors further introduce a "new" inductor

current quantity as a substitute for the continuous averaged
inductor current as shown in Figure 7.2.1. The somewhat
ambiguous justification for this subst'tution is to repre-
sent the departure of the state from the steady state and
is perturbed when a perturbation is introduced into the input
as shown in Figure 7.2.1. The newly introduced variable isn't
a true average variable. At this point the model is perturbed
and linearized. Introducing variations in the line voltage
and duty cycle ratio by the following substitutions

$$d_1 = D + \hat{d}, \quad d_2 = D_2 + \hat{d}, \quad d_3 = D_3 + \hat{d}$$

$$v_0 = V_0 + \hat{v}_0 \tag{7.2.7}$$

will cause perturbations in the 'state' and output, as shown
below.

$$\underline{x} = \underline{X} + \hat{\underline{x}} = \begin{bmatrix} \dfrac{I_{max}}{2} \\ \mathcal{V}_c \end{bmatrix} + \begin{bmatrix} \dfrac{\hat{i}_{max}}{2} \\ \hat{v}_c \end{bmatrix} \tag{7.2.8}$$

$$v_0 = V_0 + \hat{v}_0$$

Makin the above substitutions and assuming that departures
of the states from their corresponding steady state values
are small compared to the steady state values themselves al-
lows 2nd order terms to be neglected. The average model in
final form is shown below. The dc model is:

$$\underline{X} = -A^{-1}bV_I \tag{7.2.9}$$

The ac model is:

$$\hat{\underline{X}} = A\hat{\underline{x}} + b\hat{v}_I + \hat{d}[(A_1-A_3)\underline{X} + (b_1 - b_3)V_I] + \hat{d}_2[(A_1 - A_2)\underline{X} + (b_2 - b_3)V_I]$$

$$\tag{7.2.10}$$

where $\dot{\hat{\underline{x}}} = \begin{bmatrix} 0 \\ \dfrac{d\hat{V}_c}{dt} \end{bmatrix}$.

This model can be expressed in state variable, transfer function and circuit forms. But an incorrect assumption is made on the inductor current, as is summarized in the following.

In [22] while discussing the Cuk converter in discontinuous mode it is stated that "Namely, as has been customary with all so-far known cases of the discontinuous inductor currents, they are assumed to start at zero and fall to zero current level, as in" Figure 7.2.1. "This, is however wrong and leads to some contradictory results." [22] One of which is that the dc voltage gain is independent of the duty ratio. [22] Therefore, the average model for the discontinuous mode is not a general one. There are conditions for a particular case that have been incorrectly applied to a general case.

Those conditions are:

1. The inductor current is zero for a period of time. For the inductive energy storage converters such as the buck, boost and buck/boost converters this is true, but for capacitive energy storage converters such as the Cuk converter, this is not true [22]. In order to correct this, constraints must be applied to the average model after it has been developed.

2. A discrete equation has been applied to a continuous equation.

Because this particular condition is assumed for general application, constraints must be introduced after model derivation to the average model in order to analyze the Cuk converter in the discontinuous mode [22]. Therefore, this model is not general and the process to obtain the expressions is not straightforward, since constraints based on the particular type of converter must be introduced.

The transfer functions are illustrated by the block diagram in Figure 7.2.2. The blocks in the diagram are defined in Tables 7.2.1 and 7.2.2 for each converter. These transfer functions are from [16].

7.3 DISCRETE IMPULSE RESPONSE MODEL

The representation of the conventional dc-dc converters discontinuous mode by the Discrete Impulse Resonse Technique has already been discussed in Chapter II. As shown in Chapter II, the process by which the model is obtained is a very complex one. Furthermore, the expressions are very cumbersome and can only be expressed in the transfer function form. This impedes its practical usefulness and physical insight into the system operation is not easily obtainable. However, this model is accurate to one-half the switching frequency.

The discrete model transfer functions are listed in [12].
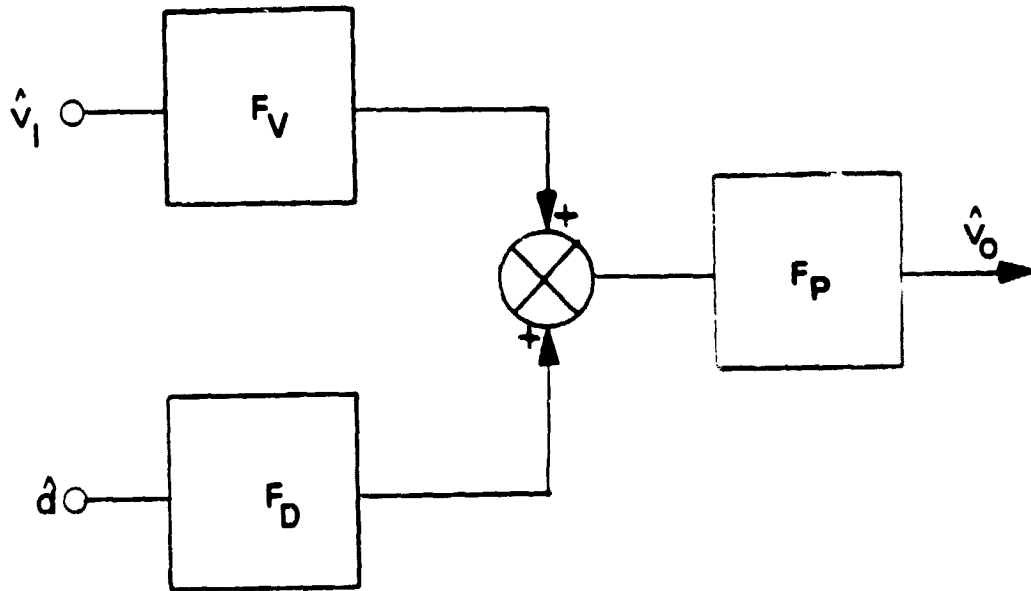
Figure 7.2.2 Block Diagram of transfer functions of
Buck, Boost and Buck/Boost converters
in Discontinuous mode.

Table 7.2.1 Block Diagram Transfer Function Parameters

	Buck	Boost	Buck/Boost
F_v	$\dfrac{V_o}{V_I}$	$\dfrac{V_o}{V_I}$	$\dfrac{N_s}{N_p}\dfrac{V_o}{V_I}$
F_D	$2\dfrac{V_o}{D}\left(1 + \dfrac{V_I}{V_I - V_o}\right)$	$2\dfrac{V_o}{D}\left(1 + \dfrac{V_o}{V_o - V_1}\right)$	$\dfrac{N_s}{N_p}\dfrac{V_I}{D_2}$
F_p	$\dfrac{1}{1 + \dfrac{s}{\omega_p}}$	$\dfrac{1}{1 + \dfrac{s}{\omega_p}}$	$\dfrac{1}{1 + \dfrac{s}{\omega_p}}$

Table 7.2.2 Fp Block Diagram Parameters

	ω_p
Buck	$\frac{1}{RC}(1 + \frac{V_I}{V_I - V_o})$
Boost	$-\frac{1}{RC}(1 + \frac{V_o}{V_o - V_I})$
Buck/Boost	$\frac{2}{R_L C}$

7.4 COMPARISON OF THE DISCRETE MODEL AND THE AVERAGE MODEL

A comparison of the discrete and average models is made on the basis of transfer functions. The transfer functions of the buck, boost and buck/boost for each have already been presented in the previous sections.

The transfer functions from both models contain only one pole and no zeroes. Any other comparisons of the expressions would be difficult to obtain because of the complexity of the expressions of the discrete model.

One example is presented here and three more are shown in Appendix B. The load, frequency and energy storage inductance are varied. This example is the boost converter with the following numerical values (refer to Figure 1.1.1):

$R = .4\Omega$

$R_c = .17\Omega$

$L = 36.2\ \mu h$

$C = 300\ \mu f$

$R_L = 50.\Omega$

$V_o = 37.5_v$

$V_I = 28_v$

$T_p = 33.3\ \mu s$

Figures 7.4.1-7.4.6 show virtually no difference in the two models.

Therefore, from the results presented, the average model is as accurate as the discrete model. However, the average model derivation is not general and certainly less rigorous. The defficiency of the average modeling technique for the discontinuous model, necessitates the development of a discrete-average modeling technique and is presented in the next section.

7.5   DISCRETE-AVERAGE MODEL IN THE DISCONTINUOUS MODE

This technique determines the solution vector for each interval T_{ON}, T_{F1} and T_{F2} in equation (7.2.1-3). The general solution for (7.2.1-3) is :

$$\underline{x}_K(t_0 + \Delta t) = e^{A_K \Delta t}[\underline{x}_K(t_0) + \int_0^{\Delta t} e^{-A_K T} b_K v_I \, dT] \quad (7.5.1)$$

with K = 1, 2, 3.

$$\text{Let} \quad e^{-A_K T} \simeq I - A_K T \quad (7.5.2)$$

$$\text{and} \quad e^{A_K t} \simeq I + A_K t. \quad (7.5.3)$$

Integrating and expanding the above equation and neglecting the higher order terms, [13] the desired solution is

Figure 7.4.1   Gain plot varying the load.
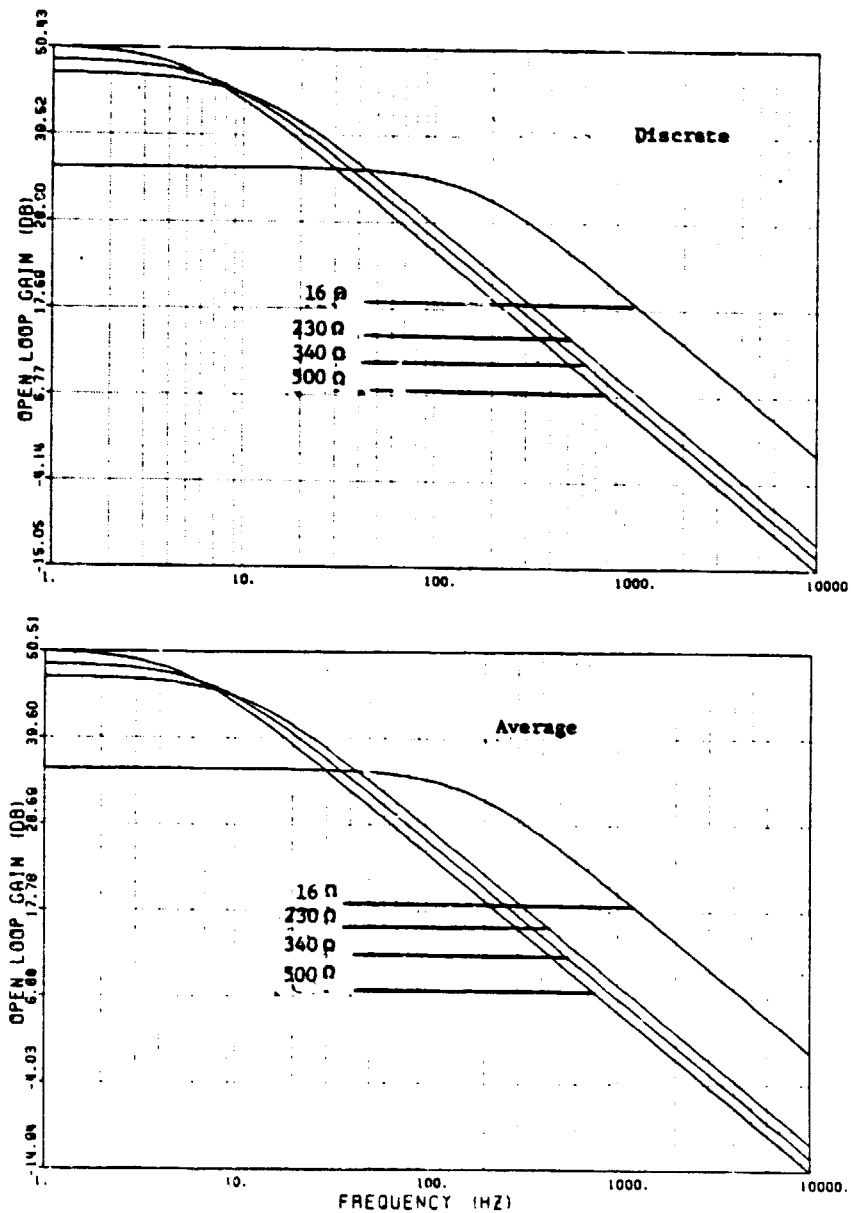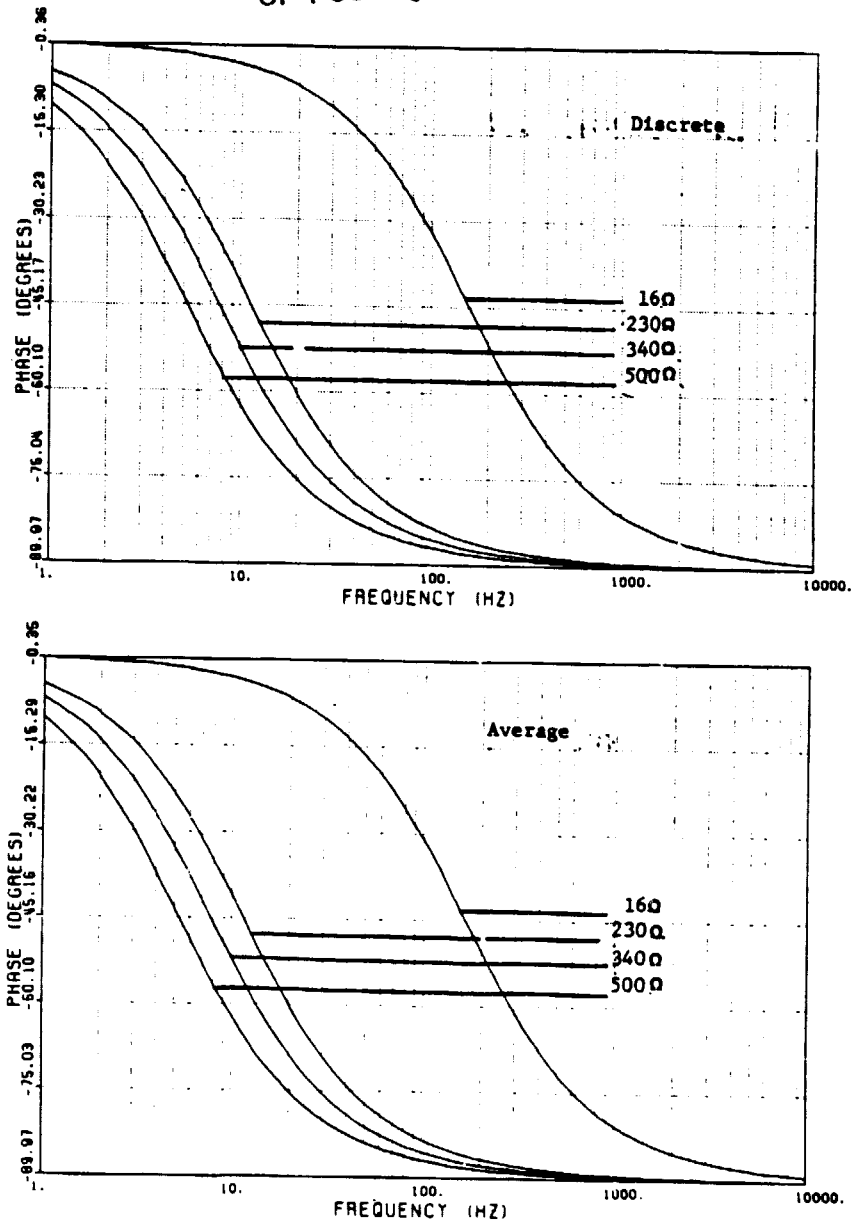
Figure 7.4.2 Phase plot varying the load.
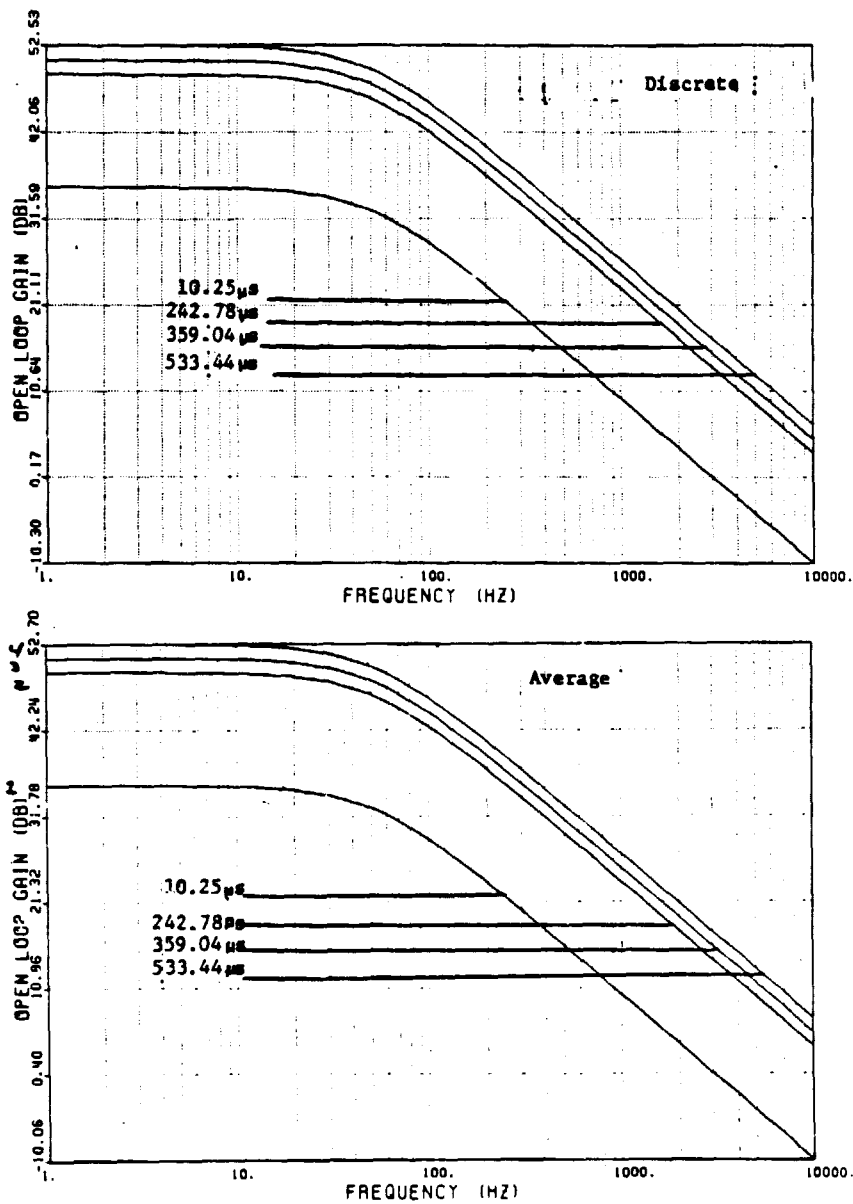
Figure 7.4.3 Gain plot varying the frequency.

214
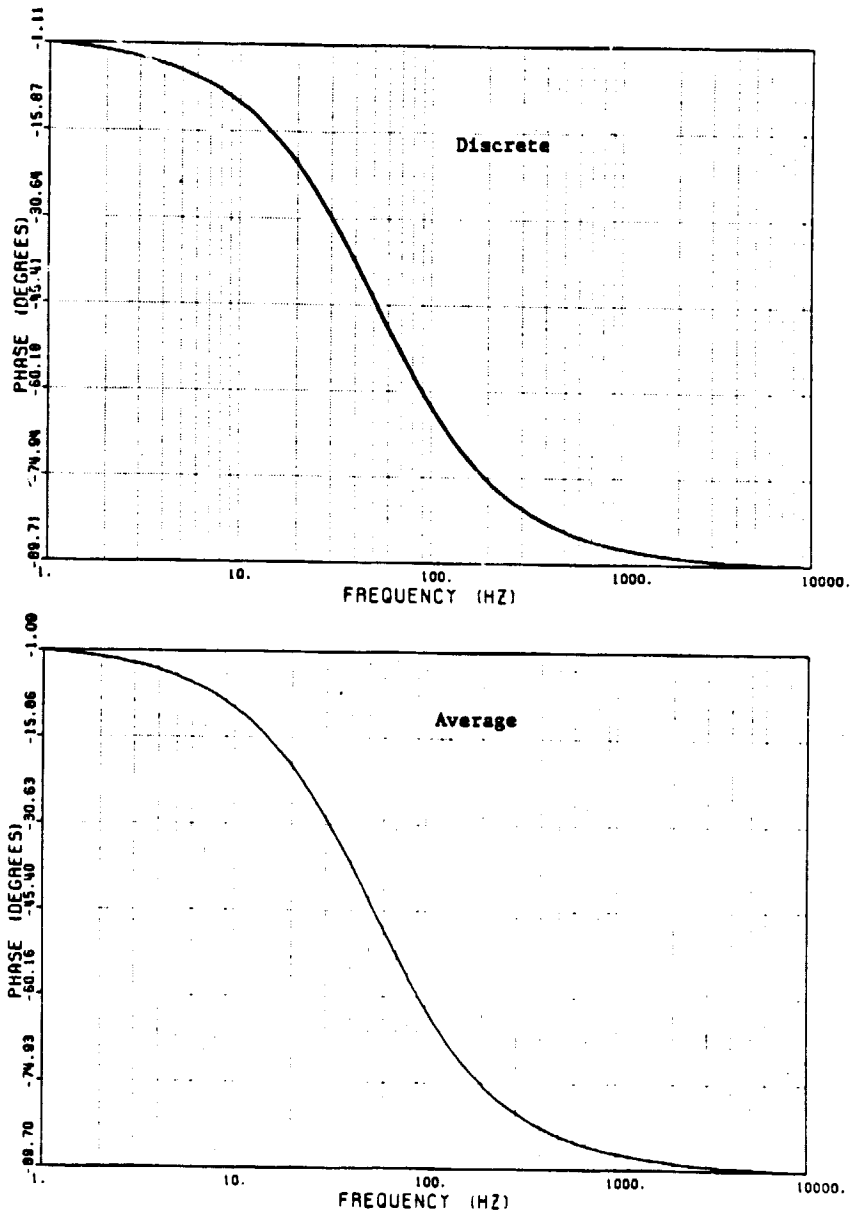
Figure 7.4.4 Phase plot varying the frequency.

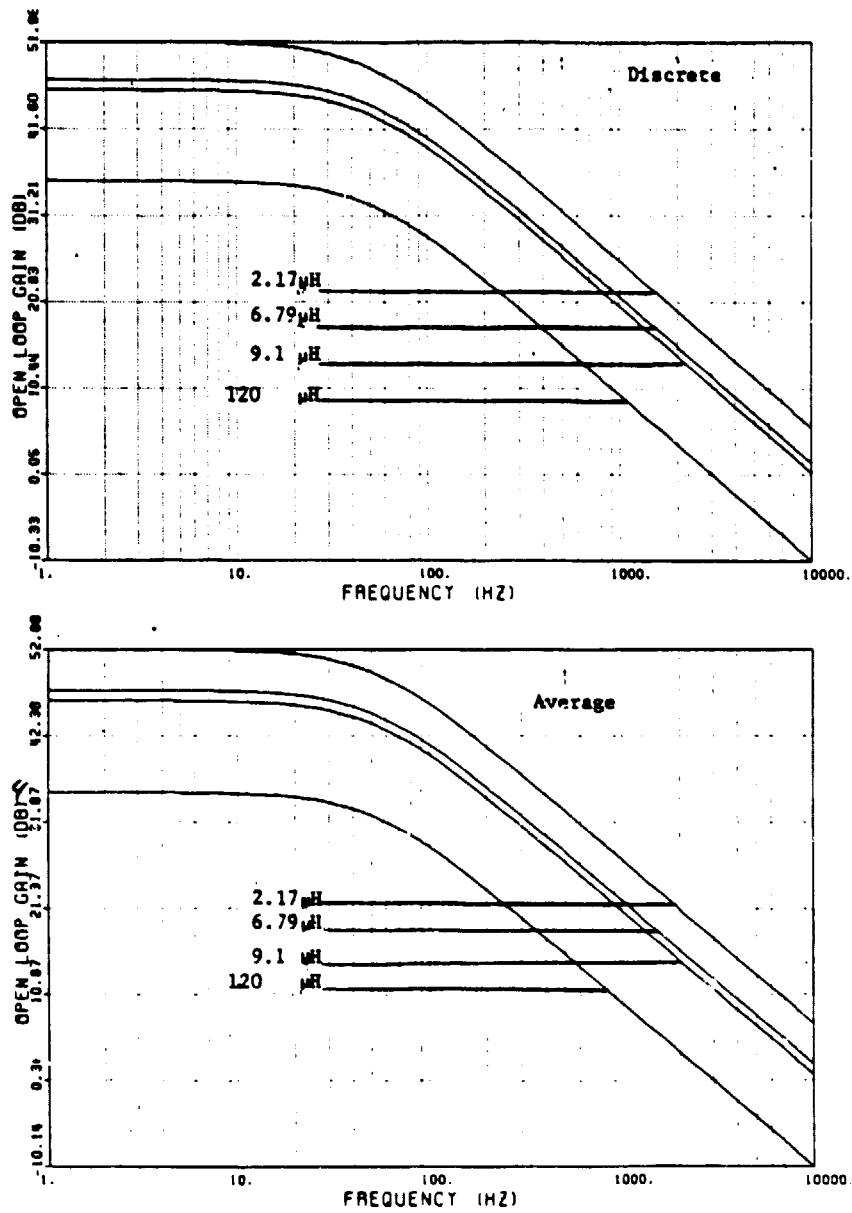Figure 7.4.5 Gain plot varying the inductance.
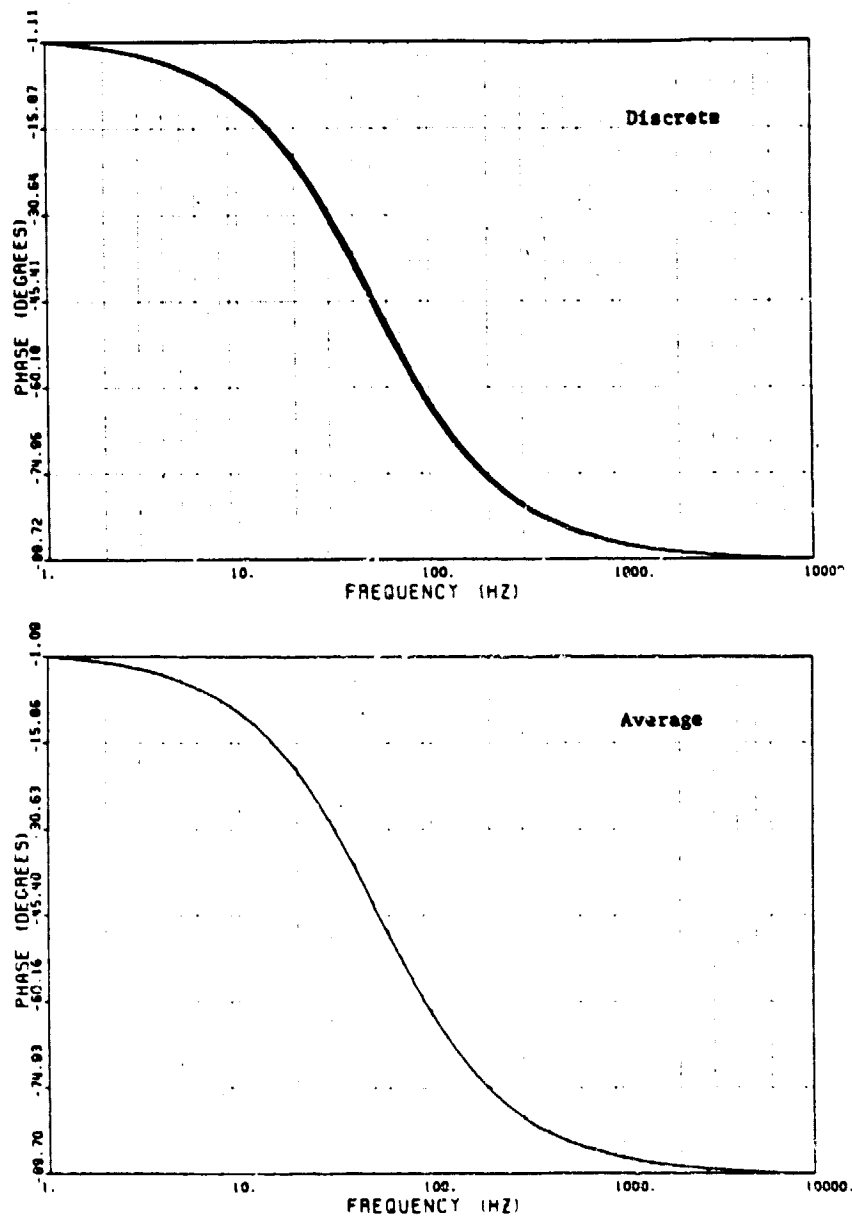
Figure 7.4.6   Phase plot varying the inductance

$$\underline{x}_K(t_0 + t) = \underline{x}(t_0) + [A_K X_K(t_0) + b_K v_I] \, t \quad (7.5.4)$$

The solution vector for the complete cycle is determined by repeated use of (7.5.4) for the intervals T_{ON}, T_{F1} and T_{F2}. Neglecting all of the higher terms, the solution is

$$\underline{x}((n+1)T_p) \simeq \underline{x}(nT_p) + [A_1\underline{x}(nT_p) + b_1v_I] \, T_{ON} \quad (7.5.5)$$

$$+[A_2\underline{x}(nT_p) + b_2v_I] \, T_{F1} + [A_3\underline{x}(nT_p) + b_3v_I] \, T_{F2}.$$

Rearranging the above equation, dividing by T_p and letting $d_1 = \dfrac{T_{ON}}{T_p}$, $d_2 = \dfrac{T_{F1}}{T_p}$ and $d_3 = \dfrac{T_{F2}}{T_p}$ results in

$$\frac{\underline{x}((n+1)T_p) - \underline{x}(nT_p)}{T_p} = (A_1\underline{x}(nT_p) * b_1v_I)d_1$$

$$(7.5.6)$$

$$+(A_2\underline{x}(nT_p) + b_2v_I)d_2 + (A_3\underline{x}(nT_p) + b_3v_I) \, d_3$$

The discrete derivative is defined as

$$\underline{\dot{x}}(nT_p) = \frac{\underline{x}((n+1)T_p) - \underline{x}(nT_p)}{T_p} \quad (7.5.7)$$

Substituting (7.5.7) into (7.5.6) the expression is shown in a general form as:

$$\underline{\dot{x}}(nT_p) = \begin{bmatrix} \dot{i}_L(nT_p) \\ \dot{v}_c(nT_p) \end{bmatrix} = \begin{bmatrix} f_1(\underline{x}, \, d_1, \, d_2, \, d_3, \, \underline{u}) \\ f_2(\underline{x}, \, d_1, \, d_2, \, d_3, \, \underline{u}) \end{bmatrix} (7.5.8)$$

where $\underline{u}$ is the input vector. The conditions for the discontinuous mode are applied as follows. The discrete derivative of the inductor current (7.2.6) is zero, so that the above system has been reduced by one order. This leaves the capacitor voltage, as shown below.

$$\dot{v}_c(nT_p) = f_2(\underline{x}, d_1, d_2, d_3, \underline{u})\Big|_{i_L(nT_p) = 0} \quad (7.5.9)$$

From the other equation

$$f_1(\underline{x}, d_1, d_2, d_3, \underline{u})\Big|_{i_L(nT_p) = 0} = 0 \quad (7.5.10)$$

expressions for d_2 and d_3 are found, substituting in to (7.5.9) leaves

$$\dot{v}_c(nT_p) = f_2(\underline{x}, d_1, \underline{u})\Big|_{i_L(nT_p) = 0} \quad (7.5.11)$$

The output expression is determined by sampling the averaged state. The appropriate sampling point must be chosen according to the type of duty cycle control employed. Figure 7.5.1 shows the discontinuous output voltage waveform for the boost and buck/boost converters. The error processor signal is the attenuated, inverted output voltage rip-
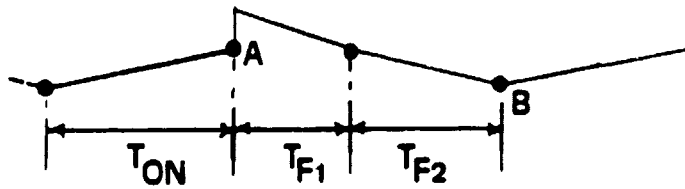
Figure 7.5.1   Boost and Buck/Boost output voltage waveform.
(Discontinuous model)

ple. The intersection of this waveform with a ramp signal determines the duty cycle. For constant frequency and constant off time control the intersection of the error processor signal and the clocked ramp signal occurs at point A, the T_{ON} part of the output voltage, similar to that described in Figure 7.5.1. For a constant frequency and constant off time controller, the sampling should be chosen at the beginning of the cycle.

$$v_o(nT_p) = \frac{R_L}{R_L + R_C} v_c(nT_p) \tag{7.5.12}$$

For the constant on time controller the intersection of the error processor signal and the clocked ramp signal occurs at point B, the T_{OFF} part of the output voltage. A modulation in the duty cycle would correspond to a modulation in the T_{OFF} part of the output voltage ripple. For this type of control, the sampling point should be chosen at the end of the cycle. For the buck, boost and buck/boost converters the output expression for the end of the cycle is the same as the one for the beginning of the cycle because i_L is equal to zero at those points in the switching cycle. The ouput expression can be expressed as:

$$v_o(nT_r) = \frac{R_L}{R_L + R_C} v_o(nT_p) \tag{7.5.13}$$
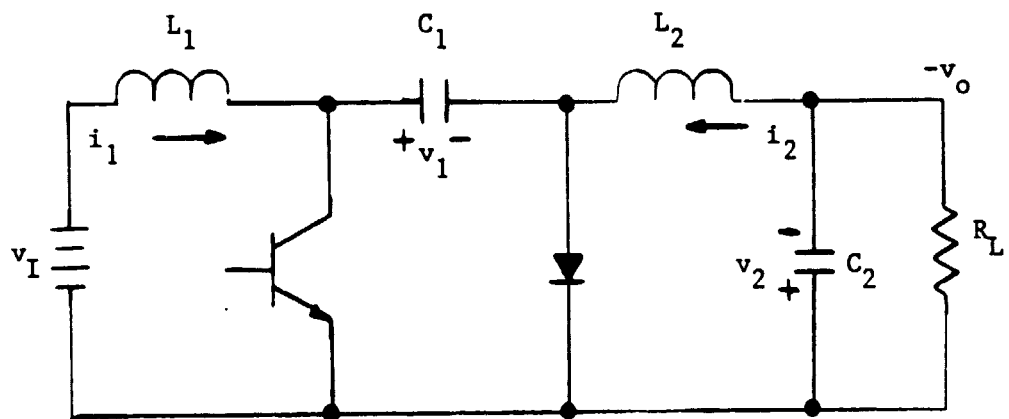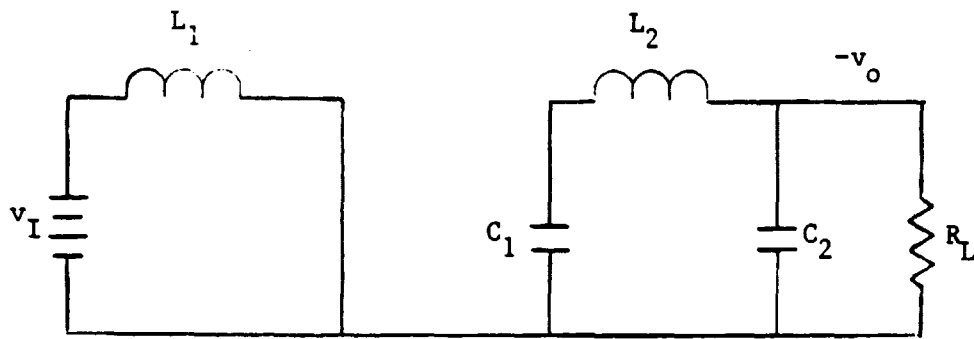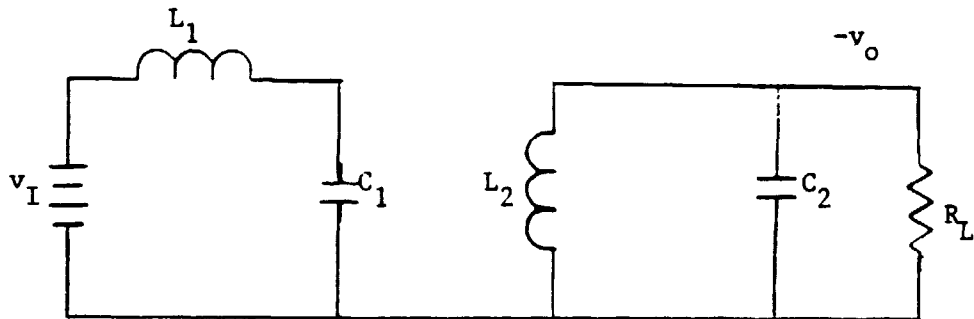
Figure 7.5.2 Cúk Converter.
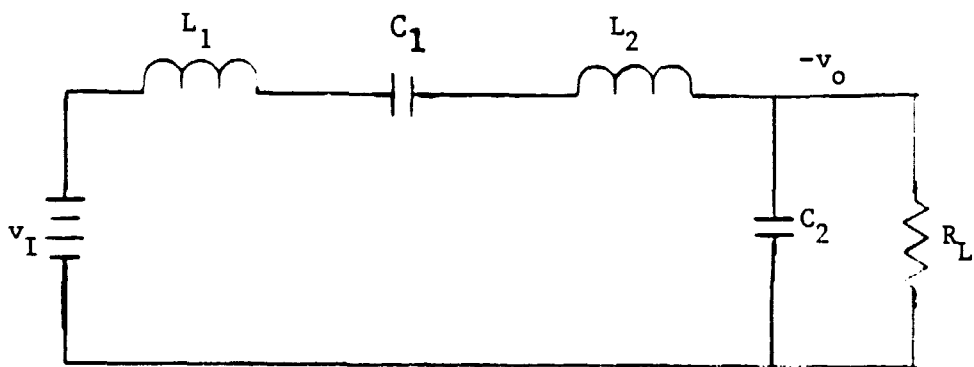
a.)

b.)

c.)

Figure 7.5.3 Cúk converter switching topologies for a
complete switching cycle.
a.) Switch on - Diode off
b.) Switch off - Diode on
c.) Switch off - Diode off

$$\underline{x} = \begin{bmatrix} i_1 \\ v_1 \\ i_2 \\ v_2^- \end{bmatrix} \qquad (7.5.15)$$

The state equations are assembled into the form of (7.5.8), resulting in

$$\underline{\dot{x}}(nT_p) = \begin{bmatrix} 0 & \dfrac{-d_2}{L_1} - \dfrac{d_3}{L_1+L_2} & 0 & \dfrac{d_3}{L_1+L_2} \\ \dfrac{1}{C_1} & 0 & \dfrac{-d}{C_1} & 0 \\ 0 & \dfrac{d}{L_2} & 0 & -\dfrac{d+d_2}{L_2} \\ -\dfrac{1}{C_2} & 0 & \dfrac{d+d_2}{C_2} - \dfrac{1}{R_L C_2} \end{bmatrix} \begin{bmatrix} i_1(nT_p) \\ v_1(nT_p) \\ i_2(nT_p) \\ v_2(nT_p) \end{bmatrix} + \begin{bmatrix} \dfrac{d+d_2}{L_1} + \dfrac{d_3}{L_1+L_2} \\ 0 \\ 0 \\ 0 \end{bmatrix} v_I \quad (7.5.16)$$

As it has been noted previously the currents i_1 and i_2 fall to a non zero level [22]. The onset of the discontinuous mode is determined by the diode current falling to zero, while the switch is off. The diode current is $i_1 + i_2$ and when that quantity falls to zero, the discontinuous mode is initialized. This results in the conditions

$$\dot{i}_1(nT_p) + \dot{i}_2(nT_p) = 0 \qquad (7.5.17) \qquad \text{and}$$

$$(i_1(nT_p) + i_1(nT_p) = 0 \qquad (7.5.18)$$

Substituting (7.5.17) and (7.5.18) in to (7.5.16) reduces the system by one order resulting in:

$$\underline{\dot{X}}(nT_p) = \begin{bmatrix} \dot{i}_1(nT_p) \\ \dot{v}_1(nT_p) \end{bmatrix} = \begin{bmatrix} 0 & -\dfrac{d_2}{L_1} - \dfrac{d_3}{L_1+L_2} & \dfrac{d_3}{L_1+L_2} \\ \dfrac{d_2+d_3}{C_1} & 0 & 0 \\ -\dfrac{1+d+d_2}{C_2} & 0 & \dfrac{1}{R_L C_2} \end{bmatrix} \begin{bmatrix} i_1(nT_p) \\ v_1(nT_p) \\ v_2(nT_p) \end{bmatrix}$$

$$+ \begin{bmatrix} \dfrac{d + d_2}{L_1} + \dfrac{d_3}{L_1 + L_2} \\ 0 \\ 0 \end{bmatrix} V_I \qquad (7.5.19)$$

The output expression is determined to be

$$V_o(nT_p) = V_2(nT_p) \qquad (7.5.20)$$

order to eliminate the d_2 and d_3 terms from (7.5.19), the equations for $i_1(nT_p)$ and $i_2(nT_p)$ are determined.

$$\dot{i}_1(nT_p) = - \left(\frac{d_2}{L_1} + \frac{d_3}{L_1 + L_2}\right) V_1(nT_p) + \frac{d_3}{L_1 + L_2} V_0(nT_p) \qquad (7.5.21)$$

$$+ \left(\frac{d + d_2}{L_1} + \frac{d_3}{L_1 + L_2}\right) V_I$$

$$\dot{i}_2(nT_p) = \frac{d}{L_2} v_1(nT_p) - \frac{d + d_2}{L_2} v_0(nT_p) \qquad (7.5.22)$$

Assume that the voltage drops across the inductors are small compared to $V_I(nT_p)$ and $V_o(nT_p)$ at the time instant equal to nT_p so that

$$V_1(nT_p) = V_0(nT_p) + V_I(nT_p) \qquad (7.5.23)$$

Substituting (7.5.23), (7.5.22) and (7.5.21) into (7.5.16) gives the following result.

$$d_2(nT_p) = \frac{V_I(nT_p)}{V_0(nT_p)} \, d(nT_p) \qquad (7.5.24)$$

Another equation relating d_3 with d_2 and d is needed, that equation is $d_3 = 1 - (d + d_2)$ (7.5.25).

Substituting the equations (7.5.24) and (7.5.25) eliminates the d_2 and d_3 terms in (7.5.16). The next step is to obtain the time equivalent system by letting $t = nT_p$, this results in:

$$\underline{\dot{x}}(t) = \begin{bmatrix} 0 & -\frac{1}{L_1}(\frac{V_I}{V_0}d) & -\frac{1}{L_1+L_2}(1-(1+\frac{V_I}{V_0})d) & \frac{(1-(1+\frac{V}{V_0})d)}{L+L} \\ \frac{1-d}{C_1} & 0 & 0 \\ \frac{-1+(1+\frac{V_I}{V_0})d}{C_2} & 0 & \frac{1}{R_L C_2} \end{bmatrix} \begin{bmatrix} i_1(t) \\ V_1(t) \\ V_2(t) \end{bmatrix}$$

$$+ \begin{bmatrix} \frac{(1+\frac{V_I}{V_0})d}{L_1} & + & \frac{1-(1+\frac{V_I}{V_0})d}{L_1+L_2} \\ 0 \\ 0 \end{bmatrix} V_I \qquad (7.5.26)$$

$$v_0(t) = V_2(t)$$

The model is perturbed by making the following substitutions, $d = D + \hat{d}$, $V_I = V_I + \hat{v}_I$, $i_1 = I_1 + \hat{i}_1$, $v_1 = V_1 + \hat{v}_1$, $V_2 = V_2 + \hat{v}_2$ and $V_0 = V_0 + \hat{v}_0$; assuming that departures from the steady state are small, allows the higher order terms to be neglected. The dc model is:

$$\underline{0} = \begin{bmatrix} 0 & -\frac{1}{L_1}(\frac{V_I}{V_0}D) -\frac{1}{L_1+L_2}(1-(1+\frac{V_I}{V_0})D) & \frac{(1-(1+\frac{V_I}{V_0})D)}{L_1+L_2} \\ \frac{1-D}{C_1} & 0 & 0 \\ -\frac{1+(1+\frac{V_I}{V_0})D}{C_2} & 0 & \frac{1}{R_L C_2} \end{bmatrix} \begin{bmatrix} I_1 \\ V_1 \\ \dot{V}_2 \end{bmatrix}$$

$$+ \begin{bmatrix} \frac{(1+\frac{V_I}{V_0})D}{L_1} + \frac{1-(1+\frac{V_I}{V_0})D}{L_1+L_2} \\ 0 \\ 0 \end{bmatrix} V_I \qquad (7.5.27)$$

$$V_0 = V_2$$

In [22] the Cúk converter dc model is determined by introducing constrants into the dc equations. " These equations were determined by averaging the state space equations for the three switched networks... specifying the dc regime " [22]. These contraints are entered after the continuous system has been derived. The dc values from that analysis and the above are determined to be the same.

The ac model is:

$$\underline{\dot{\hat{x}}} = \begin{bmatrix} 0 & -\frac{1}{L_1}\frac{V_I}{V_0}D - \frac{1}{L_1+L_2}\left(1-\left(1+\frac{V_I}{V_0}\right)D\right) & \left(1-\left(1+\frac{V_I}{V_0}D\right)\right) \\ \frac{1-D}{C_1} & 0 & 0 \\ \frac{-1+\left(1+\frac{V_I}{V_0}\right)D}{C_2} & 0 & \frac{1}{R_L C_2} \end{bmatrix} \underline{\hat{x}'}$$

$$+ \begin{bmatrix} \dfrac{\left(1+\frac{V_I}{V_0}\right)D}{L_1} + \dfrac{1-\left(1+\frac{V_I}{V_0}\right)D}{L_1+L_2} + \dfrac{V_1}{L_1} + \dfrac{V_1}{L_1+L_2} - \dfrac{V_2}{L_1+L_2} \\ + V_I\left(\frac{1}{L_1} - \frac{1}{L_1+L_2}\right)\frac{D}{V} \\ 0 \\ 0 \end{bmatrix} \hat{v}_I$$

$$+ \begin{bmatrix} \dfrac{V_1}{L_1+L_2} - \dfrac{V_2}{L_1+L_2} + V_I\left(\frac{1}{L_1}-\frac{1}{L_1+L_2}\right) + \left(\frac{V_1}{L_1}+\frac{V_1}{L_1+L_2}-\frac{V_2}{L_1+L_2}+V_I\left(\frac{1}{L_1}-\frac{1}{L_1+L_2}\right)\right)\frac{V_I}{V_0} \\ 0 \\ 0 \end{bmatrix} \hat{d}$$

$$\text{(7.5.28)}$$

$$\hat{v}_0 = \hat{v}_2$$

In [22] the system is only observed to be a third order system, there is no small signal model presented with which the above model can be compared. The system is determined to be third order by noting the behavior of the sum current $i_1 + i_2$, which rises and falls to a zero level. Again this observation is determined after the model has been placed into a continuous time system.

In summary, the discrete-average model has been determined for the discontinuous mode. The model is accurate and has been demonstrated to be general by its application to the Cúk converter. The discrete-average model with the results described above, is determined to be the more desireable one to use.

Chapter VIII

CONCLUSIONS AND FUTURE WORK

8.1 CONCLUSIONS

In Chapter I an overview of dc-dc converter models was given. The analytical techniques provided a closed form solution. From these techniques, two viable ones were chosen in order to determine a new model. The discrete technique [12] is able to track the output voltage waveform accurately, but is complex and cumbersome to use and is normally expressed in the transfer function form. The average model [14,15] averages the output voltage, is easy to use, and can be expressed in state variable, circuit, and transfer function forms. The object, then, was to combine these two models, obtaining a new model that is able to accurately track the output voltage, is easy to use and can be expressed in state variable, circuit and transfer function forms.

Chapter II presented the average model in the continuous mode and extended inputs to include the load disturbance with the input voltage and the duty cycle ratio. A boost converter example was used to illustrate the development of the generalized modeling approach. A canonical circuit model of the buck, boost, and buck/boost converters was then presented. This model preserves the input, output and state variable properties of the converter and can be applied to any feedback control scheme.

230

The canonical circuit model presented earlier in [15] cannot be used in multiloop control schemes. The discrete model for continuous mode and discontinuous mode was derived in [12]. Essentially, the discrete model tracks the envelope of the output voltage waveform, neglecting the switching ripple and concentrating on the long range trend of the waveform. The average model effectively smooths out the switching ripple, resulting in a waveform that also indicates the long range trend.

Using the boost converter as an example, the transfer functions of the average model and discrete model were compared. The difference was determined to be in $\dfrac{-s^2}{\omega_z \omega_a}$ term in the average model, which adds additional phase lag to the system, in the high modulatory frequency range. This difference is caused by the average model's representation of the voltage drop across the ESR of the output filter capacitor. This voltage drop contains two modulation components, pulse width and amplitude. The average model averages these two effects.

In Chapter IV a new model, the discrete-average model, was presented. This model samples the average state in order to determine the output voltage expression. The duty cycle control determines the selection of the proper sampling point. Consequently, the output voltage expressions for the constant frequency and constant T_{OFF} duty cycle control are different from that of the constant T_{ON} control. The power stage model selection is therefore dependent on the duty cycle control. The discrete-average model points out the excessive phase delay of

the power stage model when the constant frequency or constant T_{OFF} duty cycle is used, compared with the constant T_{ON} duty cycle control. The insight that is gained from the analysis provided by this model enables judicious selection of a duty cycle controller.

In Chapter V the discrete-average model was extended to include the load disturbance as an input. The circuit models for the buck, boost, and buck/boost converters with constant frequency control were derived. A canonical circuit model that preserves the input, output, and state variable properties of the converter was presented for the buck, boost, and buck/boost converters with the constant frequency, constant T_{OFF} and constant T_{ON} control schemes. Also, the transfer functions for each converter with each type of control were presented.

Chapter VI essentially deals with the selection of the proper model (average or discrete-average) and some measurement concerns. The output voltage for the boost and buck/boost converters is discontinuous, containing a double envelope with duty cycle modulation. If the error processor (compensation) averages these components so that all modulation components are integrated and form an integral part of the error signal, the average model was determined to be accurate. On the other hand, if the error processor (compensation) was not a good lowpass filter or performed only limited integration, the discrete-average model is the better one to use.

The measurement of loop gain is often done in closed loop

fashion by injecting an ac signal into an appropriate loca-
tion of the feedback loop. If the waveform at the point when
the injected signal is placed is "smooth" and well-behaved,
the measurement data are accurate. However, if the waveform
at the place where the disturbance is injected, is of a dis-
continuous fashion, then the measurement data is not accurate.
Since the output voltage of the boost and buck/boost conver-
ters was of a discontinuous fashion, the loop gain measurement
needed to be performed with great care. When the circumstances
determined that the measurement was proper, the model verifi-
cation was performed by opening the loop between the compensa-
tion network (error processor) and the PWM. The loop-gain
measurement was performed with a gain and phase meter and the
measurement data then compared with the analytical predictions.
If the control loop waveforms were such that they circumvented
proper measurement of gain and phase, the model could be veri-
fied only at a particular operating point at which system insta-
bility occurs. When the error processor averaged the output
voltage, effectively smoothing out the waveform, the resulting
data provided results correlating to the average model predic-
tions. However, if the error processor provided limited inte-
gration so that the error signal was a discontinuous waveform,
the results from the inaccurate data did not correlate with the
model prediction.

Ine discontinuous mode of operation was discussed in
Chapter VII. The average model derivation was presented and

the problems with generality and model derivation were pointed out. The discrete model is complex and cumbersome. Its derivation is from [12]. However, the two models were shown to produce virtually the same results. The discrete-average model was applied to this mode of operation in a fashion that was general. The process to derive the converter model was straightforward. The expressions for the buck, boost, and buck/boost converters were the same as the ones derived by the average model. The discrete-average modeling technique was demonstrated by analyzing the Cúk converter.

In summary, a new model has been developed that is almost as accurate as the Discrete Impulse Response Technique and is easy to implement in circuit and state variable forms. This new model, the discrete-average model has been shown to be a function of the particular type of duty cycle control. The proper application of this new model and the average model was also addressed and has been shown to be largely a function of the error processor in the feedback loop. In the verification process, it was shown that the accuracy of the measurement data taken by a conventional technique was affected by the conditions at which the data was collected; therefore, the model could be verified only at the particular operating point at which system instability occurs.

8.2 SUGGESTIONS FOR FUTURE WORK

As discussed previously, when the error processor is not a good lowpass filter or performs only limited integration, the

gain and phase measurement described in Chapter VI provides results that no longer relate to model prediction. This situation is caused by the pulse width modulation component in the error signal. Under this condition, the operating point at which system instability occurs is the only means of model verification. A measurement technique is needed upon which the pulse width modulation component in the error signal has no effect and from which accurate data can be determined that do correlate with the model predictions. The conventional measurement technique uses an analog signal to perturb the duty cycle, and under certain conditions has been determined to be inadequate. The process of injecting a digital signal to perturb the duty cycle should be investigated.

The error processor determines the selection of the power stage model between average and discrete-average. For an error processor that provides limited integration, the discrete-average model is the better one to use. The discrete-average model points out the excessive phase delay of the power stage model when the constant frequency or constant T_{OFF} duty cycle control is used, compared with the constant T_{ON} duty cycle control. Therefore, the discrete-average model provides insight from the modeling analysis that enables careful selection of a duty cycle controller subject to the desired system performance characteristics. This provides a basis upon which the process of choosing a particular type of duty cycle control can be determined.

BIBLIOGRAPHY

[1] R.D. Middlebrook and S. Cúk, "Modelling and Analysis Methods for DC-To-DC Switching Converters," IEEE Int. Semiconductor Power Converter Conf., 1977.

[2] H.A. Owen, A. Capel and J.G. Ferrante, "Simulation and Analysis Methods for Sampled Power Electronic Systems," IEEE Power Electronics Specialists Conference, 1976 Record pp. 45-55.

[3] A.M. Collella, M.J. O'Sullivan and D.J. Conlino, "Systems Simulation," Book, Lexington Books, p. 90.

[4] J.C. Bowers, G. Wzobrist, C. Vors, T. Rodby and J.F. O'Reilly, "A Survey of Computer-aid-Design and Analysis Programs," Technical Report AFAPL-TR-76-33.

[5] R.E. Stephenson, "Computer Simulation for Engineers," Book, Harcourt Brace Jovanovich, Inc.

[6] F.C. Lee and Y. Yu, "Computer-Aided Analysis and Simulation of Switched DC-DC Converters," IEEE Trans. on Ind. Applic., Vol IA-15, No. 5 Sept/Oct 1979, pp. 511-520.

[7] R.P. Iwens, Y. Yu and J.E. Triner, "Time Domain Modeling and Stability Analysis of an Integral Pulse Frequency Modulated DC to DC Power Converter," IEEE PESC Record pp. 80-90.

[8] F.C. Lee, R.P. Iwens, Y. Yu and J.E. Triner, "Generalized Computer-aid Discrete Time Domain Modeling and Analysis of DC-DC Converters," IEEE PESC pp. 58-69.

[9] R.P. Iwens, F.C. Lee and J.E. Triner, "Discrete Time Domain Modeling and Analysis of DC-DC Converters with Continuous and Discontinuous Inductor Current," second IFAC Symposium of Control in Power Electronics and Electrical Drives, Proceeding, Oct. 1977, Dusseldorf, West Germany.

[10] R. Prajoux, J.C. Maysinard and J. Jalade, "Accurate Mathematical Modelling of PWM Regulators," NASA Technical Translation, NASA TTF-15947.

[11] A. Capel, J.G. Ferrante and R. Prajoux, "State Variable Stability Analysis of Multi-loop PWM Controlled DC-DC Regulators in Light and Heavy Mode," IEEE Power Electronics Specialists Conference, 1975 Record, pp. 91-101.

[12] F.C. Lee, Y. Yu and J.E. Triner, "Modeling of Switching Regulator Power Stages with and Without Zero-Inductor Current Dwell Time," PESC 76 Record, pp. 62-72.

[13] H.A. Owen, J.G. Ferrante and A. Capel, "Continuous-Time Models for PWM Switched Converters in Heavy and Light Models," European Space Research and Technology Centre, Noordwijk, the Netherlands.

[14] G.W. Wester and R.D. Middlebrook, "Low-Frequency Characterization of Switched DC-DC Converters," IEEE Trans. on Aerospace and Electronic Systems VOLAES-9, No. 3 May 1973 pp. 376-385.

[15] R.D. Middlebrook and S. Cúk, "A General Unified Approach to Modelling Switching-Converter Power Stages," IEEE PESC 76 76 Record pp. 18-34.

[16] S. Cúk and R.D. Middlebrook, "A General Unified Approach to Modelling Switching DC-To-DC Converters in Discontinuous Conduction Mode," IEEE PESC 77 Record pp 36-57.

[17] R.C. Wong, G.E. Rodriguez, H.A. Owen, Jr. and T.G. Wilson, "Application of Small-signal Modeling and Measurement Techniques to the Stability Analysis of an Integrated Switching Mode Power System," IEEE Power Electronics Specialists Conference, 1980 Record, pp. 104-118.

[18] W.M. Polinka, P.R.K. Chetty and R.D. Middlebrook, "State-Space Average Modelling of Converters with Parasitics and Storage-Time Modulation," IEEE Power Electronics Specialists Conference, pp. 119-143.

[19] A.R. Brown and R.D. Middlebrook, "Sampled-Data Modeling of Switching Regulators," IEEE Power Electronics Specialists Conference, 1981 Record, pp. 349-369.

[20] E.G. Gilbert, "Controllability and Observability in Multivariable Control Systems," SIAM J. Control Ser A. Vol 2 No. 1, 1963, pp. 128-151.

[21] R.D. Middlebrook, "Predicting Modulator Phase Lag in PWM Converter Feedback Loops," 1981 Proceedings of Powercon 8 H-4, pp. 1-6.

[22] S. Cúk, "Discontinuous Inductor Current Mode in the Optimum Topology Switching Converter," IEEE PESC 78 pp. 105-123.

[23] F.C. Lee and Y. Yu, "Input Filter Design for Switching Regulators," IEEE Trans AES, Vol. AES-15, No. 5 Sept. 1979 pp. 627-634.

[24] S. Kelkar, and F.C. Lee, "A Novel Input Filter Compensation Scheme for Switching Regulators," IEEE PESC 82, pp. 260-271.

APPENDICES

APPENDIX A

Detailed Expressions for the Transfer Functions of the
Average Model and Discrete/Average Model. (sections 2.2
and 5.2)

The transfer functions in the following tables have been
derived to include the parasitic effects of R_ℓ , R_c and R_s on
the average model and the discrete-average model.

Table A.1 The Average dc model operating conditions

	BUCK	BOOST	BUCK/BOOST
I_L	$\dfrac{v_I}{D R_L}\cdot\dfrac{1+\dfrac{R_c}{R_L}}{1+\dfrac{R_c}{R_L}+\dfrac{R_\ell}{R_L}\left(1+\dfrac{R_c}{R_L}\right)}$	$\dfrac{v_I}{(D')^2 R_L}\cdot\dfrac{1+\dfrac{R_c}{R_L}}{1+\dfrac{R_c}{D'R_L}+\dfrac{R_\ell}{(D')^2 R_L}\left(1+\dfrac{R_c}{R_L}\right)}$	$\dfrac{D}{(D')^2}\dfrac{N_s}{N_p}\dfrac{v_I}{R_L}\cdot\dfrac{1+\dfrac{R_c}{R_L}}{1+\dfrac{R_c}{D'R_L}+\dfrac{R_s}{(D')^2 R_L}\left(1+\dfrac{R_c}{R_L}\right)}$
v_C	$D v_I\cdot\dfrac{1+\dfrac{R_c}{R_L}}{1+\dfrac{R_c}{R_L}+\dfrac{R_\ell}{R_L}\left(1+\dfrac{R_c}{R_L}\right)}$	$\dfrac{v_I}{D'}\cdot\dfrac{1+\dfrac{R_c}{R_L}}{1+\dfrac{R_c}{D'R_L}+\dfrac{R_\ell}{(D')^2 R_L}\left(1+\dfrac{R_c}{R_L}\right)}$	$\dfrac{D}{D'}\dfrac{N_s}{N_p}v_I\cdot\dfrac{1+\dfrac{R_c}{R_L}}{1+\dfrac{R_c}{D'R_L}+\dfrac{R_s}{(D')^2 R_L}\left(1+\dfrac{R_c}{R_L}\right)}$
$\dfrac{v_O}{v_I}$	$D\cdot\dfrac{1+\dfrac{R_c}{R_L}}{1+\dfrac{R_c}{R_L}+\dfrac{R_\ell}{R_L}\left(1+\dfrac{R_c}{R_L}\right)}$	$\dfrac{1}{D'}\cdot\dfrac{1+\dfrac{R_c}{R_L}}{1+\dfrac{R_c}{D'R_L}+\dfrac{R_s}{(D')^2 R_L}\left(1+\dfrac{R_c}{R_L}\right)}$	$\dfrac{D}{D'}\dfrac{N_s}{N_p}\cdot\dfrac{1+\dfrac{R_c}{R_L}}{1+\dfrac{R_c}{D'R_L}+\dfrac{R_s}{(D')^2 R_L}\left(1+\dfrac{R_c}{R_L}\right)}$

Table A.2 The Discrete/Average dc model operating conditions

	BUCK	BOOST	BUCK/BOOST
I_L	$D\dfrac{V_I}{R_L}\dfrac{1+\frac{R_c}{R_L}}{1+\frac{R_c}{R_L}+\frac{R_\ell}{R_L}\left(1+\frac{R_c}{R_L}\right)}$	$\dfrac{V_I}{(D')^2 R_L}\dfrac{1+\frac{R_c}{R_L}}{1+\frac{R_c}{D'R_L}+\frac{R_\ell}{(D')^2 R_L}\left(1+\frac{R_c}{R_L}\right)}$	$\dfrac{D}{(D')^2}\dfrac{N_s}{N_p}\dfrac{V_I}{R_L}\dfrac{1+\frac{R_c}{R_L}}{1+\frac{R_c}{D'R_L}+\frac{R_s}{(D')^2 R_L}\left(1+\frac{R_c}{R_L}\right)}$
V_C	$DV_I\dfrac{1+\frac{R_c}{R_L}}{1+\frac{R_c}{R_L}+\frac{R_\ell}{R_L}\left(1+\frac{R_c}{R_L}\right)}$	$\dfrac{V_I}{D'}\dfrac{1+\frac{R_c}{R_L}}{1+\frac{R_c}{D'R_L}+\frac{R_\ell}{(D')^2 R_L}\left(1+\frac{R_c}{R_L}\right)}$	$\dfrac{D}{D'}\dfrac{N_s}{N_p}V_I\dfrac{1+\frac{R_c}{R_L}}{1+\frac{R_c}{D'R_L}+\frac{R_s}{(D')^2 R_L}\left(1+\frac{R_c}{R_L}\right)}$
$\dfrac{V_O}{V_I}$	$D\dfrac{1+\frac{R_c}{R_L}}{1+\frac{R_c}{R_L}+\frac{R_\ell}{R_L}\left(1+\frac{R_c}{R_L}\right)}$	$\dfrac{1}{D'}\dfrac{1+\frac{R_c}{D'R_L}}{1+\frac{R_c}{D'R_L}+\frac{R_s}{(D')^2 R_L}\left(1+\frac{R_c}{R_L}\right)}$	$\dfrac{D}{D'}\dfrac{N_s}{N_p}\dfrac{1+\frac{R_c}{D'R_L}}{1+\frac{R_c}{D'R_L}+\frac{R_s}{(D')^2 R_L}\left(1+\frac{R_c}{R_L}\right)}$

Table A.3   Buck Converter

Transfer Function	Transfer Function
$$\frac{\hat{v}_o(s)}{\hat{d}(s)} = V_I G \frac{1+R_C Cs}{1+\frac{s}{\omega_o Q}+(\frac{s}{\omega_o})^2}$$	$$\frac{\hat{i}_L(s)}{\hat{d}(s)} = \frac{V_I}{R_L} G \frac{1+(R_L+R_C)Cs}{1+\frac{s}{\omega_o Q}+(\frac{s}{\omega_o})^2}$$
$$\frac{\hat{v}_o(s)}{\hat{v}_I(s)} = DG \frac{1+R_C Cs}{1+\frac{s}{\omega_o Q}+(\frac{s}{\omega_o})^2}$$	$$\frac{\hat{i}_L(s)}{\hat{v}_I(s)} = \frac{D}{R_L} G \frac{1+(R_L+R_C)Cs}{1+\frac{s}{\omega_o Q}+(\frac{s}{\omega_o})^2}$$
$$\frac{\hat{v}_o(s)}{\hat{i}_o(s)} = R_\ell G \frac{1+\frac{s}{\omega_1 Q_1}+(\frac{s}{\omega_1})^2}{1+\frac{s}{\omega_o Q}+(\frac{s}{\omega_o})^2}$$ $$\omega_1 = \frac{1}{\sqrt{LC}} \frac{R_L}{R_L+R_C} \sqrt{\frac{R_\ell}{R_L}}$$ $$Q_1 = \frac{1}{\omega_1} \left(\frac{R_L}{R_L+R_C}\right)^2 \frac{\frac{R_\ell}{R_L}}{L/R_C+R_\ell C}$$	$$\frac{\hat{i}_L(s)}{\hat{i}_o(s)} = -\frac{1+R_C Cs}{1+\frac{s}{\omega_o Q}+(\frac{s}{\omega_o})^2}$$

$$G=(1+R_C/R_L) / (1+R_C/R_L+\frac{R_\ell}{R_L}(1+\frac{R_C}{R_L})); \quad \omega_o=\frac{1}{\sqrt{LC}}\frac{R_L}{R_L+R_C}(1+\frac{R_C}{R_L}+\frac{R_\ell}{R_L}(1+\frac{R_C}{R_L}))^{\frac{1}{2}};$$

$$Q=\frac{1}{\omega_o}\frac{R_L}{R_L+R_C}\frac{1+\frac{R_C}{R_L}+\frac{R_\ell}{R_L}(1+\frac{R_C}{R_L})}{\frac{L}{R_L}+[R_C+R_\ell(1+\frac{R_C}{R_L})]C}$$

Table A.4 Boost Converter

Transfer Funct.	Transfer Funct.
$\dfrac{\hat{v}_o(s)}{\hat{d}(s)} = G_d \dfrac{(1+\frac{s}{\omega_2})(1-\frac{s}{\omega_4})}{(\frac{s}{\omega_o})^2 + \frac{s}{\omega_o Q} + 1}$ $G_d = \dfrac{V_I}{(D')^2} \dfrac{M}{M_p} \cdot$ $\left(\dfrac{(1+\frac{R_C}{R_L})^2 \, [1+\frac{(D'-D)R_s}{(D')^2 R_L}]}{[1+\frac{R_C}{D'R_L}+\frac{R_s}{(D')^2 R_L}(1+\frac{R_C}{R_L})]^2} \right)$ $\omega_4 = \dfrac{(D')^2 R_L}{D L_e}(1+\frac{R_s(D'-D)}{(D')^2 R_L})$ $\omega_2 = \dfrac{1}{R_C C}$	$\dfrac{\hat{i}(s)}{\hat{d}(s)} = \dfrac{V_I}{(D')^3 R_L}\left(\dfrac{(1+\frac{R_C}{R_L})G_2}{(G_1)^2} \right) \cdot$ $\dfrac{\left(1+(R_s+R_C)\frac{G_3}{G_2}\right)}{1+\frac{s}{\omega_o Q}+(\frac{s}{\omega_o})^2}$
$\dfrac{\hat{v}_o(s)}{\hat{v}_I(s)} = \dfrac{D}{D'}\dfrac{M}{M_p}\dfrac{1+\frac{R_C}{D'R_L}}{G_1} \cdot$ $\dfrac{\left(1+\dfrac{\frac{R_C C}{1+\frac{R_C}{D'R_L}}\frac{R_L}{R_L+R_C}s}{}\right)}{1+\frac{s}{\omega_o Q}+(\frac{s}{\omega_o})^2}$	$\dfrac{\hat{i}(s)}{\hat{v}_I(s)} = \dfrac{D}{(D')^2}\dfrac{M}{M_p}\dfrac{s}{R_L}\dfrac{1+\frac{R_C}{R_L}}{G_1} \cdot$ $\dfrac{\left(1+(R_s+R_C)C_s\right)}{1+\frac{s}{\omega_o Q}+(\frac{s}{\omega_o})^2}$
$\dfrac{\hat{v}_o(s)}{\hat{i}_o(s)} = \dfrac{R_s}{(D')^2} \cdot$ $\left(\dfrac{1+\frac{R_s}{R_L}}{1+\frac{R_C}{D'R_L}+\frac{R_s}{(D')^2 R_L}(1+\frac{R_C}{R_L})} \right) \cdot$ $\dfrac{\left(1+\frac{s}{\omega_1 Q_1}+(\frac{s}{\omega_1})^2\right)}{1+\frac{s}{\omega_o Q}+(\frac{s}{\omega_o})^2}$ $\omega_1 = \dfrac{1}{\sqrt{L_s C}}\sqrt{\dfrac{R_s}{R_C}}$ $Q_1 = \dfrac{1}{\omega_1}\dfrac{1}{\frac{L_s}{R_s}+R_C C}$	$\dfrac{\hat{i}(s)}{\hat{i}_o(s)} = \dfrac{-1}{D'} \cdot \dfrac{1+\frac{R_C}{R_L}}{G_1} \cdot$ $\dfrac{\left(1+R_C C_s\right)}{1+\frac{s}{\omega_o Q}+(\frac{s}{\omega_o})^2}$

$G_1 = 1 + \dfrac{R_C}{D'R_L} + \dfrac{R_s}{(D')^2 R_L}(1+\frac{R_C}{R_L})$

$\omega_o = \dfrac{D'}{\sqrt{L_s C}}\sqrt{\dfrac{R_L}{R_L+R_C}}\sqrt{G_1}$

$G_2 = (1+D)(1+\frac{R_s}{D'R_L}) + \dfrac{R_s}{(D')^2 R_L}(1+\frac{R_C}{R_L})$

$Q = \dfrac{D'}{\omega_o}\dfrac{R_L}{R_L+R_C}\dfrac{G_1}{\frac{L}{(D')^2 R_L}+(\frac{R_C}{D'}+\frac{R_s}{(D')^2}(1+\frac{R_C}{R_L}))C}$

$G_3 = 1 + \dfrac{R_C}{D'R_L} + \dfrac{R_s}{D'R_L}(1+\frac{R_C}{R_L})$

Table A.5 Buck/Boost Converter

Transfer Function	Transfer Function
$$\frac{\hat{v}_o(s)}{\hat{d}(s)} = Gd \frac{(1+\frac{s}{\omega_z})(1-\frac{s}{\omega_s})}{(\frac{s}{\omega_o})^2+\frac{s}{\omega_o Q}+1}$$ $$Gd = \frac{V_I}{(D')^2}(1+\frac{R_c}{R_L})\cdot$$ $$\left(\frac{1-\frac{R_\ell}{(D')^2 R_L}(1+\frac{R_c}{R_L})}{[1+\frac{R_c}{D'R_L}+\frac{R_\ell}{(D')^2 R_L}(1+\frac{R_c}{R_L})]^2}\right)$$ $$\omega_z = \frac{1}{R_c C}$$ $$\omega_s \frac{(D')^2 R_L \frac{R_L}{R_L+R_c} - R_\ell}{L}$$	$$\frac{\hat{i}_L(s)}{\hat{d}(s)} = \frac{V_I}{(D')^2} \frac{1+\frac{R_c}{R_L}}{D'R_L}(2+\frac{R_c}{D'R_L})\cdot$$ $$\frac{\left(1+(R_\ell+R_c)C\frac{1+\frac{R_c}{D'R_c}}{2+\frac{R_c}{D'R_L}}s\right)}{1+\frac{s}{\omega_o Q}+(\frac{s}{\omega_o})^2}$$
$$\frac{\hat{v}_o(s)}{\hat{v}_I(s)} = \frac{\left(1+\frac{R_c}{D'R_L}\right)\left(1+\frac{R_c+Cs}{D'(1+\frac{R_c}{D'R_L})}\right)}{D'G} \frac{1}{1+\frac{s}{\omega_o Q}+(\frac{s}{\omega_o})^2}$$	$$\frac{\hat{i}_L(s)}{\hat{v}_I(s)} = \frac{\left(1+\frac{R_c}{R_L}\right)}{(D')^2 R_L G} \frac{\left(1+(R_\ell+R_c)Cs\right)}{1+\frac{s}{\omega_o Q}+(\frac{s}{\omega_o})^2}$$
$$\frac{\hat{v}_o(s)}{\hat{i}_o(s)} = G_i \frac{1+\frac{s}{\omega_1 Q_1}+(\frac{s}{\omega_1})^2}{1+\frac{s}{\omega_o Q}+(\frac{s}{\omega_o})^2}$$ $$G_i = R_c/R_L + \frac{1}{D'G}(\frac{R_\ell}{D'}-R_c)$$ $$\omega_1 = \frac{D'}{\sqrt{LC}}\cdot\frac{R_L}{R_L+R_c}\cdot$$ $$\left(\sqrt{1+\frac{R_c}{D'R_L}-\frac{D'R_c}{R_L+R_c}+\frac{R_\ell}{D'R_c}}\right)$$ $$Q_1 = \frac{1}{\omega_1}\cdot$$ $$\left(\frac{1+\frac{R_\ell}{D'R_c}(1+\frac{R_c}{D'R_L})(1+\frac{R_c}{R_L})}{L/(D')^2 R_c + R_\ell C}\right)$$	$$\frac{\hat{i}_L(s)}{\hat{i}_o(s)} = \frac{1+\frac{R_c}{R_L}}{D'G} \frac{1+R_cCs}{1+\frac{s}{\omega_o Q}+(\frac{s}{\omega_o})^2}$$

$$G = 1+\frac{R_c}{D'R_L}+\frac{R_\ell}{(D')^2 R_L}; \quad \omega_o = \frac{D'}{\sqrt{LC}}\sqrt{\frac{R_L}{R_L+R_c}}\sqrt{G}; \quad Q = \frac{D'}{\omega_o}\frac{R_L}{R_L+R_c}\frac{G}{\frac{L}{D'R_L}+\frac{R_\ell C}{D'}+R_cC(1+\frac{R_\ell}{D'R_L})}$$

245

Table A.6a) Constant frequency and constant off time transfer functions. Refer to Figure 5.4.1.

	Buck	Boost	Buck/Boost
F_{V1}	$DK_{LV1}\left(1 + \dfrac{s}{\omega_{LV1}}\right)$	$\dfrac{K_{LV1}}{D'}$	$\dfrac{D}{D'}\dfrac{N_s}{N_p}K_{LV1}$
F_{V2}	$\dfrac{DK_{V2}}{R_L}\left(1 + \dfrac{s}{\omega_{V2}}\right)$	$\dfrac{K_{V2}}{(D')^2 R_L}\left(1 + \dfrac{s}{\omega_{V2}}\right)$	$\dfrac{D}{(D')^2}\dfrac{K_{V2}}{L_p^2 R_L}\left(1 + \dfrac{s}{\omega_{V2}}\right)$
F_{D2}	$V_1 K_{LD1}\left(1 + \dfrac{s}{\omega_{LD1}}\right)$	$\dfrac{V_2}{(D')^2}K_{LD1}\left(1 + \dfrac{s}{\omega_{LD1}}\right)$	$\dfrac{V_I}{(D')^2}\dfrac{N_s}{N_p}K_{LD1}\left(1 + \dfrac{s}{\omega_{LD1}}\right)$
F_{D2}	$\dfrac{V_I}{R_L}K_{D2}\left(1 + R_L + R_c)C_s\right)$	$\dfrac{V_I}{(D')^3 R_L}(K_{D2} + \dfrac{(R_L+R_c)^2}{R_L}(1 + \dfrac{R_c}{D'R_L})C_s)$	$\dfrac{V_I}{(D')^3 R_L}\dfrac{L_s}{L_p}(1 + (R_L+R_c)CC_1 s)$
F_{I1}	$R_2 K_{LI1} 1 + \dfrac{s}{\omega_1 Q_1} + (\dfrac{s}{\omega_1})^2)$	$\dfrac{R_\ell}{(D')^2}K_{LI1}(1 + \dfrac{L}{R_\ell}s)$	$\dfrac{R_c//R_L}{D'}(K_{LI1} + s\dfrac{L_s}{D'R_c}(1 + \dfrac{R_c}{R_L})K_{V2})$
F_{I2}	$-(1 + R_c Cs)$	$-\dfrac{K_{I2}}{D'}(1 + R_c Cs)$	$-\dfrac{L_s}{D'L_p}\dfrac{N_p}{N_s}K_{I2}(1 + R_c Cs)$

$$G = \frac{1 + \dfrac{R_c}{D'R_L} + \dfrac{R_s}{D'R_L}(1 + \dfrac{R_c}{R_L})}{(1 + D)(L + \dfrac{R_c}{D'R_L}) + \dfrac{R_s}{(D')^2 R_L}(1 + \dfrac{R_c}{R_L})}$$

Note: K's are defined in Table A.7, ω and Q are defined in Table A.9, $\omega_1 Q_1$ are defined in Table A.10

Table A.6b) F_P block diagram parameters

	Buck	Boost	Buck/Boost
	$\dfrac{1}{\sqrt{LC}}\sqrt{K_{LV1}}$	$\dfrac{D'}{\sqrt{LC}}\dfrac{R_L}{R_L+R_c}\sqrt{\dfrac{1}{K_{LV1}}}$	$\dfrac{D'}{\sqrt{L_sCK_{LV1}}}\dfrac{R_L}{R_L+R_c}$
	$\dfrac{1}{\omega_o}\dfrac{K_{LV1}}{\dfrac{R_L}{R_L+R_c}\dfrac{L}{R_L} + (R_c+R_\ell(1+\dfrac{R_o}{R_L}))C}$	$\dfrac{D'}{\omega_o}\dfrac{R_L}{R_L+R_c}\dfrac{L}{D'R_L} + \dfrac{R\ell C}{D'} + R_cC(1+\dfrac{R_\ell}{D'P_L})$	$\dfrac{D'}{\omega_o}\dfrac{R_L}{R_L+R_c}\dfrac{K_{LV1}}{\dfrac{L_s}{(D')^2R_L} + R_c\left(\dfrac{R_c}{D'} + \dfrac{R_s}{(D')^2}\right)\dfrac{R}{R_L}}$

Table A.7 K parameters

	Buck	Boost	Buck/Boost
K_{LV1}	$\dfrac{1 + \dfrac{R_c}{R_L}}{1 + \dfrac{R_c}{R_L} + \dfrac{R_\ell}{R_L}(1 + \dfrac{R_c}{R_L})}$	$\dfrac{1}{1 + \dfrac{R_c}{D'R_L} + \dfrac{R_\ell}{(D')^2 R_L}(1 + \dfrac{R_c}{R_L})}$	$\dfrac{1}{1 + \dfrac{R_c}{D'R_L} + \dfrac{R_s}{(D')^2}(1 + \dfrac{R_c}{R_L})}$
K_{UV1}	K_{LV1}	$\dfrac{1 + \dfrac{R_c}{D'R_L}}{1 + \dfrac{R_c}{D'R_L} + \dfrac{R_\ell}{(D')^2 R_L}(1 + \dfrac{R_c}{R_L})}$	$\dfrac{1 + \dfrac{R_c}{D'R_L}}{1 + \dfrac{R_c}{D'R_L} + \dfrac{R_s}{(D')^2}(1 + \dfrac{R_c}{R_L})}$
K_{V2}	K_{LV1}	$\dfrac{1 + \dfrac{R_c}{R_L}}{1 + \dfrac{R_c}{D'R_L} + \dfrac{R_\ell}{(D')^2 R_L}(1 + \dfrac{R_c}{R_L})}$	$\dfrac{1 + \dfrac{R_c}{R_L}}{1 + \dfrac{R_c}{D'R_L} + \dfrac{R_s}{(D')^2 R_L}(1 + \dfrac{R_c}{R_L})}$
K_{LD1}	K_{LV1}	$1 - \dfrac{R_\ell}{D'R_L}(1 + \dfrac{R_c}{R_L})$	$\dfrac{(1 + \dfrac{R_c}{R_L})(1 + \dfrac{D}{(D')^2}\dfrac{R_s}{R_L}(1 + \dfrac{R_c}{R_L}))}{1 + \dfrac{R}{D'R_L} + \dfrac{R_s}{(D')^2 R_L}\dfrac{R_c}{R_L}}$
K_{UD1}	K_{LV1}	K_{UV1}	$\dfrac{(1 + \dfrac{R_\ell}{D'R_L})^2 + \dfrac{R_s}{(D')^2 R_L}(D' - D + \dfrac{R_c}{R_L})(1 + \dfrac{R_c}{R_L})}{(1 + \dfrac{R_c}{D'R} + \dfrac{R_s}{(D')^2 R_L}(1 + \dfrac{R_c}{R_L}))^2}$
K_{D2}	K_{LV1}	$(1 + \dfrac{R_c}{R_L})(2 + \dfrac{R_c}{D'R_L})$	$\dfrac{1 + \dfrac{R_s}{D'R_L}(1 + \dfrac{R_c}{R_L})^2}{(1 + \dfrac{R_c}{D'R_L} + \dfrac{R_s}{(D')^2 R_L}(1 + \dfrac{R_c}{R_L}))}$
K_{LI1}	K_{LV1}	$\dfrac{1}{1 + \dfrac{R_c}{D'R_L} + \dfrac{R_\ell}{(D')^2 R_L}(1 + \dfrac{R_c}{R_L})}$	$\dfrac{1 + \dfrac{R_c}{D'R_L}(1 + \dfrac{R_c}{R_L})^2}{1 + \dfrac{R_c}{D'R_L} + \dfrac{R_s}{(D')^2 R_L}(1 + \dfrac{R_c}{R_L})}$
K_{UI1}	K_{LV1}	$(1 + \dfrac{R_c}{R_L})(1 + \dfrac{\dfrac{R_\ell}{(D')^2}(1 + \dfrac{R}{R_L}) - \dfrac{R_c}{D'}\dfrac{R_c}{R_L}}{1 + \dfrac{R_c}{D'R_L} + \dfrac{R_\ell}{D'R_L}(1 + \dfrac{R_c}{R_L})})$	K_{UV1}
K_{I2}		K_{UV1}	K_{UV1}

247

Table A.8 ω and Q parameters

	buck	boost	buck/boost
ω_{LV1}	$\frac{1}{R_cC}$	•	•
ω_{JV1}	LV1	$\frac{D'}{R_cC}\frac{1+\frac{R_c}{D'R_L}}{1+\frac{R_c}{R_L}}$	$\frac{D'}{R_cC}\frac{1+\frac{R_c}{D'R_L}}{1+\frac{R_c}{R_L}}$
ω_{V2}	$\frac{1}{(R_L+R_c)C}$	$\frac{1}{(R_L+R_c)C}$	$\frac{1}{(R_L+R_c)C}$
ω_{LD1}	ω_{LV1}	$-\frac{(D')^2}{L}\frac{R_L}{R_L+R_c}\frac{1}{R_{LD1}}$	$-\frac{(D')^2}{DL_S}\frac{(1+\frac{2}{(D')^2}\frac{R_S}{R_L}(1+\frac{R_S}{R_L}))^2}{R_{LD'}}$
ω_{UD1}	ω_{LV1}	(formula illegible)	(formula illegible)
ω_{D2}	ω_{V2}	(formula illegible)	(formula illegible)
ω_{LI1}	$\frac{1}{\sqrt{LC}}\frac{R_L}{R_L+R_c}\sqrt{\frac{R_c}{R_L}}$	$\frac{R_?}{L}$	(formula illegible)
Q_{LI1}	(formula illegible)	1	1
ω_{JI1}	ω_{LI1}	(formula illegible)	(formula illegible)
Q_{JI1}	Q_{LI1}	(formula illegible)	(formula illegible)
ω_{I2}	ω_{LV1}	$\frac{1}{R_cC}$	$\frac{1}{R_cC}$

Table A.9 ω_1 and Q_1

	Buck	Boost	Buck/Boost
ω_1	$\dfrac{1}{\sqrt{LC}}\dfrac{R_L}{R_L+R_c}\sqrt{\dfrac{R_\ell}{R_L}}$	$\dfrac{D'}{\sqrt{LC}}\sqrt{G}$	$\dfrac{1}{\sqrt{L_SC}}\sqrt{\dfrac{\bar{R}_S}{R_c}}$
Q_1	$\dfrac{1}{\omega_1}\dfrac{\left(\dfrac{R_L}{R_L+R_c}\right)^2\dfrac{R_\ell}{R_L}}{\dfrac{L}{R_c}+RC}$	$\dfrac{1}{\omega_1}\dfrac{\sqrt{G}}{\dfrac{L}{D'R_c/R_L}+\dfrac{R_\ell C}{D'}(1+\dfrac{R_c}{R_L})}$	$\dfrac{1}{\omega_1}\dfrac{1}{\dfrac{L_S}{R_S}+1\,C}$

$$G = \frac{R_L}{R_L+R_c}\sqrt{1+\frac{R_c}{D'R_L}\;\frac{R_c}{R_L+R_c}\;\frac{R_\ell}{(D')^2 R_c}\left(1+\frac{R_c}{R_L}\right)^2}$$

Table A.10 Constant ontime transfer functions

Refer to Figure 5.4.1.

	Buck	Boost	Buck/Boost
F_{V1}	$DK_{UN1}(1 + \dfrac{S}{\omega_{UV1}})$	$\dfrac{K_{UV1}}{D'}(1 + \dfrac{S}{\omega_{UV1}})$	$\dfrac{D}{D'}\dfrac{N_S}{N_P}K_{UV1}(1 + \dfrac{S}{\omega_{UV1}})$
F_{D1}	$V_I K_{UD1}(1 + \dfrac{S}{\omega_{UD1}})$	$\dfrac{K_{UD1}V_I}{(D')^2}(1 + \dfrac{S}{\omega_a})$	$\dfrac{V_I}{(D')^2}\dfrac{N_S}{N_P}K_{UD1}(1 + \dfrac{S}{\omega_a})$
F_{I1}	$R\,K_{UI1}(1 + \dfrac{S}{\omega_i Q_1} + (\dfrac{S}{\omega_1})^2)$	$R_c K_{UI1}(1 + \dfrac{S}{\omega_1 Q_1} + (\dfrac{S}{\omega_1})^2)$	$\dfrac{R_S}{(D')^2}K_{UI1}(1 + \dfrac{S}{\omega_1 Q_1} + (\dfrac{S}{\omega_1})^2)$

Note:

F_{V2}, F_{D2}, F_{I2} are the same as those in Table A.6

K's are defined in Table A.7

ω and Q are defined in Table A.8

ω_1 and Q_1 are defined in Table A.9

APPENDIX   B

Examples comparing the Discrete Model and
the Average Model in the Discontinuous Mode. (sec. 7.4)

Three examples are shown.   For each example the load,
frequency and energy storage inductance are varied.   In each
example the average model and discrete model produce similar
results.

The first example is of the buc converter with the
following numerical values (see Fi are 1.1.1.):

$R_i = 0 \, \Omega$, $L = 1000 \, \mu h$, $R_c = .034\Omega$, $c = 455 \, \mu f$,

$R_L = 150 \, \Omega$, $V_0 = 20 \, v$, $V_I = 40 \, v$, $t_p = 50 \, \mu s$.

Figures   B.1 - B.6   show that there is vertually no dif-
ference in the average model and the discrete model.
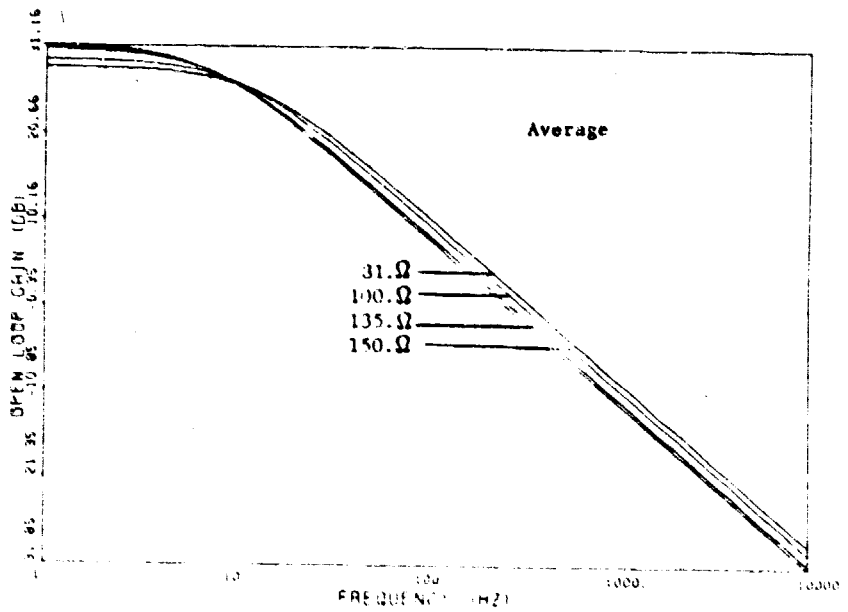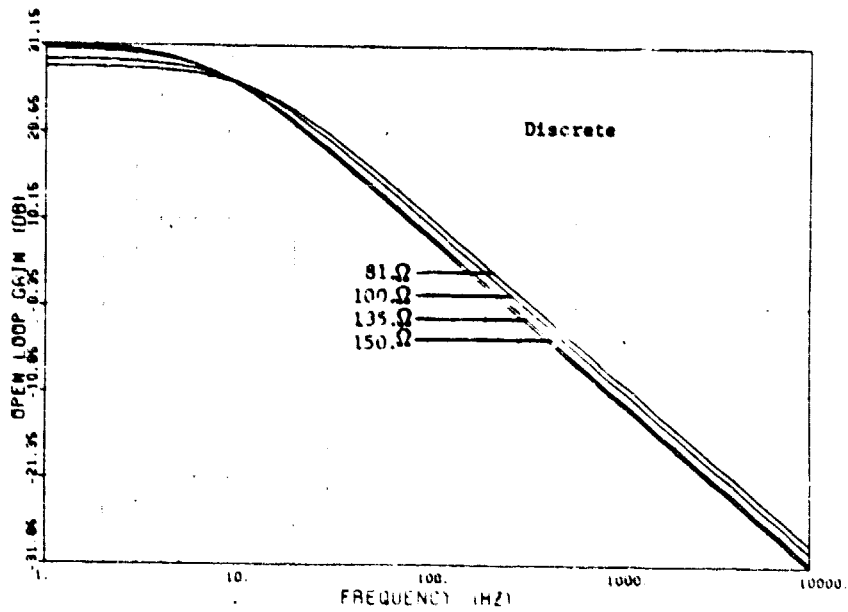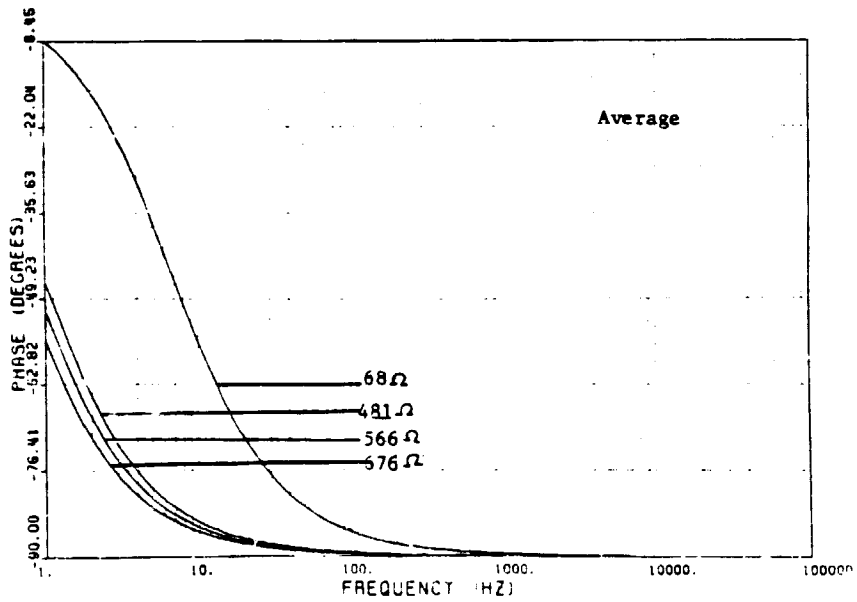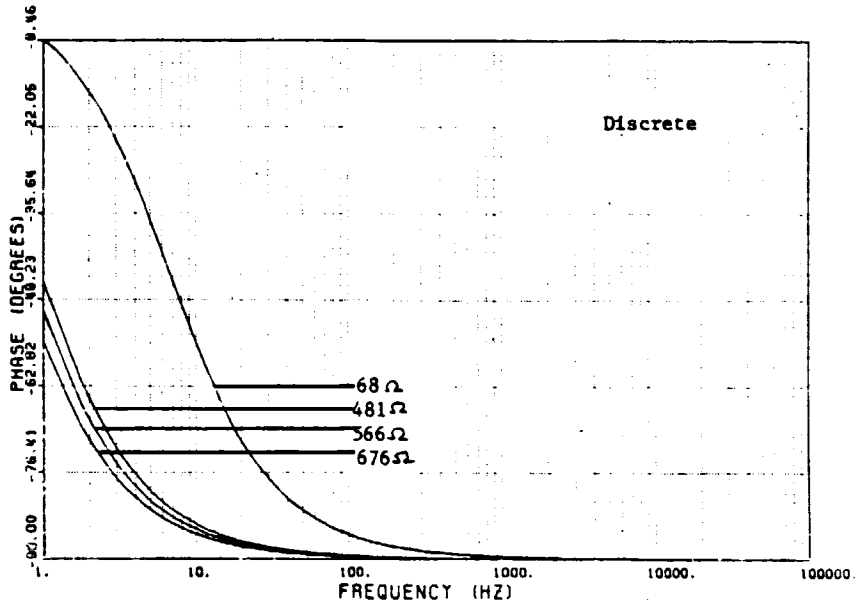
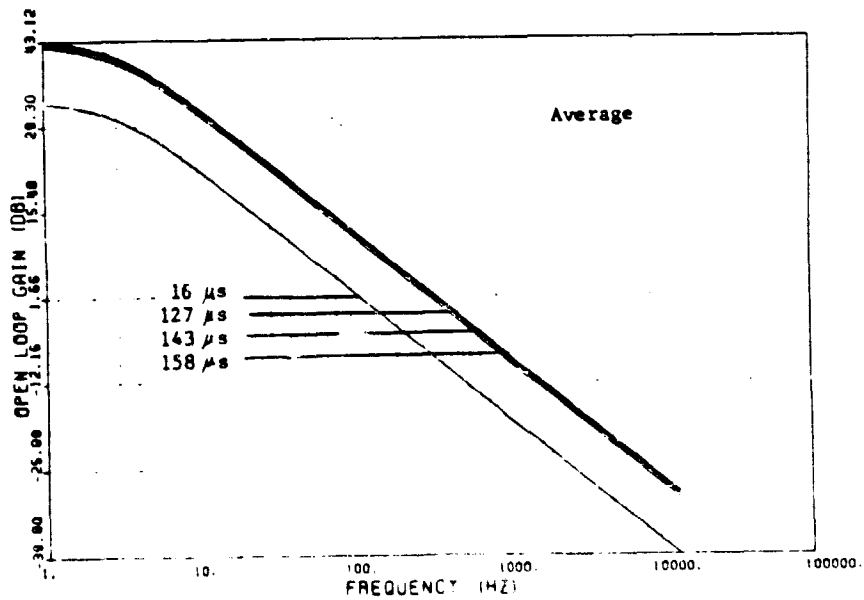Figure 8.1 Gain plot varying the load.

Figure 3.2 Phase plot varying the load.

254
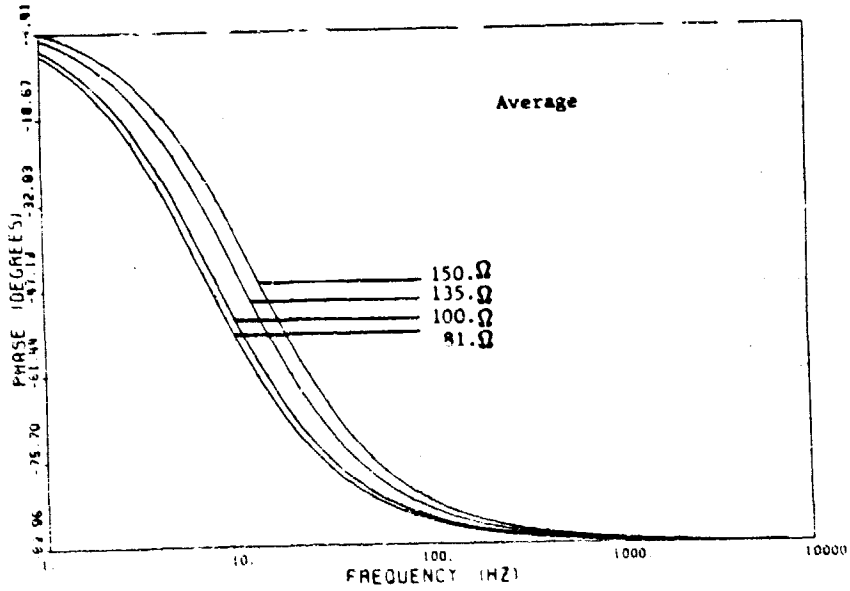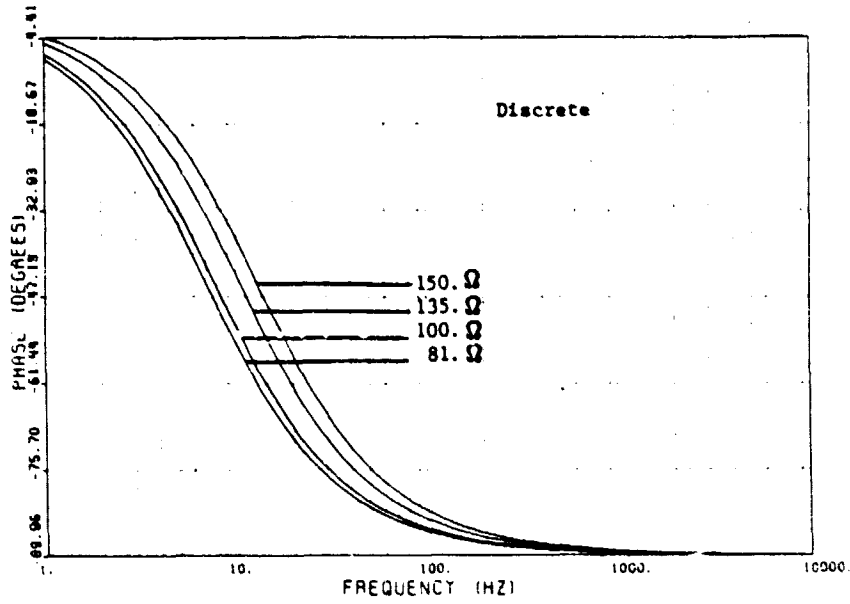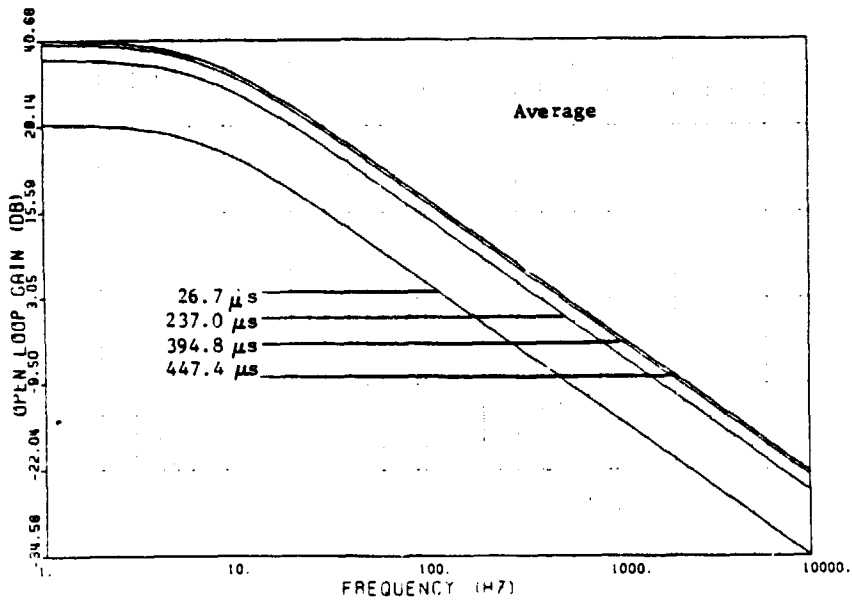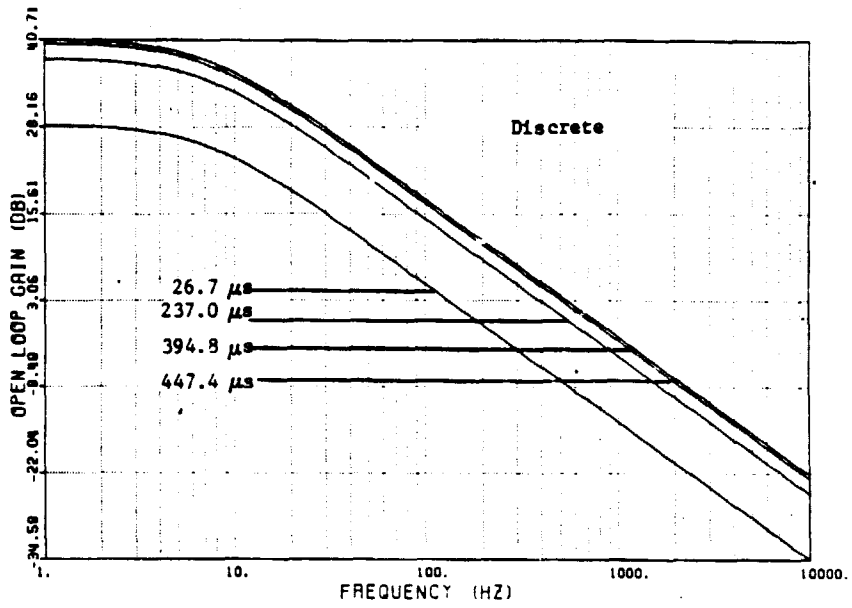
Figure B.3 Gain plot varying the frequency.
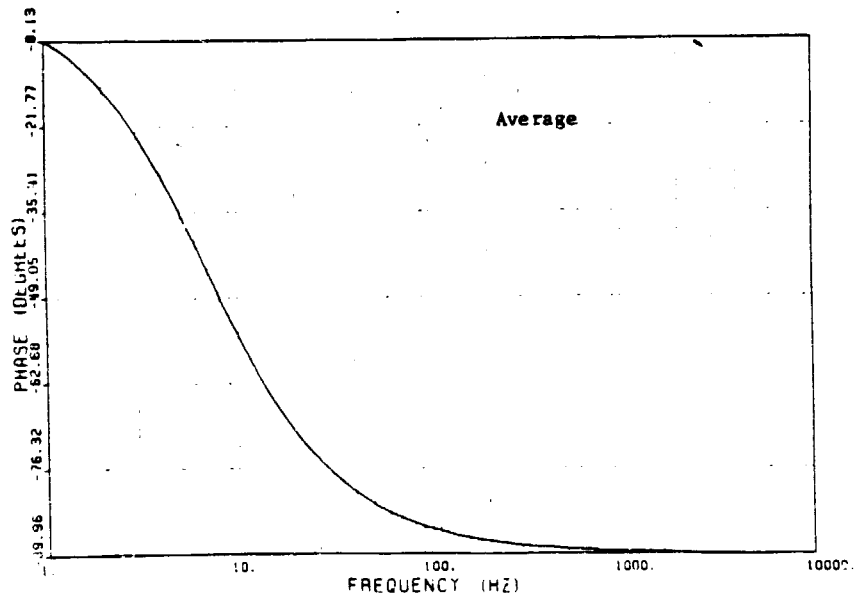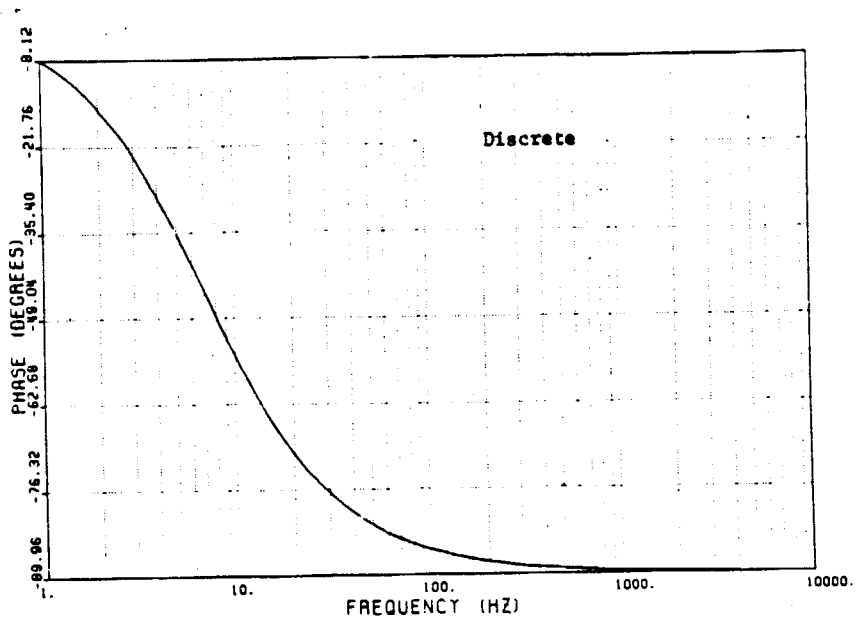
Figure B.4 Phase plot varying the frequency.
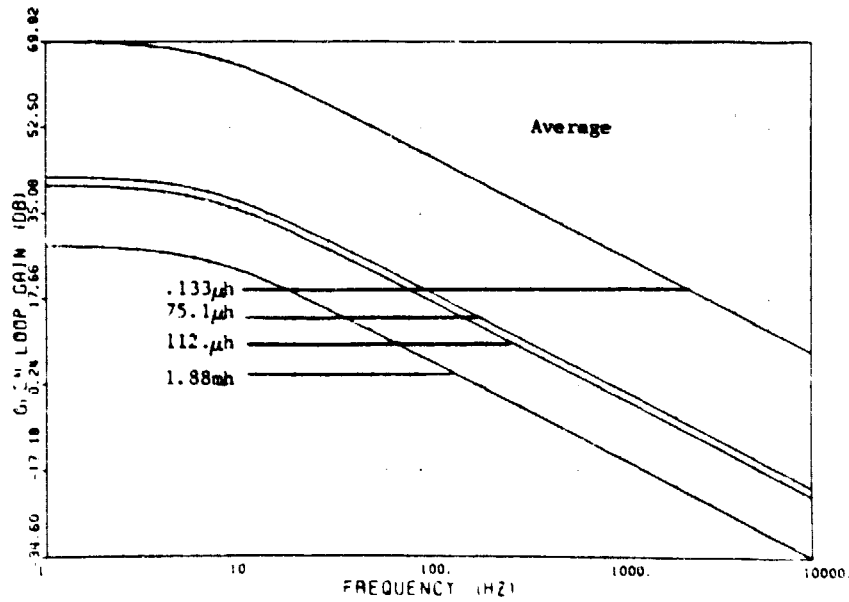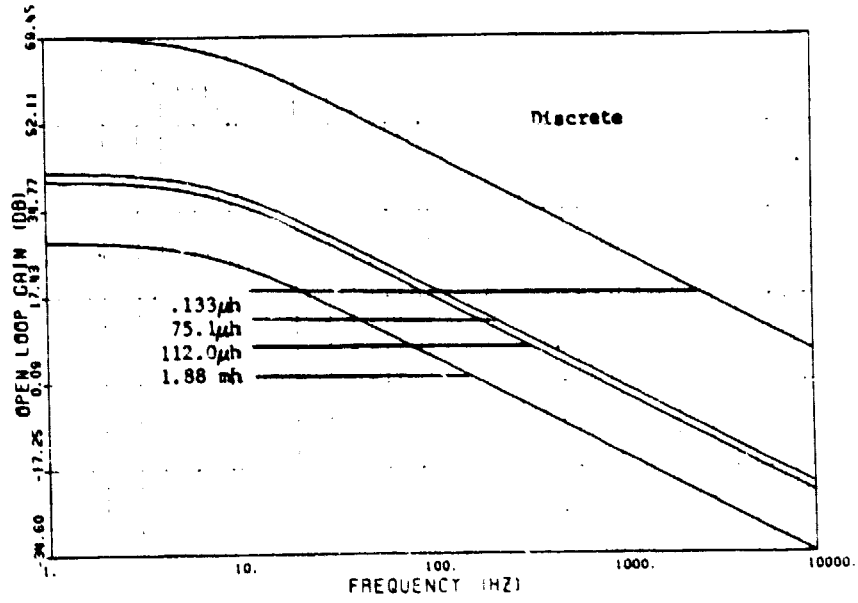
Figure B.5 Gain plot varying the inductance.
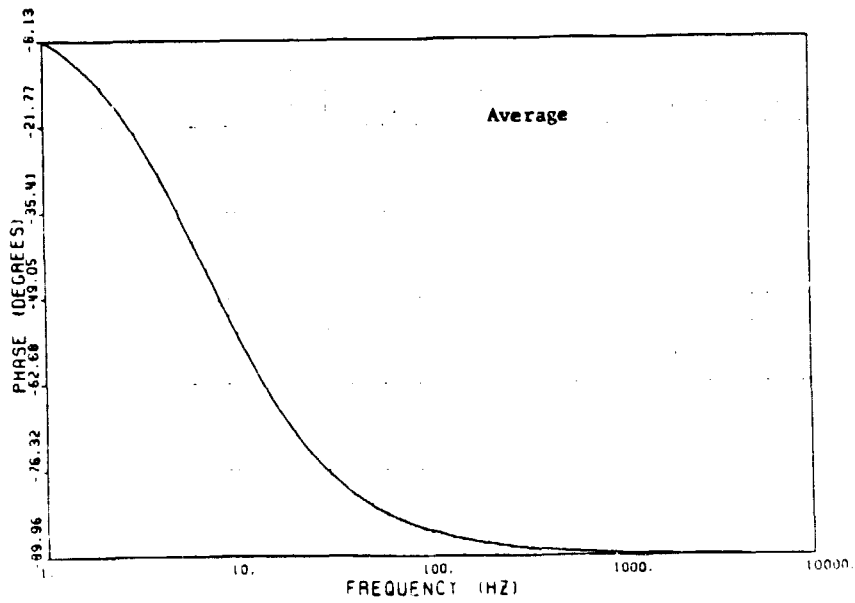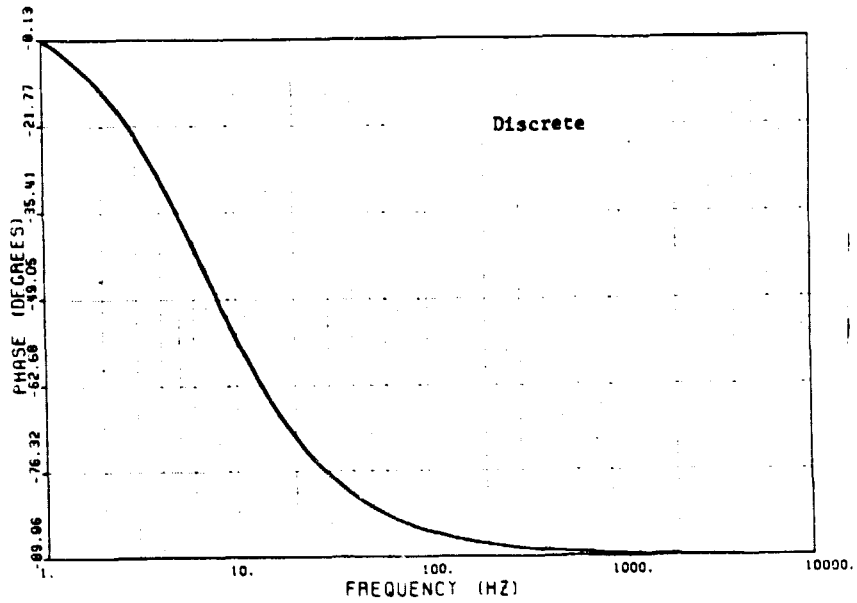
Figure B.6 Phase plot varying the inductance.

The second example is the buck/boost converter with the following numerical examples (refer to Fig. 1.1.1.):

R_s = 0. Ω

R_c = 0. Ω

C = 12 μ f

R_L = 225 Ω

$N_p = N_s$

V_o = 10. v

V_I = 60 v

L = 3.5 mh

T = 100 μ s

Figures B.7 - B.12 show virtually no difference between the two models.
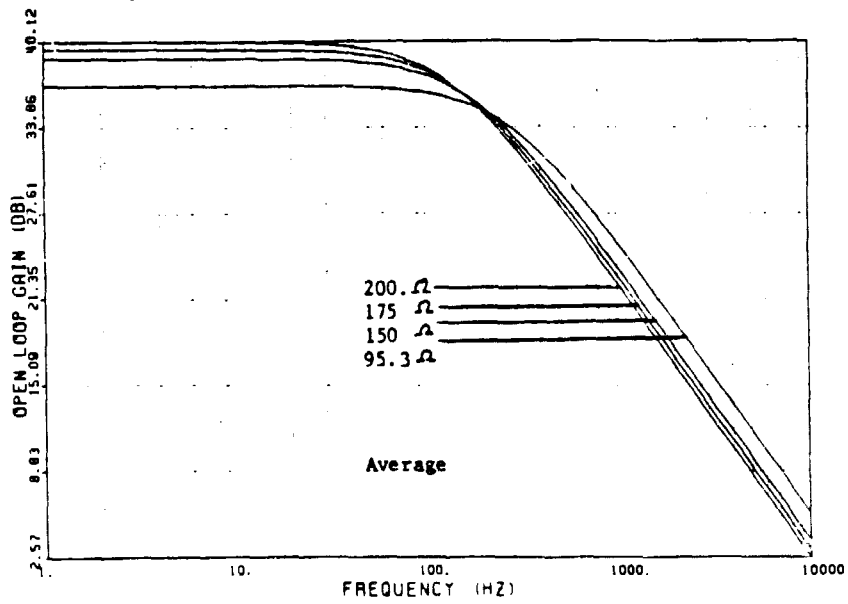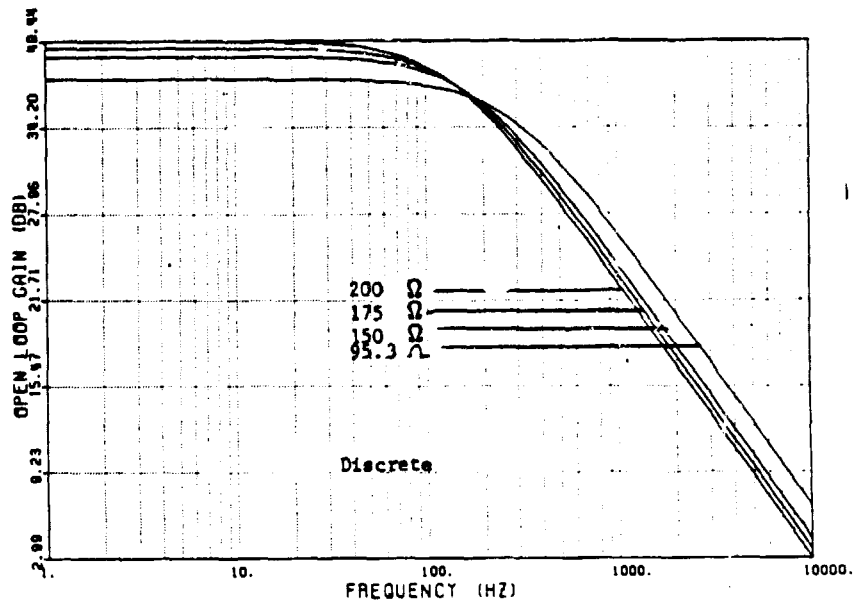
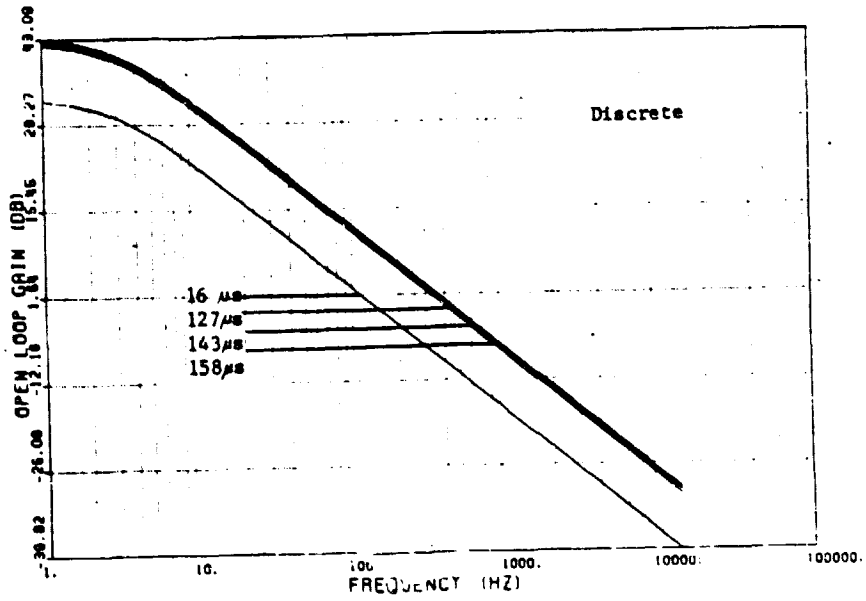Figure B.7 Gain plot varying the load.
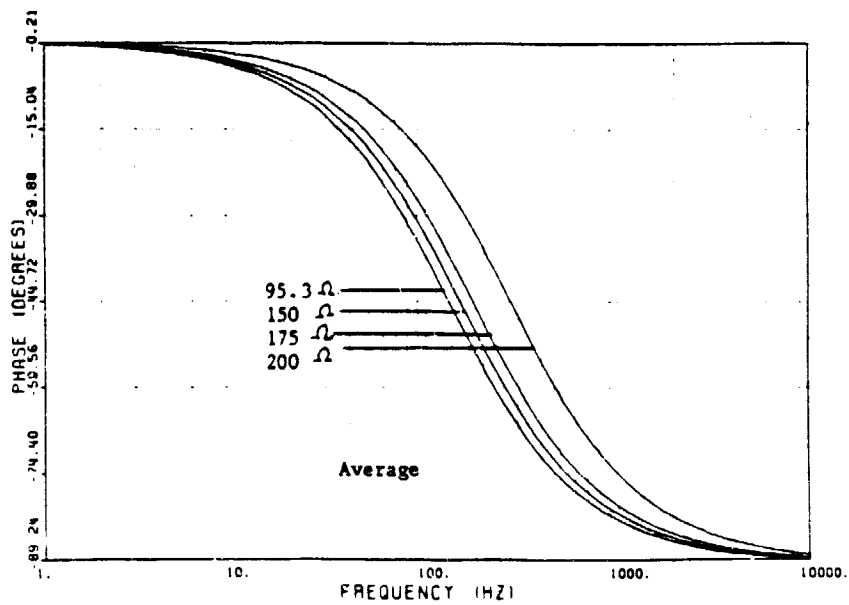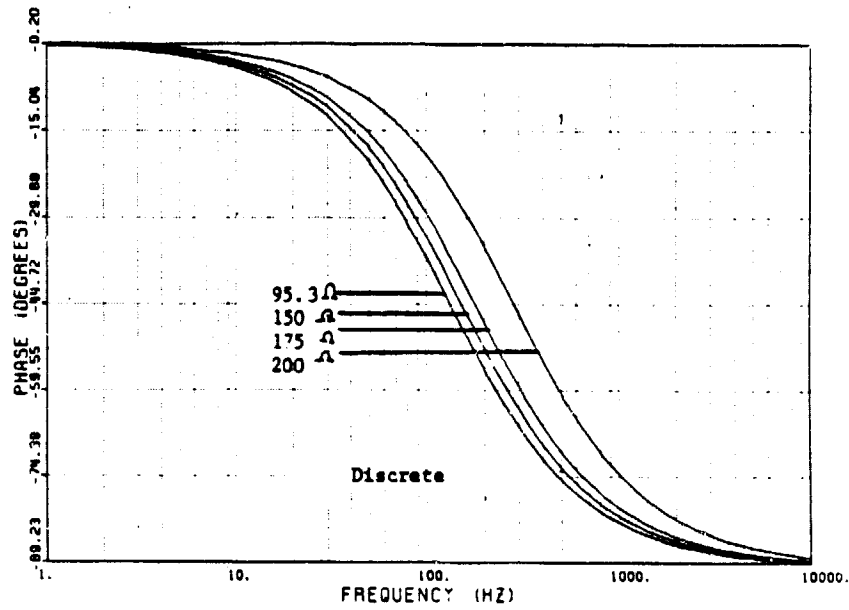
Figure B.8 Phase plot varying the load.
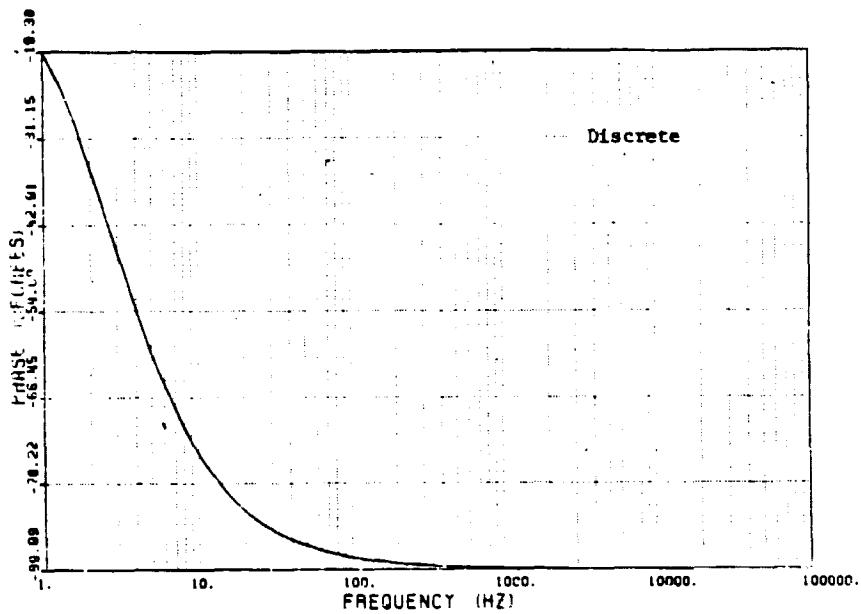
261
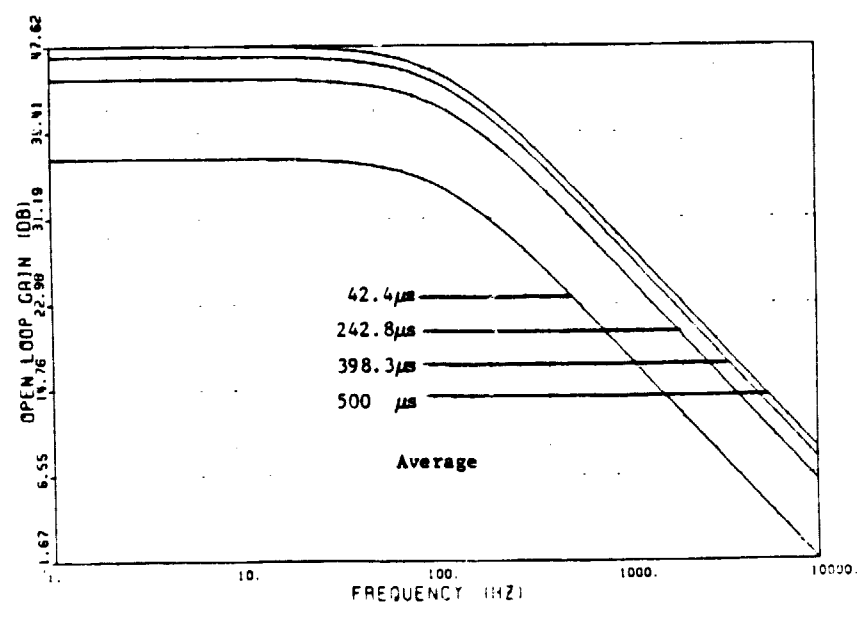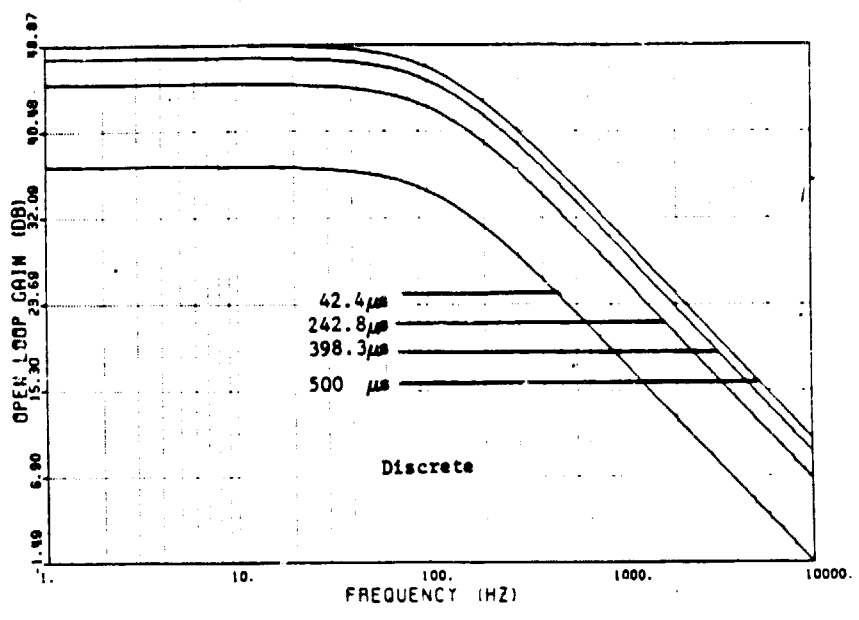
Figure B.9 Gain plot varying the frequency.
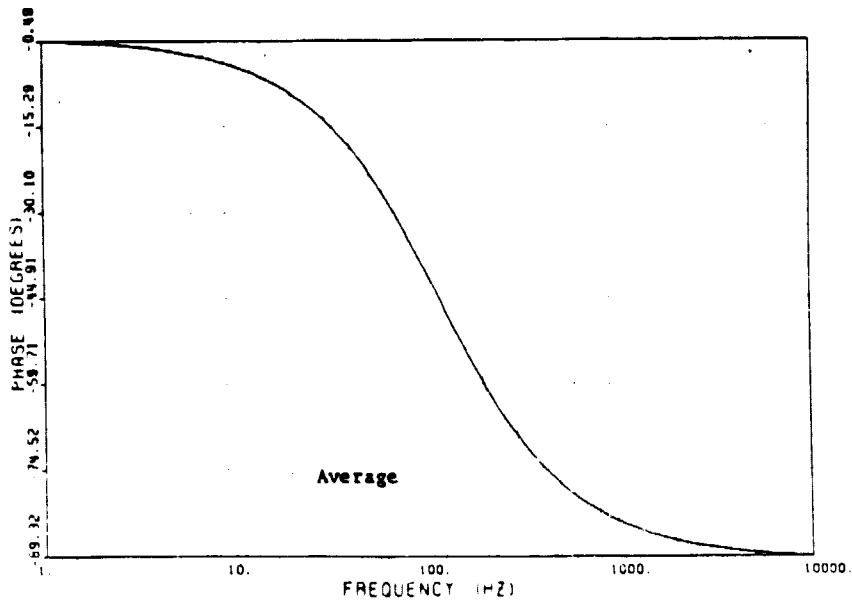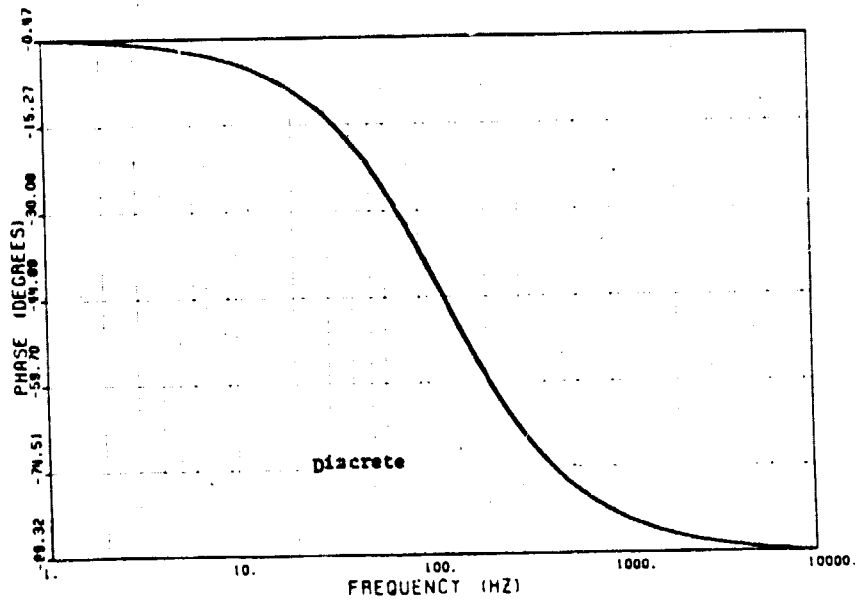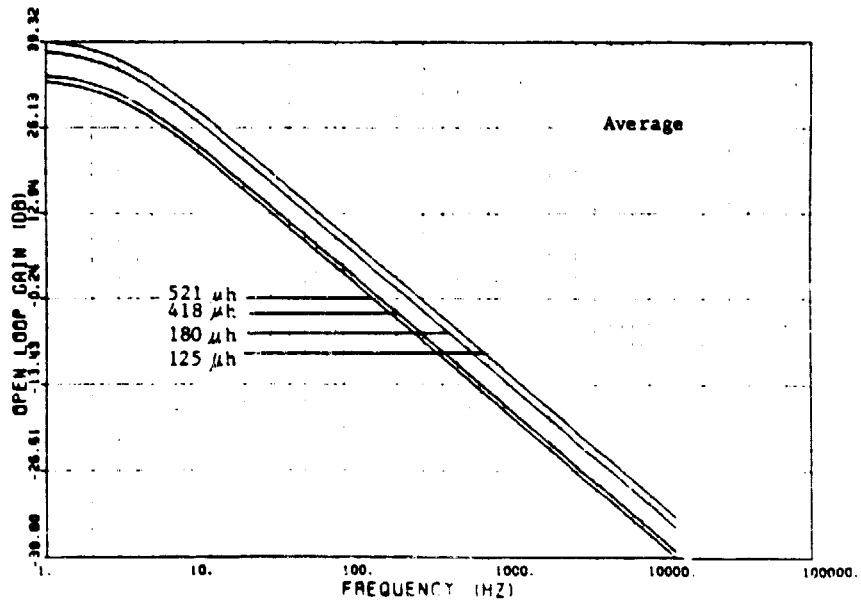
Figure B.10 Phase plot varying the frequency.
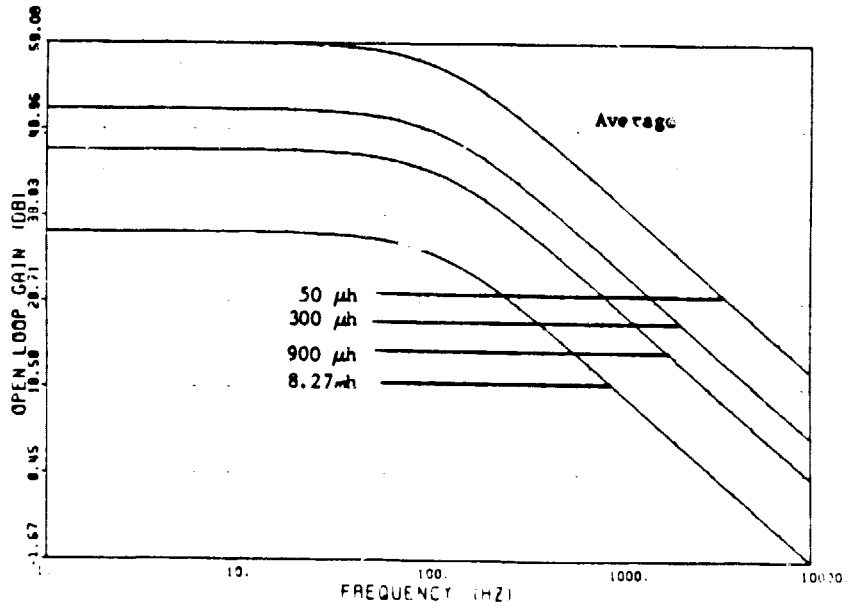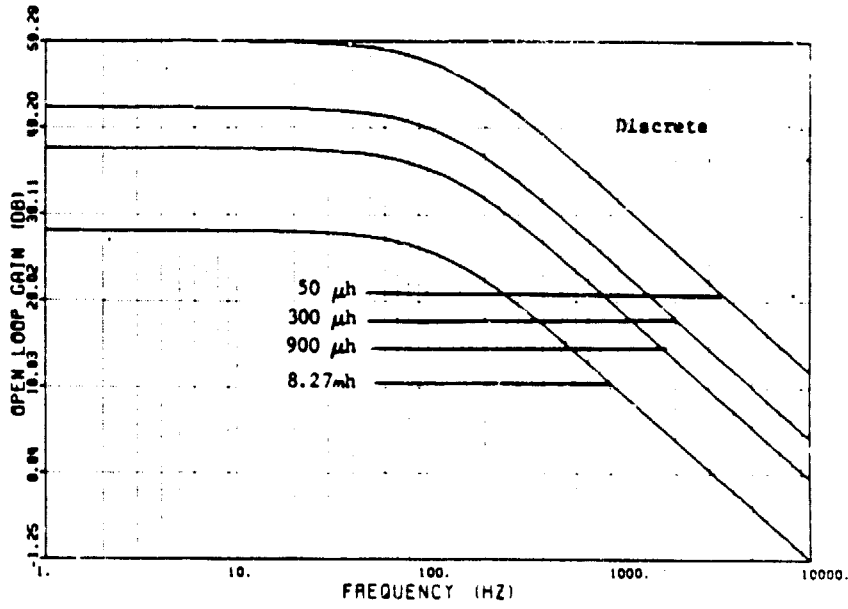
Figure B.11 Gain plot varying the inductance.

264
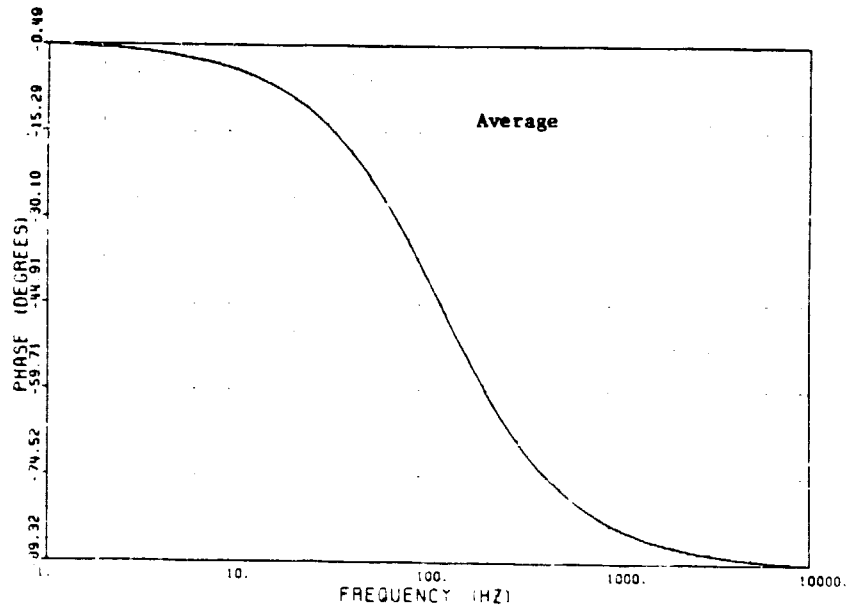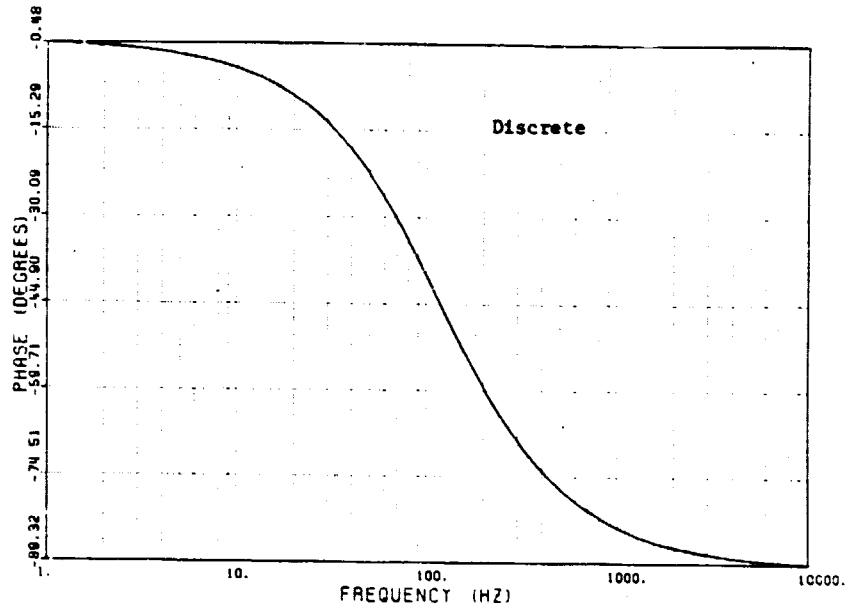
Figure B.12 Phase plot varying the inductance.

The third example is the buck/boost converter with the following numerical values (refer to Fig. 1.1.1.):

$R_s = 0. \Omega$

$R_c = .05 \ \Omega$

$C = 700 \ \mu f$

$R_L = 160 \ \Omega$

$N_p = N_s$

$V_o = 28 \ v$

$V_I = 20 \ v$

$L = 220 \ \mu h$

$T = 37.5 \ \mu s$

Figures B.13 - B.18 show virtually no difference between the two models.
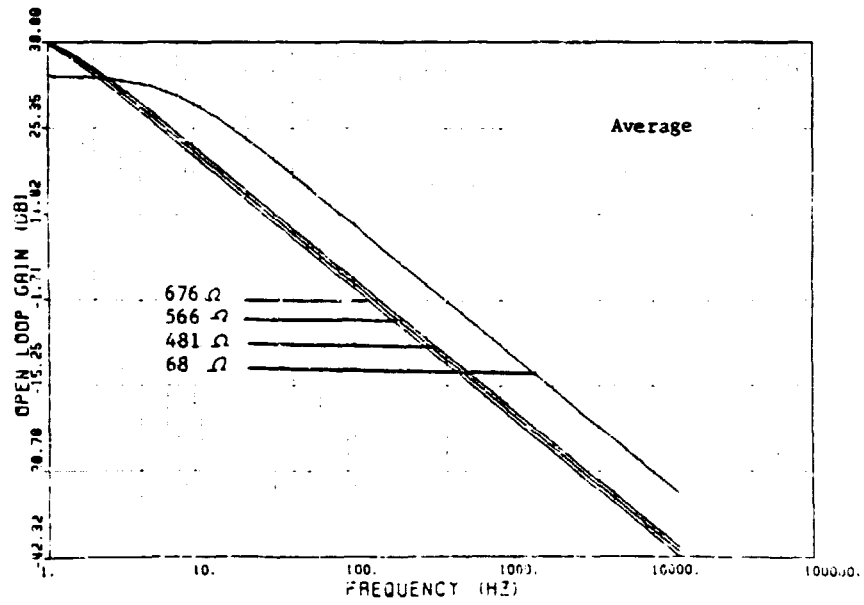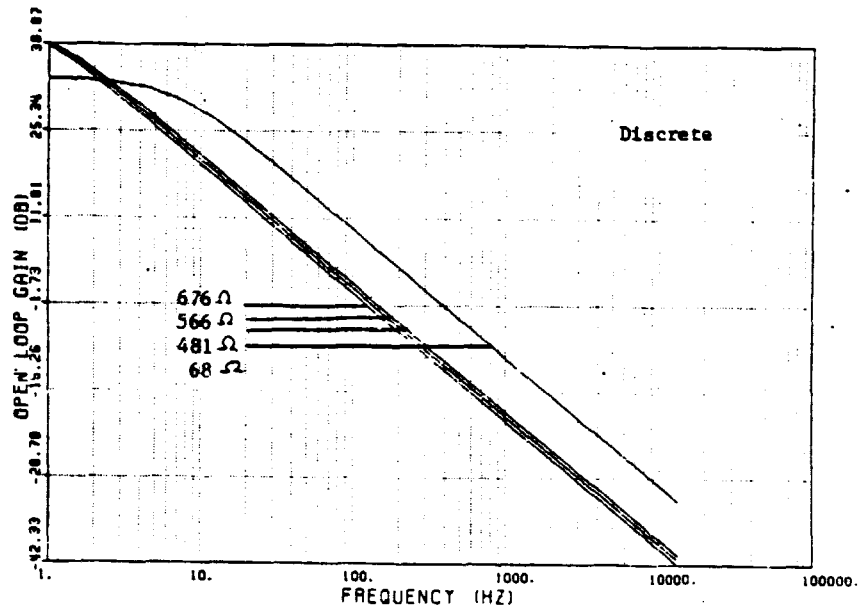
Figure B.13 Gain plot varying the load.

267

Figure B.14 Phase plot varying the load.

Figure B.15 Gain plot varying the frequency.
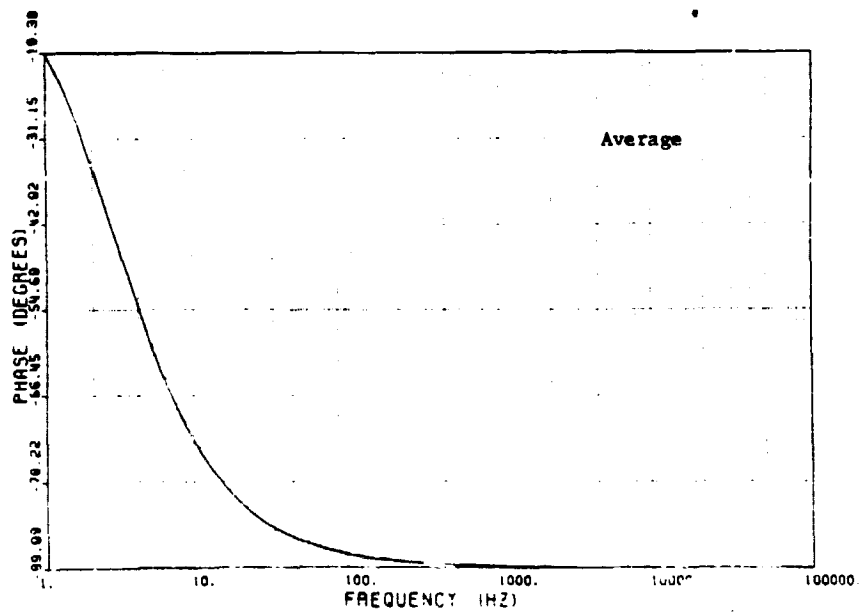
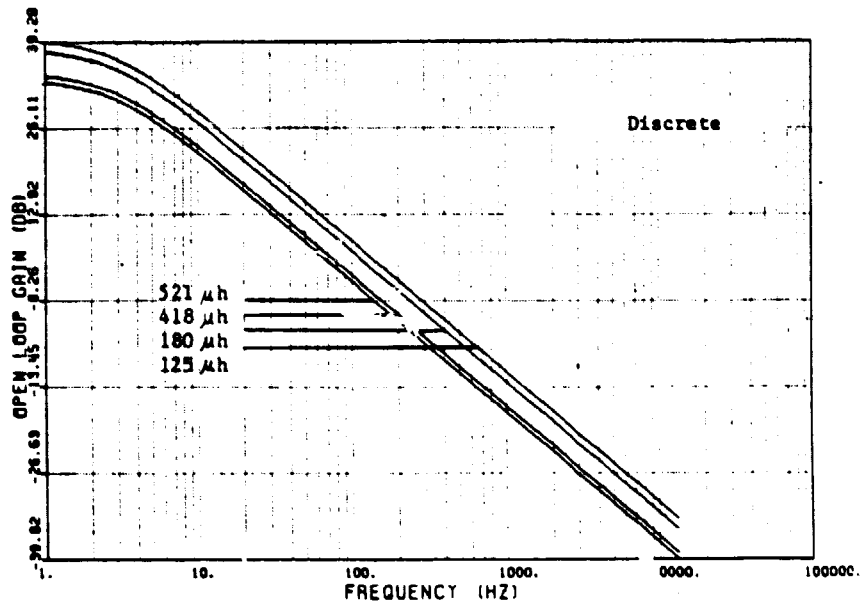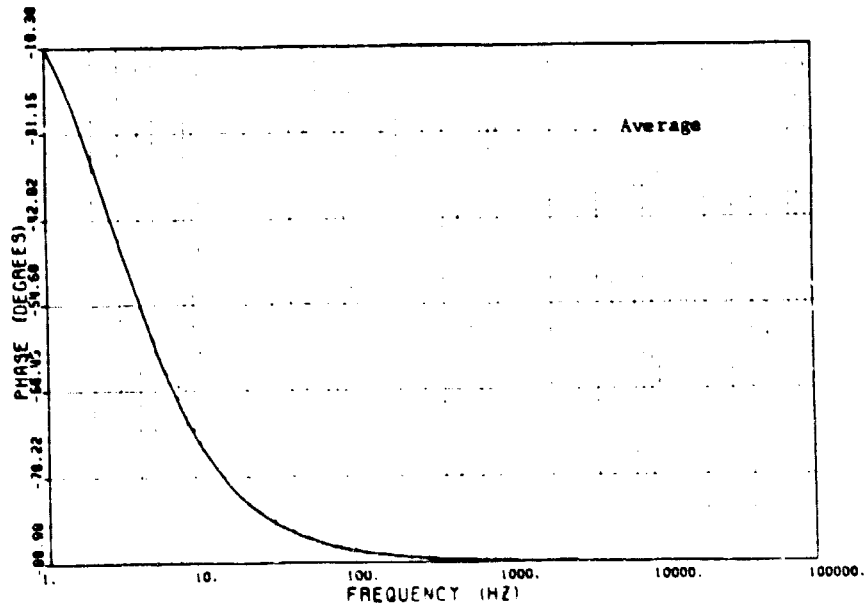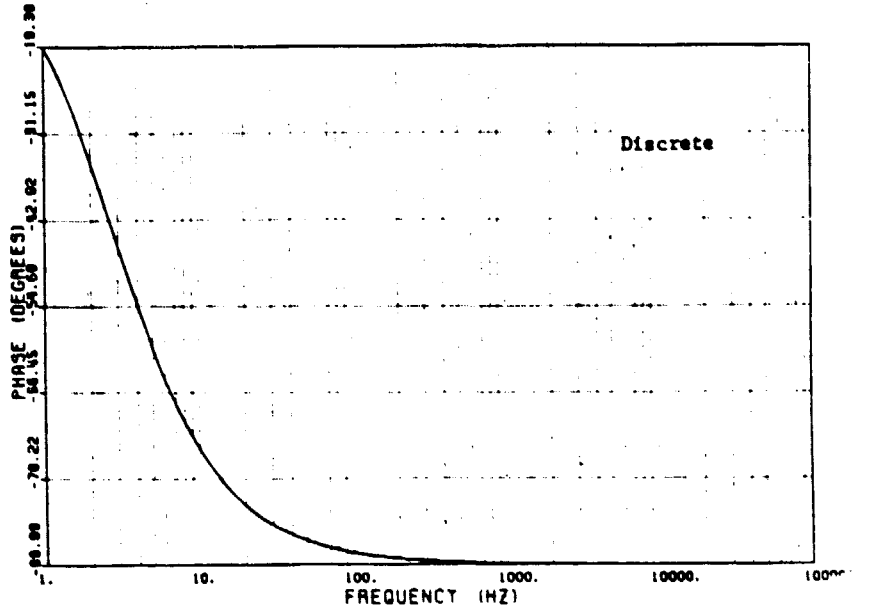Figure B.16 Phase plot varying the frequency.

Figure B.17 Gain plot varying the inductance.

Figure B.18 Phase plot varying the inductance.